A regenerator-based thermoacoustic electricity generator with different configurations for rural communities of South Sudan country

A Thesis

Submitted in partial fulfillment of the requirements
for the degree of

Doctor of Philosophy (Ph.D.)
by

Wigdan Kisha

Supervisors:

Dr. David Hann

and

Dr. Jon McKechnie



School of Mechanical, Material and Manufacturing Engineering

University of Nottingham

September 2019

DECLARATION

I, Wigdan Kisha, hereby declare that this thesis, titled "A regenerator-based thermoacoustic electricity generator with different configurations for rural communities of South Sudan country" and the whole work presented inside it represents my own ideas and has been done only by me. I further declare that

- All the work was generated during my time as a researcher at the University of Nottingham.
- None of this work has been previously submitted to obtain a research degree either at the University of Nottingham or any other institution.
- Where I used any work published by any other author, in any form, this is always adequately cited.
- The source is properly given at the point of use where I have used any work quoted from another author.
- I confirm that, the entire thesis except such quotations is the product of my own work.
- All the main sources of support used to produce this thesis have been properly and accurately acknowledged.

Wigdan Kisha	January 6, 2020

ABSTRACT

This Ph.D. thesis explores different configurations of a low-cost air-filled thermoacoustic engine for waste heat recovery and electricity generation built by the SCORE consortium. The previously tested prototypes are limited to 12.6 W maximum output from 2.5 kW heat from a biomass stove. The maximum achievable electricity output from the unpressurised air-filled system has long been a question of great interest in a wide range of thermoacoustic fields. Therefore, the aim is to push the limit of the unpressurised air-field thermoacoustic systems by enhancing the power amplification without changing the working gas, as well as the total cost due to the constraints of the application (developing world), and therefore, to meet the original 20 -100 W target set by SCORE.

This was achieved by initially completing a theoretical analysis of a looped-tube thermoacoustic electricity generator of a single regenerator unit, a feedback pipe, a loudspeaker to function as electricity harvester, and a tuning stub. The engine was heated electrically. This piece of work aims to predict the likely behaviour of the acoustic wave throughout the system components by using DeltaEC modelling. Investigation of the stub pipe for phase tuning was particularly important. It was shown that a modelling procedure of a looped-tube thermoacoustic engine coupled with a power harvester and a tuning stub could be established. DeltaEC models were constructed that simulated the real prototype with all components and energy conversions taking place. The first models predicted the behaviour of the system with different load resistances of the loudspeaker, and these models have been validated experimentally. Subsequent models were developed together with experimental work to assess the influence of the stub length on the power output. This research enabled a better understanding of the wave propagation in such complex systems by using the powerful thermoacoustic tool DeltaEC.

Based on this study, a more complex travelling wave thermoacoustic engine of two regenerators, a feedback pipe, two stubs, and a loudspeaker was accurately simulated. The system was optimised in two stages; the first one involved only operating conditions, while the second stage investigated geometrical aspects. The first optimisation was

carried out using a novel operational methodology. This innovative technique applied asymmetric heat inputs through the engine stages while maintaining the total heat flow into the system. Asymmetric impedance distribution was observed, and this caused variation in acoustic amplification. The acoustic conditions were then improved, and a stronger wave was generated along the loop. The acoustic power was higher when the heat ratio used in the first core is smaller than that supplied into the second one. The loop acoustic power was higher by almost 18% when the heat input ratio was changed from $50\% - 50\%$ to $40\% - 60\%$ with no other changes to the system configuration. For the same conditions, the electricity output showed 28.6% increasing percentage. This technique was validated in the laboratory, and the results agreed well with the models. The velocity of the air was measured using the "gradient method". In reviewing the literature, no data was found on the association between asymmetric heat inputs and acoustic amplification in two-stage thermoacoustic electricity generators. Also, No similar study of estimating the acoustic power in thermoacoustic engines using the gradient method has been made elsewhere. Subsequent optimisation of the structure of the regenerators of a dual-core thermoacoustic engine was carried out. The lengths and the hydraulic radii of the two regenerators were optimised. Fundamental analysis of regenerator performance in terms of acoustic amplification and dissipation, a time constant, heat transfer, the temperature difference, and the engine excitation was carried out. Similar models were found for the optimisation of the regenerator of a single thermoacoustic engine, but no similar numerical optimisation of regenerators of a multi-stage travelling wave thermoacoustic engine has been made elsewhere. The complexity of the optimisation becomes an issue when more than one regenerator exists, and when the cost of the system is also an important consideration. The developed models suggested optimum geometrical parameters for the regenerators. Accordingly, the generated acoustic power and the achieved efficiencies were enhanced. Compared to SCORE data, the new system has improved the loop acoustic power by 63.8%, and the electrical power by 316%.

The outcomes of this thesis could have a massive impact on atmospheric air-filled thermoacoustic engines of multiple cores, enabling producing a 100 W electricity output.

LIST OF PUBLICATIONS

Wigdan Kisha, and David Hann. "Numerical optimisation of the regenerator of a multi-stage travelling wave thermoacoustic electricity generator". *16th UK Heat transfer Conference, Nottingham, September 2019*.

Wigdan Kisha, and David Hann. "Thermoacoustic electricity generator for rural dwellings in developing world". *16th UK Heat transfer Conference, Nottingham, September 2019*.

Wigdan Kisha, Paul H.Riley, Jon McKechnie and David Hann (2018). "The Influence of Heat Input Ratio on Electrical Power Output of a Dual-Core Travelling-Wave Thermoacoustic Engine". *8th Heat Power Cycles Conference, University of Bayreuth, Germany*.

Wigdan Kisha, Paul H.Riley, Jon McKechnie and David Hann (2018). "Development of a low-cost, electricity-generating Rankine Cycle, alcohol-fuelled cooking stove for rural communities". *8th Heat Power Cycles Conference, University of Bayreuth, Germany*.

Wigdan Kisha, David Hann, and Paul H.Riley (2017). "Optimization of a Low-Cost Single Regenerator Travelling-Wave Looped-tube Thermoacoustic Engine". *15th UK Heat transfer conference, UKHTC2017, Brunel University, London*.

Wigdan Kisha, Paul H.Riley, Jon McKechnie, and David B. Hann. "Impact of thermal power distribution ratio on the performance of a multi-stage travelling-wave thermoacoustic electricity generator". *Paper submitted and under revision of Elsevier, Energy Journal*.

Wigdan Kisha, Paul H.Riley, and David Hann. "Renewable energy clean cooking stove with electrical generation for developing countries". *Paper submitted to Elsevier, Energy Journal*.

ACKNOWLEDGEMENTS

First and foremost, all the praises and thanks be to Allah, the Most Beneficent, the Most Merciful, for the strengths and His blessing in completing this thesis.
Special massive gratitude to my supervisors Dr. David Hann and Dr. Jon McKechnie for their continuous support and encouragement, both scientific and personal. This thesis might not have seen the light without their inspiring guidance, invaluable constructive criticism, and friendly advice during the study. The opportunities I have been given are highly appreciated.

I would also like to show gratitude to my project external guide Professor Paul H Riley from the City University of London for sharing his pearls of wisdom with me, for his patience, knowledge, and anecdotes throughout my Ph.D. journey. I learnt a lot from you and owe you big time for the knowledge you passed on to me over the past four years.

Besides my advisors, I would like to thank the viva voce examination committee: external examiner Prof. Zhibin Yu from University of Glasgow, and internal assessor Dr. Donald Giddings, for an intellectually stimulating and enjoyable viva.

I also immensely grateful to Dr Yousif Abakr, and Dr Goh Jenn from Malaysia campus for their valuable input and constant distractions throughout the first year of my study via Skype.

My sincere thanks go to all the students, staff, and technicians of the FluTE Research Group. Appreciation to all the technicians of L4 laboratory, Michael Fletcher, Mel Hemsley, and Sean Turner for the assistance during my laboratory works. Thanks to all other engineering technicians Andrew Plumber and Phill Bennet from L2 workshop, Mark Birkin from Electronics Workshop, and Nigel from Engine Research Group.
Special thanks to Christopher Cook from the Advanced Manufacturing research centre

for his help during the dismantling and maintenance of the early version design of the thermoacoustic rig.
Massive thanks go to Ian Homer who had to suffer from my continuous requests to maintain the electrical parts of my rig. I can't thank him enough for being patient and for all the time he spent helping me.

I want to acknowledge the backing for Ph.D. studies from the Dean of Engineering Research Excellence Scholarship, University of Nottingham. Special thanks also go to The Gordon Memorial College Trust Fund for their grants towards my living expenses.

To my parents and lifetime companions Mo Kisha and Fahima, I am indebted. Your support and encouragement can never be repaid. I am profoundly grateful to my brother Hamid, my sister Rania and her family, my lovely uncle Dr Zaroog Wahbi, my closest friend Sara, and all my friends in the UK and back in Sudan for their spiritual support and encouragement during my studies.

Heartfelt thanks go to my kind and caring daughters Rinad and Layan for their unconditional love. Thanks go to those little hands for wiping away my tears and relieving my stresses when needed. They are the ones who made it an incredible journey by letting me through all the difficulties. I love you beyond the definition of love.

Finally, to my husband Mohammed, for his unwavering love and patience, and for being my rock. I cannot thank him enough.

I am really grateful to all who believed in me, encouraged and supported me to be where I am today, and I promise to move out soon.

Wigdan Kisha

University of Nottingham
January 6, 2020

CONTENTS

Contents *Page*

Declaration **ii**

List of Publications **iv**

Abstract **iv**

Publications **vi**

Acknowledgments **viii**

List of Figures **xii**

List of Tables **xxvii**

Nomenclature **xxviii**

1 Introduction **1**

1.1 Research motivation 1
1.2 SCORE Consortium 3
1.3 Problem statement 5
1.4 Aim and objectives 5
1.5 Thesis outlines 7

2 Historical perspective of thermoacoustics **10**

2.1 Overview of thermoacoustics and thermoacoustic effect 10
2.2 Thermoacoustic technology based on the thermoacoustic effect 15
2.2.1 Mechanisms to enhance the thermoacoustic conversion 20
2.3 Thermoacoustic for waste heat recovery 24
2.4 Thermoacoustic for electricity generation 27
2.4.1 Thermoacoustic engines for micro-generation 27
2.4.2 Potential of TAE in a broader context 35
2.5 Concluding Remarks 51

3 Theoretical background of thermoacoustic systems 52
3.1 Introduction . . . 52
3.2 Classification of thermoacoustic systems . . . 52
3.2.1 Standing wave or stack-based engines . . . 55
3.2.2 Travelling wave or regenerator-based engines . . . 60
3.3 Critical performance scales and parameters . . . 62
3.3.1 Wavelength, wave amplitude and frequency . . . 62
3.3.2 Thermal penetration depth . . . 63
3.3.3 Viscous penetration depth . . . 63
3.3.4 Gas parcel displacement amplitude . . . 64
3.3.5 Mean pressure of the system . . . 65
3.3.6 Acoustic pressure amplitude ratio . . . 66
3.3.7 Acoustic power . . . 66
3.3.8 Efficiency of the system . . . 67
3.4 Thermoacoustic linearisation and Rott's approximation . . . 67
3.4.1 Thermoacoustic governing equations . . . 69
3.5 Non-linearity in thermaocoustic systems . . . 75
3.5.1 Acoustic Streaming . . . 75
3.5.2 Turbulence . . . 77
3.6 Converting thermaocoustic energy into electrical power . . . 78
3.6.1 Electromagnetic transducers . . . 79
3.6.2 Piezoelectric transducers . . . 82
3.6.3 Magnetohydrodynamic transducers . . . 83
3.6.4 Bi-directional turbines . . . 83
3.7 DeltaEC software for simulation of thermaocoustic engines . . . 84
3.8 Concluding remarks . . . 87

4 Optimisation and experimental investigation of a single regenerator travelling wave thermoacoustic system 88
4.1 Introduction . . . 88
4.2 Simplified model . . . 89
4.3 Simulation of the system . . . 93
4.3.1 The geometrical parameters of the system . . . 95
4.3.2 The operational parameters of the system . . . 97
4.3.3 DeltaEC results for the acoustic's key parameters . . . 100
4.4 Experimental investigations and validation . . . 105
4.4.1 Lab device, design and construction . . . 105
4.4.2 Measuring instruments . . . 113
4.4.3 Results and discussion . . . 116

4.4.4 Comments on uncertainty in the experimental results 126
4.5 Concluding remarks 127

5 A novel asymmetric heating method for a two-stage travelling wave thermoacoustic electricity generator 129
5.1 Introduction 129
5.2 Design concept of the current system 130
5.3 DeltaEC modelling 132
5.3.1 DeltaEC results and discussion 134
5.4 Experimental Apparatus 145
5.4.1 Principle of operation 152
5.4.2 Data acquisition (DAQ) system 153
5.4.3 Measurement of the acoustic power 156
5.4.4 Experimental results and validation 157
5.5 Concluding remarks 164

6 Optimisation of the regenerators of a double core thermoacoustic engine with asymmetric heat inputs 166
6.1 Introduction 166
6.2 Principle of the regenerator 168
6.3 The double core thermoacoustic engine 169
6.4 Optimisation of the two regenerators 170
6.4.1 Acoustic amplification within the regenerators 171
6.4.2 Acoustic dissipation 175
6.4.3 Temperature profile across the regenerator 185
6.4.4 Extracting of electrical power 194
6.5 Concluding remarks 196

7 Conclusions and recommendations for future work 198
7.1 Conclusion 198
7.1.1 Statement of the project's aim and objectives 198
7.1.2 Level of attainment of the objectives 199
7.1.3 Contribution of the thesis 203
7.2 Recommendation for future research 204

A DeltaEC calculations 206
A.1 Physical segments 206
A.1.1 DUCT 206
A.1.2 HX 207
A.1.3 STKSCREEN 208

A.1.4 STKDUCT 209
A.1.5 IESPEAKER 210
A.1.6 BRANCH 211
A.1.7 JOIN 211
A.2 The thermoviscous function and its spatial average 212
A.3 The correlations for the thermal properties factor 213

B Supplementary data for Chapter 4 **214**
B.1 DeltaEC model of the single core thermoacoustic system 214
B.2 Calibration certificate for the pressure transducers 220

C Supplementary data for Chapter 5 **222**
C.1 Detailed drawings of the double core thermoacoustic system 222
C.2 DeltaEC output file for evenly heated twin-core system 230

D Supplementary data for Chapter 6 **239**
D.1 DeltaEC output file for optimised regenerators system 239

Bibliography **250**

LIST OF FIGURES

1.1 A photograph showing South-Sudanese women preparing food over an open fire. 2

1.2 A photograph to show a portable locally-manufactured charcoal stove used by a South-Sudanese woman. This stove has a very short lifespan, typically of less than two months because of corrosion. 2

1.3 Schematic diagram to illustrate an early conceptual design of a two-stage thermoacoustic engine (TAE) integrated with a biomass cooking stove. The TAE system, the feedback loop, and the linear alternator all represent the thermoacoustic engine. The stove hobs, the chimney, and the combustion chamber are parts of the biomass stove (Chen et al. 2012). 4

1.4 A photograph of the thermoacoustic stove built by SCORE and tested at the University of Nottingham. The stove demonstrated a maximum of 12.6 W electricity from 2.5 kW heat from burning wood (Riley 2014*b*). 4

1.5 Block diagram describes the main elements of the thesis and showing the work outcomes from each part. 9

2.1 One form of apparatus for producing a singing flame. Here: S represents the length of the fuel line, L is the distance of the flame into the combustion tube (Putnam and Dennis 1956). 10

2.2 Illustration of the Sondhauss tube (Sondhauss 1850). 11

2.3 Rijke tube resonator (Rijke 1859). 12

2.4 Early thermoacoustic refrigerator of Gifford and Longsworth's achieved a temperature ratio $\mathbf{T_C/T_H \simeq 0.5}$ at 1 Hz operating frequency, and a pressure ratio $\mathbf{p_h/p_l \simeq 4}$. T_C and T_H are cold and hot temperatures, respectively, p_h and p_l represent high and low pressures, respectively (Gifford and Longsworth 1966). 13

2.5 Ceperley's travelling wave thermoacoustic engine. As shown, a travelling wave propagates across a regenerator from the cold side to the hot side, producing acoustic power. Ceperley's engine performs better than the singing pipe which uses a different type of heat exchanger called a "stack" (Ceperley 1979). 15

2.6 Schematic diagram of the first practical travelling wave thermoacoustic engine with toroidal configuration. T_H and T_c indicate the temperatures of the hot and cold heat exchangers, respectively. P is a small partition that blocked the resonance tube. x_n represents the coordinate along the loop normalized by the the total length of the loop. A number of small pressure sensors are distributed in different locations around the loop. A laser Doppler velocimetry (LDV) is used for velocity measurements (Yazaki et al. 1998). 16

2.7 Bakhaus-Swift's thermoacoustic Stirling engine and its loop. (a) Photograph of the device. (b) Details of the main components of the torus-shaped section, where it has a thermoacoustic core consists of a regenerator in between hot and cold heat exchangers, jet pump, a flow straightener, a compliance, a feedback inertance, and a resonator. Thermal insulation is provided by having a thermal buffer tube after the engine core, between the hot heat exchanger and the secondary heat exchanger. The cold heat exchangers are of the shell-and-tube type with helium gas inside the tubes and the water in the shell. The locations of the temperature and pressure sensors are indicated by T and P, and the flow of the acoustic power around the loop is shown by $\dot{W}$. (c) Lumped-element model of the engine used to simulate the acoustic components into electrical circuits (Backhaus and Swift 1999). 17

2.8 The cascade thermoacoustic engine. (a) A schematic diagram shows the entire system starting from top to bottom. The system comprises the upper resonator, the pressure housing where the cascade engine locates, the lower resonator, and load components. (b) A detailed view showing the components of the three stages of the cascade engine. The 1^{st} stage is a standing-wave engine comprises an ambient heat exchanger AHX, a stack S, a hot heat exchanger HHX, a thermal buffer tube TBT, and two flow straighteners FS; the 2^{nd} and 3^{rd} stages are travelling-wave engines and both have the same parts of the 1^{st} stage except the stack which is replaced by a regenerator R. A legend is included at the top of the figure to illustrate all the components as well as the sensors used to evaluate the performance of the cascade engine (Gardner and Swift 2003). 19

2.9 Kees De Blok's travelling wave engine with bypass pipes configuration. As it is indicated in the schematic, the engine comprises a cold heat exchanger CHX, a regenerator, a hot heat exchanger HHX, a bypass channel, and a resonator (De Blok and Van Rijt 2001). 21

2.10 Thermoacoustic Stirling heat engine with a pressure wave generator. The generation of the pressure wave achieves via two solid displacers. T_c is used to indicate the temperature of the ambient heat exchangers, and T_h is the temperature of the hot heat exchanger (Sugita et al. 2004). 21

2.11 Al-Kayiem's Looped-tube travelling-wave thermoacoustic engine with a RC load and a side-branched volume. (a) Photo of the rig. (b) Schematic diagram of the system where: AHX is the ambient heat exchanger, REG the regenerator, HHX the hot heat exchanger, TBT thermal buffer tube, SAHX secondary ambient heat exchanger (Al-Kayiem and Yu 2017). 23

2.12 Blok's travelling wave engine with hybrid configuration. (a) Photo of the engine. (b) The layout of the device which shows the bypass channel combined with the feedback torus loop. There are two engine stages and each of them has a fixed positioned regenerator clamped between a hot heat exchanger and a cold heat exchanger [Adapted from (De Blok 2008)]. 25

2.13 Blok's four stage travelling wave power converter. (a) Photo of the prototype. (b) The layout of the device which shows the engine stages and the direction of the heat flow from and into each of them and the wave propagation within the loop (De Blok 2010). 26

2.14 A schematic drawing of the travelling wave thermoacoustic engine together with the analogous lumped-element electrical circuit diagram. The main thermodynamic and acoustic components are: (a) An ambient heat exchanger. (b) A regenerator. (c) A hot heat exchanger. (d) and (f) Are two flow straighteners. (e) A thermal buffer tube. (g) An alternator. (h) An inertance tube. (i) A compliance volume. (j) A jet pump. *T* and *P* symbols represent the locations of the temperature and pressure sensors, respectively. The equivalent electrical circuit consists of two resistors *R* and *Ra*, two inductors *L* and *La*, and a capacitor *C*. More details can be found in (Backhaus, Tward and Petach 2004). 28

2.15 The thermoacoustic power converter TAPC. (a) Photo of the system showing the location of the thermoacoustic core and the two alternator (A and B). (b) The layout of the device includes: A compliance, a single TA core, a thermal buffer tube, an inertance tube, two alternators A and B (Telesz 2006). 29

2.16 Blok's four-stage travelling wave engine. (a) Experimental set-up of the flat four-stage travelling wave thermoacoustic engine. As seen, a spiralized water tube is used instead of the water tank. (b) Schematic diagram where only one acoustic feedback loop with a linear alternator is drawn (the feedback pipe connects stage 4 and stage 1. The regenerator, the upper and lower plates are also shown for the first engine stage (De Blok 2010). 30

2.17 Schematic diagram of the tested prototype showing the main system components and the measurements location used to evaluate the system performance. The acoustic and thermodynamic components include: a cold heat exchanger, a regenerator, a hot heat exchanger, a second ambient heat exchanger, an alternator, and a stub. P and T are used to show the location of pressure sensor and temperature sensors, respectively (Yu, Jaworski and Backhaus 2010*b*). 31

2.18 The looped tube travelling wave thermoacoustic engine coupled with ultra-compliant alternator. (a) A photo of the system where the main system components are: a cold heat exchanger CHX, a regenerator, a hot heat exchanger HHX, a thermal buffer tube TBT, an alternator, a stub, and a feedback pipe. (b) Schematic diagram including the equivalent acoustic circuit which developed using electrical analogy. Further details are available in (Yu, Jaworski and Backhaus 2012). . . 32

2.19 General configuration of the propane-driven thermoacoustic generator. (a) Photo of the system shows the integration of the thermoacoustic engine with the cooker. (b) The schematic diagram where the main components of the system are illustrated. The system has two thermoacoustic cores, two tuning stubs, a feedback loop, and a linear alternator. Each core comprises an ambient heat exchanger AHX, a regenerator, a hot heat exchanger HHX, and a secondary ambient heat exchanger (Chen et al. 2012). 34

2.20 Photograph of the air-filled travelling wave thermoacoustic engine integrated with a wood-burning cooking stove (Chen et al. 2012). . . 34

2.21 The single stage travelling wave thermoacoustic electricity generator. design considered for the hot heat exchangers. (a) Photo of the system showing the components of the travelling wave unit, the alternator, the matching stub, the feedback pipe, the stove, and the chimney. (b) Schematic illustration of the generator which includes the location of the measurements used to assess the performance. T/Cs are thermocouples, $P1$ to $P5$ are pressure sensors (Abdoulla-Latiwish, Mao and Jaworski 2017). 35

2.22 Schematic diagram of Wu's travelling wave thermoacoustic electricity generator showing the engine parts: A primary cold heat exchanger, a regenerator, a heater block, a thermal buffer tube, a secondary cold heat exchanger, a feedback pipe, a resonance tube, and a linear alternator (Wu et al. 2011). 36
2.23 Wu's Solar-powered travelling wave thermoacoustic electricity generator. (a) Photo of the entire system. (b) Schematic representation of the thermoacoustic loop, the linear alternator and the heat receiver with a sectional view. The generator consists of: 1. main ambient heat exchanger, 2. regenerator, 3. heater block, 4. thermal buffer tube, 5. secondary ambient heat exchanger, 6. feedback loop, 7. linear alternator, and 8. heat receiver (Wu et al. 2012). 37
2.24 (a) The four-stage 100 kW thermoacoustic power generator (TAP). (b) The flue gas exhaust $(3m \times 3m)$ with half-way the high temperature circuit heat exchanger (De Blok and Systemen 2012). 38
2.25 Schematic presentation of the travelling wave thermoacoustic engine which comprises a vibration-balanced pair of moving-magnet linear alternators. The main system components are shown by the legend at the top of the schematic, and the symbol p is used to indicate a pressure sensor (Sun et al. 2013). 39
2.26 Configuration of a travelling wave thermoacoustic electricity generator coupled with a dual-opposed linear alternator for acoustoelectric power conversion. The generator has one core comprising a main heat exchanger, a regenerator, a heater block, a thermal buffer tube, and a secondary ambient heat exchanger (Wu et al. 2014*b*). 40
2.27 The double-acting thermoacoustic Stirling electricity generator DATASEG. The arrows indicate the distances between the engines. (a) The experimental set up which includes three thermoacoustic Stirling heat engines and three linear alternators. (b) Schematic diagram where the main parts of each engine are appears (Wu et al. 2014*a*). . 40
2.28 The travelling wave thermoacoustic electric generator. (a) Photograph of the torus. (b) Schematic diagram where the main components are shown: a main ambient heat exchanger MAHX, a regenerator REG, a hot heat exchanger HHX, a thermal buffer tube TBT, a secondary ambient heat exchanger 2AHX, a feedback tube, linear alternators, and a resonator (Wang et al. 2015). 42

2.29 The two-stage travelling wave thermoacoustic electricity generator. (a) Photograph of the engine reported in the study where the two thermoacoustic engines TAE1 and TAE2, the two alternators, the ball valve BV, and the stub are shown. (b) Schematic diagram of the prototype shows details of the system components and the locations of the measurement instruments. Each thermoacoustic engine consists of a main ambient heat exchanger MAHE, a regenerator Reg, a hot heat exchanger HHE, a thermal buffer tube TBT, and a secondary ambient heat exchanger SAHE. Letters T and P are to denote the temperature and pressure readings, respectively (Kang et al. 2015). 43

2.30 The impact of the rotation angle of the ball valve on the electricity output from alternator 1 $W_{e,1}$, alternator 2 $W_{e,2}$, and the total electricity output W_{total} in the two-stage travelling wave thermoacoustic engine. (Kang et al. 2015). 44

2.31 Travelling wave thermoacoustic electricity generator with a pair of linear alternators attached via bypass configuration. (a) Photograph of engine where only a part of the resonator is appeared, and only linear alternator 2 is shown. (b) Schematic diagram of travelling wave thermoacoustic electricity generator and the equivalent electric circuit network. P_1 to P_5 denote the location of the pressure sensors. T_h is the heater temperature, T_{a1} and T_{a2} are the temperatures of the inlet and the outlet of chilling water into the main ambient heat exchanger. The coils of the linear alternators are in a series connection with a variable electric load to extract the electricity W_1 which was monitored by a power meter. Details of the electrical circuit network can be found in (Wang et al. 2016). 45

2.32 The travelling wave thermoacoustic heat engine TWTAHE. (a) A photograph of the system TWTAHE units, the alternators, and the resonance tubes. (b) Schematic diagram showing details of one engine as follows: a main ambient heat exchanger MAHX, a regenerator REG, a heater Block HB, a thermal buffer tube TBT, a secondary ambient heat exchanger SAHX. Each linear alternator formed by these elements: The winding, the moving magnet, and the piston. R and C denote the resistance and the compliance of the alternator. The elastic membrane only added in the second engine (Bi et al. 2017). 46

2.33 Schematic illustration of the four stages thermoacoustic Stirling power generator, where the components of the system are shown: each stage has thermoacoustic core, a linear alternator and a resonator. Each core consists of compliance tube, ambient heat exchanger, regenerator, hot heat exchanger, thermal buffer tube and a secondary ambient heat exchanger. The three modes used to coupled the alternator to the engine stages are also illustrates with coloured arrows. A key is provided in the middle of the diagram (Wang and Qiu 2017). 48

2.34 DeltaEC results for the electrical power output, W_e, and the corresponding relative Carnot efficiency, η_e, as a function of the loud resistance of the alternator, R_e, when three different coupling modes of the alternators were utilized: hot-end, middle, and cold-end (Wang and Qiu 2017). 48

2.35 DeltaEC results for the electrical power output, W_e, and the corresponding relative Carnot efficiency, η_e, of the four staged thermoacoustic Stirling power generator, when the position of the regenerator was changed by varying the length of the compliance tube (CT) in the range of 0.07 to 0.17 m. (a) Electrical power output as a function of the load resistance of the alternator R_e. (b) Relative Carnot efficiency as a function R_e. (c) Relative Carnot efficiency as a function of the electrical power W_e (Wang and Qiu 2017). 49

3.1 Illustration of the two major types of heat engines, the prime mover and the heat pump. The word "Engine" in the central circle is used generally to include both types of heat engines. Q denotes heat, c and h are cold and hot, T for temperature, and Q is for work. 53

3.2 Pressure and velocity as a function of time, t, in a gas through which a travelling wave exists. As illustrated, the gas undergoes a thermodynamic cycle of four processes: compression, heating, expansion, and cooling, which is the same as what occurs in the Stirling engine (Ceperley 1979). 54

3.3 Pressure and velocity as a function of time, t, for a gas in which a standing wave propagates exists. As illustrated, compression and heating of the gas are simultaneous, expansion and cooling also happen simultaneously (Ceperley 1979). 54

3.4 P-V diagram of the ideal Brayton cycle. As presented, the cycle comprises four processes: 1-2 is adiabatic compression, 2-3 is addition of heat at constant pressure, 3-4 is adiabatic expansion, and 4-1 is heat rejection at constant pressure. 55

3.5 P-V diagram of the ideal Stirling cycle where the numbers are corresponding to the thermodynamic processes of the cycle: 1-2 is isothermal expansion, 2-3 is heat removal at constant volume, 3-4 is isothermal compression, and 4-1 is heat addition at constant volume. 55
3.6 The thermoacoustic effect within a standing wave thermoacoustic system. (a) Schematic drawing of the system where the main components are shown. (b) An enlarged view to show the thermoacoustic effect on a single gas parcel in the stack during "standing wave" displacement towards the cold side. 57
3.7 The thermoacoustic effect in standing wave thermoacoustic engine. (a) Temperature T versus position x of stack and temperature versus position and time for a gas parcel within a standing wave thermoacoustic engine. The ellipse illustrates the change in the temperature of the gas parcel, while the dotted line presents the temperature gradient across the stack ΔT which is the difference between the hot side and cold side temperatures T_h and T_c, respectively. (b) P-V diagram, where dq is the heat transfer, and dW is the work done. 58
3.8 Temperature gradient created along the stack plates as a result of the bucket-brigade effect. As seen with colors, the gas parcel is heated (red) when it is in close contact with a high-temperature plate and is cooled (blue) when the parcel in direct contact with a plate of a temperature lower than the gas. Consequently, the acoustic wave get amplified [adapted from (Avent and Bowen 2015)]. 59
3.9 The thermodynamic cycle that one gas parcel undergoes during its oscillation within the regenerator in a travelling wave thermoacoustic engine. (a) P-V diagram of the cycle where the oval shape represents the travelling wave engine and the cycle numbered from 1 to 4 illustrates the Stirling cycle. (b) The thermodynamic processes undertaken by a fluid parcel during its travel from the cold side to the hot side. CHX is for cold heat exchanger, Reg. is regenerator, and HHX is for the hot heat exchanger [Adapted from (Yu, Backhaus and Jaworski 2009)]. . 61
3.10 Schematic of a thermoacoustic system showing some of the important length scales: The wavelength λ, the peak-to-peak displacement amplitude $2 \mid \xi_1 \mid$, the thermal and viscous penetration depths δ_κ and δ_ν, respectively. 65
3.11 A schematic presentation of a simple thermoacoustic engine showing the hot and cold heat exchangers, the stack, and the resonating tube. . 67

3.12 Spatial-average function f for several geometries, using r_h/δ_k on the horizontal axis yields f_k on the vertical axis, and using r_h/δ_ν yields f_ν (Swift 2003). 72
3.13 The four types of acoustic streaming that occur in thermoacoustic systems. (a) Gedeon acoustic streaming. (b) Rayleigh acoustic streaming. (c) Jet-driven acoustic streaming. (d) Acoustic streaming within a stack or a regenerator. Note: the arrows are used to indicate the time-average flow velocity (Swift 2000). 76
3.14 Boundary regime approximation of oscillatory flow, in smooth pipe of circular cross-section, as a function of peak Reynolds number, $|N_{R,1}|$, and the ratio of the pipe diameter to the viscous layer thickness, D/δ_ν (Swift 2017). 78
3.15 Overview of different mechanisms for the thermoacoustic energy into electrical power conversion. [Adapted from (Timmer, de Blok and van der Meer 2018)]. 79
3.16 Cross-section of the general purpose low-cost audio loudspeaker. The geometry shows that the motion, the magnetic field and the electric current are perpendicular. 80
3.17 The physical model of the loudspeaker (Yu et al. 2011). 81
3.18 Bi-directional turbine. (a) Illustration of the flow direction and the relative position of the rotor and the guide vanes in the turbine. (b) Schematic diagram showing the shape of the guide vanes and the rotor blade of a Wells turbine (Timmer, de Blok and van der Meer 2018). . 84

4.1 A labelled schematic of a single core thermoacoustic engine. AHX is the main ambient heat exchanger, Reg. the regenerator, HHX the hot heat exchanger, TBT the thermal buffer tube, SAHX the secondary ambient heat exchanger, L.S the loudspeaker, FB pipe is the feedback pipe. Locations labelled with P and T indicate where pressure and temperature are measured. 90
4.2 Simplified lumped-element model employed to examine the most important physical parts of the single core thermoacoustic electricity generator. A graph code key is provided on the right-hand side of the graph. 91
4.3 DeltaEC modelling procedure used to simulate a single-regenerator thermoacoustic electricity generator. This procedure is applicable to any looped-tube thermoacoustic system with a power extractor. 94

4.4 Schematic illustration of the DeltaEC segments used to develop a model for the single core thermoacoustic electricity generator. The dotted blue box shows the thermoacoustic core. The simulation starts at the top of the TA core ($x = 0$). 97
4.5 Axial distribution of the pressure amplitude of the gas throughout the engine. 101
4.6 Axial distribution of the volumetric velocity amplitude of the gas throughout the engine. 102
4.7 Axial distribution of the absolute acoustic impedance along the engine. 103
4.8 Axial distribution of the phase angle difference between the pressure and the volumetric velocity of oscillation along the engine. 104
4.9 Axial distribution of the acoustic power along the engine. 105
4.10 A general testing outline of the single core thermoacoustic electricity generator showing the main components: (a) The thermoacoustic (TA) core, (b) The loudspeaker, and (c) the cooling water pipes, feedback pipe and the tuning stub. 106
4.11 Photographs of the ambient heat exchanger. (a) The radiator with two holes drilled for the water inlet and outlet. (b) Assembly of the radiator and the upper housing. 107
4.12 Photographs of the regenerator mesh in the thermoacoustic engine unit. (a) The rectangular hole drilled for the mesh layers. (b) The Stainless Steel mesh layers after being stacked together. 109
4.13 Convoluted hot heat exchanger of the single thermoacoustic engine. (a) The convolutions. (b) The convolution after being bolted to the lower housing. (c) Back view of the HHX with a completed insulated lower housing unit. (d) Top view of the convoluted HHX and the lower housing.110
4.14 Photograph of the loudspeaker used to extract the electrical power from the acoustic power. 112
4.15 Photograph of the standards PVC pipes and fittings used to assemble part of the feedback pipe. 113
4.16 Schematic diagram of the experimental apparatus of the single core thermoacoustic electricity generator. The dotted arrows of solid circle ends indicate the temperature measurements, while the ones of solid rhombus ends are to show the pressure measurements. The letter P is to note the location of the pressure sensors. 115
4.17 SCORE software, the oscilloscope, and the power analyser during the operation of the single core thermoacoustic system. 115

4.18 The absolute pressure sensors mounted to the feedback pipe to measure the acoustic power throughout the looped-tube single regenerator thermoacoustic engine. 116
4.19 Performance characterisation of a single regenerator thermoacoustic engine: Electrical power output at four levels of heating power, when the load resistance is varied. (e) Denotes experimental data, and (s) for simulated ones. 117
4.20 Performance characterisation of a single regenerator thermoacoustic engine: Thermal-to-electrical efficiency at four levels of heating power, when the load resistance is varied. (e) Denotes experimental data, and (s) for simulated ones. 118
4.21 The computational peak stroke of the alternator against the load resistance.119
4.22 Current of the alternator against the load resistance for different heating input power. (e) Denotes experimental data, and (s) for simulated ones. 120
4.23 The numerical pressure amplitude against the load resistance of the alternator for different heating input power. 121
4.24 The numerical volumetric velocity amplitude against the load resistance of the alternator for different heating input power. 121
4.25 The numerical pressure drop across the alternator's diaphragm against the load resistance for different heating input power. 122
4.26 DeltaEC results of the pressure drop across the alternator diaphragm when the length of the stub branch varied between 45 and 70 cm. . . . 123
4.27 Experimental results and DeltaEC results of the electrical power output and the thermal-to-electrical efficiency when the length of the stub branch varied between 45 and 70 cm. 124
4.28 DeltaEC results of the local acoustic impedance in the regenerator, the phase angle in the regenerator, and the phase angle in the feedback pipe as a function of the stub length. 125

5.1 Functional diagram of the double core thermoacoustic electricity generator showing the components, the locations of the two cores within the loop, the starting point of the simulation $x = 0$, and the measurements taken to estimate the performance (pressure P and temperature T). A key is provided on the right side of the graph to show the name of the different system components. 132

5.2 Schematic illustration of the segments used to construct DeltaEC model for the double core thermoacoustic electricity generator. The amounts of heat added into the first and the second engines (HHX1 and HHX2) are Q_1 and Q_2, respectively, while the amount of electricity extracted by loudspeaker (IESPEAKER segment) is W_e. 133
5.3 Power flow diagram for the double core thermoacoustic electricity generator. 134
5.4 The variation of the peak pressure amplitude through the loop using different percentages of the total heat input. Numbers in the graph correspond to that in Figure 5.1: 1 is the regenerator of stage 2, 2 is the loudspeaker, 3 is the regenerator of stage 1 and 4 is the feedback pipe. 135
5.5 The variation of the peak volumetric velocity amplitude through the loop using different percentages of the total heat input. Numbers in the graph correspond to that in Figure 5.1: 1 is the regenerator of stage 2, 3 is the regenerator of stage 1, 4 is the feedback pipe, 5 is stub 2, 6 is stub 1.136
5.6 The variation of the acoustic impedance through the loop using different percentages of the total heat input. Numbers in the graph correspond to that in Figure 5.1: 1 is the regenerator of stage 2, 2 is the loudspeaker, 3 is the regenerator of stage 1, 4 is the feedback pipe, 5 is stub 2, 6 is stub 1.137
5.7 The variation of the phase angle through the loop using different percentages of the total heat input. Numbers in the graph correspond to that in Figure 5.1: 1 is the regenerator of stage 2, 2 is the loudspeaker, 3 is the regenerator of stage 1, 4 is the feedback pipe, 5 is stub 2, 6 is stub 1.138
5.8 The variation of the acoustic power through the loop using different percentages of the total heat input. Numbers in the graph correspond to that in Figure 5.1: 1 is the regenerator of stage 2, 2 is the loudspeaker, 3 is the regenerator of stage 1, 4 is the feedback pipe. 139
5.9 Loop acoustic power relation with the temperature difference across the regenerator when different heat percentages are used to add a total heating power range of 2.1 to 3 kW into the system. 140
5.10 Dependences of the acoustic power, and the electric power on the percentage of the heating power into the second engine, when a total heating power of 2.5 kW is added into the system. 141
5.11 Photo of the double core thermoacoustic electricity generator shows the location of the engines, the heater block, the alternator (L.A), the feedback pipe, one of the thermal buffer tubes (TBT2) and the cooling water pipes. 146

5.12 The design considered for the hot heat exchangers. (a) The dimensions of the convolutions. (b) The two hot heat exchangers after being bolted to the engine frame. 147
5.13 The electrical heaters used to supply the heat into the double core thermoacoustic electricity generator. (a) Schematic of the engine shows the location of the heater and the assembly of the heating elements. (b) Photo of the heating elements after being installed. 148
5.14 Microscopic view for the Stainless Steel mesh used to build the regenerators of the two thermoacoustic cores. (1) is the pitch, (2) is the diameter of the wire, and (3) is the width. 149
5.15 Photo of the locations of the pressure and the temperature sensors in the two cores of the current thermoacoustic system. 154
5.16 The double core thermoacoustic engine and the measuring instrumentations. (a) Schematic illustration for for the connection of the pressure and temperature sensors with the cDAQ. (b) Photo of the system while measurements are recorded. 155
5.17 Measurement of the acoustic power flows in the thermoacoustic feedback pipe. (a) The arrangement of the differential and the absolute pressure transducer in the thermoacoustic pipe. (b) Photo for the transducers after being mounted on the thermoacoustic pipe. 157
5.18 Measurement results of the performance of the double core thermoacoutsic electricity generator shows the mean pressure P_m, the amount of heat rejection Q_w, and the temperature difference across the regenerator $T_H - T_C$ as a function of time, with air at atmospheric pressure condition. 158
5.19 Experimental data for the peak pressure amplitude and the acoustic power as a function of time, when air at atmospheric pressure is used and a total heat input of 2.5 kW is evenly distributed between the two electrical heaters. 159
5.20 The loop acoustic power as a function of the heat input percentage, when a total heat input power range of 2.1 - 3 kW is added into the thermoacoustic system. 160
5.21 The harvested electrical power as a function of the heat input percentage, when the total heat input range of 2.1 - 3 kW is supplied into the thermoacoustic system. 161
5.22 The effect of the heat input percentage on the thermal-to-acoustic efficiency, considering a total heat input power range of 2.1 - 3 kW. . . . 163
5.23 The effect of the heat input percentage on the thermal-to-electrical efficiency, using a total heat input power range of 2.1 - 3 kW. 164

6.1 Numerical calculations of the change in the gain factor, g, in regenerator 1 of the dual core thermoacoustic electricity generator, when the length of the regenerator is varied in the range of 12-32 mm, and the hydraulic radius is also changed in the range of 86 - 260 μm. (a) The real part of the gain $Re[g]$. (b) The imaginary part of the gain $Im[g]$. 173
6.2 Numerical calculations of the change in the gain factor, g, in regenerator 2 of the dual core thermoacoustic electricity generator, when the length of the regenerator is varied in the range of 12-32 mm, and the hydraulic radius is also changed in the range of 86 - 260 μm. (a) The real part of the gain $Re[g]$. (b) The imaginary part of the gain $Im[g]$. 174
6.3 The simulated pressure amplitude, $|p_1|$, in the regenerators of the double core thermoacoustic electricity generator when the length of the mesh is varied in the range of 12-32 mm, and the hydraulic radius is changed in the range of 86 - 260 μm. (a) At regenerator 1. (b) At regenerator 2. 176
6.4 Numerical calculations of the thermal-relaxation dissipation components resulting from variation of the lengths and the hydraulic radii of the regenerators of the double core system. The length of each regenerator is varied in the range of 12-32 mm, while the hydraulic radius is varied in the range of 86-260 μm. (a) At regenerator 1. (b) At regenerator 2. 177
6.5 The simulated volumetric velocity $|U_1|$ in the regenerators of the double core thermoacoustic electricity generator when the length of the mesh is varied in the range of 12 - 32 mm, and the hydraulic radius is changed in the range of 86 - 260 μm. (a) At regenerator 1. (b) At regenerator 2. 179
6.6 Numerical calculations of the viscous dissipation components, $P_{vis.}$, resulted from variation of the lengths and the hydraulic radii of the regenerators of the double core thermoacoustic electricity generator. The length of each regenerator is varied in the range of 12-32 mm, while the hydraulic radius is varied in the range of 86-260 μm. (a) At regenerator 1. (b) At regenerator 2. 180
6.7 DeltaEC calculations of the impedance enhancement factor, n, at the cold end of the regenerators of the dual core thermoacoustic electricity generator, when the length of the regenerator is varied in the range of 12-32 mm, and the hydraulic radius is also changed in the range of 86 - 260 μm. (a) Conditions through regenerator 1. (b) Conditions through regenerator 2. 183

6.8 DeltaEC results of pressure drop, ΔP_1, across the regenerators of the double core thermoacoustic electricity generator when the length of the regenerator is varied in the range of 12-32 mm, and the hydraulic radius is changed in the range of 86 - 260 μm. (a) Values of Δp_1 at regenerator 1. (b) Values of Δp_1 at regenerator 2. 184
6.9 DeltaEC simulation results showing the temperature difference between the hot and cold ends of the regenerators of the double core thermoacoustic electricity generator when the length of each regenerator is changed between 12 to 32 mm, and the hydraulic radius is adjusted as 180 μm. (a) Data of regenerator 1. (b) Data of regenerator 2. 186
6.10 The relationship between the temperature difference along the regenerators of the dual core thermoacoustic electricity generator and Lautrec number *NL* as a result of varying the hydraulic radius of the pore in the range 86 - 260 μm, for length's range of 12-32 mm. (a) conditions at regenerator 1. (b) Conditions at regenerator 2. 187
6.11 The numerical results of the acoustic power flowing within the thermoacoustic loop of the double core engine when the lengths and hydraulic radii of the two regenerators are varied in the ranges 12 - 32 mm, and 86 - 260 μm, respectively. 189
6.12 The numerical results of the optimal loop acoustic power $P_{Ac.}$ produced from the double core thermoacoustic electricity generator. (a) As a function of the regenerator's length *L*. (b) As a function of the regenerator's hydraulic radius r_h. 190
6.13 Contour plot of the effect of Lautrec number, *NL*, and the regenerator length, *L*, on the acoustic power produced from the double core thermoacoustic electricity generator system. 191
6.14 The numerical results of the loop acoustic power of the double core thermoacoustic electricity generator for selected range of length: 12 - 32 mm, and hydraulic radii: 86 - 260 μm. 193
6.15 Contour plot of the effect of $\omega\tau$, and the regenerator length, *L*, on the acoustoelectric energy conversion of the double core thermoacoustic electricity generator. 194
6.16 The numerical results of the electricity extracted from the double core thermoacoustic engine when the lengths and hydraulic radii of the two regenerators are varied in the ranges 12 - 32 mm, and 86 - 260 μm, respectively. 195

LIST OF TABLES

2.1 Summary of the work done so far in electricity generation using thermoacoustic technology. 50

4.1 Design parameters of the single-stage thermoacoustic engine. 97
4.2 Electrical and mechanical parameters of the loudspeaker. 100
4.3 Comparison between the simulation and the lab measurements. 125

5.1 Performance of the two regenerators at several ratios of the thermal power. 137
5.2 Summary of DeltaEC results of the double core thermoacoustic electricity generator when the heat is being distributed into the two heaters with different ratios. 144
5.3 Specification of the regenerator mesh used in the current design. . . . 149
5.4 Design parameters of the components of the double core thermoacoustic electricity generator. 151
5.5 Specification of electromechanical parameters of the loudspeaker. . . 152
5.6 Summary of the measurements used to evaluate the performance of the current thermoacoustic system. 154

6.1 Optimal loop acoustic power and the coressponding Lautrec number *NL* for the different lengths of the regenerator. 191
6.2 Summary of DeltaEC simulation of the double core thermoacoustic electricity generator after optimisation of the two regenerators. 196

NOMENCLATURE

Roman Symbols

A	Area, m^2	108
a	Speed of sound, m/sec	62
B	Magnetic field, Tesla	81
b	A constant or function	170
C	Capacitor	46
C	Compliance, m^3/Pa	93
C	Thermal capacity, J/K	192
c	A constant or function	170
c_p	Isobaric heat capacity per unit mass, J/kg.K	63
D	Diameter, m	108
e	2.71828...	170
$\dot{E}$	Acoustic power, W	66
F	A function	86
f	Frequency, Hz	62
f	Spatially averaged thermoviscous function	71
G	Heat transfer between the gas and the solid material, W/K	192
$\dot{H}$	Rate at which total energy flows also known as total power, W	74

h	Enthalpy per unit mass, J/kg	73
h	Heat transfer coefficient per unit area, W/m^2.K	192
h	Thermoviscous function	71
I	Electric current, Amp	92
I	Power intensity, W/m^2	66
i	$\sqrt{-1}$	66
K	Stiffness of the suspension system, N/m	81
k	Thermal conductivity, W/m.K	63
k	Wave number, m^{-1}	103
L	Electrical inductance, Henry	81
L	Inertance, kg/m^4	93
L	Length, m	68
l	Thickness, m	108
M	Mass, kg	81
$\dot{m}$	Mass flow rate, kg/sec	150
NL	Lautrec number	188
$N_{R,1}$	Reynolds number	77
NR_1	Reynolds number	170
n	Impedance enhancement factor	142
n	Number of thermoacoustic stages	147
n	Number of wires	108
P	Partition	16
P	Power, W	81

p	Pressure, Pa	57
Q	Quality factor of resonance	100
q	Heat per unit mass, J/kg	56
R	Electric resistance, Ohm	81
R	Gas constant, J/kg.K	62
R	Resistance, Ohm	48
R	Resistor	46
r	Acoustic resistance per unit length, Pa.sec/m^4	169
r	Radius, m	108
s	Entropy per unit mass, J/kg.K	68
T	Temperature, K	62
t	Time, sec	66
U	Volumetric velocity, m^3/sec	66
u	Velocity amplitude of the working gas, m/sec	64
u	Velocity of the alternator's coil, m/sec	98
V	Volume, m^3	57
v	Y component of velocity, m/sec	69
W	Power, W	44
W	Work, J	56
w	Z component of velocity, m/sec	69
X	Electric reactance, Ohm	92
x	Coordinate along sound-propagation direction, m	16
y	Coordinate perpendicular to wave-propagation direction, m	68

y_0 Half of the plate spacing, m 108

Z Acoustic impedance, Pa.s/m^3 92

z Coordinate perpendicular to wave-propagation direction, m ... 68

z Specific acoustic impedance, kg/m^2.sec 102

Greek Symbols

α Thermal diffusivity, m^2/s 63

β Thermal expansion coefficient, K$^-$1 75

Δ Big difference 56

δ Penetration depth, m 59

ξ Half of the peak to peak displacement, m 56

ε The internal energy per unit mass, J/kg 73

ε Surface roughness 86

η Efficiency 18

γ Ratio of isobaric to isochoric specific heats 62

ι Transduction coefficient, Nt/Amp = Volt/(m/s) 92

κ Adiabatic bulk modulus, Pa 103

λ Wavelength, m 62

μ Dynamic viscosity, kg/m.sec 63

ν Kinematic viscosity, m^2/s 63

Π Perimeter, m 108

ϕ Phase angle, $^\circ$ 66

ϕ Volumetric porosity 108

π 3.14159 64

σ	Prandtl number	63
ρ	Density, kg/m^3	62
σ‘	Viscous stress tensor, Pa	73
τ	Amplification factor	91
τ	Thermal relaxation time	192
θ	Phase angle	171
ω	Angular frequency, sec^{-1}	64
δ	Penetration depth, m	64
ξ	Displacement amplitude of the gas parcel in x-direction, m	64

Subscripts

Ac.	Acoustic	56
Carn.	Carnot	67
C	Cold	62
$T, diss.$	Thermal dissipation	168
e	Electrical	44
1	First engine	134
1	First order	64
g	Generation	168
h	Hydraulic	108
H	Hot	62
L	Load	81
m	Mean	62
m	Mechanical	81

max.	Maximum	81
n	Normalized	16
R,Ac.	Relative Carnot efficiency of the acoustic power	150
s	Solid	66
2	Second engine	134
T	Total	134
κ	Thermal	59
total	Total	44
v	Viscous	64
vis.	Viscous dissipation	168
w	Water	150
w	Wire	108

Acronyms

Alt.	Alternator	122
BV	Ball valve	43
cDAQ	Compact data acquisition	116
CHP	Combined heat powered system	130
CHX	Cold heat exchanger	61
CT	Compliance tube	48
DATASEG	Double-acting thermoacoustic Stirling electricity generator	40
DeltaEC	Design environment for low-amplitude thermoacoustic Energy Conversion	6
DR	Drive ratio	66
FB	Feedback	90

HB	Heater block	46
HHX	Hot heat exchanger	61
L.S	Loudspeaker	90
LDV	Laser Doppler velocimetry	16
L.A	Linear alternator	48
NI	National instruments corporation	116
OWC	Oscillating water columns	83
PFC	Piezoelectric fibre composite	82
PID	Proportional integral derivative	110
PSWR	Pressure standing wave ratio	135
PVC	Polyvinyl chloride	24
PVDF	Polyvinylidene fluoride	82
PZT	Zirconate titanate	82
RC	Resistance-compliance acoustic load	24
REG	Regenerator	24
Reg.	Regenerator	61
RPN	Reverse polish notation	97
2AHX	Secondary ambient heat exchanger	48
SAHX	Secondary ambient heat exchanger	24
SCORE	Stove for Cooking Refrigeration and Electricity	3
SWG	Standard wire gauge	110
TAE	Thermoacoustic engine	43
TAP	Thermoacoustic power generator	38

TASHE	Thermoacoustic Stirling heat engine	17
TA	Thermoacoustic	97
TBT	Thermal buffer tube	24
T/C	Thermocouple	35
TWTAEG	Travelling wave thermoacoustic electricity generator	36
TWTAHE	Travelling wave thermoacoustic heat engine	46
USB	Universal serial bus	116

Other Symbols

$\langle\ \rangle$	Spatial average perpendicular to x	71
$\|\ \|$	Magnitude of a complex number	64
overline	Time average	74
$Re[\ ]$	Real part of a complex number	66
$\sim$	Complex conjugate	66

CHAPTER 1

INTRODUCTION

1.1 Research motivation

A recently developed country, South Sudan, has an estimated population of 8.26 million. South Sudan is the least electrified country, and it has been severely influenced by decades of conflict. Access to the national grid is at less than 1% due to the reduced level of power generation as well as the weak distribution network. Even those who have an electricity supply face frequent power cuts due to shortages and irregular maintenance of the power units resulting from the economic situation of the country. Energy deficiency has profoundly affected both the service and social sectors. Furthermore, shortages in the fuel supply have further diminished food security, and 47% are food-deprived (Dagne 2012). On the other hand, approximately 50% of the South Sudan population rely on firewood for lighting, while more than 27% still live in the dark with no lighting facilities. Likewise, nearly 97% of the population of South Sudan rely on firewood, charcoal, and kerosene for their cooking activities, which can cause severe medical issues. The cooking method mostly used by South-Sudanese people is the traditional three-stone fire as displayed in Figure 1.1. However, in some areas, a charcoal stove (Figure 1.2) is much more accessible.



Figure 1.1: A photograph showing South-Sudanese women preparing food over an open fire.



Figure 1.2: A photograph to show a portable locally-manufactured charcoal stove used by a South-Sudanese woman. This stove has a very short lifespan, typically of less than two months because of corrosion.

In addition to the adverse health effects related to indoor air pollution, gathering firewood for cooking and heating purposes requires travelling long distances. This job is mainly done by South-Sudanese women and children, which puts women in particular at risk of gender-based violence. Due to all these issues, the development of South Sudan without access to electricity is still only a dream. Therefore, efficiently inexpensive electricity-generating stoves may help them combat health problems associated with the combustion of charcoal and firewood in addition to their functionality as electricity generators. Furthermore, these low-cost energy-generating stoves could be beneficial to cut down the amount of poverty in the countries of interest. Also, they could become a viable solution to prevent deforestation and environmental degradation, not only for the country of interest, but also for all rural communities around the world. Efficiently designed cooking stoves are desirable to enable rural households to save time and money for activities that can generate income, or can be directed instead towards education activity.

1.2 SCORE Consortium

The SCORE (**S**tove for **Co**oking **R**efrigeration and **E**lectricity) consortium was established in 2007 (The University of Nottingham 2007). It was managed by the University of Nottingham and worked with Practical Action to develop clean, efficient cooking stoves that could provide electricity to rural communities that are not connected to the electrical power grid. At the initial stages of the project, the SCORE team has considered several technologies for generating electricity such as steam engines, integrated solar stoves, thermoelectric systems, Stirling engines, and thermoacoustic devices. An assessment of these technologies carried out in 2014 (Riley 2014*a*) has identified that thermoacoustics integrated into a stove is more cost-effective than most other electrical generation technologies except hydroelectricity, although the decreasing cost and increasing efficiency of solar power in recent years has brought the latter back into contention (Shahsavari and Akbari 2018*a*; Shahsavari and Akbari 2018*b*). Additionally, thermoacoustic systems were adopted for other several reasons, such as their flexibility in using heat source, their ability to operate with inert gasses as their working fluid, and their simplicity, since they have fewer moving components which facilitates the manufacturing and maintenance processes.

Thermoacoustic systems are based on the thermoacoustic effect, which generates acoustic energy when a fluid interacts with a solid thermodynamic media via its thermoacoustic core. The thermoacoustic core consists of a section of porous media in between ambient and hot heat exchangers. The expansion and contraction of the air between these heat exchangers causes pressure fluctuations. These pressure fluctuations propagate around the loop to return to the heat exchangers. If the pressure fluctuations return in phase, a strong acoustic field can be generated. An alternator can be used to harvest these oscillations to produce electrical current. The power generated from these thermoacoustic systems can be utilized to offer lighting and mobile charging facilities, and enable international connection via TVs and small radio sets.
Figure 1.3 shows schematic illustration of a thermoacoustic engine integrated with a cooking stove, while Figure 1.4 displays one of the thermoacoustic stove developed by the SCORE.
In addition to the electricity generators (Abdoulla-Latiwish, Mao and Jaworski 2017; Ehsan et al. 2015; Chen et al. 2013, Yu, Jaworski and Backhaus 2010*b*), the SCORE team has done related research in the development of coolers and refrigerators based on thermoacoustic technology (Saechan and Jaworski 2018).

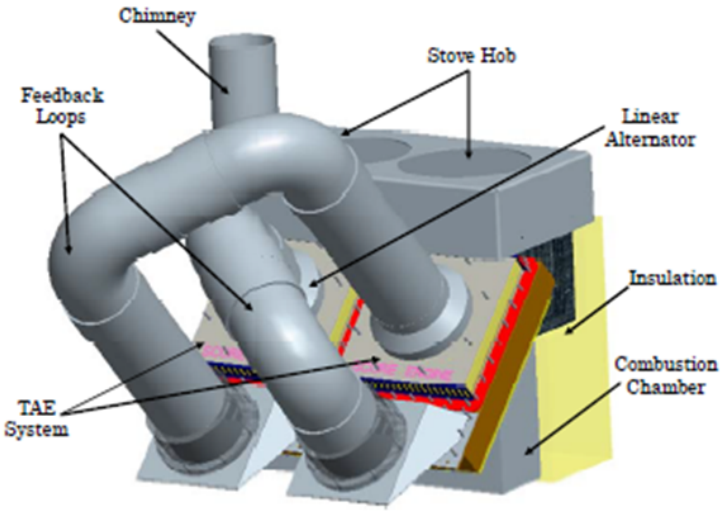


Figure 1.3: Schematic diagram to illustrate an early conceptual design of a two-stage thermoacoustic engine (TAE) integrated with a biomass cooking stove. The TAE system, the feedback loop, and the linear alternator all represent the thermoacoustic engine. The stove hobs, the chimney, and the combustion chamber are parts of the biomass stove (Chen et al. 2012).



Figure 1.4: A photograph of the thermoacoustic stove built by SCORE and tested at the University of Nottingham. The stove demonstrated a maximum of 12.6 W electricity from 2.5 kW heat from burning wood (Riley 2014*b*).

1.3 Problem statement

In the preliminary stage of the SCORE project, social science research (Sanchez, Owala and Okello 2012; Sanchez, Dennis and Pullen 2013) of selected rural communities has been established to meet local communities requirements; such as their cooking habits, energy needs, etc. The outcomes of these studies reflected that there is a clear need for developing such devices since approximately 3 billion people in remote areas worldwide rely on biomass fires for cooking. Additionally, in many societies, the cooking activities are done indoors within a dwelling with the smoke swirling around the house. The cooking time of two meals was found to be nearly five hours every day and, therefore, smoke inhalation becomes a severe health hazard. Likewise, nearly 2 billion lack access to electricity, which affects education, health care, and other critical services in those areas. Furthermore, the social studies have revealed that the electrical power rating of an ideal power generating stove in the developing world should target a range of electrical power output of 20 - 100 W, with a manufacturing cost that should ideally not exceed 200 pounds (Sanchez et al. 2012).
On the other hand, some studies for other remote communities pointed out that even a modest electricity output within the range of 15 to 20 W per rural dwelling could have a massive impact on the lives of people living in poverty all around the world by providing some essential needs such as lighting. Delivery of these Watts of electricity as a secondary product from a firewood cooking process would therefore be of immense advantage from the social perspective. Besides, there is no efficiency limitation for such technologies because the waste heat produced from cooking activities isn't otherwise utilised.

To make the thermoacoustic technology a viable alternative, several researchers around the world have developed a range of variations (Kruse et al. 2017; Piccolo 2018; Yang et al. 2019). However, neither SCORE nor other inventors have managed to reach more than 20 W electricity using air-filled thermoacoustic systems.

1.4 Aim and objectives

The current research aims to improve the performance of the air-filled thermoacoustic engine developed earlier by the SCORE team, and therefore, to meet the original 20 - 100 W electrical power target. The target is the people of the country of South Sudan. However, benefits are extendible so as to include all remote areas of the developing world. The SCORE experimental investigations indicated that a maximum electricity output of 12.6 W with 0.5% thermal-to-electrical efficiency can be gained from their double stage looped-tube travelling wave thermoacoustic engine utilising air at atmospheric pressure as the working gas (Chen et al. 2013). The other goals are to

maximize the acoustic amplification within the engine's core and minimize the acoustic dissipations without adding new parts or additional cost.

The initial stage of the current research involves comprehensive revision of the functionality of the SCORE systems, with extra efforts being devoted to the single core engine as well as the dual-core engine. A series of numerical optimizations, as well as experimental investigations, will be performed to look for ways to maximise the power output while maintaining the cost. All the parametric studies of the thermoacoustic performance will be conducted with the help of the widely used simulation software DeltaEC (Design environment for low-amplitude thermoacoustic Energy Conversion). The software will allow a deeper physical understanding of the wave performance throughout the different system components. Also, it will allow the exploration of the merits of alternative configurations before the system is tested.
One of the issues encountered with the experimental investigations carried out by SCORE is the repeatability (Riley 2014*b*) where the reason behind that couldn't be identified. Through the use of a simulation tool, however, the user will be able to understand the behaviour of all the system components and counteract the complexity of such a system, and determine any inconsistencies. The specific objectives needed to achieve the research aims can be broken down as follows:

1. To understand the thermoacoustic effect, acoustoelectric concept, and thermoacoustic modelling using DeltaEC software.
2. To consequently develop a modelling procedure and construct an optimised model for the single core looped-tube thermoacoustic electricity generator to mimic the wave performance.
3. To investigate, in particular, on the effect of the load resistance of the loudspeaker on the acoustoelectric conversion.
4. To investigate the effect of the stub branch pipe on the acoustic field, and prove it functions in minimizing the disturbance in the field as a result of the existence of the loudspeaker.
5. To experimentally test the single core thermoacoustic engine with the same conditions applied in the theoretical simulation.
6. To validate the numerical models against the experimental results and analyse the application of a single-core system for electricity production.
7. To perform numerical modelling of the double-core looped tube thermoacoustic electricity generator built by SCORE (Riley 2014*b*) based on the modelling procedure used for the single core system.

8. To investigate a new operational technique of the double-core engine numerically by supplying the heating power into the two cores using unevenly amounts.
9. To numerically demonstrate a potential of enhanced performance of the double core engine using the suggested novel operational technique with no additional cost.
10. To test the experimental apparatus of the double-core thermoacoustic electricity generator to find the optimum conditions, and therefore, to confirm the results obtained theoretically. The novelty is to prove the validity of the suggested operational technique.
11. To further optimise the regenerator units of the double-core thermoacoustic electricity generator for the maximum acoustic output.
12. To evaluate the thermoacoustic and thermoelectric performance of the optimised double-core thermoacoustic system, and compare the findings with those achieved previously by SCORE.

1.5 Thesis outlines

The overall structure of this thesis consists of seven chapters, including this introductory chapter. A brief introduction and concluding remarks are provided in some chapters. In this section, a chapter-by-chapter overview of the contents is presented.

- **Chapter 1** discusses the lack of electrical power supply and healthy cooking in rural areas all around the globe, considering South Sudan as a case study for the technology application. The chapter also gives an overview of the topic by providing the preface of the SCORE project and its development on thermoacoustic electricity generators. This is followed by a background on the research. All these serve as the backbone of the motivation behind this research, which will be conducted experimentally and numerically using the powerful thermoacoustic software DeltaEC.

- **Chapter 2** provides the theoretical background of thermoacoustic systems, including the types of thermoacoustic systems, and the principles of thermoacoustics that are essential for the development and operation of thermoacoustic systems. This is followed by discussing scale lengths that are crucial to the thermoacoustic performance. The linear thermoacoustic theory, together with Rott's approximation, is also discussed in great detail. Additionally, acoustic streaming and turbulence effects in oscillatory flow are also included. The

conversion of acoustic power into electricity is provided. Finally, modelling of thermoacoustic systems with DeltaEC software is given.

- **Chapter 3** includes a comprehensive overview of thermoacoustics. It starts by explaining the thermoacoustic effect along with advances in thermoacoustic engines. A recent advance in thermoacoustic technology for waste heat recovery and electricity generation is also provided in this chapter.

- **Chapter 4** describes the numerical and experimental investigation of a single core thermoacoustic engine in a looped tube arrangement. For this system, the analogy between the acoustic components and A/C electric circuit is developed. This provides a physical understanding of the operation of the thermoacoustic system, and allows DeltaEC to accurately simulate the system by estimating the values of the guesses needed to meet the targets. The development of the DeltaEC model of the engine is also described along with the performance of the acoustic wave through the system components. Following this, the experimental apparatus is described along with the measuring devices as well as the experimental procedure. Finally, a verification of the experimental data against simulation ones is given.

- **Chapter 5** focuses on a two-stage travelling wave thermoacoustic electricity generator in a looped tube configuration, with new operational methodology. A DeltaEC model is developed for the thermoacoustic generator, and then the laboratory device is shown with the measurement instrumentations needed to evaluate the viability of the suggested operational technique. Finally, validation results are provided.

- **Chapter 6** considers the regenerator part. Numerical optimization of the two regenerators of a dual-core travelling wave thermoacoustic electricity generator is performed. Results and discussion of the optimization procedure are provided including analysis of acoustic amplification, acoustic dissipations, temperature profile, and harvesting of electrical power.

- **Chapter 7** discusses the conclusions drawn from this research, including this research's contribution to the thermoacoustic field and provides proposals for future development.

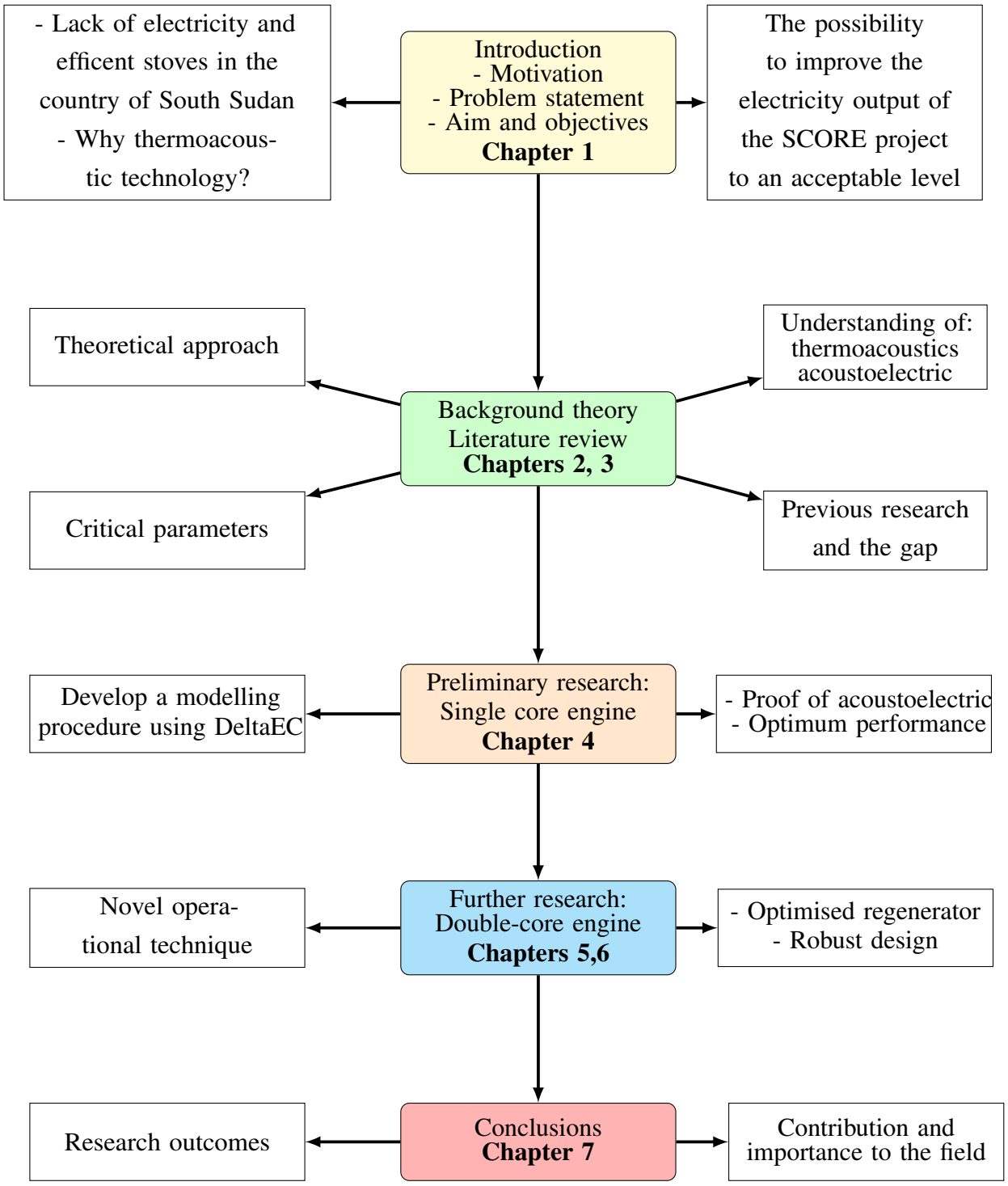


Figure 1.5: Block diagram describes the main elements of the thesis and showing the work outcomes from each part.

CHAPTER 2

HISTORICAL PERSPECTIVE OF THERMOACOUSTICS

2.1 Overview of thermoacoustics and thermoacoustic effect

The thermoacoustic phenomenon has been observed independently for more than two hundred years since glass blowers recognized that when a hot glass bulb placed at the end of a cold glass pipe, the tip of the pipe would emit sound. The first combustion driven oscillations (also named as the singing flame) were recognized by Byron Higgins as early as 1777. Higgins noticed that when a hydrogen diffusion flame placed at certain lengths inside a vertical tube opened at both sides as shown in Figure 2.1, oscillations occasionally occurred and the sound heard (Higgins 1802).

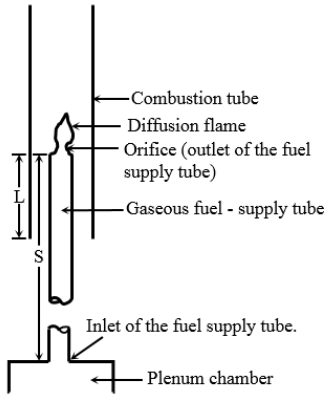


Figure 2.1: One form of apparatus for producing a singing flame. Here: S represents the length of the fuel line, L is the distance of the flame into the combustion tube (Putnam and Dennis 1956).

The tone had a frequency correlated to one of the longitudinal sound modes of the pipe. The existence of the "singing", the mode order, and the amplitude of oscillation all depend on different parameters such as the flow rate of the fuel, the properties of the fuel, and the configuration of the fuel line (Putnam and Dennis 1956).
Carl Sondhauss investigated the thermoacoustic effect in a different way to the previous studies. In their research, a glass tube (later named a Sondhauss tube) that was opened at one end and closed at another was tested by attaching a glass bulb to the closed end as shown in Figure 2.2. Carl discovered that when the glass bulb exposes to a gas flame, the temperature at the closed side of the tube increases, and as a result, sound oscillation is beginning to emit from the open side until the bulb cools (Sondhauss 1850).

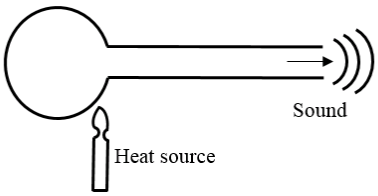


Figure 2.2: Illustration of the Sondhauss tube (Sondhauss 1850).

In the meantime, another example of the singing flame was the Rijke tube found by Rijke (1859). He qualitatively analysed the strong acoustic oscillation that occurred as a result of placing a heated wire gauze inside an open-ended upright glass tube. The glass tube as shown in Figure 2.3 was 35 mm in diameter and 80 cm in length with the wire 20 cm away from the bottom end. Heat was supplied through a spirit lamp and, when the wire gauze glowed red, the heat supply was stopped. The air which was passing up through the hot wire screen was heated and expanded. As a result, an oscillating pressure wave in the form of sound was emitted from the open top end for several seconds until the gauze cooled down.
The acoustic oscillation associated with the Rijke tube and Sondhauss tube was studied extensively by means of theoretical investigations and experimental tests (Feldman Jr 1968*a*). The most important note is that the Sondhauss tube doesn't need a convection flow to sustain the acoustic oscillation.

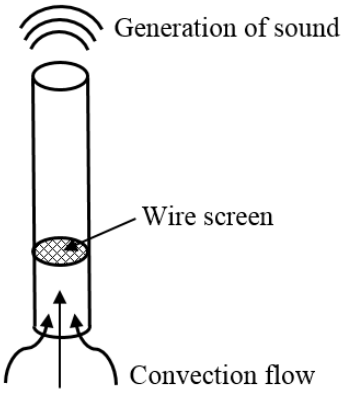


Figure 2.3: Rijke tube resonator (Rijke 1859).

A large version of Rijke tube was developed by Lord (1945) to explain the thermoacoustic pressure oscillations. Rayleigh understood that the acoustic oscillations occur in a channel that has a temperature gradient along its end, and this could lead to the generation of acoustic power. Rayleigh's criteria is stated as:

"If heat be given to the air at the moment of greatest compression, or be taken from it at the moment of greatest rarefaction, the vibration is encouraged. On the other hand, if heat be given at the moment of greatest rarefaction, or abstracted at the moment of greatest condensation, the vibration is discouraged" (Lord 1945).

Although Rayleigh's criterion has been widely recognised as an explanation of sustaining the thermoacoustic pressure oscillations, the criterion didn't explain the start-up of the oscillation and didn't provide any mathematical treatment.

A later realization of thermoacoustic oscillation was made by Taconis et al. (1949). They recognized the effect "named as Taconis waves" when the end of a gas-filled glass tube was inserted in a liquid at cryogenic temperatures producing a singing sound, the same as Rijke's device, consequent to its removal and after warming to the ambient temperature.
Gifford and Longsworth (1966) also encountered thermoacoustic phenomena in a device called a pulse-tube refrigerator as shown in Figure 2.4. In this device, part of the tube was fitted using a set of Stirling-type regenerator plates to develop locally isothermal processes along their length, while the other part of the tube was left empty. Pulses were generated at the regenerator end of the tube by switching between high and low pressure gas containers at a fast rate of 1 Hz. They expressed the phenomenon as:

"If any closed chamber is pressurized and de-pressurized by delivery and exhaustion of gas from one point on its surface and the flow is essentially smooth, heat pumping will occur away from the point on its surface" (Gifford and Longsworth 1966).

This resulted from changes in the temperature that associated with the pressure changes in the working gas, and their phase difference relative to the oscillating gas flow.

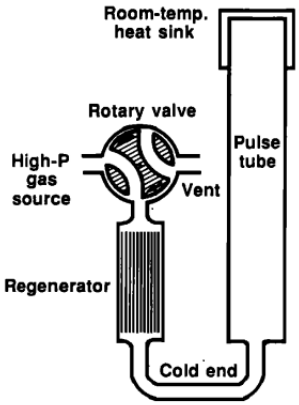


Figure 2.4: Early thermoacoustic refrigerator of Gifford and Longsworth's achieved a temperature ratio $\mathbf{T_C/T_H \simeq 0.5}$ at 1 Hz operating frequency, and a pressure ratio $\mathbf{p_h/p_l \simeq 4}$. T_C and T_H are cold and hot temperatures, respectively, p_h and p_l represent high and low pressures, respectively (Gifford and Longsworth 1966).

Although investigations and observations of the thermoacoustic pressure and temperature oscillations were quite abundant through the mid-20^{th} century, they are considered only as scientific demonstrations that are capable of producing a loud sound.

Carter, White, and Stelle made great efforts to improve the Sondhauss tube (Feldman Jr 1968*b*). They suggested that the thermoacoustic effect can be enhanced by having a better heat transfer between the working gas and the solid wall. Accordingly, small glass tubes were layered into a bundle named as a stack and placed inside the Sondhauss tube. The stack has since been described as having precisely spaced parallel plates through which the sound wave propagates. Following that, hot and cold heat exchangers are attached at both sides of the stack to obtain a large temperature gradient and to investigate the feasibility of producing acoustic power.

Bell Laboratories came up with two inventions of singing pipes (Hartley 1951; Marrison 1958). The two patents considered a concept of using thermoacoustic phenomena to generate electrical power by converting heat into acoustic power via a thermoacoustic engine and then extracting electricity from the acoustic energy using an electrodynamic transducer. Although the concept was very encouraging in its attempt to deliver electricity from heat energy and the suggested devices were attractive because of their simplicity, it was inapplicable due to the weak oscillating waves which degraded the thermoacoustic conversion efficiency.

Nickolass Rott analysed the Taconis waves and Sondhauss tubes and published in a series of papers the governing equations of thermoacoustics (Rott and Zouzoulas 1976;

Tijani, Zeegers and De Waele 2002) which established the theoretical thermoacoustics, named later as "linear thermoacoustic theory". These publications contributed to the understanding of thermoacoustic phenomena and were considered as a standard theory in the field of thermoacoustics. Mathematical expressions to describe the acoustic oscillations of the working gas in a channel with an axial temperature gradient and with a lateral channel dimension to allow thermal interaction between gas parcels and solid wall were developed and explained well.
Using the linear thermoacoustic theory allows prediction of the performance of a thermoacoustic system under low-pressure amplitude of oscillation. However, the accuracy of the predictions obtained from the linear theory, compared to the measurements, substantially reduces at high-pressure amplitudes of the acoustic oscillation. Underestimations in the thermoacoustic performance may be as a result of the non-linear effects, minor losses, turbulence, or acoustic streaming arising in the thermoacoustic system.

The theoretical thermoacoustic was established firstly for thermally generated acoustic oscillations. Later, Swift (1988*b*) reviewed the theory of thermoacoustics, and explained in a number of published articles and a textbook (Swift 2003) how Rott's theory can be expanded and also applied to build efficient thermoacoustic refrigerators.

Subsequently, a significant development in thermoacoustic theory was introduced by Los Almos National Lab. They developed a software named DeltaEC (**D**esign **e**nvironment for **l**ow-amplitude **t**hermo**a**coustic **E**nergy **C**onversion) to implement the linear thermoacoustic theory to design practical thermoacoustic systems, to achieve the desired levels of performance. Nowadays, DeltaEC is broadly applied to design, analyse, and predict the performance of thermoacoustic systems (Ward, Clark and Swift 2008).
Independently, P. Merkli and H. Thomann from the Swiss Federal Institute of Technology worked out an extended acoustic theory (Merkli and Thomann 1975*a*). The theory concentrated on the amplitudes outside the shock region. The most striking result was that cooling takes place in the section of the tube of the highest dissipation (velocity anti-nodes) as a result of friction, and heating occurs in the part of the tube with the minimum velocity amplitude. Also, it is noted that these effects depend strongly on the Prandtl number. The results were verified against the experimental data, and they showed good agreements. Although their extended acoustic theory was not valid for proper resonance conditions, it provided an insight into what can be expected when the laminar flow is assumed, and non-linear effects are dominated.

2.2 Thermoacoustic technology based on the thermoacoustic effect

The most important breakthrough occurred when Ceperley compared the thermoacoustic effect with the Stirling engine in his published article about a piston-less Stirling engine (Ceperley 1979; 1985). Ceperley was the first one who noted that the thermoacoustic conversion efficiency could be further improved by using a porous medium (regenerator) as in Figure 2.5 to allow for propagation of a travelling wave instead of a standing wave. One reason for the efficiency enhancement is that a standing wave results from a constructive interference between two travelling waves, thus the pressure and velocity amplitudes of oscillation can be approximately double the amplitudes in the initial travelling wave propagated along the system, which increases the dissipated acoustic power.

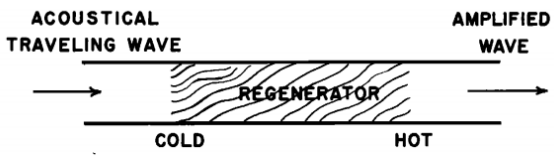


Figure 2.5: Ceperley's travelling wave thermoacoustic engine. As shown, a travelling wave propagates across a regenerator from the cold side to the hot side, producing acoustic power. Ceperley's engine performs better than the singing pipe which uses a different type of heat exchanger called a "stack" (Ceperley 1979).

He also recognized that when the wave propagates from the cold side to the hot side of the regenerator, the interaction between the working gas and the adjacent solid material undergoes a Stirling-like thermodynamic cycle (Callen 1985), where the gas particles experience contraction during the displacement toward the high temperature and expansion during the displacement toward the low temperature. Hence, Rayleigh criterion can be met by achieving the correct time-phasing between the pressure and the velocity, while the efficiencies are boosted by the implementation of a reversible thermodynamic cycle.

Since this discovery, interest in thermoacoustics and its applications has spread worldwide. Significant work has been devoted to improve the performance of thermoacoustic systems as well as improving efficiency by developing a precise methodology to design and construct such efficient functional devices and, more fundamentally, extending thermoacoustic theory beyond the linear limit. Yazaki et al. (1998) used the travelling wave concept to design the first practical regenerator-based thermoacoustic engine, using a novel feedback mechanism. The feedback was arranged as a loop of a uniform diameter to overcome the zero acoustic power

generation in travelling wave mode faced by Ceperley (1985). The device is shown schematically in Figure 2.6. It consisted of a core made from one stack in between two heat exchangers. Air at atmospheric pressure selected as the working gas and the device operated at 268 Hz frequency. The results proved that spontaneous gas oscillations were running throughout the thermoacoustic loop from the cold side to the hot side of the engine as travelling waves. The device functioned as a travelling wave engine because the phase difference between the oscillating pressure and the volumetric velocity was almost zero. Accordingly, a stack and a pair of heat exchangers in a toroidal configuration consider as a travelling wave engine.

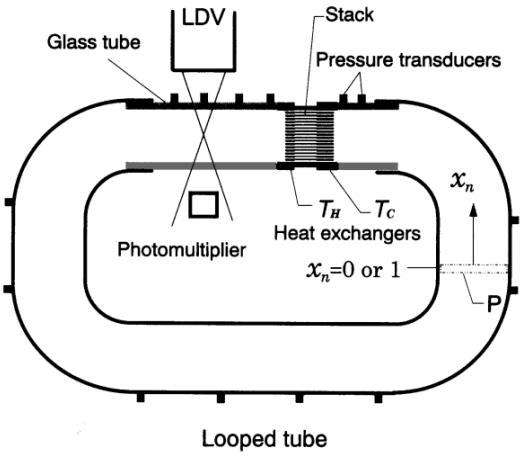


Figure 2.6: Schematic diagram of the first practical travelling wave thermoacoustic engine with toroidal configuration. T_H and T_c indicate the temperatures of the hot and cold heat exchangers, respectively. P is a small partition that blocked the resonance tube. x_n represents the coordinate along the loop normalized by the the total length of the loop. A number of small pressure sensors are distributed in different locations around the loop. A laser Doppler velocimetry (LDV) is used for velocity measurements (Yazaki et al. 1998).

Viscous dissipations recognized during the experimental tests, and they attributed to the low acoustic impedance within the engine core which caused by the high acoustic velocities in the regenerator and within the feedback loop. Viscous losses are a function of the acoustic velocity and can be mitigated by keeping the acoustic impedance high, particularly in the regenerator. This enables continuous pressure wave amplification while suppressing the viscous dissipations within the regenerator.

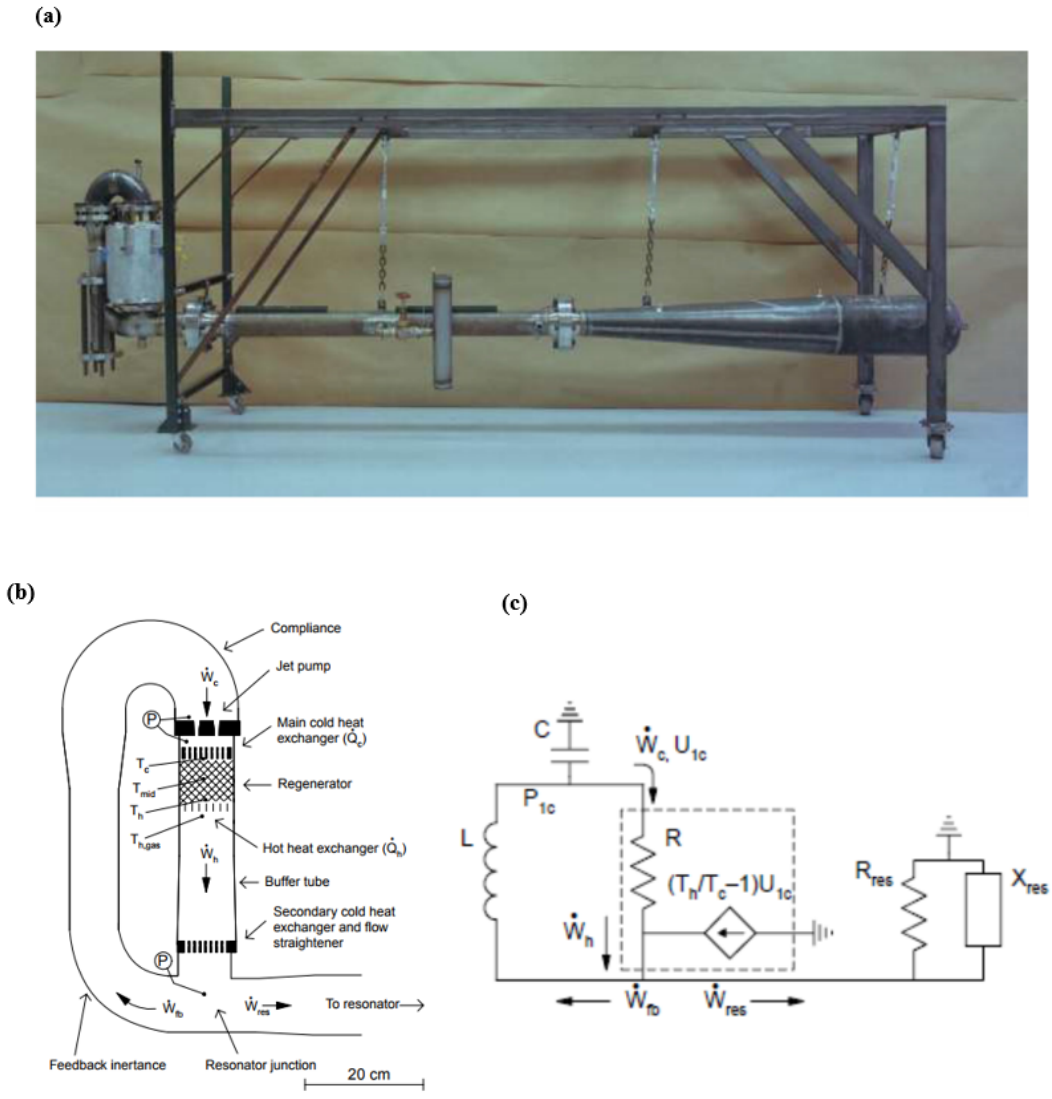


Figure 2.7: Bakhaus-Swift's thermoacoustic Stirling engine and its loop. (a) Photograph of the device. (b) Details of the main components of the torus-shaped section, where it has a thermoacoustic core consists of a regenerator in between hot and cold heat exchangers, jet pump, a flow straightener, a compliance, a feedback inertance, and a resonator. Thermal insulation is provided by having a thermal buffer tube after the engine core, between the hot heat exchanger and the secondary heat exchanger. The cold heat exchangers are of the shell-and-tube type with helium gas inside the tubes and the water in the shell. The locations of the temperature and pressure sensors are indicated by T and P, and the flow of the acoustic power around the loop is shown by $\dot{W}$. (c) Lumped-element model of the engine used to simulate the acoustic components into electrical circuits (Backhaus and Swift 1999).

Based on this and to enhance the thermoacoustic performance of the travelling wave thermoacoustic engine, Backhaus and Swift (1999) have made a major breakthrough which was the invention of the thermoacoustic Stirling heat engine (TASHE). The new invention, (Figure 2.7), is made from a short loop of a quarter wavelength. This loop was connected to a long standing wave resonating tube to improve the regenerator

impedance, and therefore, to control the non-linearity within the system.
Essentially, the torus (in the absence of the long resonator pipe) of Backhaus and Swift's travelling wave engine is considered as an acoustic version of the free-piston Stirling engine. The principal idea incorporated in this work was to simulate the free-piston Stirling engine utilizing a compact acoustic construction. The system operated at 80 Hz frequency and used helium at a mean pressure of 30 bar as the working gas. In the first set of results, the measured temperature at the middle of the regenerator didn't match the theoretically derived one. This was mainly because of non-linear effects i.e. Gedeon streaming and Rayleigh streaming. Therefore, much effort was made to improve engine performance and to reduce viscous dissipations. A compact acoustic configuration was adopted to minimize the acoustic losses and to achieve better acoustic impedance within the regenerator.
Also, as seen in Figure 2.7 (b), a large compliance bend and an inertance feedback were both added to the torus part of the engine to create a positive feedback such that the acoustic wave propagated into to the cold side of the regenerator with a zero time-phasing. This ensures excellent amplification of the travelling wave. The regenerator was positioned in the feedback loop where the acoustic impedance was inherently high because of its compact design. Moreover, a jet pump and a thermal buffer tube were introduced in the new design to suppress the acoustic streaming. The results showed that the maximum thermal efficiency of the system $\eta_{thermal-to-acoustic}$ is 0.3 which corresponds to 42% Carnot efficiency (Bejan 2016) where the hot temperature of the gas was $725^{\circ}C$ and occurred near a pressure ratio (defined as the ratio of the peak pressure to the mean pressure) $\frac{|p_1|}{p_m}$ of 0.06 (Backhaus and Swift 1999; 2000).

Gardner and Swift (2003) improved the performance of the TASHE by using a novel concept named as "cascade" thermoacoustic engine which was simpler to build. The cascade device comprised one standing wave stage and a two-stage travelling wave in a series connection and with a straight-line arrangement, as appears in Figure 2.8.
The working principle of the engine is that the two travelling wave engines are used to amplify the acoustic power generated from the standing wave engine. Above the standing wave stage, the upper section of the resonator is designed for minimum acoustic dissipation. Another unique feature is that the first stage thermal buffer tube has a taper angle design to eliminate Rayleigh streaming. Additionally, at the end of the thermal buffer tubes there are flow straighteners to prevent any possible jet-driven streaming.

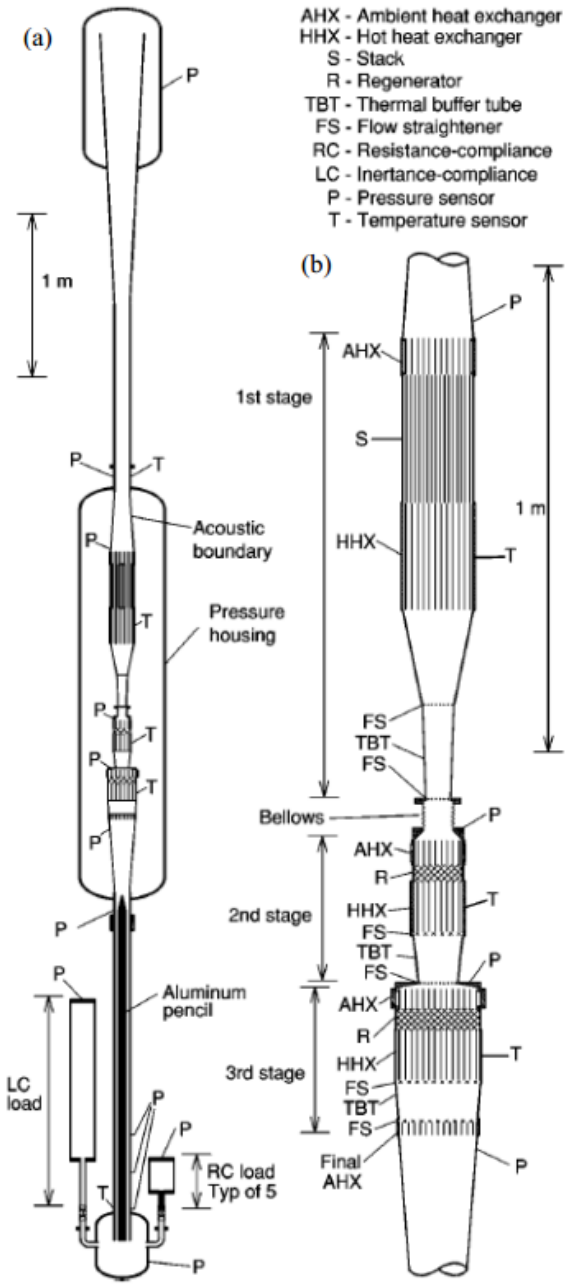


Figure 2.8: The cascade thermoacoustic engine. (a) A schematic diagram shows the entire system starting from top to bottom. The system comprises the upper resonator, the pressure housing where the cascade engine locates, the lower resonator, and load components. (b) A detailed view showing the components of the three stages of the cascade engine. The 1^{st} stage is a standing-wave engine comprises an ambient heat exchanger AHX, a stack S, a hot heat exchanger HHX, a thermal buffer tube TBT, and two flow straighteners FS; the 2^{nd} and 3^{rd} stages are travelling-wave engines and both have the same parts of the 1^{st} stage except the stack which is replaced by a regenerator R. A legend is included at the top of the figure to illustrate all the components as well as the sensors used to evaluate the performance of the cascade engine (Gardner and Swift 2003).

The efficiency of the system is enhanced due to the travelling wave engine stages. Running of the cascade engine delivered 2 kW of acoustic power with a thermal efficiency of 20% using argon as the working gas at a mean pressure of 2.33 MPa, and the engine operated at 60 Hz frequency. It is noticed that about one-third of the acoustic power generated from the first stage is lost in the upper section of the resonator. Also, the dissipation in the hot heat exchanger and flow straighteners below the last stage is higher than for the middle stage, because in the third stage these components were installed farther away from zero Rayleigh streaming and thus they experienced high acoustic velocities. The authors claim that efficiency can probably reach around 35-40% of Carnot's efficiency with further improvements.

2.2.1 Mechanisms to enhance the thermoacoustic conversion

Many research efforts have been made using different resonator geometries to reduce the power dissipation while maintaining the resonance (Sun et al. 2009; Zhou et al. 2008). It is recognised that the alternative forms of resonator tube can enhance the system performance in terms of the pressure amplitude of oscillation. One example to improve the performance and minimize the harmful parasitic losses is by using a technique that provides the resonance as well as directly extracting the acoustic power.

A new design concept for the travelling wave thermoacoustic engine was introduced by De Blok and Van Rijt (2001) who suggested utilizing bypass pipes as a feedback mechanism for the regenerator. The system is shown in Figure 2.9. He concluded that the location and size of the bypass pipes influence the time-phasing between the pressure and the velocity of oscillation. Furthermore, the bypass channels should be larger than the viscous depth in order to reduce the viscous dissipations. Also, the flow velocity in the channels should be kept slow, hence a larger diameter is required. The insights gained from Blok's research is that the bypass channels should be roughly 5% or more of the cross-sectional area of the regenerator.

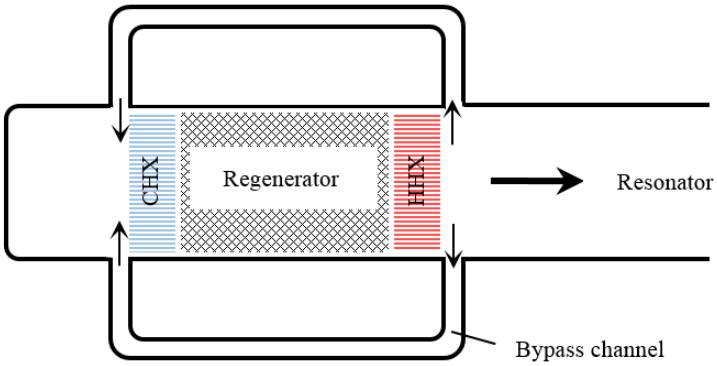


Figure 2.9: Kees De Blok's travelling wave engine with bypass pipes configuration. As it is indicated in the schematic, the engine comprises a cold heat exchanger CHX, a regenerator, a hot heat exchanger HHX, a bypass channel, and a resonator (De Blok and Van Rijt 2001).

An alternate design of the long resonator pipe in the TASHE was suggested by Sugita et al. (2004), as shown in Figure 2.10. The concept is to utilize solid displacers to act as an acoustic resonator instead of the commonly used long and heavy tubes. Despite its complicated design system, adding mechanical moving components to the engine helped to compact the entire system down. The experimental work verified that the solid displacers design is effective in suppressing non linear effects, and is also effective in increasing the pressure ratio. In their experiments, helium gas was supplied at a mean pressure of 1.5 MPa. The work amplification ratio obtained from this design was 1.6 with the maximum output of 22 W for the thermal input of approximately 260 W.

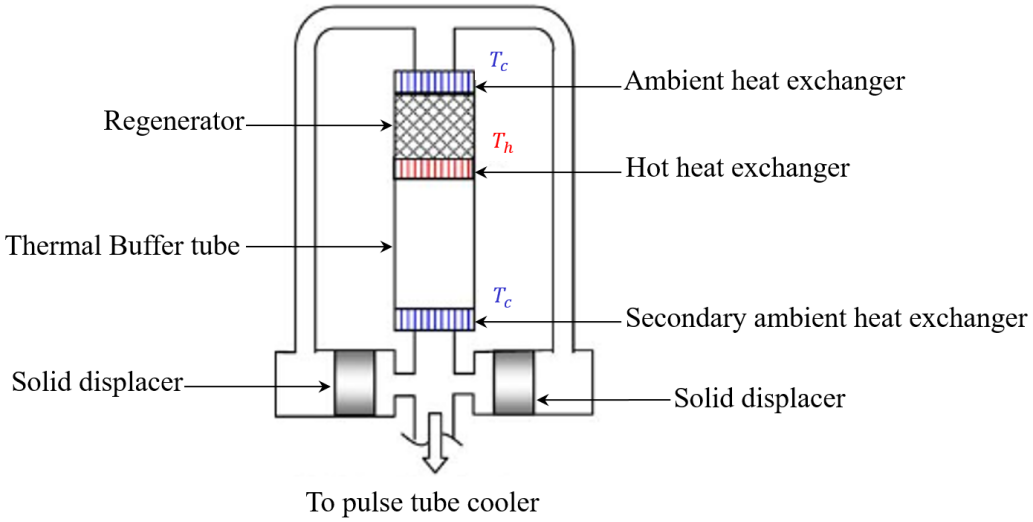


Figure 2.10: Thermoacoustic Stirling heat engine with a pressure wave generator. The generation of the pressure wave achieves via two solid displacers. T_c is used to indicate the temperature of the ambient heat exchangers, and T_h is the temperature of the hot heat exchanger (Sugita et al. 2004).

Luo et al. (2005) explored the potential of the thermoacoustic Stirling engine to achieve a higher pressure ratio (pressure ratio can be defined as the ratio of the maximum pressure amplitude in the system to the mean pressure). This investigation identified that the pressure ratio is limited because of the shock waves occurred in the resonator pipe. To overcome the creation of these shock waves, the resonator tube is tapered along its length. The surface area of the resonator tube is still large for viscous dissipation. The experiments showed that with 3 kW heating power and at an average pressure of 1.5 MPa, a high pressure ratio of 1.40 was achieved, which is very useful as a powerful driving source of thermoacoustic refrigerators or pulse tube cryocoolers. Furthermore, a relatively low onset temperature of 73 K was achieved, which confirms the feasibility of the engine for low heat recovery applications.

Yu et al. (2007) in their published work concluded that the high efficiency in thermoacoustic engines could be achieved by several new techniques. One method utilized an "inert" feedback loop (inertance tube) to bring the time-phasing between the oscillating pressure and the velocity to near zero in the regenerator. This adds positive feedback to the regenerator and, therefore, the self-oscillation is sustained. Another method uses an acoustic compact network which enables high acoustic impedance within the regenerator to suppress the viscous dissipation. One extra technique involves introducing a thermal buffer tube to separate the secondary cold heat exchanger from the hot heat exchanger and thus the parasitical heat losses can be minimised. Likewise, one can add a jet pump to a thermoacoustic system to suppress the Gedeon and Rayleigh streamings (DC flow) (Swift 2017). Lastly, the method used previously by Backhaus which suggested adding a long branch resonating tube of a quarter-wavelength to the torus. In comparison with the original one wavelength mode of the torus, this way provides the acoustic resonance to allow the system working at a moderate low frequency.
Low frequency reduces the total size and effective length of the acoustic network and thus minimizes the acoustic dissipation in a travelling wave loop. Moreover, standing wave components would be added to the system by the resonator tube and thus would correct the phase timing because of the thermal lag. As a result, the acoustic velocity can be reduced as well as the viscous dissipation. However, it should be pointed out that, the long standing wave resonator has pros and cons. Essentially, it is a Helmholtz resonator which dissipates much of the generated acoustic power due to its large surface, and this affects the maximum thermal efficiency that could be achieved from the system.

Most recently, Al-Kayiem and Yu (2017) considered a novel phase tuning technique in their looped tube travelling wave thermoacoustic engine. The concept proposed using a side-branched variable acoustic volume to tune the phase difference between the oscillating pressure and the acoustic velocity throughout the engine. In this study, comprehensive numerical investigations were executed using DeltaEC software to

capture the performance parameters of the system. Accordingly, the prototype was constructed and tested to demonstrate the function experimentally.

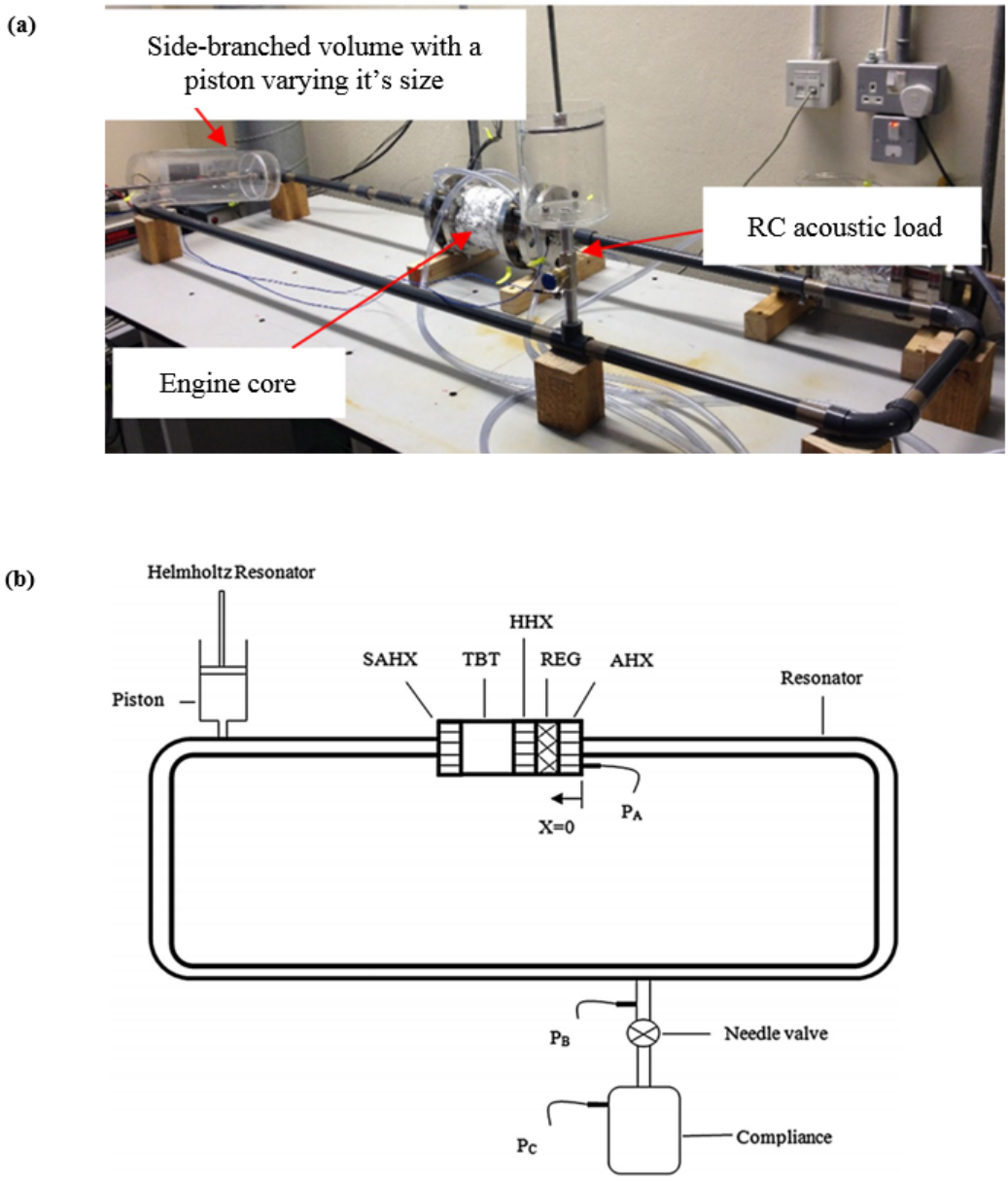


Figure 2.11: Al-Kayiem's Looped-tube travelling-wave thermoacoustic engine with a RC load and a side-branched volume. (a) Photo of the rig. (b) Schematic diagram of the system where: AHX is the ambient heat exchanger, REG the regenerator, HHX the hot heat exchanger, TBT thermal buffer tube, SAHX secondary ambient heat exchanger (Al-Kayiem and Yu 2017).

The engine as shown schematically in Figure 2.11 consists of a regenerator in between two heat exchangers (cold and hot), a thermal buffer tube, a secondary ambient heat exchanger, a feedback pipe, a resistance-compliance "RC" acoustic load for acoustic power extraction, and a side-branched acoustic volume of 12.6 cm diameter. The volume of the side-branched acoustic volume is controlled by the piston located 70 cm

away from the secondary ambient heat exchanger and is attached to the engine loop. Air at atmospheric condition was used as the working gas and the system worked at a frequency of 60.5 Hz. From the results, the acoustic power extracted by the RC load was 16 W and the measured efficiency of 0.35% was much lower than the predicted one of 6.1%. The onset temperature achieved in this system was about 247 °C which was also much greater than the calculated one. There are several reasons behind the low performance of the system. One is the massive heat losses resulting from the insufficient thermal insulation around the hot heat exchanger and the thermal buffer tube. The others are the acoustic streaming and acoustic losses resulting from the sudden transition of the cross-sectional areas along the engine. Also, leakage of sound waves resulted from using PVC pipes and fittings. However, the numerical and experimental outputs demonstrated that the usage of a side-branched acoustic volume would enhance the overall performance of the system. This is because the volume introduces a parallel acoustic compliance to the feedback tube that is, in essence, an acoustic wave-guide. Part of the acoustic volumetric flow shunts away from the feedback tube at the spot where the volume is placed. Hence, the acoustic impedance can be adjusted throughout the engine's feedback and thus, the time-phasing between the pressure and velocity of oscillation.

2.3 Thermoacoustic for waste heat recovery

To date, travelling wave thermoacoustic energy conversion is recognized as highly efficient. A travelling wave engine with the torus configuration has reached a high thermal efficiency of 30% at a high operation temperature of 725°C (Backhaus and Swift 2000), allowing the thermoacoustic engine to be compared to that of the internal combustion engine of 28% - 40%. Therefore, thermoacoustic technology is expected to be implemented for applications infeasible (economically or practically) with the conventional techniques, and also for the waste heat and solar energy field. However, a number of challenges would be associated with this technology, such as the integration of the thermoacoustic systems with the heat recovery sources and the possibility of reducing the temperature gradient for energy excitation.

Solar and industrial waste heat applications have an operating temperature of 70°C, and it can go up to 400°C for exhaust heat of a combined heat and power system. At these low temperatures, the ratio between the useful acoustic power and the acoustic power of the loop has an immediate effect on the overall system performance. It is well-known that this ratio can be improved by deploying more than one thermoacoustic engine. However, it is hard to realize the correct time-phasing inside more than two engines when using the torus configuration.

De Blok (2008) discovered that, in the torus-type thermoacoustic system, the combination of the high acoustic impedance and the acoustic losses within the standing wave resonating tube raise the value of the temperature difference needed for the system excitation. Accordingly, a novel geometry with a hybrid configuration was suggested for waste heat recovery. The system consists of a combination of a bypass pipe and a travelling wave feedback loop as depicted in Figure 2.12.

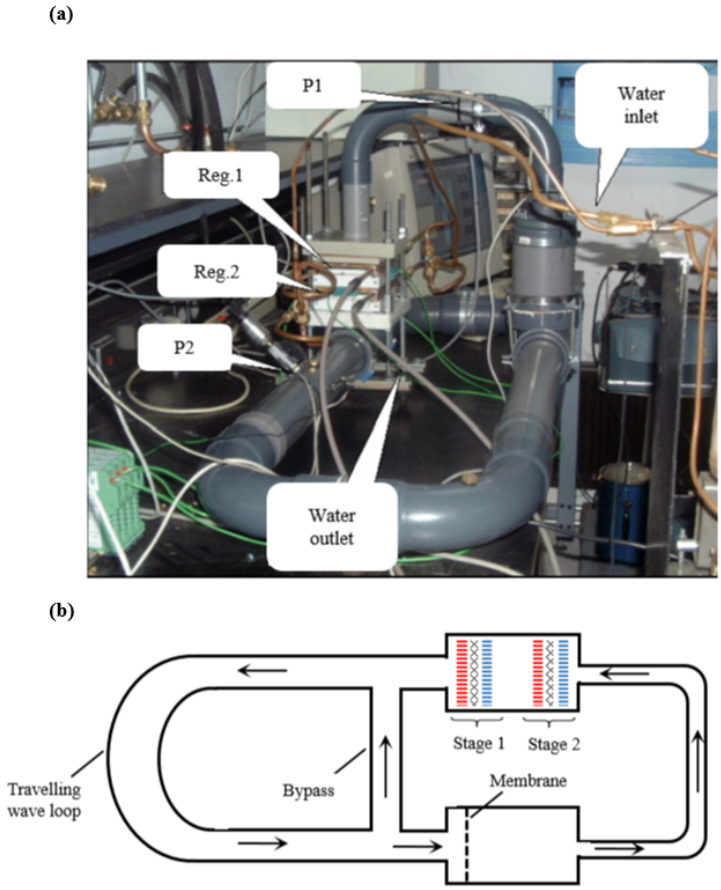


Figure 2.12: Blok's travelling wave engine with hybrid configuration. (a) Photo of the engine. (b) The layout of the device which shows the bypass channel combined with the feedback torus loop. There are two engine stages and each of them has a fixed positioned regenerator clamped between a hot heat exchanger and a cold heat exchanger [Adapted from (De Blok 2008)].

In this device, air at atmospheric pressure was employed as the working gas. The torus consisted of two identical regenerators placed in between two heat exchangers. The system was powered by a dedicated gas-fired water heater, while a car radiator was used to remove the process heat. The bypass channel was combined with the acoustic wave guide to act as an "overflow" pipe with access volumetric flow directed away from the regenerator units. With minimized volumetric flow the regenerator may be designed with a low acoustic impedance to minimize the flow resistance and with a large cross sectional area to enhance the heat transfer. By implementing this, a travelling wave looped resonator (compromising the bypass pipe and the feedback

wave guide) was obtained. The acoustic wave in this system remains at travelling wave phasing in almost every area because the configuration of the engine remains essentially a toroidal loop. Therefore, the temperature gradient was greatly decreased. The region of pure travelling wave in the hybrid configuration is relatively large because most of the engine components experience travelling wave time-phasing conditions. This allows for placing more than a single regenerator in order to increase the amount of the acoustic power produced from the engine at a low operating temperature. The prototype recorded the lowest temperature difference of 65°C. However, there is no sufficient experimental data to prove whether the efficiency of this new type of engine was higher than the toroidal type with a standing wave resonator or not.

Subsequently, De Blok (2010) invented a new multiple-regenerator travelling wave thermoacoustic engine to support his previous concept (Figure 2.13).

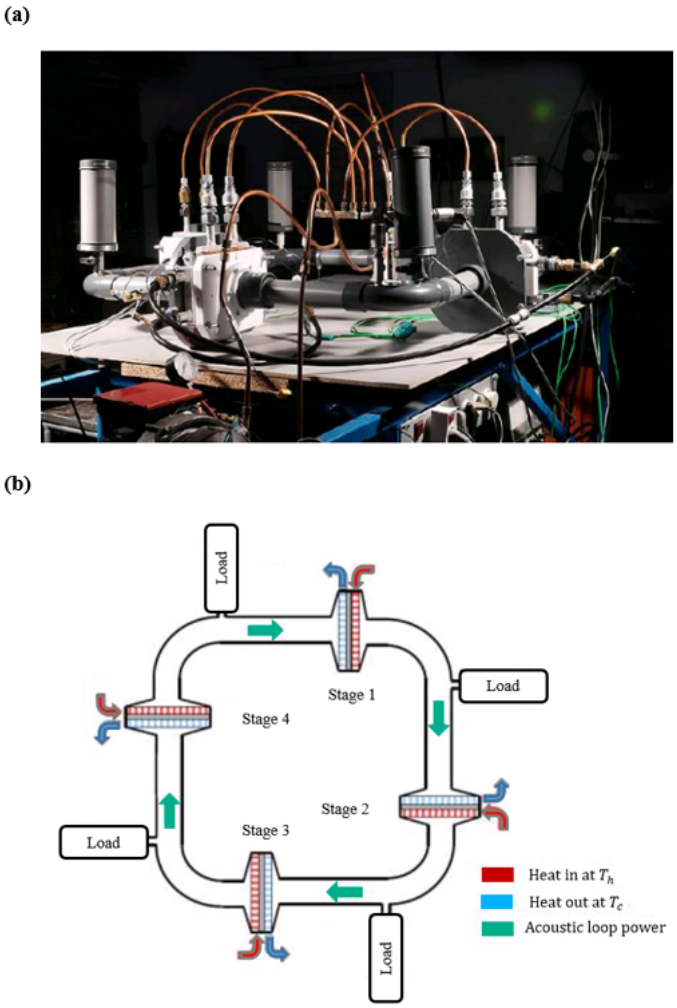


Figure 2.13: Blok's four stage travelling wave power converter. (a) Photo of the prototype. (b) The layout of the device which shows the engine stages and the direction of the heat flow from and into each of them and the wave propagation within the loop (De Blok 2010).

The invention relates to reducing both the onset and the operation temperature of a thermoacoustic engine by reducing the acoustic dissipations and increasing acoustic power gain in a thermoacoustic integrated device, in such a way that the known limitations are terminated. According to the prototype Figure 2.13, the acoustic power gain would be increased by a series connection of multiple thermoacoustic energy converters mutually coupled by acoustic wave guides. In this configuration, the local acoustic velocity inside the regenerator units of the energy converter was reduced by an increase in the cross-sectional area of each regenerator with respect to the local cross-sectional area of the wave guide which in turn led to a reduction in the viscous losses.
De Blok (2010) concluded that the preferred implementation of the prototype is to utilize four identical thermoacoustic energy converters with quarter wave-length mutual acoustic spacing. Travelling wave time-phasing was obtained almost everywhere in this particular case and was achieved by the fact that reflections with a mutual distance of $(1/4)\lambda$ tend to cancel each other out. As a result, acoustic impedance in each stage was matched "by default" without any extra acoustic adjustment and the production cost was potentially decreased because of the identical parts per stage. The acoustic power was extracted on multiple positions and with different phases through the length of the prototype (one wave-length).

2.4 Thermoacoustic for electricity generation

The research on thermoacoustic technology and its applications continued and prior studies have noted the possibility of implementing thermoacoustic technology for power generation. To establish the viability of this, several attempts have been made to convert the acoustic power generated from thermoacoustic engines into electricity, utilizing different system configurations and acoustoelectric transducers. The advances in thermoacoustic electricity generators can be categorised into two groups as follows:

2.4.1 Thermoacoustic engines for micro-generation

Helium-filled engines

A novel thermoacoustic travelling wave generator was designed and built by Backhaus, Tward and Petach (2004) to test the ability to convert high temperature heat into acoustic power with high thermal efficiency with no moving parts. In their system as displayed in Figure 2.14, the long standing wave resonating tube was replaced with two moving coil-type linear alternators which were attached to the torus. The alternators were used to induce and sustain an acoustic resonance in the torus as well as to deliver electricity from the acoustic power. Essentially, a loop tube configuration was adopted where the loop pipe was filled with 55 bar Helium under 120 Hz. After careful optimisation, the results yielded that the engine efficiency (acoustic power delivered to the alternator

piston over the heat added to the system) is 24%, the alternator efficiency is 75%, and the thermal-to-electrical efficiency is 18% at a pressure ratio of 0.063 where the electrical output is 39 W. Also, it is noticed that the electrical power output increased significantly by 49% (from 39 W to 58 W) when the pressure ratio was increased from 0.063 to 0.098. In this travelling wave electricity generator, high-cost linear alternators have been utilized. However, it is possible to integrate low-cost commercially available loudspeakers to TA systems to extract electricity from the generated acoustic power (Yu, Saechan and Jaworski 2011; Yu, Jaworski and Backhaus 2012).

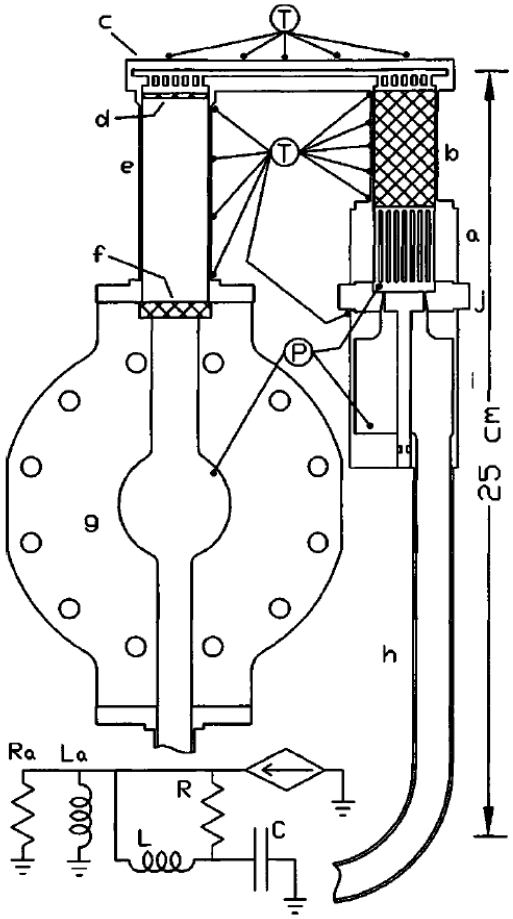


Figure 2.14: A schematic drawing of the travelling wave thermoacoustic engine together with the analogous lumped-element electrical circuit diagram. The main thermodynamic and acoustic components are: (a) An ambient heat exchanger. (b) A regenerator. (c) A hot heat exchanger. (d) and (f) Are two flow straighteners. (e) A thermal buffer tube. (g) An alternator. (h) An inertance tube. (i) A compliance volume. (j) A jet pump. *T* and *P* symbols represent the locations of the temperature and pressure sensors, respectively. The equivalent electrical circuit consists of two resistors *R* and *Ra*, two inductors *L* and *La*, and a capacitor *C*. More details can be found in (Backhaus, Tward and Petach 2004).

Another thermoacoustic power converter was fabricated and tested by Telesz (2006) as shown in Figure 2.15. The system interfaces a thermoacoustic Stirling engine with two linear alternators to deliver 100 W electrical power from a heat input. It operated

at 100 Hz frequency using helium at 31 bar as the working gas, and with a hot side temperature of 649 °C. The maximum electrical power extracted from the system was 70 W with 26.3% thermal-to-acoustic efficiency (40% of Carnot efficiency) and 16.8% thermal-to-electric efficiency. The performance values of the system have not achieved the original design goals as a result of the DC heat leaks. Besides, the alternators were damaged during the initial shakedown testing because they had over-stroke on numerous occasions.

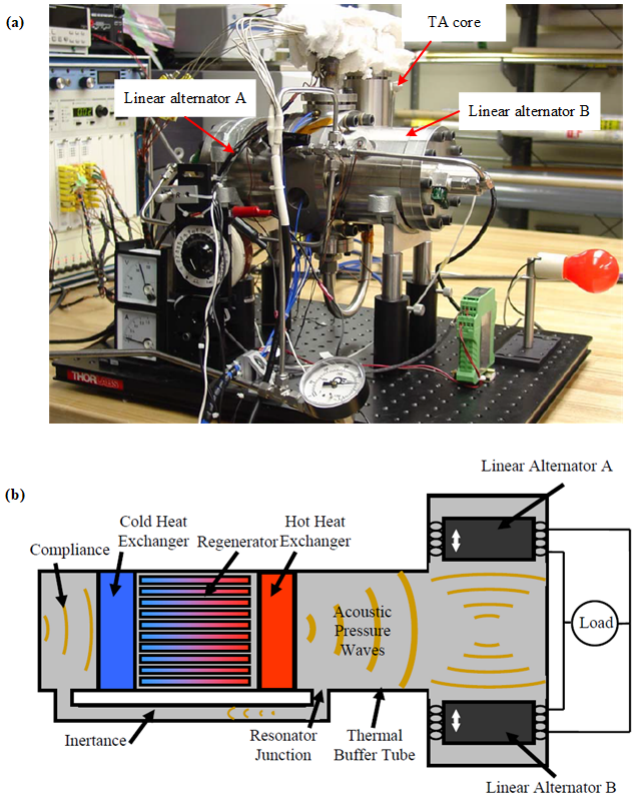


Figure 2.15: The thermoacoustic power converter TAPC. (a) Photo of the system showing the location of the thermoacoustic core and the two alternator (A and B). (b) The layout of the device includes: A compliance, a single TA core, a thermal buffer tube, an inertance tube, two alternators A and B (Telesz 2006).

Air-filled engines

Aster Thermoacoustics research company implemented the concept of the four-stage travelling wave thermoacoustic engine into a cooking stove (De Blok 2010). In addition to the hot water, the system was designed to provide electrical power. The prototype was very thin (about 50 mm) and was placed between a heating source (i.e. wood fire) and a water storage tank filled with the heated water. Each stage of the system consisted of an aluminium upper and lower plate with internal fins performing as ambient and hot heat exchangers, respectively. An isolation layer containing the regenerator was

placed between the two plates. Figure 2.16 displays the conceptual design of the flat multi-stage thermoacoustic engine. For measuring purposes a spiralled water tube was used instead of the water reservoir. The acoustic inputs and outputs of engine stage were 90° rotated with respect to each other and interconnected by a short tube of 43 mm. In the preliminary tests, a single cheap alternator was used to extract the electric power from the system. With air atmospheric pressure as the working gas, the system delivered 5.4 W electrical power with acoustic-to-electric conversion of 31%. The loop acoustic power was 34 W, while the net acoustic production was 17.6 W, which proves that the acoustic losses are low in spite of the bends and the area transitions.

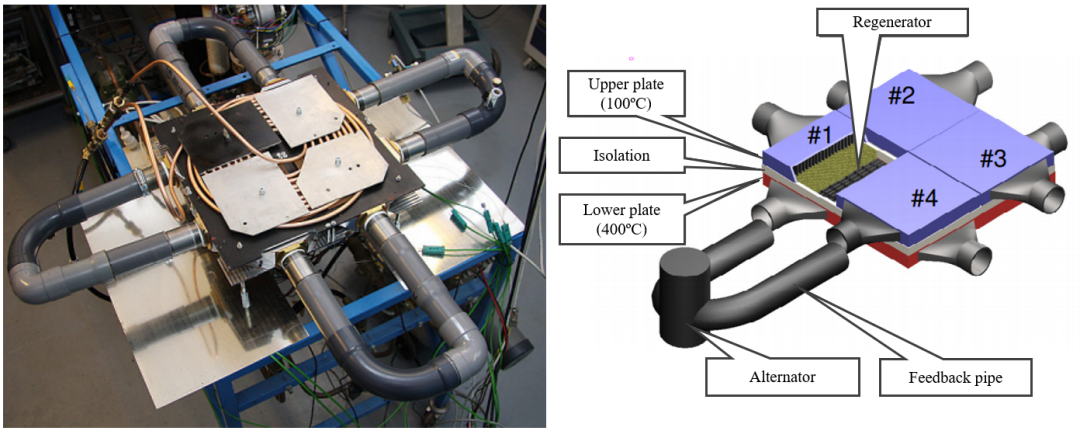


Figure 2.16: Blok's four-stage travelling wave engine. (a) Experimental set-up of the flat four-stage travelling wave thermoacoustic engine. As seen, a spiralized water tube is used instead of the water tank. (b) Schematic diagram where only one acoustic feedback loop with a linear alternator is drawn (the feedback pipe connects stage 4 and stage 1. The regenerator, the upper and lower plates are also shown for the first engine stage (De Blok 2010).

Further research was carried by Yu, Jaworski and Backhaus (2010*b*), who designed and constructed a looped tube travelling wave thermoacoustic generator, to investigate the concept of a low-cost thermoacoustic system for developing world applications. Their thermoacoustic system is schematically represented in Figure 2.17. It consisted of a single regenerator unit, a feedback loop, a tuning stub, and a loudspeaker. The loudspeaker was placed in the loop after the secondary cold heat exchanger and was employed as a linear alternator to convert the acoustic power production into electricity. Air at atmospheric pressure was used as the working gas and the system was worked at 75 Hz frequency. During the test, 800 W of heat was supplied to the system through an electrical heater, and only 5.18 W of the supplied heat was harvested by the loudspeaker with 50% acoustic-to-electric conversion efficiency and 0.65% heat-to-electric efficiency. The results prove the possibility and the feasibility of

using commercially available, inexpensive ordinary loudspeakers to design affordable thermoacoustic electricity generators. However, the power and the efficiency figures were not very encouraging.

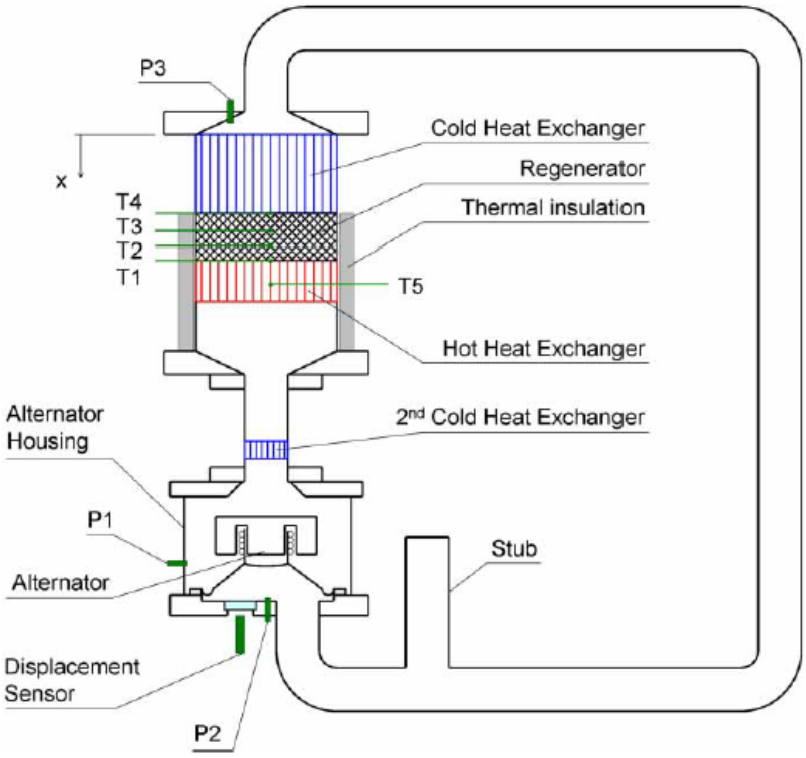


Figure 2.17: Schematic diagram of the tested prototype showing the main system components and the measurements location used to evaluate the system performance. The acoustic and thermodynamic components include: a cold heat exchanger, a regenerator, a hot heat exchanger, a second ambient heat exchanger, an alternator, and a stub. P and T are used to show the location of pressure sensor and temperature sensors, respectively (Yu, Jaworski and Backhaus 2010*b*).

To investigate the acoustoelectric efficiency, Yu, Saechan and Jaworski (2011) and their research group developed an experimental technique to characterise the performance of ordinary, low-cost loudspeakers for the linear alternator applications in low-cost thermoacoustic engines. In this research, a particular loudspeaker (model B&C 3PS38) was chosen, based on the force factor as well as both the electrical and the mechanical resistances, to serve as a case study to demonstrate the acoustoelectric conversion efficiency. The experimental outputs showed that the transduction efficiency of the selected loudspeaker (model B&C 3PS38) could reach up to 60% when the optimum load resistance was adopted, while it could go up to 40%, when the load resistance approaches the electrical resistance of the loudspeaker coil. In addition, the results identified that the transduction efficiency is not significantly influenced by the displacement

amplitude which is critical for using ordinary audio loudspeakers to develop affordable thermoacoustic electricity generators, where the high stroke and low pressure drop across the loudspeaker diaphragm are preferable. Furthermore, it is useful and possible to replace the linear alternators with the commercially available, inexpensive audio loudspeakers. Also, their developed methodology is valid and reliable for identifying and characterising the transduction efficiency of the alternator.

Yu, Jaworski and Backhaus (2012) continued their research in thermoacoustic engines and proposed a novel concept of a looped tube travelling wave thermoacoustic electricity generator.

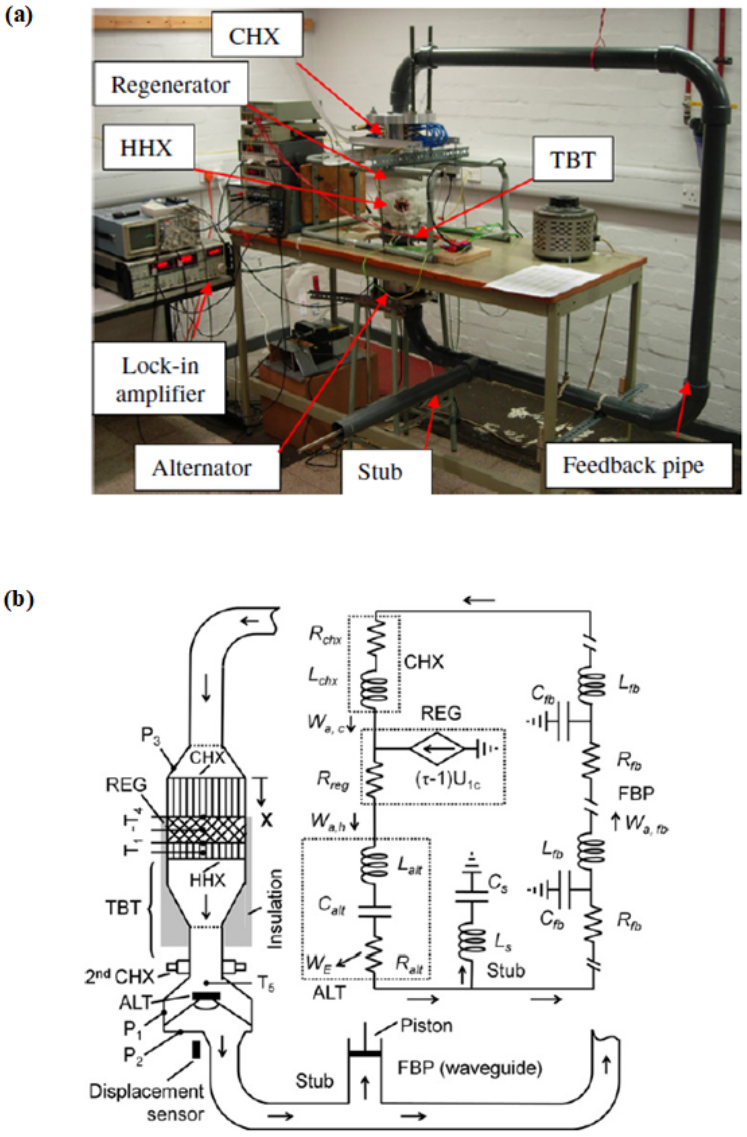


Figure 2.18: The looped tube travelling wave thermoacoustic engine coupled with ultra-compliant alternator. (a) A photo of the system where the main system components are: a cold heat exchanger CHX, a regenerator, a hot heat exchanger HHX, a thermal buffer tube TBT, an alternator, a stub, and a feedback pipe. (b) Schematic diagram including the equivalent acoustic circuit which developed using electrical analogy. Further details are available in (Yu, Jaworski and Backhaus 2012).

The system as shown schematically in Figure 2.18 has one unit which consists of; a cold heat exchange CHX, a regenerator, a hot heat exchanger HHX, a thermal buffer tube TBT, a feedback pipe, a linear alternator, and a stub. The linear alternator was of ultra-compliant type and was attached to the engine loop to convert acoustic energy into electrical power. The side branch stub was used to correct the impedance of the acoustic field within the system changed by the installation of the linear alternator. The cold heat exchanger used in this system was carefully designed to obtain a phase-shifting inertance. The physics of this new concept was captured and demonstrated using a simple acoustic impedance circuit, while DeltaEC software was used to investigate the performance of the whole system in detail. The experimental data showed that the engine can produce 11.6 W electrical power with 1.3% thermal-to-electrical efficiency, which is an indication of the potential to develop a low-cost thermoacoustic electricity generator for low grade heat recovery. Also, the numerical outputs suggested that the system can perform better and achieve much greater efficiencies when pressurised helium is selected as the working gas and a better alternator as an electro-dynamic transduction mechanism. Therefore, the author recommended that further research should be undertaken to investigate the implication of mean pressure on performance.

For the SCORE project, two types of low-cost, looped tube travelling wave thermoacoustic systems have been comprehensively assessed, based on the systematic heat transfer, by Chen et al. (2012). In essence, the two systems were designed to deliver an acceptable level of electricity to be used by rural households. One of the devices (shown in Figure 2.19) was powered by waste heat from a propane-driven cooking stove, and was successfully demonstrated to produce 15 W electrical power with 3.26% thermal-to-electrical efficiency using a low-cost loudspeaker as a linear alternator. The second system (shown in Figure 2.20) utilized waste heat from a wood-burning cooking stove and successfully demonstrated 12.6 W of electricity when using air under atmospheric condition and 22.7 W of electricity when the system was pressurised to 50 kPa gauge pressure. The heat-to-electrical efficiency was quite low on both devices as a result of the high acoustic losses and the inefficient linear alternators being used (35% acoustic-to-electric conversion efficiency). However, the price per Watt is cheap (Riley 2014*a*).

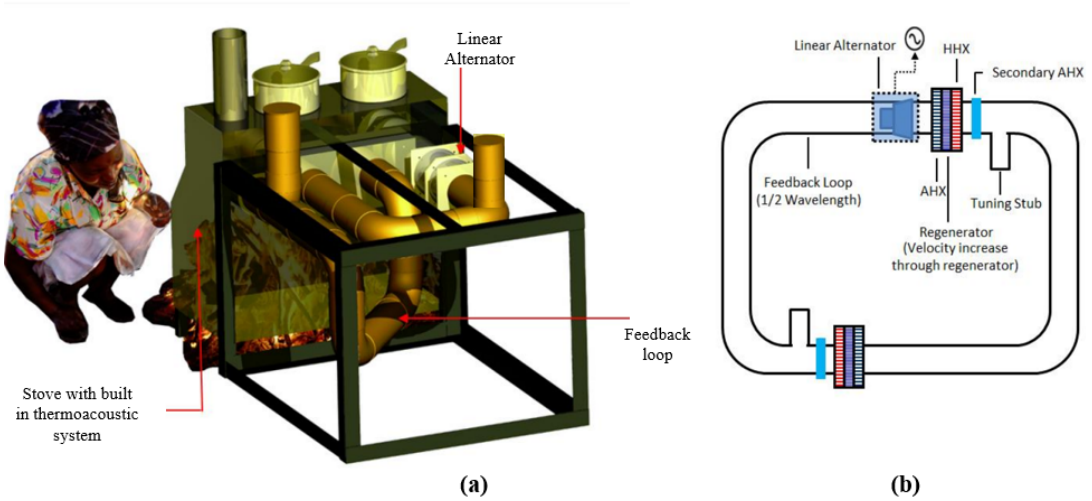


Figure 2.19: General configuration of the propane-driven thermoacoustic generator. (a) Photo of the system shows the integration of the thermoacoustic engine with the cooker. (b) The schematic diagram where the main components of the system are illustrated. The system has two thermoacoustic cores, two tuning stubs, a feedback loop, and a linear alternator. Each core comprises an ambient heat exchanger AHX, a regenerator, a hot heat exchanger HHX, and a secondary ambient heat exchanger (Chen et al. 2012).

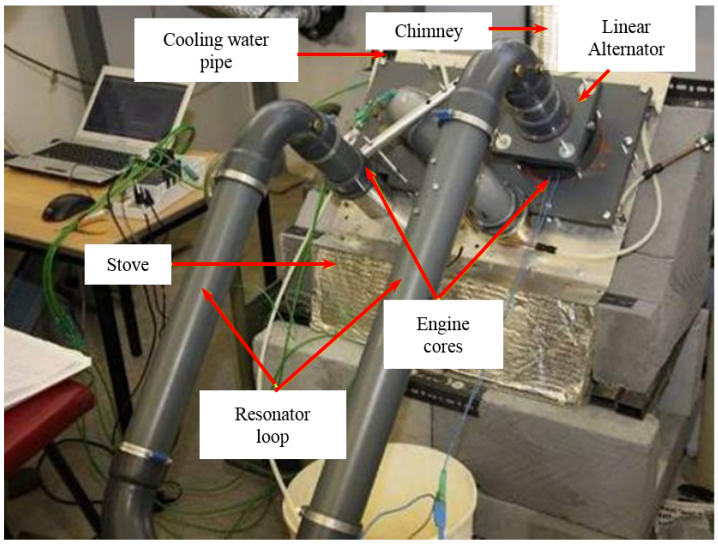


Figure 2.20: Photograph of the air-filled travelling wave thermoacoustic engine integrated with a wood-burning cooking stove (Chen et al. 2012).

The most recent travelling wave thermoacoustic prototype for micro-generation was developed and constructed by (Abdoulla-Latiwish, Mao and Jaworski 2017). The system has one thermoacoustic core with a looped-tube configuration as displayed in Figure 2.21. The heat source was flue gas from a propane burner, and the system used air at atmospheric pressure. The acoustoelectric conversion was obtained via an audio loudspeaker connected to a side branch pipe. The prototype delivered around

18 W of electrical power with thermal-to-acoustic and thermal-to-electric conversion efficiencies of around 3.5% and 1.9%, respectively. The performance was reduced due to the acoustic dissipations and the efficiency of the loudspeaker.

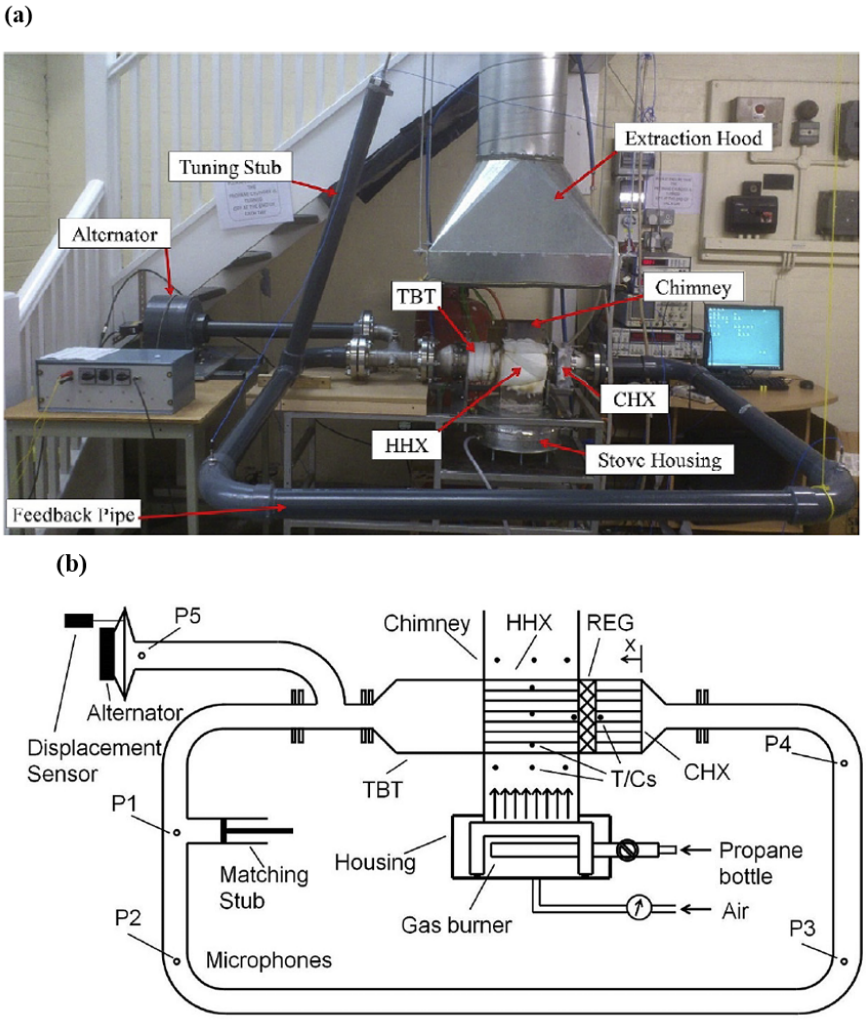


Figure 2.21: The single stage travelling wave thermoacoustic electricity generator. design considered for the hot heat exchangers. (a) Photo of the system showing the components of the travelling wave unit, the alternator, the matching stub, the feedback pipe, the stove, and the chimney. (b) Schematic illustration of the generator which includes the location of the measurements used to assess the performance. T/Cs are thermocouples, $P1$ to $P5$ are pressure sensors (Abdoulla-Latiwish, Mao and Jaworski 2017).

2.4.2 Potential of TAE in a broader context

A travelling wave thermoacoustic electricity generator (TWTAEG) was built and tested by Wu et al. (2011). The engine was based on Stirling cycle and used a linear alternator to achieve the power conversion. Figure 2.22 illustrates the schematic diagram of the TWTAEG which includes the feedback loop, a resonator tube and a linear alternator. The working gas was 3.54 MPa pressurized helium and the system operated at a

frequency of 74 Hz. An electrical heater was adopted to supply the heat into the system. In their experiments, an electrical power output of 450.9 W was obtained with 15% thermal-to-electrical conversion efficiency and 481 W electrical output achieved with a thermal-to-electrical efficiency of 12.65%. Unfortunately, the acoustic work was not totally turned into useful electrical power because of the large acoustic losses in the resonator pipe. Also, the acoustic-to-electrical efficiency of the linear alternator was poor due to the high mechanical damping coefficient.

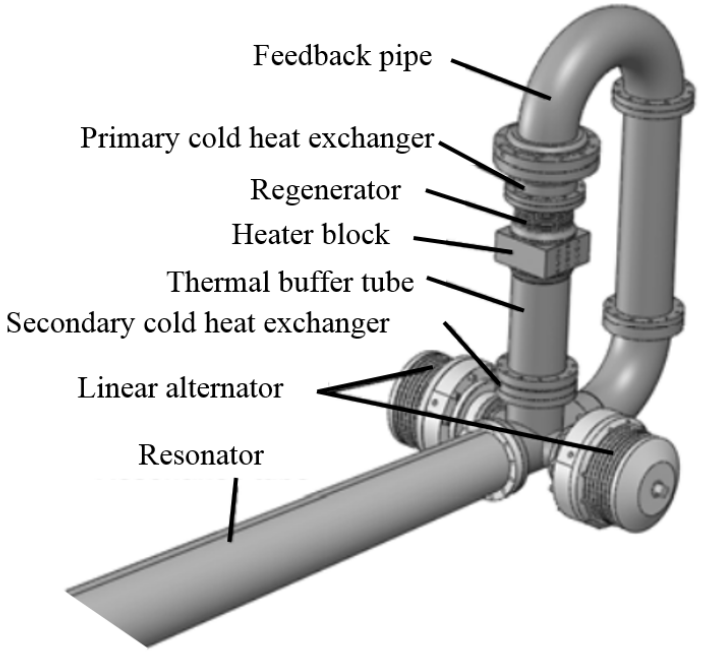


Figure 2.22: Schematic diagram of Wu's travelling wave thermoacoustic electricity generator showing the engine parts: A primary cold heat exchanger, a regenerator, a heater block, a thermal buffer tube, a secondary cold heat exchanger, a feedback pipe, a resonance tube, and a linear alternator (Wu et al. 2011).

Wu et al. (2012) applied a linear alternator in their 1 kW solar-powered travelling wave thermoacoustic system to generate electric power from solar energy as depicted in Figure 2.23. The rig operated at a frequency of 74 Hz and used 3.5 MPa pressurized helium as the working gas. The electricity generator was integrated with a solar dish collector and a heat receiver. In the first set of tests, the solar energy was simulated using electrical cartridge heaters. The maximum electrical power output extracted by the alternator was 481 W with 15% thermal-to-electrical efficiency. Thereafter, the solar dish was used to heat up the system and only 200 W electrical power was obtained from the integrated system. This inconsistency may be due to the design problems related to the solar collector.

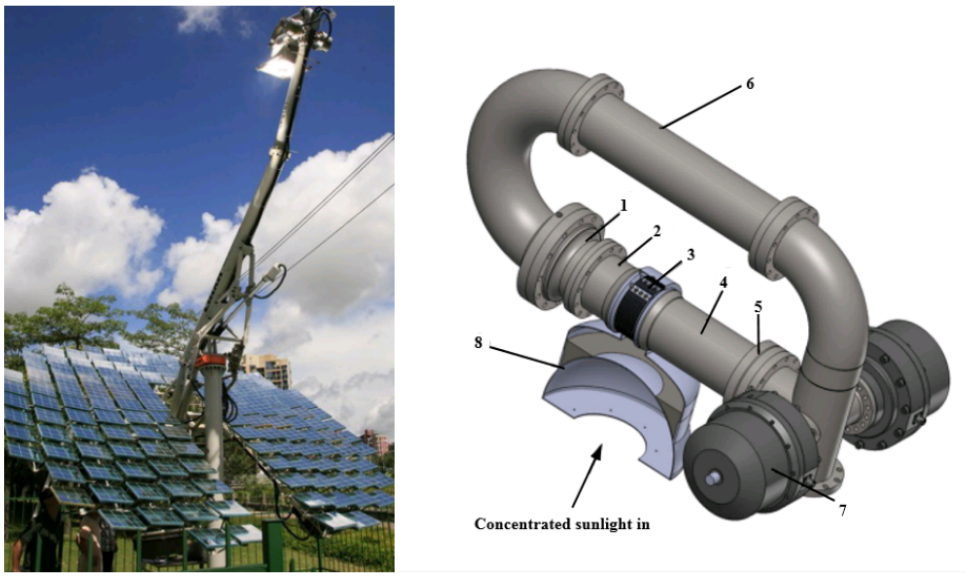
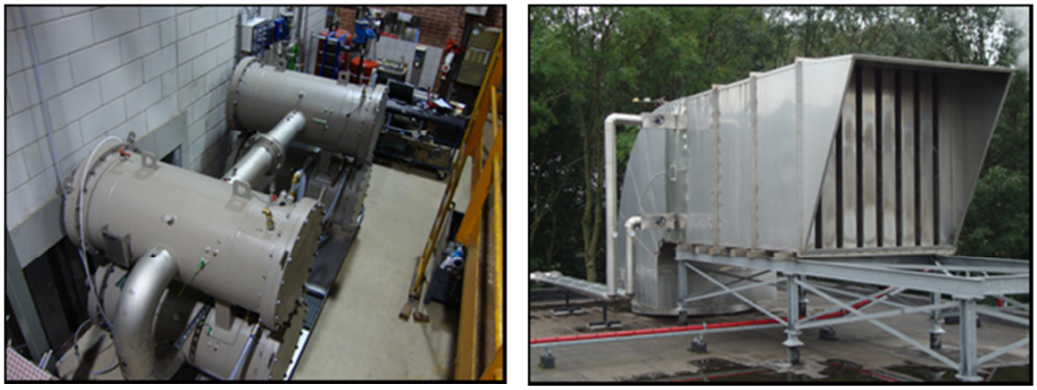


Figure 2.23: Wu's Solar-powered travelling wave thermoacoustic electricity generator. (a) Photo of the entire system. (b) Schematic representation of the thermoacoustic loop, the linear alternator and the heat receiver with a sectional view. The generator consists of: 1. main ambient heat exchanger, 2. regenerator, 3. heater block, 4. thermal buffer tube, 5. secondary ambient heat exchanger, 6. feedback loop, 7. linear alternator, and 8. heat receiver (Wu et al. 2012).

At the industrial scale, a pilot 100 kW thermoacoustic power generator was invented and tested to partially convert the exhaust gas at 150 - 160 °C from a paper manufacturing plant into electrical power (De Blok and Systemen 2012). This study set out to prove the economic feasibility of the thermoacoustic power generator and to verify the scalability of thermoacoustic engine from low power rate to industrial power levels. The pilot had four-regenerator units and feedback loop and used 7.5 bar pressurised helium as the working gas. The system worked at 40 Hz operating frequency. The housing was assembled from four pressure cylinders mutually connected by a pair of straight and a pair of bended feedback pipes, each with an equal acoustic length of 1.5 m as shown in Figure 2.24. The heat exchangers and the regenerator were in transverse position. Waste heat was extracted firstly from the production process using a commercial available heat exchanger and, after that, heat was transferred from a heat exchanger at the roof down to an intermediate heat exchanger close to the thermoacoustic power generator. From the intermediate heat exchanger, thermal oil was utilized to transfer heat to the hot heat exchangers of the thermoacoustic power generator inside each vessel. The cold heat exchangers were connected to a water reservoir. Hence, heat removed from the power generator was utilized to pre-heat the production process water. The linear alternators were mounted inside each pressure vessel and utilized to extract part of the acoustic power production into electricity.



(a) (b)

Figure 2.24: (a) The four-stage 100 kW thermoacoustic power generator (TAP). (b) The flue gas exhaust $(3m \times 3m)$ with half-way the high temperature circuit heat exchanger (De Blok and Systemen 2012).

In this work, the measured values agreed well with the simulation. The achieved output power was 1.64 kW with 7.5 bar pressurised helium and at 1.7% drive ratio. Although the outcome is encouraging because it confirms the scalability of thermoacoustic engines from laboratory size up to industrial levels in practical applications, the total temperature drop along the heat exchangers was in the order of 40 °C, which is a considerable amount of the available input temperatures from low-grade heat or solar energy (e.g. 160°C).

More recent research has been into the coupling mechanism of a linear alternator with a travelling wave thermoacoustic electricity generator (Sun et al. 2013). Early system used an equivalent acoustic circuit of the linear alternator which was developed using the electrical analogy to evaluate the overall performance of the acoustic system. Based on that, a travelling wave thermoacoustic electricity generator with a pair of linear alternators was built and tested as shown in Figure 2.25. The system used helium at 3.0 MPa as a working gas at 65 Hz operating frequency. Under the most powerful operating conditions, the thermoacoustic electricity generator produced 345.3 W electrical power with a thermoelectric conversion efficiency of 9.34%. The system delivered 321.8 W of electricity with 12.33% thermoelectric efficiency at the best operating point.

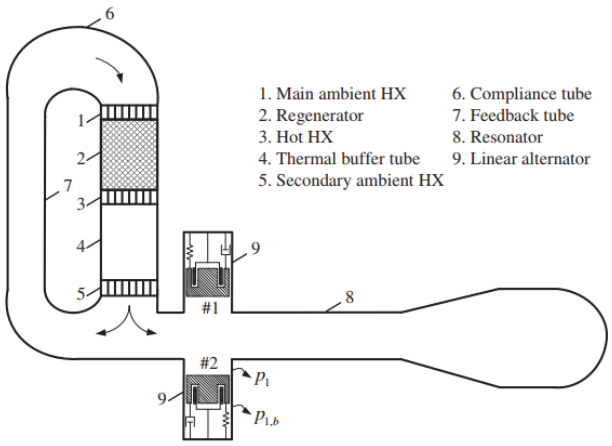


Figure 2.25: Schematic presentation of the travelling wave thermoacoustic engine which comprises a vibration-balanced pair of moving-magnet linear alternators. The main system components are shown by the legend at the top of the schematic, and the symbol p is used to indicate a pressure sensor (Sun et al. 2013).

Both the numerical and experimental data showed that the mechanical and electrical resonances are important in boosting the performance of the thermoacoustic electricity generator. Besides, the electric power output can be improved considerably by using a gas with higher pressure amplitude in the system.

Wu et al. (2014*b*) designed and investigated a 1 kW travelling wave thermoacoustic electricity generator. The system comprises a feedback tube, a single core unit, a section of a plastic membrane to suppress the DC flow in the thermoacoustic loop, and a linear alternator. The linear alternator was a dual-opposed configuration and had two linear motors as illustrated in Figure Figure 2.26. The first experiments were achieved with 4.0 MPa pressurised helium and at 74 Hz working frequency. The heating temperature was 650 °C. A maximum electrical power of 638 W and a drive ratio of 4.5% were obtained. The electricity output was considerably lower than the calculated one because of the high friction losses of the alternator piston. Therefore, the group attempted to enhance the overall performance of the thermoacoustic system by charging 4.5% mole fraction of argon gas into the system. Accordingly, a maximum electricity output of 1043 W with 19.8% thermal-to-electrical efficiency was obtained at 64 Hz operating frequency, 4.0 MPa mean pressure, and 650 °C heating temperature. Overall, this study strengthens the idea that the coupling mechanism of the linear alternator to the system is crucial to improve the performance of the system.

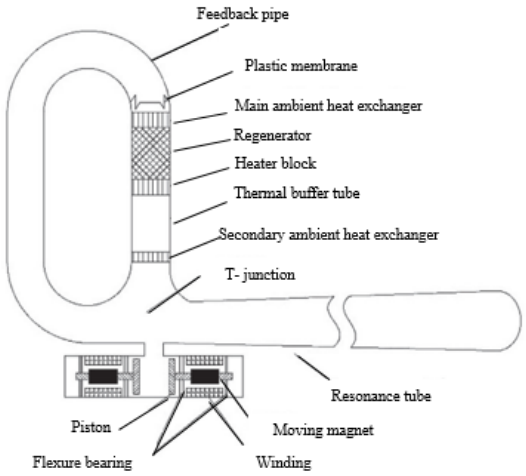


Figure 2.26: Configuration of a travelling wave thermoacoustic electricity generator coupled with a dual-opposed linear alternator for acoustoelectric power conversion. The generator has one core comprising a main heat exchanger, a regenerator, a heater block, a thermal buffer tube, and a secondary ambient heat exchanger (Wu et al. 2014*b*).

A novel three-cylinder double-acting thermoacoustic Stirling electricity generator "DATASEG" capable of converting thermal power into electricity was introduced by Wu et al. (2014*a*). The system employed three thermoacoustic Stirling heat engines and three linear alternators as shown in Figure 2.27.

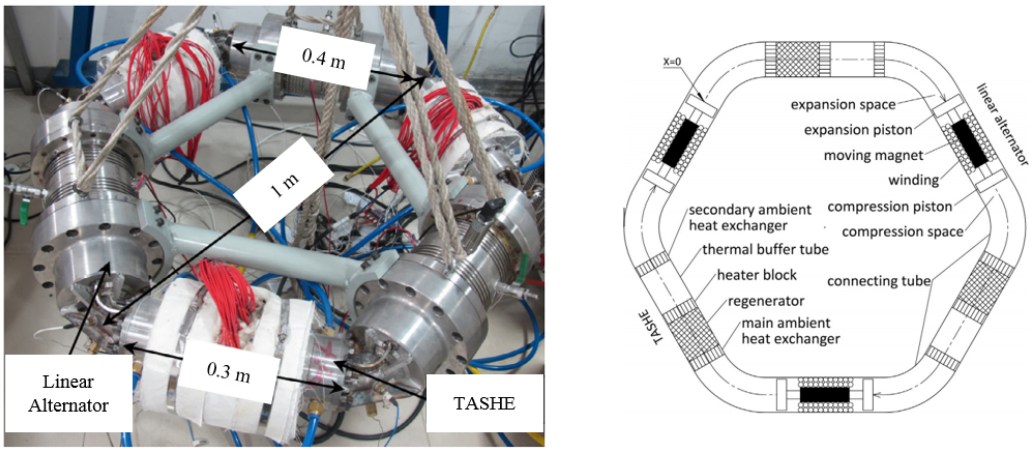


Figure 2.27: The double-acting thermoacoustic Stirling electricity generator DATASEG. The arrows indicate the distances between the engines. (a) The experimental set up which includes three thermoacoustic Stirling heat engines and three linear alternators. (b) Schematic diagram where the main parts of each engine are appears (Wu et al. 2014*a*).

Prior to the design stage and based on the linear thermoacoustic theory, modelling work was performed utilizing a DeltaEC tool to gain a detailed understanding of the entire system, and also to determine the thermodynamic parameters of the system. Afterwards, the system was built and tested. In the preliminary tests, a maximum electrical power of about 1570 W with a maximum thermal-to-electric conversion efficiency of 16.8% was obtained using 5 MPa pressurized helium with 86 Hz working frequency and 3.12 kW heat input power from each heater block. These findings contribute in several ways to understanding the concept of using multiple regenerator units in thermoacoustic systems. However, there was a dramatic increase in the mechanical damping coefficient of the piston due to the deformation of the cylinder wall as a consequence of the high thermal stress during the experimental tests. Also, there was a reduction in the permitted displacement due to the equilibrium position of the piston shifting. Moreover, there were significant differences in the performance of the three engines as well as the three alternators, such as the heating temperature, the piston displacement and the output electric power from the alternators. Thereby, the system performance was highly degraded.

Another travelling-wave thermoacoustic electricity generator capable of producing up to 500 W electrical power was studied using both numerical and experimental methods (Wang et al. 2015). The experimental rig is schematically shown in Figure 2.28 and consists of a single regenerator unit, feedback tube, a resonator and two linear alternators. The performance parameters and the operating characteristics of the engine under different conditions were predicted. From the preliminary experiments, a maximum electrical power of 473.6 W with a maximum thermal-to-electric efficiency of 14.5% was achieved when the mean pressure, the heating temperature and operating frequency are fixed at 2.48 MPa, 650 °C and 66 Hz, respectively. The energy flow evaluation showed that the dominant losses were from the acoustic power dissipations within the resonating pipe, particularly at low load resistances. Moreover, significant losses were caused by the acoustic dissipation in the hot heat exchangers, thermal buffer tube, and the feedback pipe. From the numerical results, it found that the generated acoustic power could be effectively improved up to 776.5 W as a result of increasing the mean pressure of the gas from 2.48 MPa to 3.2 MPa.

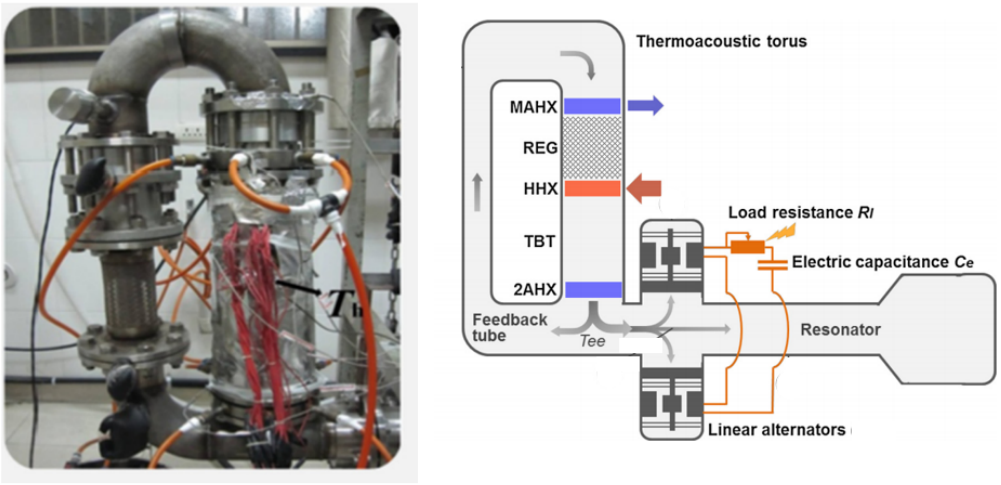
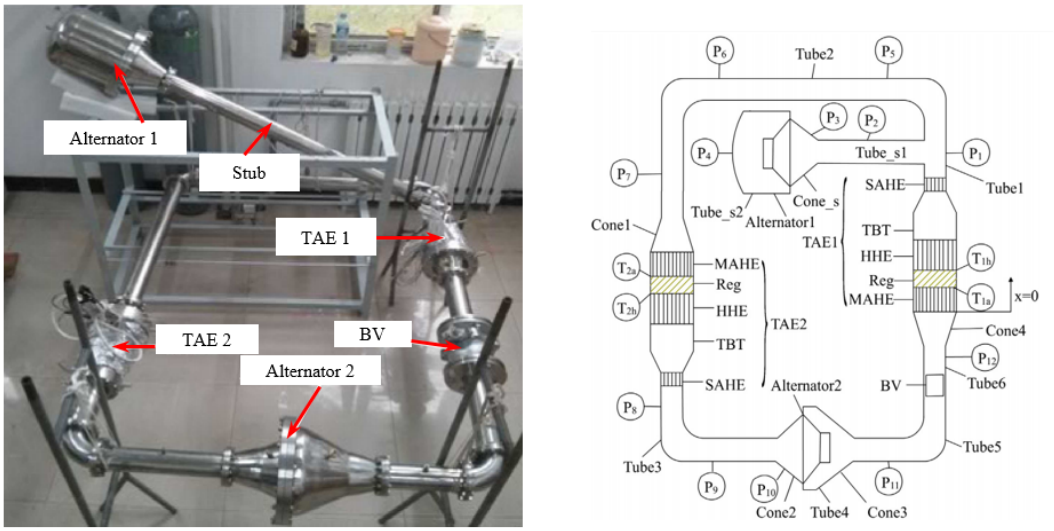


Figure 2.28: The travelling wave thermoacoustic electric generator. (a) Photograph of the torus. (b) Schematic diagram where the main components are shown: a main ambient heat exchanger MAHX, a regenerator REG, a hot heat exchanger HHX, a thermal buffer tube TBT, a secondary ambient heat exchanger 2AHX, a feedback tube, linear alternators, and a resonator (Wang et al. 2015).

Kang et al. (2015) examined the ability of two low-impedance linear alternators to provide electrical output from a double stage travelling wave thermoacoustic engine. A combination of quantitative and qualitative approaches was used to address the coupling mechanism between the alternators and the engine. In addition to the two thermoacoustic cores, a ball valve was installed in the engine loop in order to partially modify the acoustic field altered as a consequence of manufacturing faults. The prototype was constructed and tested as shown in Figure 2.29 with 1.8 MPa pressurised helium as the working gas and the system worked at a frequency of nearly 171 Hz. After the engine started oscillation, the ball valve was slightly rotated between fully open (0°) and fully closed (90°). Adjusting the angle of the ball valve would enable introducing local acoustic resistance, and as a result, the acoustic field within the engine loop can be tuned. As shown in Figure 2.30, the electric power output from the alternators was influenced by the rotating angle of the ball valve and it reached a maximum when the angle was about 10°. Based on this, the turning angle kept constant through the tests, while the total heat input power was varied between 3 and 6 kW with the same input amount through the two heaters.



(a) (b)

Figure 2.29: The two-stage travelling wave thermoacoustic electricity generator. (a) Photograph of the engine reported in the study where the two thermoacoustic engines TAE1 and TAE2, the two alternators, the ball valve BV, and the stub are shown. (b) Schematic diagram of the prototype shows details of the system components and the locations of the measurement instruments. Each thermoacoustic engine consists of a main ambient heat exchanger MAHE, a regenerator Reg, a hot heat exchanger HHE, a thermal buffer tube TBT, and a secondary ambient heat exchanger SAHE. Letters T and P are to denote the temperature and pressure readings, respectively (Kang et al. 2015).

It is recognized that when the total heat power reached 5.4 kW, the thermal-to-electric efficiency recorded a higher value of 3.43% and the temperatures at the hot sides of the two regenerators were 512 and 452 °C, respectively. The total electric power output had a maximum value of 204 W using a total heat input power of 6 kW and with hot-end temperatures at the two regenerators of about 597 and 511 °C, respectively. Interestingly, the research demonstrated the a travelling wave thermoacoustic engine of multiple stages has enormous potential for developing inexpensive electricity generators. However, the performance was low because the thermal dissipation was very large and non-linear behaviour existed in the system as a result of the high pressure amplitude. Therefore, and in order to improve the overall performance, further research work is needed to fully understand the implications of the non-linearity on thermoacoustic engines and also to explore the optimal acoustic field for such a complicated system.

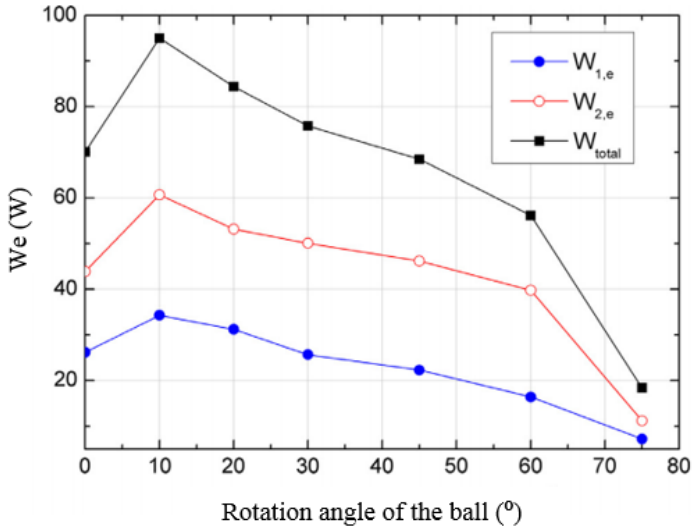


Figure 2.30: The impact of the rotation angle of the ball valve on the electricity output from alternator 1 $W_{e,1}$, alternator 2 $W_{e,2}$, and the total electricity output W_{total} in the two-stage travelling wave thermoacoustic engine. (Kang et al. 2015).

Wang et al. (2016) built an acoustically matched travelling wave thermoacoustic electricity generator capable of generating 750 W electric power. The novel approach used in this research was that the linear alternators were coupled to the system with a by-pass configuration. The aim was to investigate the influence of the coupling mechanism on the system performance. The system as depicted in Figure 2.31, consists of a single regenerator unit, a resonator tube, an inertance tube, and a compliance tube. A silica membrane is installed immediately above the main ambient heat exchanger to eliminate the harmful Gedeon streaming arising in the thermoacoustic loop. The appropriate phase relationship between the oscillating pressure and velocity in the regenerator is adjusted by the acoustic network formed by the resonator tube, the inertance tube, and the compliance tube. A flow straightener composed of several mesh screen layers was used to suppress the jet streaming in the thermal buffer tube which could have a negative impact on the performance. The appropriate acoustic impedances for efficient and powerful operation of the system and the linear alternators were investigated and analysed based on linear thermoacoustic theory. Accordingly, a prototype was constructed and tested at an operating frequency of 65.5 Hz using pressurised helium at 3.16 MPa and with heating temperature of 650°C. When the acoustic impedances were well matched, it found that a maximum electricity output of 750.4 W and a highest thermoelectric conversion efficiency of 16.3% were obtained. Numerical calculations revealed that the electric power output could reach more than 1300 W with 20% thermal-to-electrical conversion if the helium gas pressurised up to 5 MPa.

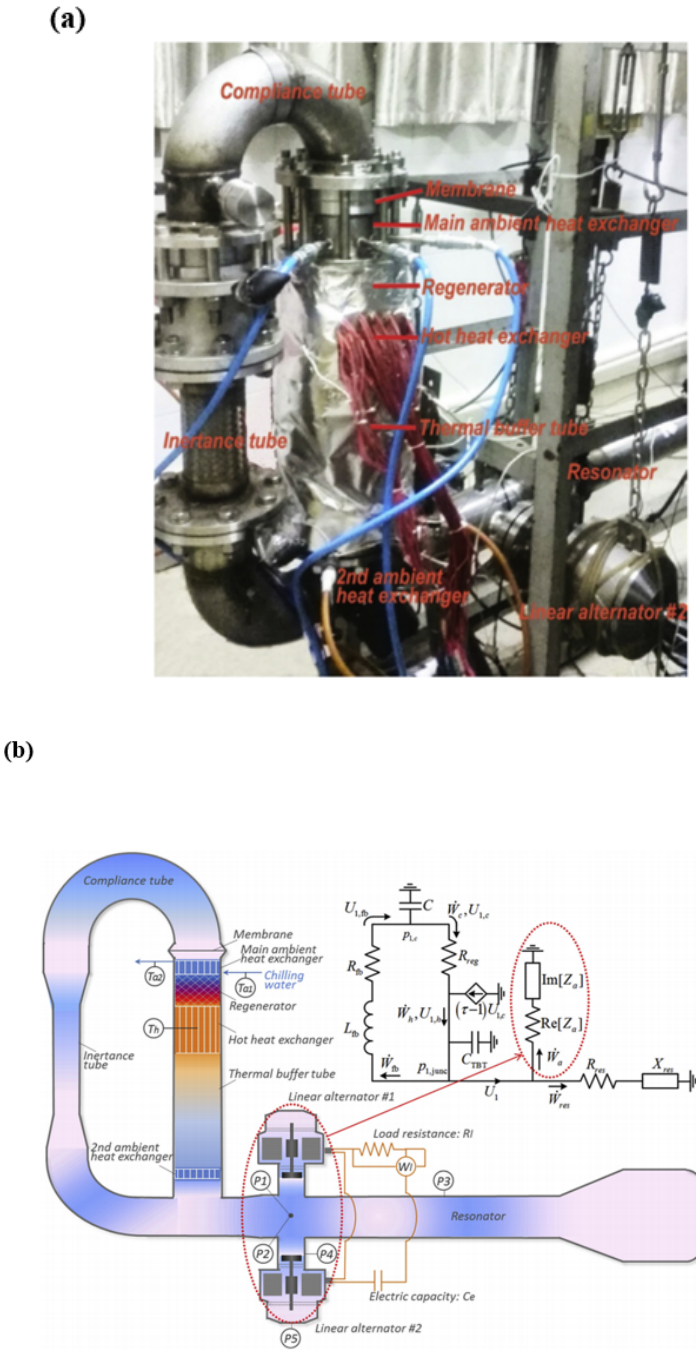


Figure 2.31: Travelling wave thermoacoustic electricity generator with a pair of linear alternators attached via bypass configuration. (a) Photograph of engine where only a part of the resonator is appeared, and only linear alternator 2 is shown. (b) Schematic diagram of travelling wave thermoacoustic electricity generator and the equivalent electric circuit network. P_1 to P_5 denote the location of the pressure sensors. T_h is the heater temperature, T_{a1} and T_{a2} are the temperatures of the inlet and the outlet of chilling water into the main ambient heat exchanger. The coils of the linear alternators are in a series connection with a variable electric load to extract the electricity W_1 which was monitored by a power meter. Details of the electrical circuit network can be found in (Wang et al. 2016).

The results of this study have important implications for the acoustic matching and developing of high-performance thermoacoustic electricity generators. However, there were some deviations between the experimental and theoretical outcomes, mainly due to the large thermal dissipations through the hot heat exchanger, including the heat radiation and convection to the environment, and the secondary ambient heat exchanger via the thermal buffer tube, and the conduction heat transfer via the pipes and regenerator mesh layers, which degraded the overall system performance.

Lately, a new multi-stage travelling wave thermoacoustic heat engine TWTAHE was proposed by Bi et al. (2017). It consists of a three-stage travelling wave thermoacoustic heat engine and three linear alternators. The three engine stages were connected end-to-end using slim resonating tubes to achieve a travelling wave acoustic field within the regenerator, which is required in order to obtain an efficient engine. The slim tubes act as inertance tubes, which enhance the phase shifting effect, and therefore, minimize the acoustic losses. The alternators were designed with a dual-opposed arrangement with two linear motors moving in opposite directions; thus, the vibration can be eliminated. The two motors connected as a bypass at the end of each resonating tube as shown in Figure 2.32.

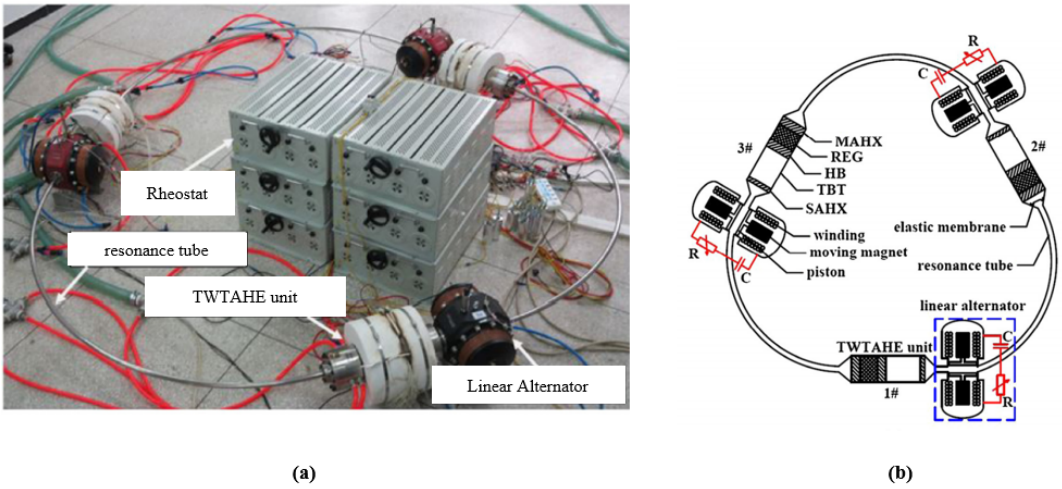


Figure 2.32: The travelling wave thermoacoustic heat engine TWTAHE. (a) A photograph of the system TWTAHE units, the alternators, and the resonance tubes. (b) Schematic diagram showing details of one engine as follows: a main ambient heat exchanger MAHX, a regenerator REG, a heater Block HB, a thermal buffer tube TBT, a secondary ambient heat exchanger SAHX. Each linear alternator formed by these elements: The winding, the moving magnet, and the piston. *R* and *C* denote the resistance and the compliance of the alternator. The elastic membrane only added in the second engine (Bi et al. 2017).

An elastic membrane was installed only in engine 2 to suppress the DC flow. The system used helium at 6 MPa as the working gas. The operating frequency was 70 Hz and the cooling and heating temperatures were 25 and 650°C, respectively. The influence

of the load resistance and the electric capacitance on the system performance was investigated to address the coupling mechanism between the alternators and the system. The preliminary results showed that the acoustic impedance of the linear alternator can be highly influenced by both the electric resistance and electric capacitance, thereby the system performance can be greatly changed. It found that the maximum electricity output of 4.69 kW with 15.6% thermal-to-electric efficiency can be achieved using an electric capacitance of 11.1 μF, and the maximum thermal-to-electric efficiency of 18.4% with electric power of 3.46 kW can be obtained using an electric capacitance of 12.5 μF. Additionally, the highest total electricity output of 3.02 kW can be achieved using 20 Ω load resistance, and the maximum thermal-to-electric efficiency of 14.6% can be obtained using a load resistance of 35 Ω . The most striking observation to emerge from this research is that proper load resistance and electric capacitance are important parameters to achieve an efficient system performance. However, the parasitic heat transfer and the alternator's friction losses were considerably high which dropped the electricity rate.

Another four stages thermoacoustic Stirling power generator in a looped tube arrangement was systematically studied by Wang and Qiu (2017). A numerical model for the system was developed to investigate the coupling characteristics of the linear alternators, and the regenerators on the overall performance. The system comprised four thermoacoustic cores and four linear alternators as presented in Figure 2.33, and operated at 70 Hz frequency using 3 MPa pressurized helium as the working gas. Three coupling modes of the alternators were investigated: near the cold end of the thermoacoustic core, in the middle of the resonator, and near the hot end of the core. It was observed that, more electrical power was delivered when the alternators were installed next to the cold side of the thermoacoustic core, while less power was obtained when the alternators were coupled at the middle of the resonators. The worst performance resulted from the high pressure amplitude at the middle of the resonator as seen in Figure 2.34, which in turn caused high acoustic dissipation. The data showed that the thermoacoustic prototype can produce up to 1223 W electrical power with the hot-end coupling mode, and the corresponding relative Carnot efficiency was 20%.

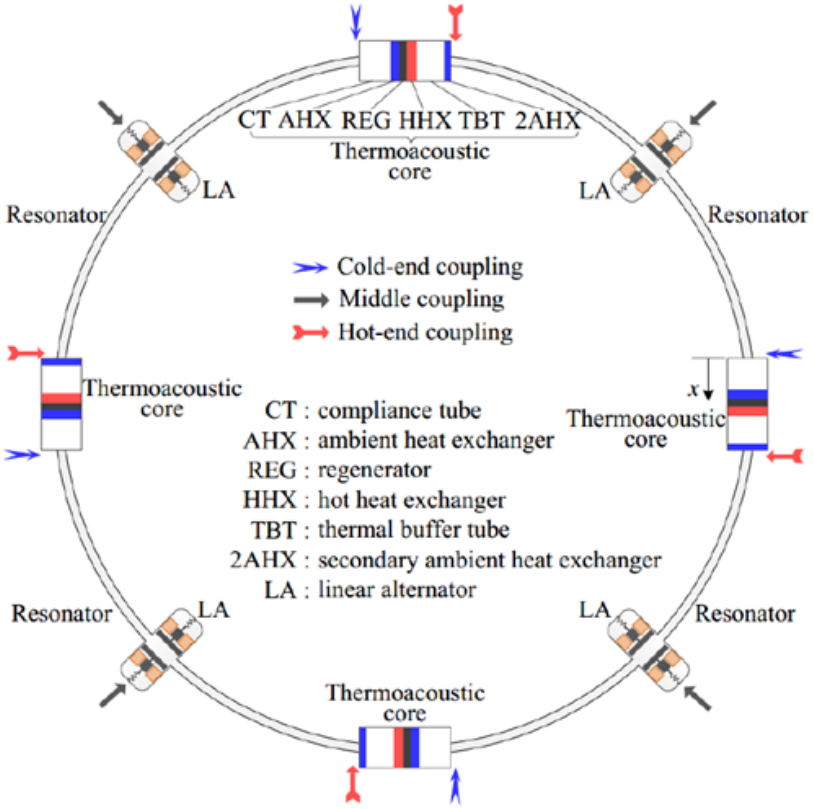


Figure 2.33: Schematic illustration of the four stages thermoacoustic Stirling power generator, where the components of the system are shown: each stage has thermoacoustic core, a linear alternator and a resonator. Each core consists of compliance tube, ambient heat exchanger, regenerator, hot heat exchanger, thermal buffer tube and a secondary ambient heat exchanger. The three modes used to coupled the alternator to the engine stages are also illustrates with coloured arrows. A key is provided in the middle of the diagram (Wang and Qiu 2017).

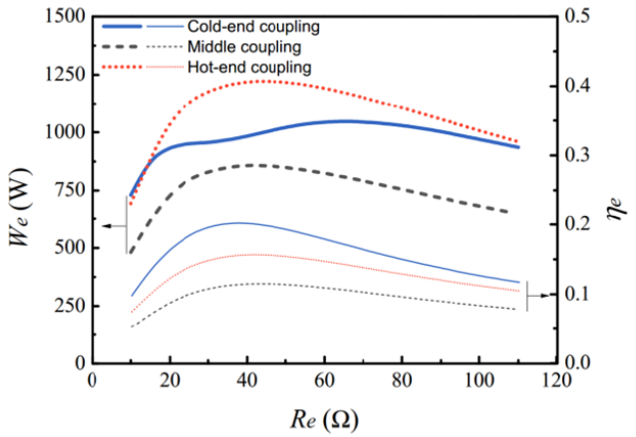


Figure 2.34: DeltaEC results for the electrical power output, W_e, and the corresponding relative Carnot efficiency, η_e, as a function of the loud resistance of the alternator, R_e, when three different coupling modes of the alternators were utilized: hot-end, middle, and cold-end (Wang and Qiu 2017).

Furthermore, it was realized that the location of the regenerator has a significant effect on the electricity output, and therefore, the overall performance of the system as illustrated in Figure 2.35. The position of the regenerator was adjusted by varying the length of the compliance tube (named as CT in Figure 2.35). Also, the length of the thermal buffer tube was also adjusted in order to maintain the same total length of the loop. The contribution of this study has been to confirm the impact of regenerator position on the overall performance. Besides, the length of the compliance tube should be selected carefully depending on the design target.

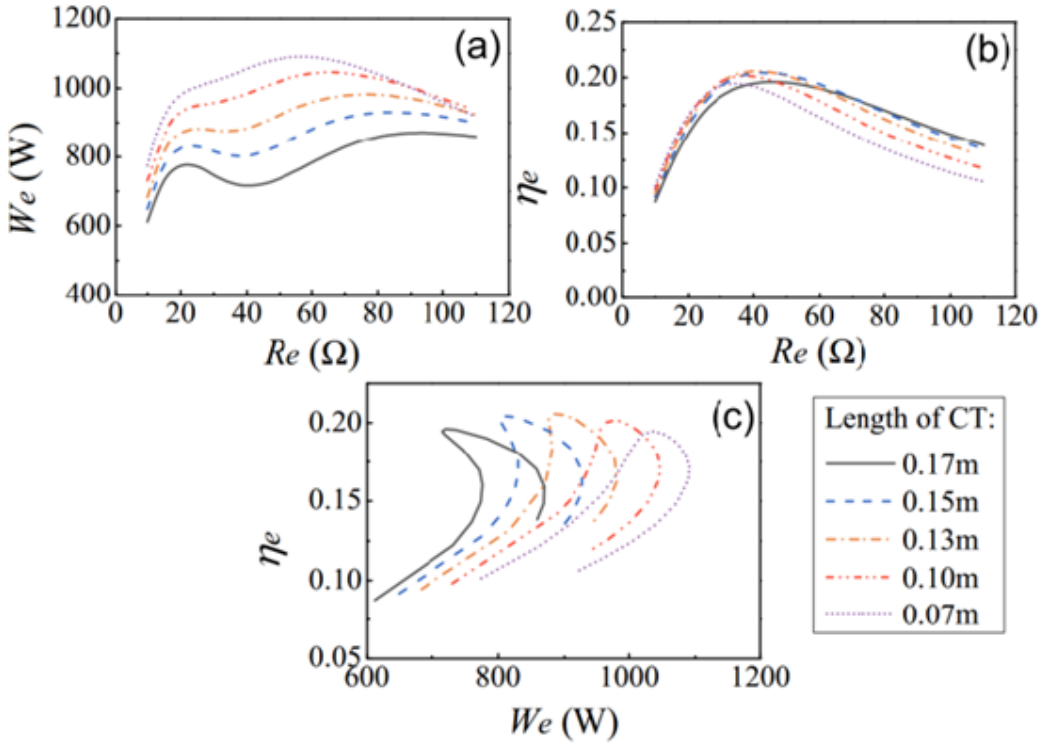


Figure 2.35: DeltaEC results for the electrical power output, W_e, and the corresponding relative Carnot efficiency, η_e, of the four staged thermoacoustic Stirling power generator, when the position of the regenerator was changed by varying the length of the compliance tube (CT) in the range of 0.07 to 0.17 m. (a) Electrical power output as a function of the load resistance of the alternator R_e. (b) Relative Carnot efficiency as a function R_e. (c) Relative Carnot efficiency as a function of the electrical power W_e (Wang and Qiu 2017).

Table 2.1: Summary of the work done so far in electricity generation using thermoacoustic technology.

Author and year	TA units	Frequency (Hz)	Pressure (bar)	Acoustic power (W)	Electric power (W)	Thermal-to-electrical efficiency (%)
Air-filled resonator						
Yu, Jaworski and Backhaus (2010*b*)	1	75	1	Not reported	5.18	0.65
De Blok (2010)	4	70	1	17.6	5.4	0.27
Yu, Jaworski and Backhaus (2012)	1	70	1	27	11.6	1.3
Chen et al. (2012)	2	72	1	460	15	0.59
Chen et al. (2012)	2	80	1.5	65.2	22.7	1.13
Abdoulla-Latiwish, Mao and Jaworski (2017)	1	64	1	221	17.8	1.9
Helium-filled resonator						
Backhaus, Tward and Petach (2004)	1	120	55	77.3	58	18
Telesz (2006)	1	100	31	109.6	70	16.8
Wu et al. (2011)	1	74	35.4	Not reported	1640	8.2
Wu et al. (2012)	1	74	35.4	Not reported	200	12.7
De Blok and Systemen (2012)	4	40		Not reported	200	12.7
Sun et al. (2013)	1	65	30	Not reported	345.3	9.34
Wu et al. (2014*a*)	3	86	50	4131.6	1570	16.8
Wang et al. (2015)	1	66	24.8	1425	473.6	14.5
Kang et al. (2015)	2	171	18	864	204	3.34
Wang et al. (2016)	2	65.5	31.6	Not reported	750.4	16.3
Bi et al. (2017)	3	70	60	6500	4690	15.6
Wang and Qiu (2017)	4	70	30	1900	1223	
Helium/Argon filled resonator						
Wu et al. (2014*b*)	1	64	40	1865	1043	17.7

2.5 Concluding Remarks

In this chapter, the review of the relevant research work in the field of thermoacoustic technology have been explored. Particular attention has been paid to the early history and technical development in thermoacoustics, the invention of thermoacoustic engines for capturing waste heat and electricity generation. The current research focuses on providing electric power to the remote and rural area of South Sudan country where access to the electricity grid is minimal. Since the target is rural households, the working gas will be air. However, as discussed in section 3.4 and 3.5, the most powerful systems were operated with inert gases, and those who used air at atmospheric pressure produced a maximum electricity output of around 18 W. Therefore, the capability of improving the power output from air-filled thermoacoustic systems to acceptable levels represents the primary goal of the current research and presents a challenging question that needs to be answered. Perhaps the most serious limitation of using the air-filled engines is the cost due to the nature of the application. Additionally, the system has to be of simple construction; thus, it can be manufactured and assembled locally. The literature search (particularly section 3.3) highlights that the looped-tube travelling wave thermoacoustic engine coupled with a commercially available inexpensive audio loudspeaker(/s) is a highly attractive solution in these circumstances. It might be beneficial for its standing alone nature, simplicity, and the affordability of using a looped tube configuration for the thermoacoustic engine. However, the wave performance throughout the system is very complex, which requires numerical investigations together with the experimental tests. As identified in the literature, the software package DeltaEC is accurate and can help to simulate complex wave equations throughout the parts forming the thermoacoustic system of interest; thus it will be used to develop the theoretical models.

CHAPTER 3

THEORETICAL BACKGROUND OF THERMOACOUSTIC SYSTEMS

3.1 Introduction

This research focuses on thermoacoustic systems to demonstrate the feasibility of producing the required electrical power from acoustic energy. Before the details of this work are explained, it is necessary to introduce the different types of thermoacoustic systems. Also, to understand which principles of thermoacoustics are essential for the design and operation of these systems, and useful for achieving energy conversion. At the beginning of this chapter in section 2.2, the classification of thermoacoustic systems is described. In section 2.3, the scale lengths that are crucial to the performance of thermoacoustic systems are explained. Following that, the linear thermoacoustic is discussed in section 2.4. The concept of acoustic streaming and its impact on system performance is discussed in section 2.5, together with the observation of turbulence in oscillatory flow. Section 2.6 deals with the production of electricity from thermoacoustic power. Section 2.7 provides details about modelling of thermoacoustic systems using DeltaEC software. General comments are presented to conclude the chapter in section 2.8.

3.2 Classification of thermoacoustic systems

Generally, thermaocoustic systems can be categorized under two main groups: thermoacoustic engines and thermoacoustic refrigerators/coolers, based on the direction of energy conversion between the heat energy and the acoustic power within the porous media (Swift 1988*b*). Thermoacoustic engines use an acoustic wave to prompt the compression and expansion of the working gas. When an acoustic wave propagates across a

porous media with a temperature gradient across its ends, it generates acoustic power as a result of the displacement of the gas parcels caused by the velocity component of the acoustic wave. Thus, the gas is transported from a high temperature region to a colder region. Alternatively, thermoacoustic refrigeration works by using an acoustic wave to create a hydrodynamic heat pumping effect, which in turn generates a temperature gradient across a porous structure in the direction of the acoustic wave propagation. The temperature gradient in the heat pump is typically much lower than in the heat engine. Figure 3.1 presents the two basic types of heat engines.
It is noteworthy that the refrigerator performs similar functions as the heat pump. The only one difference between them is of the working temperatures. The operating temperatures in the refrigerator are of the colder level and atmosphere, whereas the operating temperatures in the heat pump are of hotter level and atmosphere.

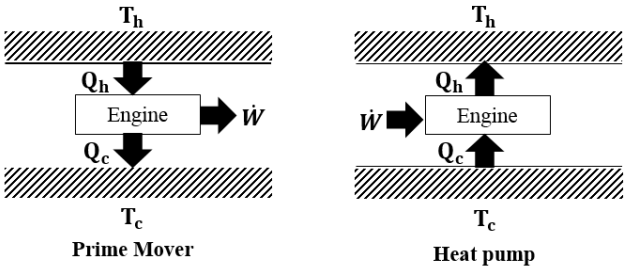


Figure 3.1: Illustration of the two major types of heat engines, the prime mover and the heat pump. The word "Engine" in the central circle is used generally to include both types of heat engines. Q denotes heat, c and h are cold and hot, T for temperature, and Q is for work.

It is usual to use the wave type to classify the thermoacoustic systems into: travelling wave thermoacoustic devices where the oscillating pressure and the velocity of the gas along the regenerator are in phase, as shown in Figure 3.2, and pure standing wave devices where the velocity of the gas across the stack is 90 degrees out of phase with the oscillating pressure, as in Figure 3.3. Wheatley, Swift and Migliori (1986*a*) categorized the thermaoacoustic systems depending on the wave type as well as the device functionality: whether the device was of the power producing type or of the power consuming type. Therefore, thermoacoustic systems could be classified into four types as follows: Standing Wave Engine, Travelling Wave Engine, Standing Wave Refrigerator, Travelling Wave Refrigerator.

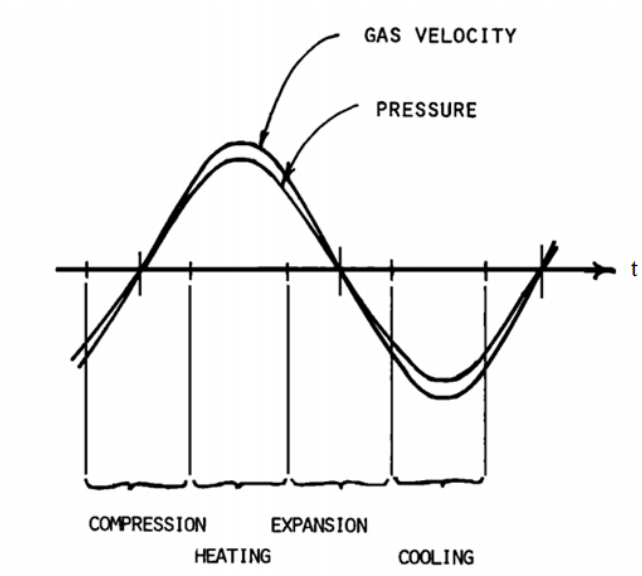


Figure 3.2: Pressure and velocity as a function of time, t, in a gas through which a travelling wave exists. As illustrated, the gas undergoes a thermodynamic cycle of four processes: compression, heating, expansion, and cooling, which is the same as what occurs in the Stirling engine (Ceperley 1979).

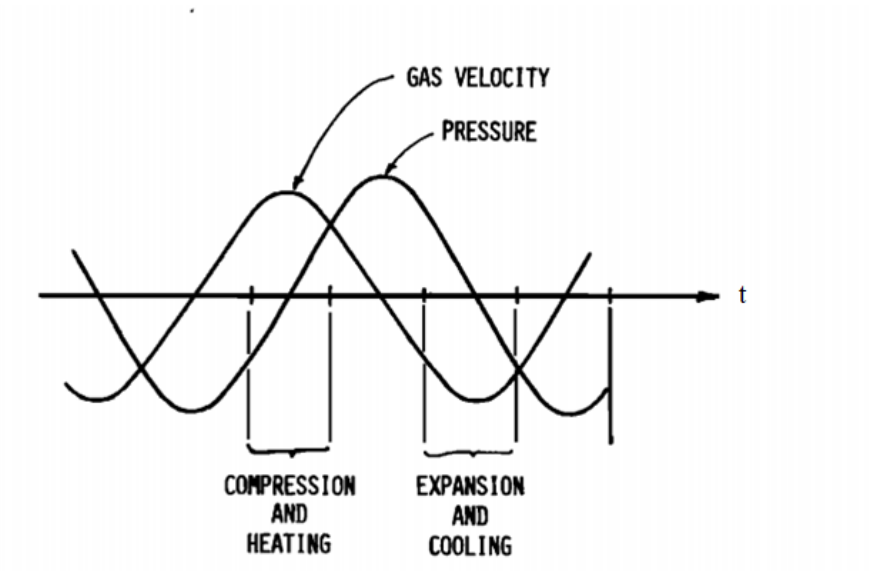


Figure 3.3: Pressure and velocity as a function of time, t, for a gas in which a standing wave propagates exists. As illustrated, compression and heating of the gas are simultaneous, expansion and cooling also happen simultaneously (Ceperley 1979).

The thermodynamic cycle of the standing wave devices is similar to the Brayton cycle (Dunn et al. 2015; Poese et al. 2004) as shown in Figure 3.4 comprising two reversible adiabatic processes and two constant pressure processes, while in the travelling wave devices the movement of the gas parcels is comparable to the Stirling cycle as in Figure 3.5, which consists of two constant temperature processes and two reversible constant volume processes.

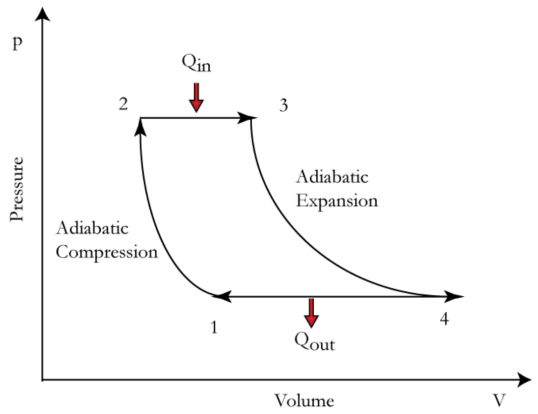


Figure 3.4: P-V diagram of the ideal Brayton cycle. As presented, the cycle comprises four processes: 1-2 is adiabatic compression, 2-3 is addition of heat at constant pressure, 3-4 is adiabatic expansion, and 4-1 is heat rejection at constant pressure.

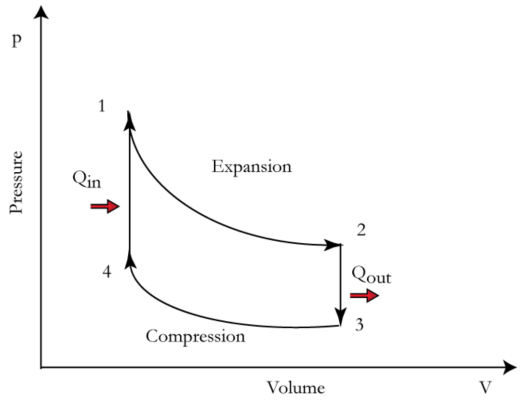


Figure 3.5: P-V diagram of the ideal Stirling cycle where the numbers are corresponding to the thermodynamic processes of the cycle: 1-2 is isothermal expansion, 2-3 is heat removal at constant volume, 3-4 is isothermal compression, and 4-1 is heat addition at constant volume.

This thesis explores the performance of a looped tube travelling wave thermoacoustic engine with different configurations using experimental techniques and advanced acoustic models. Therefore, the thermoacoustic prime movers type is the main focus rather than the thermoacoustic coolers. A detailed explanation of the thermodynamic cycles of the standing wave engine and the travelling wave engine is introduced in the next sections.

3.2.1 Standing wave or stack-based engines

Thermoacoustic engines are devices whose main function is to convert thermal power into mechanical energy utilising the so-called thermoacoustic effect. Generally, in a thermoacoustic engine, heat is added to the hot end of the stack (or the regenerator) via the hot heat exchanger, thus the gas parcels carry heat from the hot heat exchanger to the hot end of the stack/regenerator. Heat is transferred further towards the cold heat

exchanger and to certain locations between the hot and cold ends of the stack/regenerator by the gas parcels which receive heat from the solid material of the regenerator. After this point, the gas parcels transfer heat to the regenerator wall, which is found near the regenerator cold side. Therefore, an axial temperature gradient will be created across the hot and cold ends of the stack. When the thermoacoustic onset conditions are met, the acoustic oscillations arise spontaneously until it approaches a steady state.

The research studies on thermoacoustic systems conducted firstly on the design and fabrication of the standing wave type because of their simple arrangement. The schematic diagram and the working principles of a standing wave thermoacoustic engine are illustrated in Figure 3.6. The engine consists of a stack which is sandwiched between hot and cold heat exchangers, and all these components are placed inside a half wave-length ($\lambda/2$) gas filled resonator. Intense oscillating pressure and velocities are generated along the resonator as a result of the large temperature gradient ΔT across the stack. Electrical power could be extracted from the acoustic power contained in the resonator by means of electrodynamic transduction mechanisms such as a linear alternator.

Figure 3.6(b) shows the thermoacoustic effect on one gas parcel in the channels between the stack plates. The temperature of the stack surface is higher than the temperature of the gas parcel near the hot side, and the opposite is right near the cold side. The gas parcel firstly undergoes an adiabatic compression. It travels from the cold side to the hot side as a result of the high temperature difference. The new pressure amplitude increases to double the initial pressure and consumes an acoustic power of dW with an increase in the volume and an increase in the temperature from T^- to T^+. After that, the gas parcel experiences irreversible heat transfer dq from the adjacent solid wall of the stack at constant pressure, as indicated by point 2 in the time-position diagram Figure 3.7. As a result, the temperature of the gas parcel increases further to T^{++}. Following this, the gas parcel expands adiabatically and produces an acoustic power of dW^+ and its temperature drops to T. Heat dq starts flowing from the gas parcel to the adjacent stack wall which makes the temperature of the parcel to drop to T^- without any change in the pressure (point 4 in Figure 3.7). This brings the gas parcel back to its initial condition and the thermodynamic cycle can be repeated again as long as the temperature gradient through the stack is maintained. $dW^+ - dW$ represents the net acoustic power generated from the cycle. 2ξ is the peak to peak displacement of the gas parcel.

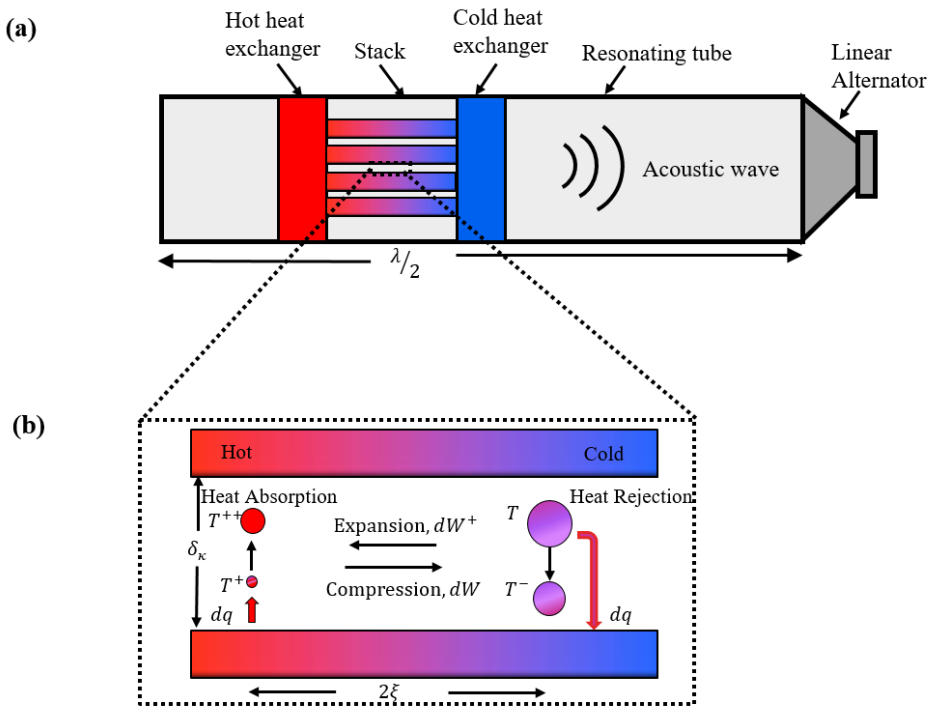


Figure 3.6: The thermoacoustic effect within a standing wave thermoacoustic system. (a) Schematic drawing of the system where the main components are shown. (b) An enlarged view to show the thermoacoustic effect on a single gas parcel in the stack during "standing wave" displacement towards the cold side.

By virtue of the thermoacoustic effect, the system absorbs amounts of heat at the higher temperature T_h and rejects amounts of heat at a low temperature of T_c, and delivers acoustic power $P_{Ac.}$. Pure standing wave engines have a phase difference of 90 degrees between the pressure and velocity amplitudes of oscillation. However, this phase difference is less than 90 degrees in practical standing wave engines to allow acoustic power flow to the acoustic load. Furthermore, in practical applications, the thermal expansion of the gas parcel takes place at a higher pressure than the thermal contraction presented in the P-V diagram Figure 3.7 (b). Accordingly, $\oint pdV > 0$, which indicates that the gas has done work on the surroundings, and the system can deliver an amount of acoustic power greater than zero.

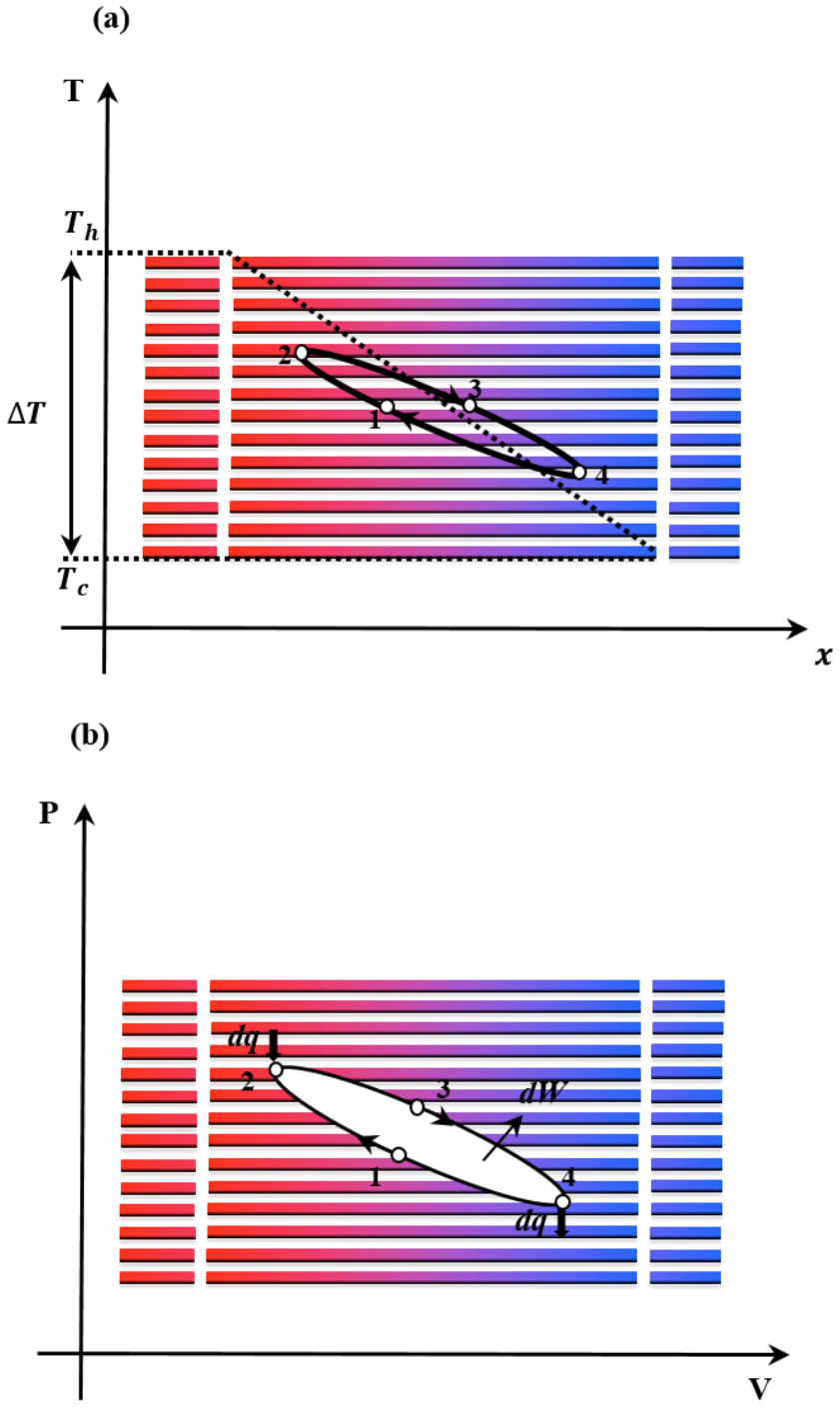


Figure 3.7: The thermoacoustic effect in standing wave thermoacoustic engine. (a) Temperature T versus position x of stack and temperature versus position and time for a gas parcel within a standing wave thermoacoustic engine. The ellipse illustrates the change in the temperature of the gas parcel, while the dotted line presents the temperature gradient across the stack ΔT which is the difference between the hot side and cold side temperatures T_h and T_c, respectively. (b) P-V diagram, where dq is the heat transfer, and dW is the work done.

It can be noted that each fluid parcel inside the stack acts like a "bucket brigade" (see Figure 3.8); this is because each of the parcels absorbs an amount of heat from one location within the stack and rejects it to another neighbouring location. Therefore, an effective heat transfer can be generated from one side of the stack to the other as a result of the combination of the small thermoacoustic effects in each gas parcel.

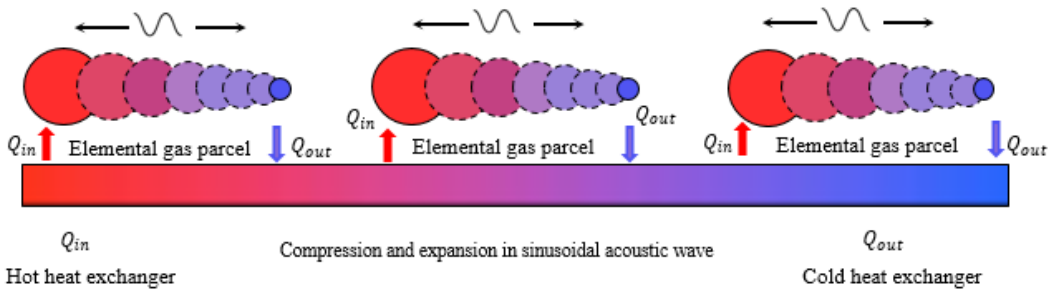


Figure 3.8: Temperature gradient created along the stack plates as a result of the bucket-brigade effect. As seen with colors, the gas parcel is heated (red) when it is in close contact with a high-temperature plate and is cooled (blue) when the parcel in direct contact with a plate of a temperature lower than the gas. Consequently, the acoustic wave get amplified [adapted from (Avent and Bowen 2015)].

In the standing wave thermoacoustic device, the thermal contact and heat transfer between the gas parcel and the stack plates must be deliberately imperfect, to enable the thermal expansion and rarefaction to be in the same phase with the oscillating pressure and displacement or 90 degrees out of phase with the velocity amplitude of oscillation. The imperfect thermal contact can be obtained when the gaps between the stack plates is roughly a few δ_κ. If it were good enough, the temperature of the gas parcel would be equal to (or near) the temperature of the adjacent plate; if too weak, no thermal expansion/contraction or work would take place. In addition, the exchange of heat only happens at the peaks of the gas parcel's displacement which causes an inherent irreversibility, and therefore, degrades the thermoacoustic efficiency of the system. With such phasing, the thermoacoustic effect in the P-V diagram Figure 3.7 (b) would turn into a reciprocating line rather than a narrow ellipse, and no work would occur. A standing wave device with a perfect regenerator will not perform because the oscillating pressure and velocity are not in phase (Riley 2014*b*).

In conclusion, standing wave thermoacoustic engines have been utilized to generate acoustic energy from thermal power. This type of engine is agreed to be fundamentally inefficient because of the limitation of the intrinsically irreversible thermodynamic cycle (Backhaus and Swift 2000). The maximum thermal efficiency achieved according to the open literature was only 18% (Swift 1992). According to the principles of thermodynamics and in order to increase the thermal efficiency of the standing wave engine, the heat transfer between the gas parcel and the stack solid material should be

enhanced. In contrast, the most important design characteristic of the standing wave engine is the imperfect heat transfer which causes the required time condition between the pressure and the velocity to obtain the desired phase to sustain the oscillation (Swift 1992).

3.2.2 Travelling wave or regenerator-based engines

One more type of thermoacoustic heat engine is known as the travelling wave or thermoacoustic-Stirling engine. Travelling wave thermoacoustic devices became the focus of great research interest to overcome the efficiency limitation of the standing wave thermoacoustic engines, and to improve the efficiency of the traditional Stirling engine, as well as simplifying its design and minimizing the number of moving parts the engine contains. The travelling wave thermoacoustic engine is similar to the standing wave engine in its working principles; both of the engines generate acoustic power from thermal energy. However, the second thermodynamic medium in the travelling wave engine called "regenerator" differs from the stack in the standing wave engine.

The key principle of the travelling wave engines is that the gas parcels within the regenerator undergo a thermal expansion thermodynamic process when the pressure is maximum, and a thermal contraction process when the pressure is minimum. Consequently, the working gas in the regenerator does useful work in each acoustic oscillation cycle and generate acoustic power. In the conventional Stirling engine, the oscillating gas motion and oscillating pressure are caused by the moving pistons. However, they can also occur spontaneously without using pistons, as long as the temperature difference along the regenerator is large enough.

The thermodynamic cycle of the travelling wave engine differs from that of the standing wave engine. The travelling wave engine is typically an ideal reversible process with the capacity for high thermal to acoustic conversion (Ceperley 1979). The travelling wave dominates oscillating pressure in phase with velocity, and an excellent thermal contact is crucial to ensure that the temperature of gas parcel is always equivalent to that of the solid plate at a certain location (Backhaus and Swift 1999). Broadly, a travelling wave thermoacoustic engine comprises a core and an acoustic resonator. The engine core consists of a regenerator in between two heat exchangers (hot and cold). Heat is extracted from the heat source through the hot heat exchanger, while the ambient heat exchanger is to remove heat from the gas to an external heat sink at the ambient temperature. The hot and ambient heat exchangers build up and maintain a steep temperature gradient across the regenerator where the thermoacoustic effect takes place, and thermal energy is converted into acoustic power.

The regenerator is the medium that is responsible for providing the required time-phasing between the pressure and the velocity amplitudes in travelling wave systems

Ceperley (1985). It consists of very thin pores that are made of a porous material, so the gas and the solid temperatures within the regenerator can be assumed to be equal, thus providing excellent thermal contact. Good thermal contact can be achieved by having a regenerator of a channel size less than the thermal penetration depth. Four processes form the complete thermodynamic cycle that the fluid parcel undergoes in a travelling wave engine as shown in Figure 3.9. At the beginning, the gas parcel will be compressed adiabatically near the hot end of the regenerator before absorbing heat at constant volume from the regenerator surface due to the high temperature gradient and the excellent thermal contact. After that, the gas parcel adiabatically expands while it moves toward the cold end of the regenerator. The parcel moves further towards the cold end, almost exhausting heat at constant volume to the wall due to the temperature difference. In the last step, the parcel compressed isothermally with heat rejection to the wall. The elliptical shape represents a real thermoacoustic engine cycle with a notable overlap between compression and heat absorption, and an overlap between expansion and heat rejection.

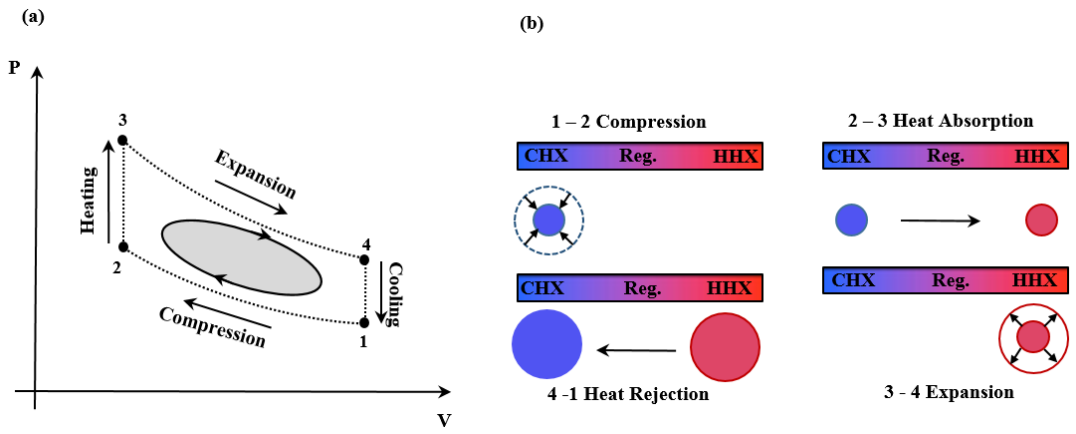


Figure 3.9: The thermodynamic cycle that one gas parcel undergoes during its oscillation within the regenerator in a travelling wave thermoacoustic engine. (a) P-V diagram of the cycle where the oval shape represents the travelling wave engine and the cycle numbered from 1 to 4 illustrates the Stirling cycle. (b) The thermodynamic processes undertaken by a fluid parcel during its travel from the cold side to the hot side. CHX is for cold heat exchanger, Reg. is regenerator, and HHX is for the hot heat exchanger [Adapted from (Yu, Backhaus and Jaworski 2009)].

Unlike the standing wave engine, Figure 3.9(b) illustrates using colors that the solid wall of the regenerator and the gas parcel have similar temperatures at each point because of the small size of the flow channels. This makes the gas parcel to displace towards the hot end and experience thermal expansion when the pressure is higher, and similarly, the gas parcel moves towards the cold end and undergoes thermal contraction when the pressure is lower, leading to amplification of the acoustic power. Another key benefit of the travelling wave engine is its onset temperature (defined as the difference between

the hot and cold temperatures along the regenerator at the time when the oscillation starts) which is considerably less than that of standing wave engine when they work at the same frequency and wavelength due to the excellent thermal contact between the gas and the solid surface.
The regenerator in a travelling wave engine functions as an acoustic amplifier, where the acoustic power gets amplified with a ratio proportional to the ratio of the hot and cold temperatures across the regenerator, T_H/T_C (Backhaus and Swift 2000).

3.3 Critical performance scales and parameters

There are several useful length scales and parameters in the design and the operation of thermoacoustic systems. In a thermoacoustic system, the operation of the device is affected by its dimensions and the thermophysical properties of the working fluid. The physical properties includes the ratio of specific capacities, thermal conductivity, density, viscosity, Prandtl number, isothermal and adiabatic bulk modulus, toxicity, and impact on the environment. In this section, theses critical parameters will be defined and explained.

3.3.1 Wavelength, wave amplitude and frequency

The wavelength, λ, can be defined as the separation of the wave from crest-to-crest, or it is the distance over which the waves shape repeats. The wave amplitude is the height of the wave or the distance from one crest to the principle axis. The relationship between wavelength and frequency can be expressed as follows:

$$\lambda = \frac{a}{f} \tag{3.1}$$

Here: a is the speed of sound (m/sec), f is the oscillating frequency (Hz). λ is the wavelength (m) and it is determined by the length of the resonating tube. In general, the standing wave thermoacoustic systems are built to operate in a quarter-wavelength, half-wavelength or full-wavelength mode.

The speed of the sound, a, for ideal gases can be defined as follows:

$$a = \sqrt{\frac{\gamma P_m}{\rho_m}} = \sqrt{\gamma R T_m} \tag{3.2}$$

Where: γ is the ratio of isobaric to isochoric specific heats, P_m is the mean pressure of the working gas (Pa), T is the mean temperature of the gas in (K), ρ_m is the mean density of the gas (kg/m^3), R is the gas constant (J/kg.K). From Equation 3.2, it is obvious that the speed of sound depends strongly on the type of working fluid as well as its temperature. Therefore, the size of the system / operating frequency and the choice

of the working gas should be determined early in the design stage of any thermoacoustic device because they are related to other important characteristic parameters.

3.3.2 Thermal penetration depth

There are two more important characteristic lengths in the direction perpendicular to the gas motion, referred to as thermal and viscous penetration depths. The thermal penetration depth, δ_κ, is approximately the distance that heat can diffuse laterally through the gas during a given time interval and it is related to the frequency of oscillation and the properties of the working gas. The thermal penetration depth is expressed as:

$$\delta_\kappa = \sqrt{2k/\omega\rho c_p} = \sqrt{2\alpha/\omega} \tag{3.3}$$

Here: k and α are the thermal conductivity and thermal diffusivity of the working gas, respectively. c_p is the specific heat of the working gas per unit mass at constant pressure. The thermal penetration length is crucial in understanding the heat exchange component in thermoacoustic systems, because the diffusive heat transport between the working gas and the nearest solid boundary is only significant within this region (Garrett 2004).

3.3.3 Viscous penetration depth

The viscous penetration depth, δ_ν, represents the distance over which viscous shear forces diffuse laterally during a time interval of the order of the oscillation divided by π. The viscous penetration depth is expressed as follows:

$$\delta_\nu = \sqrt{2\mu/\omega\rho} = \sqrt{2\nu/\omega} \tag{3.4}$$

Here: μ and ν are the dynamic and kinematic viscosities of the working gas, respectively. Viscous shear forces occur within this boundary layer thickness, which dissipates part of the acoustic power of the system. The square of the ratio of the viscous penetration depth to the thermal penetration depth gives the Prandtl number, σ, which is the ratio of kinematic viscosity to thermal diffusivity of the gas. In the thermoacoustic field, Prandtl can be used to characterise the relative magnitude of the viscous and the thermal effects.

$$\left(\frac{\delta_\nu}{\delta_\kappa}\right)^2 = \frac{\mu c_p}{\kappa} = \sigma \lesssim 1 \tag{3.5}$$

Where c_p is the isobaric heat capacity per unit mass. A lower Prandtl number leads to a more beneficial balance between viscous dissipations and thermal efficiency. The selection of a working fluid is therefore crucial to the performance of the thermoacoustic systems. For typical gases, the Prandtl number is close to unity. Therefore, viscous and thermal penetration depths are comparable. The thermal and the viscous depths are

very important in thermoacoustic processes because they determine the required plate spacing within the stack or regenerator. Therefore, at a distance much larger than these depths from the solid boundary (e.g. plates of stack), there is no thermal or viscous contact between the gas and the solid boundaries.

3.3.4 Gas parcel displacement amplitude

Another important length in the direction of the wave propagation is the displacement amplitude of the gas parcel, $|\,\xi_1\,|$, which is the ratio of velocity amplitude, $|\,u_1\,|$, to the wave angular frequency, ω.

$$|\,\xi_1\,| = \frac{|\,u_1\,|}{\omega} = \frac{|\,u_1\,|}{2\pi f} \tag{3.6}$$

Here: $|\,u_1\,|$ is the velocity amplitude of the working gas (m/sec), f is the working frequency (Hz), ω is the angular frequency ($\sec^{-1}$).

The peak-to-peak displacement amplitude, $2\,|\,\xi_1\,|$, can be defined as the maximum displacement of the gas parcel in x-direction during each acoustic cycle. In thermoacoustic devices, the displacement amplitude is always shorter than the wavelength, λ, and is much larger than the thermal and viscous penetration depths, δ_k and δ_v. (Swift 1988*b*).

$$\delta_\kappa, \delta_\upsilon \ll |\,\xi_1\,| \ll \lambda \tag{3.7}$$

Generally, the gas displacement amplitude is selected to be an appropriate length of the heat exchanger in the thermoacoustic devices. The heat transfer mechanisms with different lengths of heat exchangers are shown in Figure 3.10. If the length of the heat exchanger equals to peak-to-peak displacement amplitude $2\,|\,\xi_1\,|$, heat will be transferred from the right end of the stack to the right side of the heat exchanger. However, having a heat exchanger with a length of less than $2\,|\,\xi_1\,|$ will allow some gas parcels from the end of the stack to "overshoot" the heat exchanger. Thereby, heat is not efficiently transferred by these gas parcels to and from the heat exchanger. In contrast, if the length of the heat exchanger is greater than $2\,|\,\xi_1\,|$, some parcels will oscillate completely in the heat exchanger. These parcels don't directly affect the heat exchange between the stack and the heat exchanger.

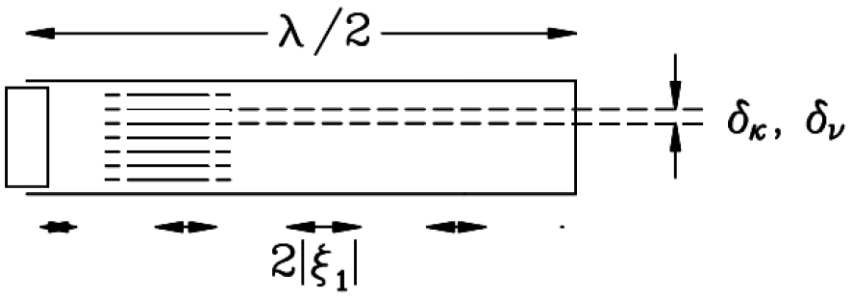


Figure 3.10: Schematic of a thermoacoustic system showing some of the important length scales: The wavelength λ, the peak-to-peak displacement amplitude $2 \mid \xi_1 \mid$, the thermal and viscous penetration depths δ_κ and δ_ν, respectively.

3.3.5 Mean pressure of the system

The internal mean pressure has a strong influence on the performance of the thermoacoustic systems. Increasing the internal mean pressure would increase the compression and the rarefaction effects of the gas parcels. Therefore, the acoustic power can be increased significantly by increasing the operating mean pressure because the power density is proportional to the mean pressure of the working gas ($P_{Ac.} \propto P_m$) (Ceperley 1979). Also, acoustic dissipations increase rapidly as mean pressure decreases. However, the design of the resonator pipe should be selected to stand the high pressures, which means that the total cost of the engine is higher. Moreover, increasing the mean pressure decreases the thermal boundary layer around the solid wall where the thermal interaction between the gas parcels and the solid plate takes place. The relationship between the thermal penetration depth and the mean pressure of the working gas can be written as:

$$\delta_k \propto \frac{1}{\sqrt{P_m}} \tag{3.8}$$

High mean pressure requires small penetration depth which results in small flow channel of the regenerator which in turn adds difficulties to the design (Yu, Jaworski and Backhaus 2010*a*). Furthermore, Hariharan, Sivashanmugam and Kasthurirengan (2013) discovered that, for a dual core thermoacoustic engine, the onset temperature at which the acoustic oscillations starts, increased with an increase in the mean pressure. The critical temperature gradient, $\Delta T_{critical}$, is given as follows:

$$\Delta T_{critical} = \frac{\omega A |p_1|}{\rho_m c_{p,s} |U_1|} \tag{3.9}$$

Where: A is area, ρ_m is the mean density of the fluid, $c_{p,s}$ is the specific heat capacity of the solid plate, $|p_1|$ and $|U_1|$ are the peak pressure and volumetric flow rates of oscillation, respectively. The sensitivity of temperature gradient to changes in the mean

pressure can be clearly realized, since the mean density is also a function of the mean pressure.

3.3.6 Acoustic pressure amplitude ratio

Acoustic pressure amplitude ratio, "also known as Drive ratio", is an important parameter for evaluating the strength of self-excited oscillations in thermoacoustic systems (Shen et al. 2009). It represents the percentage of the oscillating acoustic pressure, $|p_1|$, to the mean pressure, p_m:

$$DR = \frac{|p_1|}{p_m} \times 100\% \tag{3.10}$$

The oscillating pressure, p_1, can be related to the mean pressure of the working gas as follows:

$$p_1 = -\frac{\gamma \Delta U_1}{i\omega A \Delta x} p_m \tag{3.11}$$

3.3.7 Acoustic power

Power can be shown using the products of first-order variables such as the pressure amplitude, p_1, and the volumetric velocity amplitude, U_1. Introductory acoustic books expressed general acoustic intensity, $I_{Ac.}$ as:

$$I_{Ac.} = \frac{\omega}{2\pi} \oint Re[p_1 e^{i\omega t}] Re[u_1 e^{i\omega t}] dt = \frac{1}{2} Re[p_1 \widetilde{u_1}] \tag{3.12}$$

Acoustic intensity is defined as the time-averaged acoustic power per unit area in an acoustic wave. In thermoacoustics, great care should be taken to identify the type of energy and power such as heat, enthalpy, etc.
Swift (2003) showed the integral of the acoustic intensity across the cross-sectional area of the channel which gives the acoustic power flowing in x-direction as:

$$\dot{E}_2(x) = \frac{\omega}{2\pi} \oint Re[p_1(x) e^{i\omega t}] Re[U_1(x) e^{i\omega t}] dt \tag{3.13}$$

$$= \frac{1}{2} Re[p_1 \widetilde{U_1}] = \frac{1}{2} Re[\widetilde{p_1} U_1] \tag{3.14}$$

$$= \frac{1}{2} |p_1||U_1| \cos(\phi_{pU}) \tag{3.15}$$

Where: ϕ_{pU} is the phase angle between the pressure amplitude, p_1, and the volumetric velocity amplitude, U_1. The tilde "$\sim$" denotes complex conjugation, and the subscript "2" refers to the second order which is the product of the two first order quantities, p_1 and U_1.

3.3.8 Efficiency of the system

In a travelling-wave thermoacoustic engine, the hot heat exchanger is used to supply heat, $\dot{Q}_h$, to the engine at a high temperature of T_H. Acoustic power is then being produced in the regenerator by the thermoacoustic phenomena, and heat, $\dot{Q}_c$, is rejected from the engine via the cold heat exchanger at a low temperature of T_C. The well-known Carnot thermal efficiency of temperatures serves as a useful measures of efficiency for the simplest thermodynamic systems, such as the simple heat engine. The Carnot ratio is given as:

$$\eta_{Carn.} = 1 - \frac{T_C}{T_H} \tag{3.16}$$

Typically, thermoacoustic prime movers and coolers that were developed for high efficiency have operated at or above 20% of Carnot thermal efficiency; as of early 2001, the highest reported efficiency represents 40% of Carnot thermal efficiency (Backhaus and Swift 1999; 2000) .

3.4 Thermoacoustic linearisation and Rott's approximation

Rott (1969; 1973; 1975; 1980) was the first to introduce the linear thermoacoustic theory. The theory was developed to apply to thermally generated oscillations, but it can be applied also to thermoacoustic refrigerators. The linear theory can be used to predict the performance of a thermoacoustic system under low pressure amplitude of the acoustic oscillation. However, when the amplitude of the oscillation is high (higher than 3% of the mean pressure), the accuracy of linear theory predictions compared to the measurement substantially decreases. This may be caused by non-linear effects, minor losses, acoustic streaming, or turbulence occurring in the system. The linear theory is based on the linearisation of the continuity, momentum and energy equations. As shown in Figure 3.11. below, a stack is sandwiched between an ambient and a hot heat exchanger, all inside a half-wavelength resonator of length L.

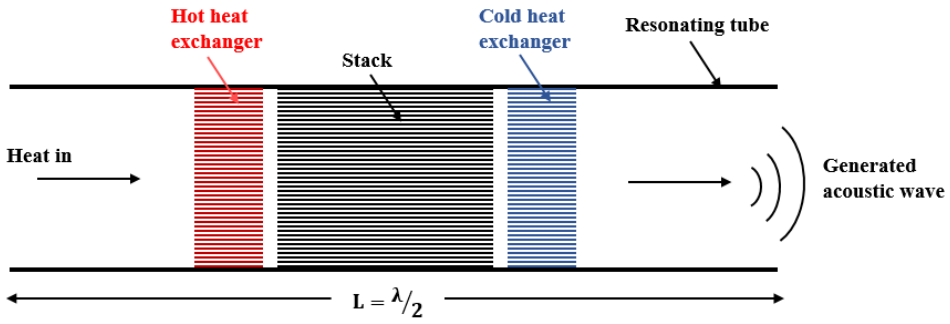


Figure 3.11: A schematic presentation of a simple thermoacoustic engine showing the hot and cold heat exchangers, the stack, and the resonating tube.

The assumptions required to simplify the continuity, momentum and energy equations can be summarized as:

- A steady state condition.
- The stack plates are rigid and stationary.
- The acoustic wave only propagates in x direction, and the transverse pressure gradient across the pore are neglected i.e. $\partial p/\partial y = 0, \partial p/\partial z = 0$.
- The second-order terms, such as turbulence and acoustic streaming, are negligible due to the limitation of the linear theory to the low amplitude of oscillations. These effects have to be considered in case of high-pressure amplitudes.
- Oscillating variables have harmonic time dependence at a single angular frequency ω.
- The time dependences of the temperature, pressure, density and volume flow rate are sinusoidal.
- The temperature dependence of viscosity is neglected (viscosity is constant), which can be important at large temperature gradients.
- The temperature oscillations of the gas along the stack are much smaller than the absolute temperature.

The steady state sinusoidal oscillation of variables such as temperature T, density ρ, and entropy s, can be expressed in the complex notation as follows:

$$T(x,y,z,t) = T_m(x) + Re[T_1(x,y,z)e^{i\omega t}] \tag{3.17}$$

$$\rho(x,y,z,t) = \rho_m(x) + Re[\rho_1(x,y,z)e^{i\omega t}] \tag{3.18}$$

$$s(x,y,z,t) = s_m(x) + Re[s_1(x,y,z)e^{i\omega t}] \tag{3.19}$$

Here: The subscript "m" indicates the steady state mean values of the variables which depend only on x not on y or z. While the first order term of a variable that indicates the oscillation refers with the subscript "1". The complex notation makes use of the identity $e^{i\omega t} = \cos(\omega t) + i\sin(\omega t)$ and $i = \sqrt{-1}$. Terms higher than first order are omitted by the linear thermoacoustic theory. x refers to the direction of the wave propagation, while the y and z are the transverse directions. The pressure, p, and the velocity, u, can be expressed in a format different from that of ρ, T and s. The mean pressure of the device is independent of x, y and z (must be uniform in space), since any gradient in the mean pressure would accelerate the gas. The oscillating pressure is assumed only as a function of x. Hence, the other gradients in the oscillating pressure are neglected.

Therefore, the pressure is written as:

$$p(x,y,z,t) = p_m(x) + Re[p_1(x)e^{i\omega t}] \tag{3.20}$$

For the oscillating velocity, it is assumed that net mass flow in the system is zero. Therefore, the mean velocity part is zero. Hence, the velocity vector is written as:

$$u(x,y,z,t) = Re[u_1(x,y,z)e^{i\omega t}] \tag{3.21}$$

3.4.1 Thermoacoustic governing equations

The continuity equation

With the linear approximations, simplified versions of the equations of the general continuity equation, the momentum equation and the energy equation can be derived. The continuity equation is an expression of a scientific conservation principle that fluid mass is conserved. The change of the mass within any microscopic control volume in a fluid can only be caused by the difference between the fluid particles flowing into the region and fluid particles that flow out of the region (matter can be neither created nor destroyed).
Consider a mass inside a cubical volume, $dxdydz$, that only changes as a result of net inflow or outflow through the six faces of the cube. The mass in the cube is $\rho dxdydz$. The mass flow rate at one of the faces can expressed as:

$$\left[\rho u - \frac{d}{dx}(\rho u)\frac{dx}{2}\right]dydz \tag{3.22}$$

Where u is the x component of the velocity v. Similarly, υ and w are the y and z components, respectively, of v. All six faces yield the well-known continuity equation:

$$\frac{\partial \rho}{\partial t} + \nabla.(\rho v) = 0 \tag{3.23}$$

Substituting the complex-notation expressions of the density and the velocity, Equation 3.18 and Equation 3.21, and applying the linear theory assumptions yields a first-order equation:

$$\frac{\partial}{\partial t}Re[\rho_1(x,y,z,t)e^{i\omega t}] + \nabla.\rho_m(x)Re[v_1(x,y,z)e^{i\omega t}] = 0 \tag{3.24}$$

Equation 3.24 can be re-written as:

$$\frac{\partial \rho_1}{\partial t} + \nabla.(\rho_m v_1) = 0 \tag{3.25}$$

Recall that $\partial/\partial t$ in the first term is identical to $i\omega$. Therefore, Equation 3.25 can always be written in an abbreviated form:

$$i\omega\rho_1 + \nabla.(\rho_m v_1) = 0 \tag{3.26}$$

Since ρ_1 depends only on x not y and z, further simplification of the continuity equation brings:

$$i\omega\rho_1 + \frac{d\rho_m}{dx}u_1 + \rho_m \nabla.v_1 = 0 \tag{3.27}$$

Substituting Equation 3.17, Equation 3.18, and Equation 3.20 into the ideal-gas law $P = \rho RT$ yields:

$$p_m + Re[p_1(x)e^{i\omega t}] = \rho_m(x) + Re[\rho_1(x,y,z)e^{i\omega t}] * R * T_m(x) + Re[T_1(x,y,z)e^{i\omega t}] \tag{3.28}$$

Neglecting the second-order term with the product of ρ_1 and T_1 gives an abbreviated form of the first-order ideal-gas equation of state as follows:

$$p_1 = \rho_m R T_1 + R T_m \rho_1 \tag{3.29}$$

This relationship can also be derived by differentiating the ideal-gas law to yield:

$$dp = \rho R dT + RT d\rho \tag{3.30}$$

Associating the small variables such as p_1 with the small differentials such as dp gives the acoustic version. The first-order ideal-gas equation is often more usefully expressed as:

$$\frac{p_1}{p_m} = \frac{T_1}{T_m} + \frac{\rho_1}{\rho_m} \tag{3.31}$$

Thermoacoustic continuity and oscillating temperature equations

From the continuity equation, the second term is the product of mean density and the velocity vector which can be presented only in the x direction since the velocities in y and z directions are much smaller than the velocity in x direction. Therefore, neglecting the y and z components gives:

$$i\omega\rho_1 + \frac{d}{dx}(\rho_m u_1) = 0 \tag{3.32}$$

Integration of Equation 3.32 over the cross sectional area of the channel gives the spatial average over the channel as:

$$i\omega\langle\rho_1\rangle + \rho_m \frac{d\langle u_1\rangle}{dx} = 0 \tag{3.33}$$

where the $\langle\rangle$ brackets refer to the spatial averaged or the cross-sectional average. The spatially averaged density can be obtained using Equation 3.31 as:

$$\langle \rho_1 \rangle = -\frac{\rho_m}{T_m}\langle T_1 \rangle + \frac{\rho_m}{p_m} p_1 \tag{3.34}$$

An expression for the spatially average oscillating temperature over y and z, $\langle T_1 \rangle$, is derived from the general equation of heat transfer, for which the appropriate acoustic approximation is:

$$i\omega\rho_m c_p T_1 + \rho_m c_p \frac{dT_m}{dx} u_1 = i\omega p_1 + k\left(\frac{\partial^2 T_1}{\partial y^2} + \frac{\partial^2 T_1}{\partial z^2}\right) \tag{3.35}$$

when $dT_m/dx \neq 0$. Considering the y and z dependences of u_1 and allowing for arbitrary geometries (Arnott, Bass and Raspet 1991), gives:

$$T_1 = \frac{1}{\rho_m c_p}(1-h_k)p_1 - \frac{1}{i\omega A}\frac{dT_m}{dx}\left[\frac{(1-h_k)-\sigma(1-h_\nu)}{(1-f_\nu)(1-\sigma)}\right]U_1 \tag{3.36}$$

Here: h_k and h_ν are the thermal and viscous functions, respectively. The spatially averaged version of Equation 3.36 can be expressed as follows:

$$\langle T_1 \rangle = \frac{1}{\rho_m c_p}(1-f_k)p_1 - \frac{1}{i\omega A}\frac{dT_m}{dx}\left[\frac{(1-f_k)-\sigma(1-f_\nu)}{(1-f_\nu)(1-\sigma)}\right]U_1 \tag{3.37}$$

f_k and f_ν are the spatial average of the thermal and viscous functions h_k and h_ν, respectively. f_k and f_ν are functions of ratio of the hydraulic radius of the channel, r_h, to the thermal and viscous penetration depths, δ_k and δ_h, respectively.

For oscillating flow within the channel, f_k indicates the transition from isothermal to adiabatic, while f_h represents the transition from viscous to inviscid flow. h_ν function and its spatial average f_ν are known for many geometries of thermoacoustic cores (see **Appendix A**).

The real and the imaginary parts of the spatial average, f, are plotted against the ratio of the hydraulic radius to the penetration depth, r_h/δ in Figure 3.12. In all geometries, the boundary-layer limit is approached when the hydraulic radius r_h is larger than the penetration depth, δ. The majority of the fluid experiences zero viscous shear force and has a uniform velocity profile which allows both f-functions to approach zero. When $r_h/\delta \approx 0$, the gas has a perfect thermal contact with the wall to expand and compress.

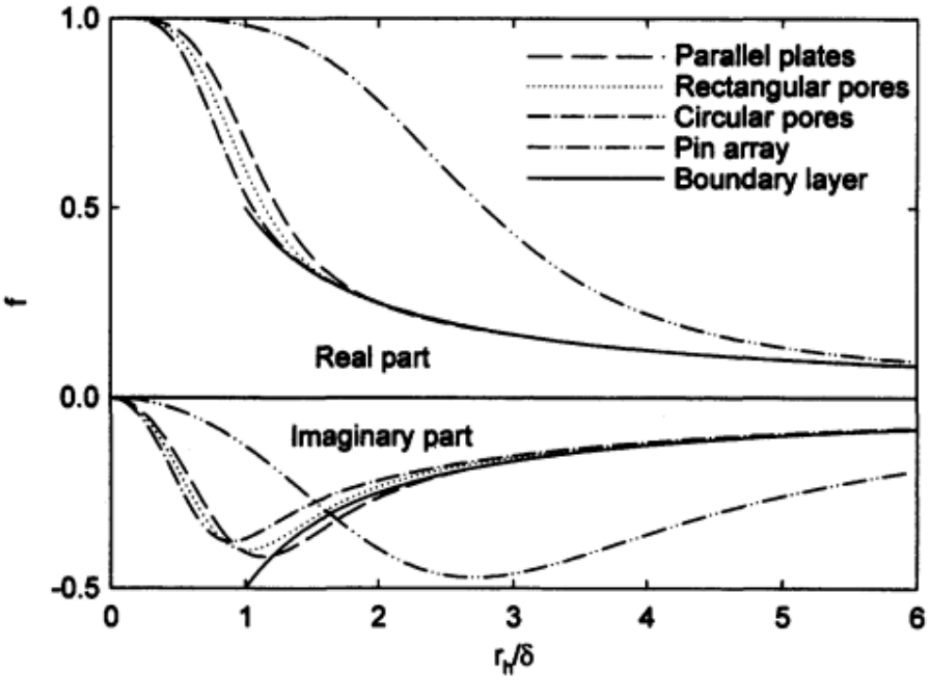


Figure 3.12: Spatial-average function f for several geometries, using r_h/δ_k on the horizontal axis yields f_k on the vertical axis, and using r_h/δ_v yields f_v (Swift 2003).

In the continuity equation, the x dependence of the mean density should be taken into account yielding:

$$i\omega\langle\rho_1\rangle + \rho_m \frac{d\langle u_1\rangle}{dx} = 0 \tag{3.38}$$

Combining Equation 3.37 and Equation 3.38 gives:

$$dU_1 = \frac{-i\omega A dx}{\gamma p_m}[1+(\gamma-1)f_k]p_1 + \frac{(f_k - f_v)}{(1-f_v)(1-\sigma)}\frac{dT_m}{T_m}U_1 \tag{3.39}$$

This is a first-order differential equation where the two terms indicate that a gradient in U_1 can be caused either by pressure or by velocity along the temperature gradient. The dependence on the mean temperature gradient results from the thermoacoustic effect taking place.

The momentum (Navier-Stokes) equation

The momentum equation, or Navier-Stokes equation, expresses Newton's second law for fluid which states that the mass of an object multiplied by its acceleration is equal to the sum of the forces acting on it. For viscous fluid, the momentum equation is given as:

$$\rho\left[\frac{\partial v}{\partial t} + (v.\nabla)v\right] = -\nabla p + \mu\nabla^2 v \tag{3.40}$$

The left hand side of Equation 3.40 represents the density times the acceleration. The forces that act on a microscopic element of fluid are presented on the right hand side; the first term is the pressure gradient, while the second term results from the viscous shearing force. The derivative in the x direction in the second term is neglected because the viscous penetration depth is much smaller than the wavelength. Therefore, the x component of the momentum equation for oscillating flow becomes as follows:

$$i\omega\rho_m u_1 = -\frac{\partial p}{\partial x} + \mu\left(\frac{\partial^2 u_1}{\partial y^2} + \frac{\partial^2 u_1}{\partial z^2}\right) \tag{3.41}$$

where u_1 is the x component of the first-order of the velocity vector. Equation 3.41 is a differential equation for $u_1(y,z)$ with boundary condition $u_1 = 0$ at the solid surface. Therefore, the solution for u_1 is:

$$u_1 = \frac{i}{\omega\rho_m}[1-h_\nu]\frac{dp_1}{dx} \tag{3.42}$$

where h_ν is the thermoviscous function which depends on the channel geometry. By integrating Equation 3.42 over the cross sectional area of the channel, the momentum equation becomes:

$$dp_1 = \frac{i\omega\rho_m}{(1-f_\nu)}\frac{dx}{A}U_1 \tag{3.43}$$

where f_ν is the spatial average of thermoviscous function h_ν. This first-order differential equation is simply the approximation of the momentum equation describing how the pressure changes as a function of the volume flow rate and the geometrical properties of the channel. By combining Equation 3.37 and Equation 3.38, eliminating U_1, to obtain a second-order differential equation in p_1 which is named as Rott's "wave" equation:

$$[1+(\gamma-1)f_k]p_1 + \frac{\gamma p_m}{\omega^2}\frac{d}{dx}\left(\frac{1-f_\nu}{\rho_m}\frac{dp_1}{dx}\right) - \frac{a^2}{\omega^2}\frac{(f_k-f_\nu)}{(1-\sigma)}\frac{1}{T_m}\frac{dT_m}{dx}\frac{dp_1}{dx} = 0 \tag{3.44}$$

The energy equation

The energy equation is a statement of the first law of thermodynamics which says that a change in the energy of the system can occur only through the energetic interaction of the system with its surroundings. This equation can be presented as:

$$\frac{\partial}{\partial t}\left(\rho\varepsilon + \frac{1}{2}\mid v\mid^2\right) = -\nabla.\left[\left(\rho h + \frac{1}{2}\rho\mid v\mid^2\right)v - k\nabla T - v.\sigma'\right] \tag{3.45}$$

Here: ε is the internal energy per unit mass, σ' is the viscous stress tensor and h is the enthalpy per unit mass. The term on the left hand side in Equation 3.45 is a derivative of the total energy, which is the sum of the internal energy and the kinetic

energy. The quantity inside the square brackets on the right side is the energy flux density, because its divergence causes change in the energy per unit volume. The first term inside the bracket is the net energy flow due to mass leaving the boundary of the system. The second term is the heat-flux density which is the microscopic vector version of the conduction heat transfer to the control volume $Q^{\circ} = kAdT/dx$. The last term is the work due only to viscous shear forces on the control volume. From equation Equation 3.45, the total energy flow can be written as:

$$\dot{H} = \left(\rho h + \frac{1}{2}\rho \mid v \mid^2 \right) v - k\nabla T - v.\sigma' \tag{3.46}$$

The enthalpy, h, can be expressed as:

$$h = \varepsilon + \frac{p}{\rho} \tag{3.47}$$

meaning that thermoacoustic total power, $\dot{H}$, should be at most first order in the oscillating variables, as same as the acoustic power. Therefore, $\rho|v|^2$ is negligible. Rott's acoustic approximation to the time-averaged total energy flow flux in x-direction, integrated over the cross-sectional area of the channel , A, can be written as:

$$\dot{H} = \sum_{j=0}^{2} \int \left[\overline{\rho h u} - \overline{kdT/dx} - (\overline{v.\sigma'})_x\right]_j dA \tag{3.48}$$

The second term in the above equation is due to the thermal conduction and it has second order that is assumed to be much lower than the first order component. Hence,

$$\int (\overline{kdT/dx})_0 \, dA = (Ak + A_{solid}k_{solid}) \, dT_m/dx \tag{3.49}$$

The third term in Equation 3.48 is due to the stress tensor and is usually negligible. Therefore, Equation 3.49 simplifies to:

$$\dot{H} = \frac{1}{2}\rho_m \int Re[h_1 \tilde{u}_1] - (Ak + A_{solid}k_{solid}) \, dT_m/dx \tag{3.50}$$

The second term represents the conduction of heat, including conduction in both the working gas and the solid (e.g., stack or regenerator). The first term represents the time-averaged enthalpy flux, which can be written as a function of the temperature and the pressure:

$$dh = c_p \, dT + \frac{(1 - T\beta)dp}{\rho} \tag{3.51}$$

$$h_1 = c_p T_1 \tag{3.52}$$

Here: $\beta = -\frac{1}{T}$ and it represents the thermal expansion coefficient. Therefore, the total energy can be given as:

$$\dot{H} = \frac{1}{2}\rho_m c_p \int Re[T_1 \tilde{u}_1]\, dA - (Ak + A_{solid} k_{solid})\, dT_m/dx \tag{3.53}$$

using Equation 3.36 and Equation 3.42, for T_1 and U_1 , and solving the total energy equation, Equation 3.53, gives:

$$\dot{H} = \frac{1}{2} Re\left[p_1 \tilde{U}_1 \left(1 - \frac{f_k - \tilde{f}_v}{(1+\sigma)(1-\tilde{f}_v)}\right)\right] + \frac{\rho_m c_p |U_1|^2}{2A\omega(1-\sigma^2)|1-f_v|^2}$$
$$Im(f_k + \sigma \tilde{f}_v)\frac{dT_m}{dx} - (Ak + A_{solid} k_{solid})\, dT_m/dx \tag{3.54}$$

Equation 3.44 and Equation 3.54 can be solved by integrating them along the length of the solid material. However, this equation describes only the total energy flow in standing wave systems. The energy flow equation that is used in unison with the thermoacoustic continuity equation and thermoacoustic momentum equation is considered as the basis for all models of thermoacoustic systems.

3.5 Non-linearity in thermaocoustic systems

The thermoacoustic effect developed based on the wave approximation and by only supposing small amplitudes of acoustic waves. However, practical thermoacoustic systems always work at high amplitudes. One may expect that non-linearity will take place in such devices. These non-linear effects have a harmful effect on the overall performance of thermoacoustic devices and contribute to the dissipation of the acoustic power.

3.5.1 Acoustic Streaming

The motion of the gas particles and the convective heat transfer are critical for thermoacoustic effect. During the operation of thermoacoustic devices, undesirable mass transfer can exist, and may result in unwanted convective heat transfer in the system. Acoustic streaming refers to a second order mass flow that is superimposed on the large first order acoustic oscillatory flow, and is induced by first order acoustic velocity (Swift 2017). For the design and operation of thermoacoustic systems, it is important to understand the consequences of acoustic streaming because it can greatly affect the total power flow in the system. It can be considered as an extra heating power requirement in a thermoacoustic engine or undesirable heat dissipation that causes losses of cooling power in a thermoacoustic refrigerator. In order to eliminate the non-linear effect in thermoacoustic systems, many researchers have addressed the acoustic streaming phenomena (Backhaus and Swift 2000; Olson and Swift 1997). According to their

work, acoustic streaming in thermoacoutsic systems may be divided into four types (Swift 2000), taking place mostly in looped-tube travelling wave arrangements. The four types are illustrated in Figure 3.13.

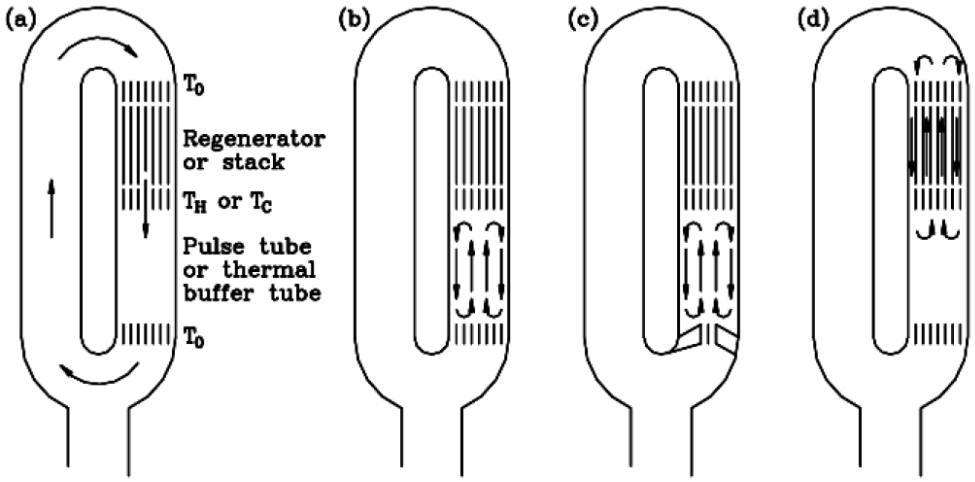


Figure 3.13: The four types of acoustic streaming that occur in thermoacoustic systems. (a) Gedeon acoustic streaming. (b) Rayleigh acoustic streaming. (c) Jet-driven acoustic streaming. (d) Acoustic streaming within a stack or a regenerator. Note: the arrows are used to indicate the time-average flow velocity (Swift 2000).

Gedeon streaming was discovered and explained first by Gedeon (1997), who noticed the existence of a non-zero time averaged mass flow in a pulse tube or Stirling with a loop passage for steady energy flux. An extra component needs to be installed in the thermoacoustic system such as a jet pump or a flexible membrane to cancel out the time-averaged mass flow (Swift, Gardner and Backhaus 1999; Luo et al. 2005; Luo et al. 2006; Qiu et al. 2006).

Rayleigh streaming was proposed first by Rayleigh (1896) before it was investigated and proven by other researchers. Rayleigh streaming is a forced convection within the thermal buffer tube that happens due to thermal and viscous boundary layer effects at the side wall (Olson and Swift 1997). This streaming can be eliminated by tapering the wall zone through which the streaming occurs into a particular angle. It can occur in both standing wave and travelling wave thermoacoustic devices unlike Gedeon streaming which is specific to travelling wave systems.

Jet-driven streaming refers to the time-averaged toroidal circulation that occurs inside the thermal buffer tube, when a periodic suction and ejection of a viscous fluid exists through an orifice or a change in cross-section. The jet streaming can be diminished by adding flow straighteners to the inlet. However, these straighteners can also dissipate part of the acoustic power of the loop and this should be considered in the design of the flow straighteners (Swift 2017).

To date, little information of mass streaming within a stack or a regenerator is available

in the literature unlike the other types of acoustic streaming (Swift 2017). In thermoacoustic regenerator-based systems, the streaming instability can be observed inside the regenerator when a narrow jet blows strongly at the cold end of the regenerator as a result of an abrupt transition from a small cross section driver duct to the larger cross-section ambient heat exchanger and regenerator.

3.5.2 Turbulence

Understanding of the dynamic and mechanisms of flow transition to turbulence is important in thermoacoustic systems to get a rough idea about whether deviations from Rott's acoustic approximation might be expected. Many experimental works have observed that laminar-turbulent transition in oscillatory flow occurred at a Reynolds number, $N_{R,1}^{\delta_v}$, based on the viscous boundary layer thickness of a range of 500 to 550, independent of the particular flow geometry (channel, pipe, oscillating plate) (Hino et al. 1983; Merkli and Thomann 1975*b*). The resulting transition is characterized by the sudden explosive occurrence of turbulence towards the end of the acceleration phase of the cycle. Reynolds Stoke-layer thickness can be defined as:

$$N_{R,1}^{\delta_v} = \frac{\langle u \rangle \rho \, \delta_v}{\mu} \tag{3.55}$$

Where: $\langle u \rangle$ is the mean velocity of the oscillatory flow.

The laminar-turbulent transition for an oscillatory flow in a tube of a radius, r, appears roughly at the following values (Akhavan, Kamm and Shapiro 1991):

$$N_{R,1} \cong 2000, \; For \; r < 2\delta_v \tag{3.56}$$

$$\frac{N_{R,1}}{r/\delta_v} \cong 1000, \; For \; r > 2\delta_v \tag{3.57}$$

Therefore, the Reynolds number based on the peak acoustic volumetric velocity, $|U_1|$, and the diameter of the flow channel,D, can be given as:

$$N_{R,1} = \frac{\rho_m |U_1| D}{A\mu} \tag{3.58}$$

At the high amplitudes necessary to produce high acoustic power, various components in thermoacoustic systems operate in all regimes shown in Figure 3.14. Thermal buffer tubes and pulse tubes typically work in the weakly turbulent flow regime, but may be conditionally turbulent. Resonator parts may often enter conditionally or fully turbulent zone. For other parts of non-circular cross sections but having parallel walls, Figure 3.18 provides reasonable guidance, using $D \sim 4r_h$.

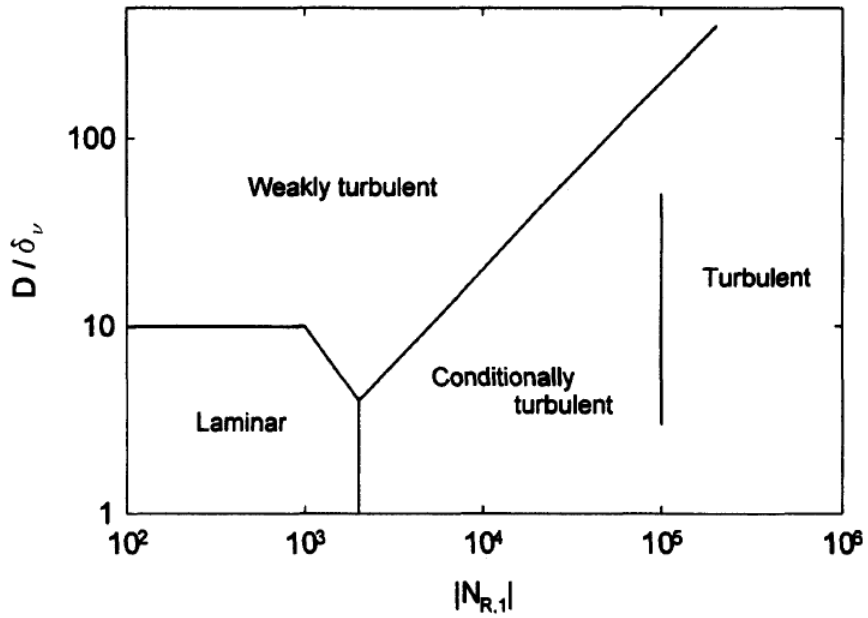


Figure 3.14: Boundary regime approximation of oscillatory flow, in smooth pipe of circular cross-section, as a function of peak Reynolds number, $|N_{R,1}|$, and the ratio of the pipe diameter to the viscous layer thickness, D/δ_ν (Swift 2017).

3.6 Converting thermaocoustic energy into electrical power

Thermoacoustc engines potentially produce electrical power in a reliable way and at a reasonable cost (Chen et al. 2013; Yu, Jaworski and Backhaus 2010*b*). So far, electromagnetic components are widely used to achieve the electrical power extraction. This is achieved by using a relatively low-cost ordinary loudspeaker or by using the more costly but dedicated linear alternator. Other methods that have been utilized practically are piezoelectric devices, magnetohydrodynamic devices, and Bi-directional turbines. Figure 3.15 shows a schematic overview of the four mechanisms that can be used to harvest thermoacoustic electrical power.

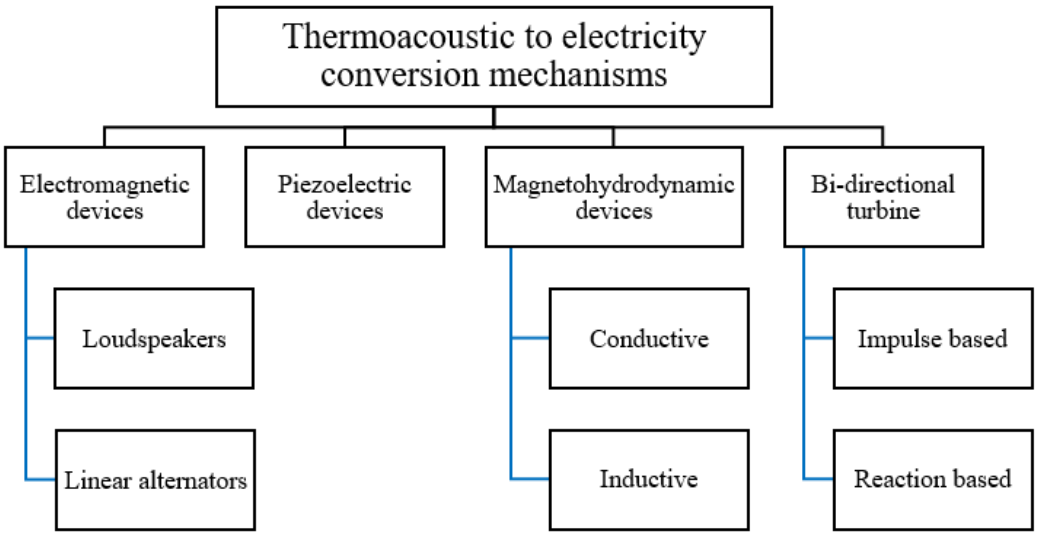


Figure 3.15: Overview of different mechanisms for the thermoacoustic energy into electrical power conversion. [Adapted from (Timmer, de Blok and van der Meer 2018)].

3.6.1 Electromagnetic transducers

Electromagnetic devices, such as linear alternators and loudspeakers, can be used for converting thermoacoustic power into electricity. The main principle of the conventional loudspeakers is that the thermoacoustic power produces mechanical movement from electrical power. Also, loudspeakers can be used in reverse to produce electrical power by using an electrical motor in reverse as a generator. Fundamentally, both the linear alternator and the loudspeakers can be classified as electromagnetic devices. However, the main purpose of the linear alternators is to extract electricity from acoustic power at a single resonance frequency. In contrast, the loudspeakers are designed to produce sound over a large frequency range, and thus linear alternators and loudspeakers have different characteristics.

Commercially audio loudspeakers are used to extract electricity in thermoacoutsic systems (Chen et al. 2013; Jaworski and Mao 2013; Abdoulla-Latiwish, Mao and Jaworski 2017), mainly because of their relatively low cost and availability. However, the transduction efficiency of loudspeakers is poor (Swift 2017), since the design is concerned about linearity rather than efficiency, and due to the flat response over a large frequency range that they have.

Although linear alternators are better than loudspeakers in terms of transduction efficiency, they are excluded when the cost is an important factor. It should be noted that loudspeakers are used in low power thermoacoustic applications, because of their fragile cones, limited peak strokes, and high impedance mismatch at a high mean pressure of the working gas (Swift 2017). Loudspeakers are suitable where there is a low pressure drop across the cone, of order of kPa (Jaworski and Mao 2013).

The modelling and analysis of using a loudspeaker as a thermoacoustic power converter have been described and explained by many researchers (Yu, Saechan and Jaworski 2011; Kang et al. 2015). The loudspeaker consists mainly of a moving coil inside a static magnetic field where the voice coil is connected to the cone and its suspension. Normally, the cone is fabricated from paper, plasticized cloth or carbon fibre. The magnet includes three parts: the front plate, the yoke pole piece, and the rear plate. The loudspeaker is made from low-cost iron material and a large ferrite magnet. Vent holes are provided to allow the air displaced by the moving coil to pass to the outside, as shown schematically in Figure 3.16.

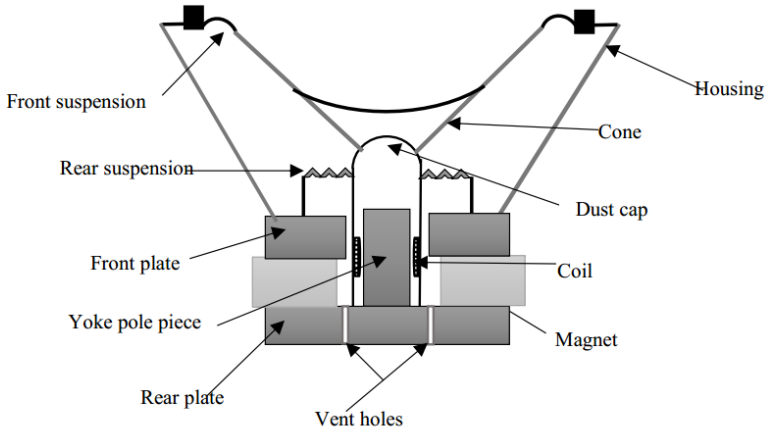


Figure 3.16: Cross-section of the general purpose low-cost audio loudspeaker. The geometry shows that the motion, the magnetic field and the electric current are perpendicular.

The simple physical model of the loudspeaker is presented in Figure 3.17. The acoustic wave employs an oscillatory pressure on the loudspeaker's diaphragm that has an area of A. The total mass of the moving diaphragm and the coil is M. The stiffness of the suspension system is K. The mechanical resistance is R_m. The coil has electrical resistance R_e and electrical inductance L. The product of the magnetic field B and the wire length l produces a force factor Bl. To extract the electrical power from the acoustic power, a load resistor R_L is connected to the coil's terminals.

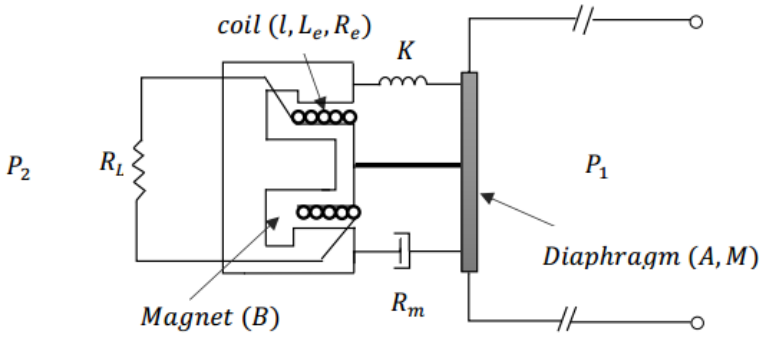


Figure 3.17: The physical model of the loudspeaker (Yu et al. 2011).

The power extracted by the loudspeaker can be expressed as (Yu et al. 2011):

$$P_e = \frac{1}{2}\frac{|U_1|^2}{A^2}\frac{(Bl)^2 R_L}{(R_e+R_L)^2} \tag{3.59}$$

The extracted electrical power reaches a maximum value when $R_L = R_e$, therefore Equation 3.59 becomes:

$$P_{e,max.} = \frac{1}{8}|U_1|^2\frac{(Bl)^2}{A^2 R_e} = \frac{1}{8}|U_1|^2\frac{(Bl)^2}{A^2 R_L} \tag{3.60}$$

The maximum electrical power output of a given loudspeaker can be estimated from Equation 3.60 which can be used as an indicator for selecting a suitable loudspeaker as a linear alternator. Equation 3.60 shows that the maximum output is proportional to the $|U_1|^2$ and to $\frac{(Bl)^2}{A^2 R_e}$ or $\frac{(Bl)^2}{A^2 R_L}$. The first term $|U_1|^2$ represents the square of the volume flow rate, which is determined by both the geometrical and the operational parameters of the engine, and is limited to a certain value for a particular engine.
$\frac{(Bl)^2}{A^2 R_e}$ term represents the acoustic impedance of the loudspeaker. For a given volume flow rate, the acoustic impedance should be increased to increase the electrical output. For the loudspeaker used in this engine, ωL_e is much less than R_L or R_e, the inductance of the loudspeaker is negligible. Therefore, the efficiency of the loudspeaker can be expressed as:

$$\eta_e = \frac{(Bl^2)R_L}{R_m(R_e+R_L)^2 + (Bl^2)(R_e+R_L)} \tag{3.61}$$

The transduction efficiency reaches a maximum value when

$$R_L = R_e\sqrt{1+\frac{(Bl)^2}{R_e R_m}} \tag{3.62}$$

Therefore, the maximum efficiency can be written as (Swift 2017):

$$\eta_{e,max.} = \frac{(Bl)^2\sqrt{1+\frac{(Bl)^2}{R_eR_m}}}{R_mR_e\left(1+\sqrt{1+\frac{(Bl)^2}{R_eR_m}}\right)^2+(Bl)^2\left(R_e+\sqrt{1+\frac{(Bl)^2}{R_eR_m}}\right)} \tag{3.63}$$

Linear alternators refer to moving coil and moving magnet configurations. The moving coil alternators share the same principle of the loudspeakers, except they don't have the fragile paper cone that ordinary loudspeakers have. In the moving magnet alternators, the structure with the coil is fixed and the magnet is forced to move linearly by the acoustic wave. Both of these linear alternators are addressed as electricity producing parts in thermoacoustic systems, but the moving magnet alternators are used more frequently. Linear alternators have a small range of mechanical resonance, a larger mass compared to loudspeakers, and a high transduction efficiency. Moreover, linear alternators have a large power output due to the larger peak stroke and can also work at higher mean pressures of the working gas. However, precise manufacturing is required for these dedicated parts.

3.6.2 Piezoelectric transducers

In a thermoacoustic engine, piezoelectric materials such as ceramics and certain crystals, can be placed inside the thermoacoustic engine to produce electricity from the acoustic power. In principle, piezoelectric materials create a voltage difference through their opposite sides during mechanical deformation. When these faces are connected in an electrical circuit, a current will be induced, and as a result electricity will be produced. If the sides are connected in a circuit and a voltage difference is applied across them, they will mechanically deform, and this can be used in thermoacoustic field to generate acoustic waves. Ceramic lead zirconate titanate (PZT) is the most widely used device (Zhao 2013; Nouh, Aldraihem and Baz 2014). It is high quality but it can't experience high strain due to its brittle nature. Other piezoelectric materials used in thermoacoustic systems are piezoelectric fibre composite (PFC) and polyvinylidene fluoride (PVDF) and these have better resistance to cracking and are more flexible compared to the PZT. An extensive review on piezoelectric materials, including different tuning schemes and several spatial arrangements, can be found in the work carried out by Anton and Sodano (2007). Generally, the piezoelectric material has small mass and small inertia, thus it is efficient at a small wave length and a relatively high operating frequency (Avent and Bowen 2015; Smoker et al. 2012). This reduces the size of the resonator and therefore the thermoacoustic engine. To date, most of the thermoacoustic work done using piezoelectric elements is in standing wave system designs (Jensen and Raspet 2010; Lihoreau et al. 2002; Matveev et al. 2007). There is not any experimental

work done on travelling wave designs using piezoelectric materials, but only numerical modellings (Aldraihem and Baz 2012; Nouh, Aldraihem and Baz 2013). Research work shows it is possible that the transduction efficiency of piezoelectric elements is in the range of 70% to 90%.

3.6.3 Magnetohydrodynamic transducers

The Magnetohydrodynamic devices utilize an electrically conducted fluid that is forced to oscillate by the acoustic wave of the thermoacoustic system. The oscillating fluid is used to achieve direct conversion of the acoustic power into electrical power, when a magnetic field is applied over the oscillating fluid. The electrical power can be produced in an inductive or conductive manner. This type of power harvesters is suitable with applications that required no maintenance, such as outer space (Alemany et al. 2015). The electrically conducted fluid that is usually used is liquid sodium (Swift 1988*a*; Vogin and Alemany 2007), because it has a relatively low density and high electrical conductivity. However, it is a highly reactive and hazardous substance and can cause serious damage to the thermoacoustic system, as reported by Swift (1988*a*). The theoretical efficiency obtained using this transducer is in the range of 60% to 72%. However, there are not too many experimental investigations to confirm these figures. There is only one thermoacoustic system which filled with liquid sodium at mean pressure of 200 bar and was able to produce up to 300W electrical power with acoustic-to-electrical efficiency of 45% (Wheatley, Swift and Migliori 1986*b*; Swift 1988*a*; Migliori and Swift 1988). To ensure optimum performance of this power harvester in a thermoacoustic engine, a good coupling with the acoustic field is crucial.

3.6.4 Bi-directional turbines

A bi-directional turbine, Figure 3.18, can be used to convert acoustic energy into mechanical energy and into electricity if it is connected to a generator. There is no available literature about the bi-directional turbine in thermoacoustic applications. However, they have been used to convert marine wave energy into electricity in oscillating water columns (OWC) (Setoguchi and Takao 2006; Thakker, Jarvis and Sahed 2008; Pereiras et al. 2011).

In on-shore and off-shore power plants, the waves force a water column in a chamber to move upwards and downwards. The chamber is opened to the atmosphere and the oscillatory flow of air drives the bi-directional turbine that has rotated independently. Comparing this to a thermoacoustic application, where similar oscillatory flow conditions which exist, making it possible to employ it as a thermoacoustic power converter. The efficiency of the bi-directional turbines depends strongly on the density of the working fluid. When a bi-directional is placed in OWC plants, the achieved conversion efficiency is in the range of 25% to 40%, using air at atmospheric pressure. For ther-

moacoustic systems, the mean pressure of the working gas can be up to 40 bar, so the conversion efficiency of the turbine can be up to 85% due to the high density of the gas (De Blok, Owczarek and François 2014). Therefore, a bi-directional turbine can be a low-cost and scalable candidate for thermoacoustic power conversion and they can compete with the linear alternators. However, the coupling of a bi-directional turbine with thermoacoustic systems requires a stable operational frequency and amplitude which should be considered carefully.

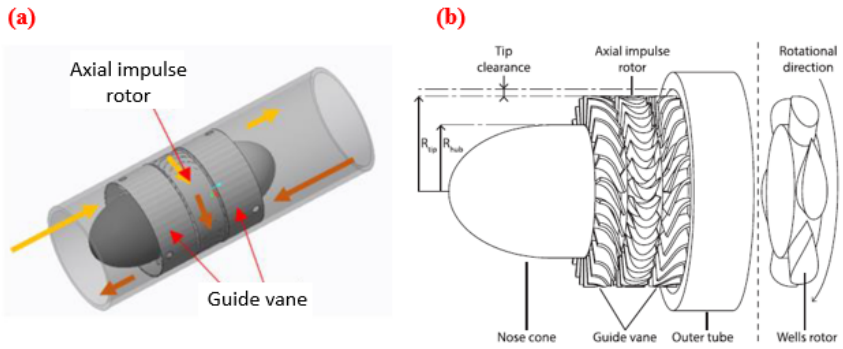


Figure 3.18: Bi-directional turbine. (a) Illustration of the flow direction and the relative position of the rotor and the guide vanes in the turbine. (b) Schematic diagram showing the shape of the guide vanes and the rotor blade of a Wells turbine (Timmer, de Blok and van der Meer 2018).

3.7 DeltaEC software for simulation of thermaocoustic engines

DeltaEC is a numerical code developed by Los Alamos group (Ward, Clark and Swift 2008) based on thermoacoustic theory. The software package is widely used to compute details of how thermoacoustic engines and refrigerators perform under different conditions, assuming one-dimensional approximation for the system geometry and the energy flow through the path of the wave propagation. DeltaEC integrates the wave equation and the other equations such as the energy equation, in a gas or in a very compressible, thermodynamically active fluid, in a geometry defined earlier by the user assuming a time dependence, $Re(e^{i\omega t})$, for all the oscillation variables. The time dependence assumption enables transforming the temporal part of the governing equations into algebraic equations of time, instead of differential equations in time. Therefore, the governing equations become much easier to solve (Chinn 2010).

The geometry of the thermoacoustic device is modelled as a sequence of segments that reflect the actual physical aspects of the system, such as ducts, cones, heat exchangers, transducers, thermoacoustic regenerators and stacks. The input data for each segment can be introduced and also modified through DeltaEC's user interface. The software allows the user to select the type of working fluid and also provides a pre-programmed

option to include gases as well as liquids. With a full model built from the desired segments, a DeltaEC user will go through a process of setting the Guess-Target lists that the code uses to converge to solution using an iterative shooting method.
The Guess lists, as the name suggests, includes values of the unknown parameters. On the other hand, the TARGET list contains boundary conditions of the model or desired values of the parameters the user is trying to find. For example, the user can guess the volumetric velocity for 1 Pa oscillating pressure and 100 Hz operating frequency, when the TARGET is set to infinite complex acoustic impedance at a closed ** END of the simulation. The solver enables the user to determine the changes in the state of the working gas, such as the oscillatory variables (pressure and volumetric velocity), the acoustic power, and the total energy flow, throughout the thermaocoutsic system components.
The output data can be examined via the user interface, built-in graphics displays, the operating system's text utilities, or any spreadsheet or visuals software. However, for novice users, DeltaEC sometimes becomes quite frustrating when the GUESS list is set out of the vicinity of the actual solution. Moreover, the model can be easily diverged if one parameter is changed in a single big step. Some useful strategies to get the model successfully converged is to assure energy conservation by checking the values of the heat flux in the heat exchangers, and the work flux through the stack, and also check the values of the acoustic parameters and the temperatures to ensure there is a physical meaning behind them (Poese and Garrett 2000), and match the experimental data, if applicable. One extra technique to avoid a TARGET convergence issue is to use the incremental plot feature to let DeltaEC automatically accomplish large change in a particular variable via a series of small steps. The "incremental plot" option is very useful when it is required to optimise a design for one part that has many variables such as regenerator (length, position or channel size).
As mentioned before, the software deals with one-dimensional sequences of segments. Therefore, the wave equation for x-independent cross-sectional area A, without thermal or viscous losses, can be expressed as:

$$p_1 + \frac{a^2}{\omega^2}\frac{dp_1^2}{dx^2} = 0 \tag{3.64}$$

This second order equation can be considered as two coupled first-order equations with respect to the pressure p_1 and the volumetric velocity U_1

$$\frac{dp_1}{dx} = \frac{-i\omega\rho_m}{A}U_1 \tag{3.65}$$

$$\frac{dU_1}{dx} = \frac{-i\omega A}{\rho_m a^2}p_1 \tag{3.66}$$

This perspective is defined in (Swift 2003) where Equation 3.65 and Equation 3.66 are derived from the momentum equation and the continuity equation, respectively.
The momentum and continuity equations can be different depending on the local circumstances of every segment. DeltaEC utilizes arduous governing equations that allow for the possibility of the acoustic power dissipation along the ends of the ducts. For instance, in a boundary layer approximation in large cross-sectional ducts and shallow cones, these equations are different:

$$\frac{dp_1}{dx} = \frac{-i\omega\rho_m}{A}\left[1 - \frac{1-i}{2}\frac{\Pi}{A}\delta_v\right]^{-1} U_1 \tag{3.67}$$

$$\frac{dU_1}{dx} = \frac{-i\omega A}{\rho_m a^2}\left[1 + \frac{1-i}{2}\frac{\Pi}{A}\frac{\gamma-1}{1+\varepsilon_s}\delta_\kappa\right] p_1 \tag{3.68}$$

Here: A and Π are the cross-sectional area and the perimeter of the acoustic duct, respectively, δ_v and δ_κ are the viscous and the thermal penetration depth, respectively, γ the ratio of the isobaric to isochoric specific heats, and ε_s is a correction factor for the thermal properties of the solid material (also known as surface roughness).
To pass from one end of a segment to the beginning of the adjacent segment, DeltaEC uses continuity of the pressure, p_1, and the volumetric velocity, U_1, of oscillation. Locally within a particular segment, the propagation of the acoustic wave depends on the local variables such as area and perimeter, as well as the global parameters of the model such as the working frequency. DeltaEC starts at the beginning of the first segment of a series of segments and integrates the momentum equation, $F_{momentum}$, and the continuity equation, $F_{continuity}$, via each segment, sequentially, to the end of the model, using the local variables and p_1 and U_1 themselves, as:

$$\frac{dp_1}{dx} = F_{momentum}(p_1, U_1, T_m, p_m, \omega, geometry, gas\ properties, solid\ properties, etc.) \tag{3.69}$$

$$\frac{dU_1}{dx} = F_{momentum}(p_1, U_1, T_m, p_m, \omega, geometry, gas\ properties, solid\ properties, etc.) \tag{3.70}$$

Here: most variables on the right-hand sides of Equation 3.71 and Equation 3.70 vary with x.
For an ideal thermoacoustic core, due to the large heat capacity of the solid material, all the thermodynamic processes on the interface between the working gas and the solid material are assumed to be isothermal. However, in real applications, the case is completely different because the heat capacity of the solid material is insufficient. Therefore, the equations built within DeltaEC are coupled with a correction factor, ε_s , for the finite thermal conductivity. Accordingly, the governing equations can be

expressed as:

$$\left[1+\frac{(\gamma-1)f_k}{1+\varepsilon_s}\right]p_1+\frac{\gamma p_m}{\omega^2}\frac{d}{dx}\left(\frac{1-f_v}{\rho_m}\frac{dp_1}{dx}\right)-\beta\frac{a^2}{\omega^2}\frac{(f_k-f_v)}{(1-\sigma)(1+\varepsilon_s)}\frac{1}{T_m}\frac{dT_m}{dx}\frac{dp_1}{dx}=0 \tag{3.71}$$

$$\frac{dU_1}{dx}=\frac{-i\omega A}{\gamma p_m a^2}\left(1+\frac{(\gamma-1)f_k}{1+\varepsilon_s}\right)p_1+\frac{\beta(f_k-f_v)}{(1-f_v)(1-\sigma)(1+\varepsilon_s)}\frac{dT_m}{dx}U_1 \tag{3.72}$$

$$\frac{dT_m}{dx}=\frac{\dot{H}_2-\frac{1}{2}Re\left[p_1\tilde{U}_1\left(1-\frac{T_m\beta(f_k-\tilde{f}_v)}{(1+\varepsilon_s)(1+\sigma)(1-\tilde{f}_v)}\right)\right]}{\frac{\rho_m c_p|U_1|^2}{2A\omega(1-\sigma)|1-f_v|^2}Im\left(\tilde{f}_v+\frac{(f_k-\tilde{f}_v)(1+\varepsilon_s f_v/f_k)}{(1+\varepsilon_s)(1+\sigma)}\right)-Ak-A_sk_s} \tag{3.73}$$

$$\dot{H}_2=\frac{1}{2}Re\left[p_1\tilde{U}_1\left(1-\frac{T_m\beta(f_k-\tilde{f}_v)}{(1+\varepsilon_s)(1+\sigma)(1-\tilde{f}_v)}\right)\right]+\frac{\rho_m c_p|U_1|^2}{2A\omega(1-\sigma)|1-f_v|^2}\frac{dT_m}{dx}$$
$$Im\left(\tilde{f}_v+\frac{(f_k-\tilde{f}_v)(1+\varepsilon_s f_v/f_k)}{(1+\varepsilon_s)(1+\sigma)}\right)-(Ak+A_sk_s)\frac{dT_m}{dx} \tag{3.74}$$

The correlations for the correction factor, ε_s, are provided in **Appendix A**.

3.8 Concluding remarks

This chapter has shown a review of the basics of thermodynamics and fluid mechanics, on which thermoacoustic relies. A discussion of the critical spatial scales, basic assumptions, and notation is then presented. The linear thermoacoustic theory with the basic equations that govern the operation of thermoacoustic systems is introduced with emphasis on describing the temperature, flow and power field. Non-linear effects in thermoacoustic systems are also explained with some examples. Also, mechanisms of thermoacoustic power conversion are discussed. Finally, the simulation of thermoacoustic systems using the DeltaEC package is presented with some useful guidance. As mentioned in the introductory chapter, the driving force for this study is the low cost of the system because it targets one of the developing countries (South Sudan). Therefore, the most suitable candidate to achieve the acoustoelectric conversion is the ordinary inexpensive audio loudspeaker. Also, the available specialised software DeltaEC will be used to develop theoretical models to predict behaviour of the thermoacoustic engines. The critical parameters in section 2 will be considered in both theoretical and experimental investigations to analyse and assess the thermoacoustic systems considered in this study, and compare alternative designs. Before starting these investigations, it is worthy discuss the advances in thermoacoustics and what has been done so far by other researchers, and this will be addressed in the next chapter.

CHAPTER 4

OPTIMISATION AND EXPERIMENTAL INVESTIGATION OF A SINGLE REGENERATOR TRAVELLING WAVE THERMOACOUSTIC SYSTEM

4.1 Introduction

The literature survey presented in Chapter three suggests that the looped-tube engine is a good alternative for waste heat recovery. This differs from the torus configuration which requires a high temperature difference (hundreds of Kelvin) to start oscillation. In fact, a looped-tube engine type is the simplest means of implementing the travelling wave thermoacoustic engine. The simple construction is an advantage for some low-cost niche applications, such as developing energy systems for rural communities in the developing world (Chen et al. 2012; Riley 2014*b*). In the looped-tube travelling wave thermoacoustic engine, the thermoacoustic core acts as an acoustic power amplifier, a certain amount of acoustic power feeds into the cold side of the regenerator, and then it is amplified by the thermodynamic cycle taking place in the regenerator. The amplified acoustic power flows out from the hot side of the regenerator. The looped-tube resonator acts as an acoustic wave-guide, which provides a feedback passage to transfer part of the acoustic power back to the cold side of the regenerator for amplification. Therefore, self-sustained acoustic oscillation can be induced. In order to be viable and competitive with conventional energy conversion systems, thermoacoustic systems must work on a low operating temperature with a range of 70 to 200°C, while maintaining relative Carnot efficiency (De Blok 2008; Zhang et al. 2016).

Typically thermoacoustic engines which have a single core are more useful for high temperature operation, which adds an extra challenge when adapting the engine for low temperature applications. A thermoacoustic engine with fewer stages might require a higher temperature to start oscillation but could outperform an engine with multi stages and a higher temperature difference. Therefore, having fewer engine stages could be beneficial in reducing the system's complexity and cutting down the investment costs.

On these grounds, the research present in this chapter describes a single-stage looped tube thermoacoustic travelling wave engine. The main criteria for designing the thermoacoustic electricity generator are the relatively low-cost of construction coupled with a beneficial level of electricity for a single household in a rural community and to prove the viability of the SCORE project. Moreover, the construction of the generator has to be as simple as possible to promote wider use and acceptance of the technology. Certainly, such a design will necessarily be different from the conventional thermoacoustic systems which generally seek either delivery of high power or high efficiency.

The engine is investigated by means of theoretical calculations as well as experimental tests to strengthen and support the numerical data. The design, construction and lab testing of the prototype is described. The theoretical model of the acoustic field is developed using DeltaEC software. A comprehensive analysis of the constructed theoretical model is provided as well as the verification of the simulation against the obtained experimental data. The effect of different operational and design parameters such as the input heat, the stub length, and the alternator load resistance on functionality are observed.

4.2 Simplified model

As described in the introduction, the looped-tube thermoacoutsic engine is one type of travelling wave engine (Yazaki et al. 1998). The configuration of this engine type is relatively simple and the performance is much better than the standing wave thermoacoustic engine. Using this looped-tube arrangement gives the advantage of coupling the alternator in the near-travelling wave region. Therefore, the pressure drop across the alternator diaphragm can be greatly reduced. Moreover, this configuration helps to suppress the boundary-layer driven streaming.

The present concept of the single core thermoacoustic engine is schematically depicted in Figure 4.1. The system comprises several major elements. The thermoacoustic core is the essence of the thermoacoustic engine and it builds up from a regenerator sandwiched in between an ambient heat exchanger (AHX) and a hot heat exchanger (HHX). In this model, the hot heat exchanger works as a heat source and the ambient heat exchanger works as a heat sink. Together they induce a steep temperature gradient

across the regenerator which causes a sharp increase in the volumetric velocity (power amplification effect). Below the engine core, there is a thermal buffer tube (TBT), which is placed between the hot heat exchanger and the secondary ambient heat exchanger (SAHX) to stop heat circulation to the loudspeaker housing. The loudspeaker (L.S) is connected in series to the engine and is installed near one of the ambient heat exchangers. The loudspeaker functions as a linear alternator, to deliver electricity from acoustic power after it is produced in the engine core. The alternator introduces an acoustic load to the thermoacoustic generator, which disturbs the acoustic field within it. If the acoustic load (alternator) is not matched properly, acoustic reflections and a high standing wave ratio would arise, and therefore also large acoustic dissipations. For efficient power extraction, the load has to be properly matched with the acoustic field by adding a stub-matching technique, to cancel out the reflections caused by the alternator, and to suppress acoustic impedance disturbance in the loop caused by the core and the loudspeaker. Therefore, a matching-stub is added to the engine to compensate for impedance mismatching. The looped wave-guide is closed by a feedback pipe (FB pipe).

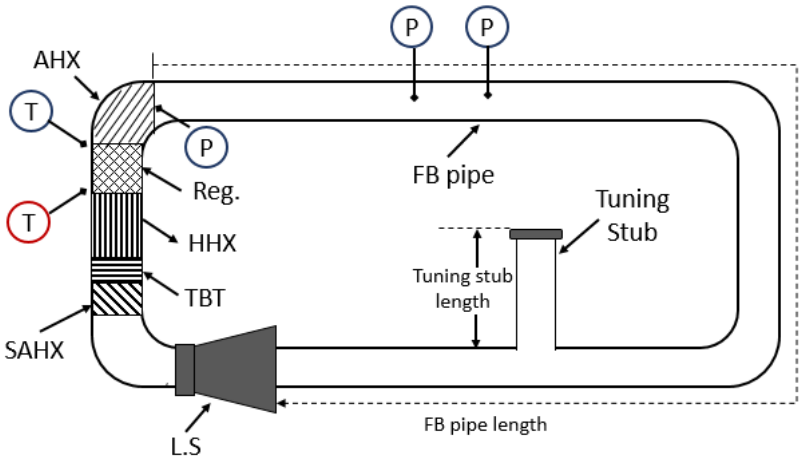


Figure 4.1: A labelled schematic of a single core thermoacoustic engine. AHX is the main ambient heat exchanger, Reg. the regenerator, HHX the hot heat exchanger, TBT the thermal buffer tube, SAHX the secondary ambient heat exchanger, L.S the loudspeaker, FB pipe is the feedback pipe. Locations labelled with P and T indicate where pressure and temperature are measured.

To have a further understanding of the acoustic field, and to examine the most important physical parameters in the single core thermoacoustic engine, a simplified lumped element model that is equivalent to the acoustic circuit is developed and presented in Figure 4.2. The lumped impedance model was initially developed by Backhaus and Swift (2000) for the thermoacoustic Stirling heat engine TASHE, and has been used extensively by many other researchers (Luo et al. 2005; Tang et al. 2011; Ghorbanian and Karimi 2014; Yu, Jaworski and Backhaus 2012). The simplified lumped-element

model divides the system into elements that have spatial dimensions much smaller than the acoustic wavelength. This allows the spatial dependence of the elements to be approximated as constant, thus the individual elements are only functions of time and neighbouring elements. Each component of the current engine is replaced with its equivalent lumped-element (Swift 2017).

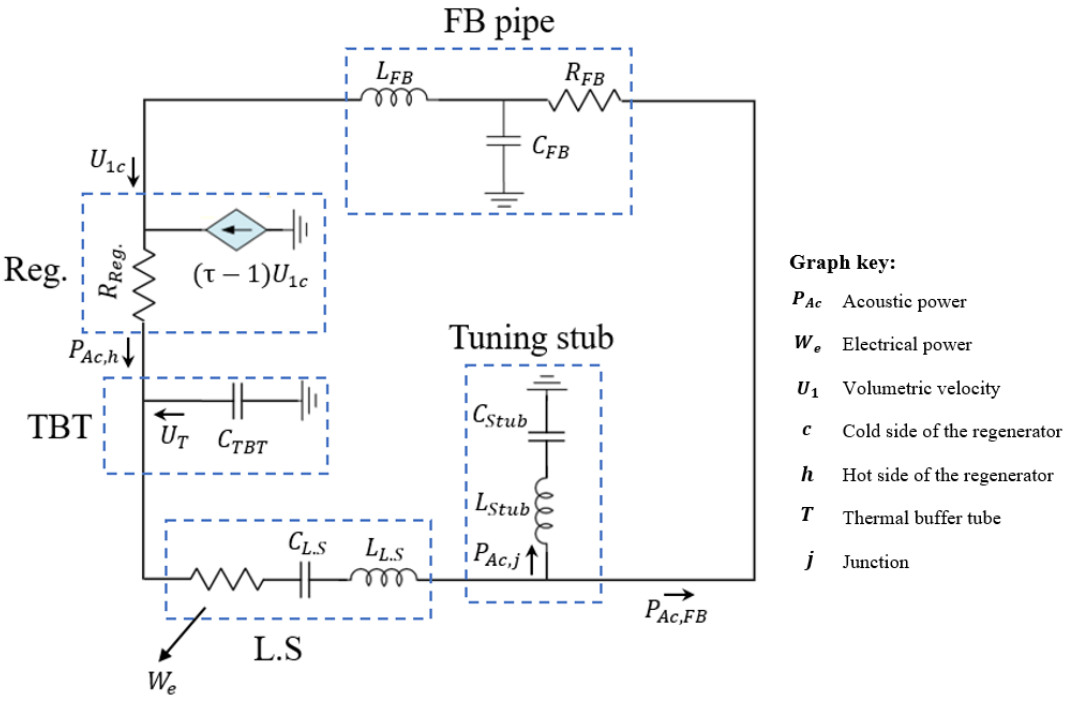


Figure 4.2: Simplified lumped-element model employed to examine the most important physical parts of the single core thermoacoustic electricity generator. A graph code key is provided on the right-hand side of the graph.

The regenerator is modelled as the combination of a resistance and a controlled current source. In the regenerator, the inertance part of the impedance of the regenerator is negligible compared to the resistive part. The resistive part is such, due to the viscous flow in the small-passages of the screen bed that forms the regenerator. Therefore, the viscous resistance is modelled as, $R_{Reg.}$ in Figure 4.2. The controlled current source, $(\tau - 1)U_1$, is used to replicate the acoustic velocity amplification and temperature gradient characteristics of the regenerator. Here τ is the amplification factor, and can be defined as the ratio of the temperature of the hot side of the regenerator to the temperature of the cold side, $\tau = T_H/T_C$.

The compliance appearing below the regenerator is used to model the compressibility of the working gas in the thermal buffer tube.

The loudspeaker is described approximately by the following harmonic-approximation

equations (Swift 2017):

$$\Delta p_1 = \frac{\iota}{A_{L.S}} I_1 + \frac{R_m + iX_m}{A_{L.S}^2} U_1 \tag{4.1}$$

$$I_1 = \frac{\iota}{A_{L.S} * (R_e + iX_e)} U_1 \tag{4.2}$$

Here: Δp_1 is the pressure drop across the loudspeaker diaphragm, I_1 is the complex electric current through the loudspeaker, $A_{L.S}$ is the area of the loudspeaker, ι is the transduction coefficient, which is also called the Bl product, R_e is the winding resistance of the coil, R_L is the load resistance, X_e is the electrical reactance, R_m is the mechanical resistance, and X_m is the mechanical reactance.

Substituting Equation 4.2 into Equation 4.1, and dividing both sides by U_1, gives the impedance of the loudspeaker as:

$$Z_{L.S} = \frac{\Delta p_1}{U_1} = \frac{1}{A_{L.S}^2} \left[\frac{\iota^2}{(R_e + R_L + iX_e)} + (R_m + iX_m) \right] \tag{4.3}$$

The electrical and mechanical reactances are given by:

$$X_e = \omega L_e \tag{4.4}$$

and

$$X_m = \omega M - \frac{K}{\omega} \tag{4.5}$$

Where: ω is the angular velocity, L_e is the electrical inductance of the loudspeaker, M is the moving mass of the coil and the cone, and K is the stiffness. The electrical reactance, X_e, can be omitted because it is much less compared to the electrical or the load resistances, R_e or R_L. Therefore, the impedance of the loudspeaker can be re-written as:

$$Z_{L.S} = \frac{1}{A_{L.S}^2} \left[\frac{(Bl)^2}{(R_e + R_L)} + (R_m + iX_m) \right] \tag{4.6}$$

The right hand side of Equation 4.6 shows that the loudspeaker introduces three components: the first component represents the total effect of the electrical resistance of the coil, the load resistance and the mechanical resistance, the second component is the inertance which replicates the inertial effect of the moving mass of the coil, and the last component is the compliance which represents the spring effect. Therefore, the three elements of the loudspeaker are replaced by a resistance, $R_{L.S}$, an inertance $L_{L.S}$, and a compliance $C_{L.S}$, and are connected in series in the impedance circuit of the thermoacoustic system as shown in Figure 4.2.

For a section of acoustic duct that has a length Δx that is much less than a quarter of the wavelength, and has a closed end, the acoustic impedance can be given as a combination

of an acoustic inertance, L_{Stub}, and an acoustic compliance, C_{Stub}. The compliance is assigned to the closed side of the acoustic duct because the compressibility of the gas is much more important than its inertia at that location, where $|p_1|$ is high and $|U_1|$ is low. Similarly, an inertance is assigned to the open side of the duct, because the inertia is important where the volumetric velocity $|U_1|$ is high. Therefore, the impedance of the stub can be given as (Yu, Jaworski and Backhaus 2012):

$$Z_{Stub} = \frac{i\omega L_{Stub}}{3} - \frac{i}{\omega C_{Stub}} \tag{4.7}$$

The inertance and the compliance are expressed as:

$$L_{Stub} = \frac{\rho_m \Delta x}{A_{Stub}} \tag{4.8}$$

$$C_{Stub} = \frac{V_{Stub}}{\gamma p_m} \tag{4.9}$$

Here: A_{Stub} is the cross-sectional area of the stub, V_{Stub} is the volume of the stub, and γ is the ratio of specific heats. The inertia and the compressibility of the working gas in the feedback pipe are replaced by an acoustic inertance L_{FB} and an acoustic compliance C_{FB}, respectively.

4.3 Simulation of the system

The simplified lumped-element model discussed in the previous section provides a qualitative understanding of the physical characteristics of the current system. However, the process of design and optimisation of such a system is very complex and involves mechanical, acoustic and electrical components. Therefore, and in order to obtain the predictions of the performance of the energy extractor, a computational analysis is performed using DeltaEC software. The steps involved in DeltaEC simulation of the single core thermoacoustic electricity generator are outlined in Figure 4.3.

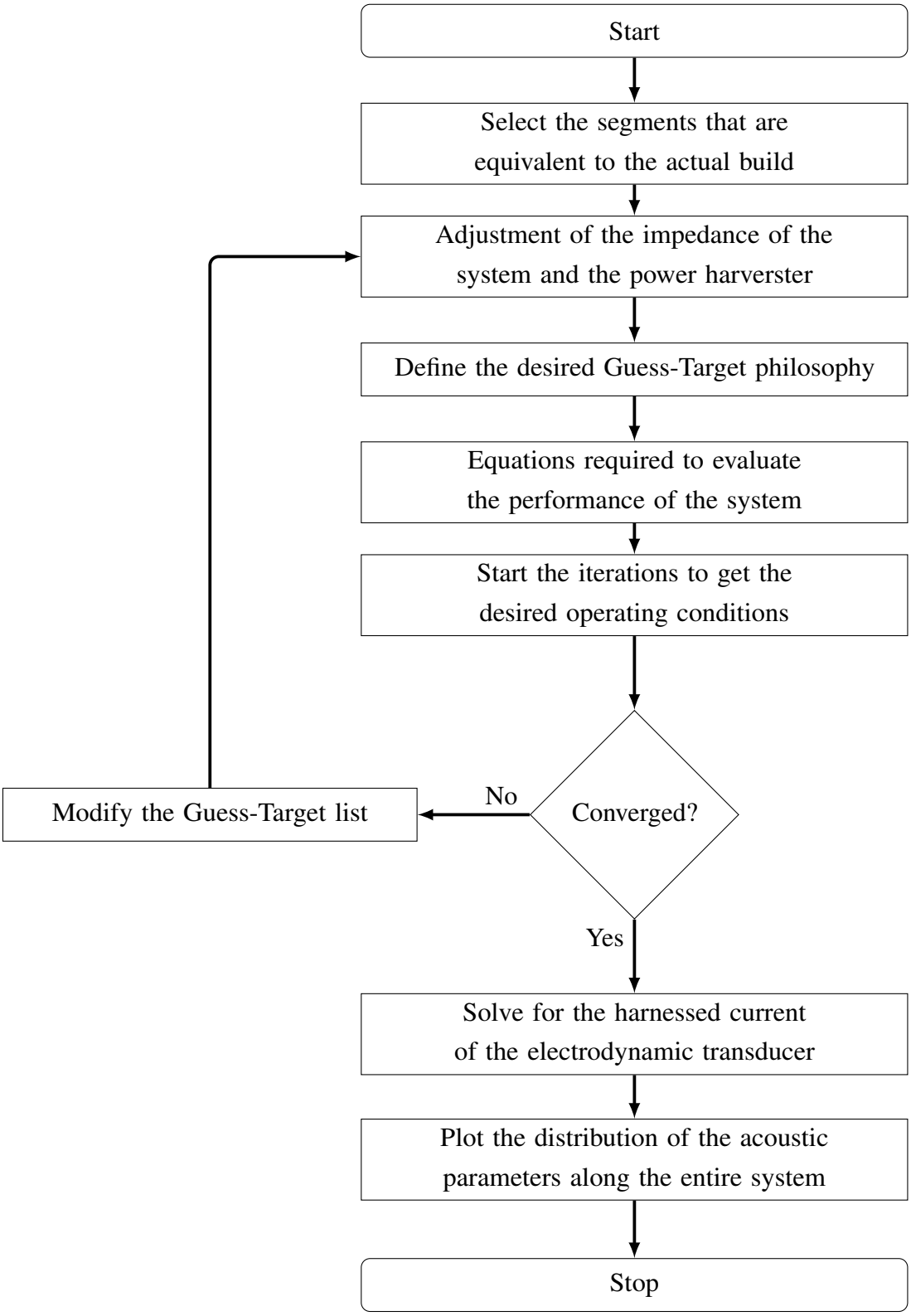


Figure 4.3: DeltaEC modelling procedure used to simulate a single-regenerator thermoacoustic electricity generator. This procedure is applicable to any looped-tube thermoacoustic system with a power extractor.

4.3.1 The geometrical parameters of the system

To realize the acoustic wave propagation and the power conversion within the system, a number of segments were chosen to model the entire system based on the actual prototype built by the SCORE project. The segments used to develop the DeltaEC thermoacoustic engine model are schematically illustrated in Figure 4.1. The functions of these can be explained as follows (Ward, Clark and Swift 2008):

- DUCT: As the name suggests, this is basically a pipe that has a cross-section and dimensions defined by the user. This segment was used in the model to represent the feedback loop and all other connectors.
  HX: This segment is used to simulate all the heat exchangers of the physical thermoacoustic electricity generator, to allow for heat addition and heat removal from the DeltaEC model.

- STKSKREEN: This segment represents the geometry and the material of the regenerator. Generally, there are two different segments to simulate different pore geometries. However, STKSCREEN has a stacked-screen mesh which accurately represented the regenerator used in the actual rig. The length of the STKSCREEN represents the total thickness of all the screens layers after being stacked together. Here, the regenerator is 12 mm long, and has an area equal to 0.04 m^2, with 73.3% volumetric porosity, and 56 μm hydraulic radius.

- STKDUCT: This segment represents the thermal buffer tube which is the section of the resonator between the hot heat exchanger and the secondary ambient heat exchanger. The input parameters for this segment are similar to the DUCT segment except for one extra parameter which is the cross-sectional area of the wall material A_{Solid}. The mean temperature along the STKDUCT is not constant, thus it is necessary to consider the changes in the temperature as it would affect the oscillating frequency. In this segment, the mean temperature of the working gas is not constant, and it is important to understand the changes in the temperature as this would affect the operating frequency. A common practice for the heat upstream of the thermal buffer tube is to be assumed as a guess, corresponding to a temperature target downstream of the STKDUCT. With HX, STKCREEN and STKDUCT, small changes in the guessed heat tend to largely change the downstream temperature during the shooting method. If long DUCTs or any other temperature-sensitive segments are located after the temperature-target segment, any targets after the long segments can be highly affected by the changes in the heat guess. The stability of the shooting-method can be improved in such cases by adding a segment that fixes the temperature immediately before of the long segment(s).

- BRANCH represents a side branch with specified impedance and it is used to model the tuning stub, to show how to split the volume flow rate between the feedback pipe and the stub. In BRANCH segment, the user specifies the real and the imaginary parts of the acoustic impedance, assumed dependent of oscillation frequency at the the low-frequency limit $\omega r/a << 1$ (Garrett 2017), where r is the radius of the branch pipe. The calculations used to estimate the stub impedance are obtained using Equation 4.7.

- IESPEAKER: This segment is used to simulate the alternator connected in series in the thermoacoustic prototype, with the function of extracting electricity from the loop acoustic power. The input parameters for the IESPEAKER include the moving mass of the coil, the spring constant, the force factor, the electrical resistance of the coil, the mechanical resistance, the inductance and the complex current. The values of the input parameters of all above-mentioned segments are summarized in Table 4.1, while the governing equations for each physical segment employed to construct DeltaEC model for the current engine are provided separately in Appendix A.

- JOIN: This segment was used on both ends of the thermal buffer tube, and between the regenerator and the adjacent heat exchangers, to model adiabatic-isothermal interface losses there.

In addition to the above segments, it should be noted that a segment named as "RPN" was added many times in the model. Essentially, RPN is a user-defined segment that doesn't refer to any physical component, but it is a segment that is often used to display some interesting algebraic calculations, such as the penetration depths and the local acoustic impedance in various parts of the simulation. The calculations are obtained using a Reverse Polish Notation, hence the name "RPN" (Burks, Warren and Wright 1954).

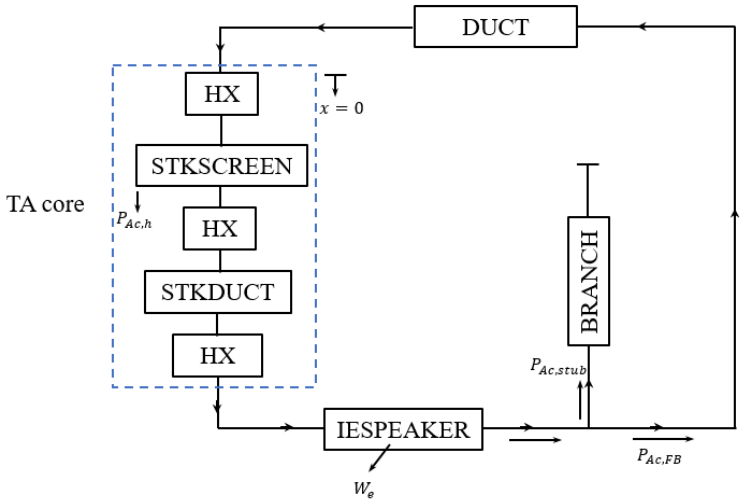


Figure 4.4: Schematic illustration of the DeltaEC segments used to develop a model for the single core thermoacoustic electricity generator. The dotted blue box shows the thermoacoustic core. The simulation starts at the top of the TA core ($x = 0$).

Table 4.1: Design parameters of the single-stage thermoacoustic engine.

Component	Specification
Main ambient heat exchanger	Length: 25 mm, porosity: 0.115, plate spacing: 2.934 mm
Regenerator	Length: 12 mm, porosity: 0.733, hydraulic radius: 56 µm
Hot heat exchanger	Length: 40 mm, porosity: 0.7, plate spacing: 9 mm
Thermal buffer tube	Wall area: 0.00116 m^2
Secondary ambient heat exchanger	Length:10 mm, porosity 0.713
Tuning stub	Diameter: 70 mm, length: 0.07 m
Feedback pipe	Area: 0.0038 m^2, diameter: 7 cm

4.3.2 The operational parameters of the system

Fundamentally, the size of a thermoacoutsic system is determined mainly by the operating frequency or vice-versa, as the engine has to operate on the resonant frequency defined by the initial acoustic boundary conditions. The frequency plays a vital role in the performance of the thermoacoustic engine, because it's linearly proportional to the power density (Swift 2017). Also, the voltage induced in the alternator's coil is proportional to the velocity of the coil, u. The coil velocity can be expressed as a

function of the operating frequency as follows:

$$u = 2\pi f x \tag{4.10}$$

Where: f is the operating frequency (Hz), x is the displacement amplitude of the loudspeaker's coil (mm). Moreover, the alternator has its own resonant frequency which is inversely proportional to the square root of the moving mass and the compliance of the suspension. The force required to drive the alternator strongly depends on the frequency. However, the cone itself is relatively weak and fragile, and can be easily damaged if a high force is applied. Therefore, it is necessary to select the system operating frequency as close as possible to the alternator's resonant frequency. For a given displacement amplitude, a high operating frequency would induce a high voltage on the alternator's coil.

Consequently, the operating frequency is inversely proportional to the thermal penetration depth. A high operating frequency leads to small pore size for the regenerator, and hence high material cost of the engine core. In this model the system operating frequency is selected to be 75 Hz which is a compromise between the requirements from the regenerator geometrical parameters (i.e. matching the hydraulic radius of the regenerator) and the linear alternator working conditions (i.e. operating on the natural acoustic mode). The operating frequency leads to a total engine length of about 4.4 metres.

The system uses air under atmospheric pressure as the working gas, after careful consideration of the cost and the availability of the gas itself in developing countries. The material and manufacturing costs of the entire system were considered, because the size of the feedback pipe depends on the wavelength which is related to the speed of sound of in the working gas. For a given operating frequency, a working gas with a low acoustic speed would help to reduce the length of the feedback pipe, which in turn would cut down the total cost. On the other hand, short feedback pipe will lead to lower power dissipations.
The acoustic power density is proportional to the mean pressure of the working gas, P_m. Working on mean pressure higher than 1 bar required a smaller regenerator flow channel, because the thermal penetration depth is inversely proportional to the square root of the mean pressure. The small size of the channels adds extra challenges to the construction of the system.
The type of the working gas, the mean pressure and the operating frequency all are initialized in the *BEGIN* segment in the DeltaEC model. These global parameters are shared among the downstream segments such as ducts, heat exchangers, ...etc.

In essence, thermoacoustic engines convert thermal power into acoustic energy, while thermoacoustic coolers use the acoustic energy input to produce refrigeration capabilities. The acoustic/electric energy conversion required in either type of the thermoacoustic systems is usually achieved by an electro-dynamic transduction mechanism. Thermoacoustic systems typically use high efficiency flexure-bearing supported linear alternators. A flexure-bearing consists of a stack of several spiral-cut circular metal plates with a piston attached to its center. The stack of plates forms a bearing that is relatively soft in the axial direction and is extremely stiff with respect to radial, rocking or twisting motion of the piston.

Although, these linear alternators perform the acoustic-to-electric power conversion with high transduction efficiency and reliability (Saha et al. 2012), they have very high acoustic impedance at the working frequency of the system and have to be installed at a high impedance region in the thermoacoustic field. The high acoustic impedance mostly causes a high pressure drop. Therefore, most linear alternators employ a clearance seal which is basically a small radial gap of about 10 μm between the cylinder and the piston to avoid friction losses (Backhaus, Tward and Petach 2004). However, part of the working gas can escape via the gap when the pressure difference between the two sides of the piston is high, which might cause acoustic streaming.

In some thermoacoustic engine configurations, the piston faces the engine, while its back is enclosed. Such streaming will allow the gas to accumulate on one side of the piston and therefore, the mean pressure at the two sides of the piston will be unequal. Moreover, such linear alternator tends to be costly because the clearance seal requires a high-cost manufacturing process. The high cost of these alternators would eliminate the advantage of developing low-cost thermoacoustic power converters targeted by the SCORE project. However, in less demanding applications where low-cost is a key component in the design process, inexpensive commercially available audio loudspeakers can also be good candidates for producing electrical power at a fraction of the cost (Yu, Saechan and Jaworski 2011). However, the function of the loudspeakers is to convert an audio signal into a corresponding sound rather than producing electricity. In addition, loudspeakers do not match precisely the requirements of thermoacoustic electricity generators due to their fragile paper cones, limited strokes, and the relatively low transduction efficiency. Therefore, integration of loudspeakers with thermoacoustic systems brings new challenges and design issues, which should be addressed. In the current engine design, a test alternator is built utilizing an ordinary audio loudspeaker JL6W3v3-3 to act as an electro-acoustic transducer. The parameters of the loudspeaker are listed in Table 4.2 (Riley 2014*b*).

Table 4.2: Electrical and mechanical parameters of the loudspeaker.

Component	**Value**	**Unit**
Nominal diameter	165	mm
The moving mass of the transducer, **M**	20	g
Mechanical quality factor, $\mathbf{Q_m}$	11	-
Linear excursion, $\mathbf{x_{max}}$	9.4	mm
Bl product	7	T.m
Electrical resistance of the coil, $\mathbf{R_e}$	4	Ω
Electrical inductance of the coil, $\mathbf{L_e}$	0.001	H
The spring constant of the transducer, **K**	4337	N/m
The mechanical resistance of the transducer, $\mathbf{R_m}$	0.18	N.s/m

Where: *Bl* is the product of magnetic field strength in the coil gap and the length of the wire immersed in the magnetic field.

4.3.3 DeltaEC results for the acoustic's key parameters

For further understanding of the thermodynamic characteristics of the engine, axial distribution of the key acoustic parameters obtained from DeltaEC are plotted and shown in **??** to Figure 4.9 where the mean pressure is 1 bar, and the maximum temperature of the HHX is 650 °C. The working frequency is 75 Hz, and the input heating power is 1.5 kW. The load resistance of the alternator is 30 Ω. In these plots, the *x*-axis starts at the joint between the feedback pipe and the main ambient heat exchanger, and passes counter-clockwise through the other parts of the engine until it ends up in the feedback pipe where the acoustic power transports back to the AHX, as shown in Figure 4.4. The pressure amplitude of oscillation, the volumetric velocity amplitude and the phase angles of them are set to be equal at the first and the final ends of the model. The total length of the engine is around 4.4 m.

The axial distribution of the pressure amplitude is demonstrated in Figure 4.5. The regenerator locates at the left end of the curve (i.e. in the range of x = 0.026 m to x = 0.038 m). As presented in the Figure, there are two crests and two troughs of the pressure amplitude throughout the engine. The two pressure amplitude nodes are at x = 0.75 m and x = 3.35 m, respectively. The two pressure amplitude anti-nodes appears at the cold end of the regenerator at a distance x = 0.025 m, and at the feedback pipe, close

to the middle of the system (x = 2.2 m). At the location of the regenerator, the pressure amplitude drops from 5.3 kPa to 4.8 kPa. Also, the pressure amplitude decreases by 178 Pa across the alternator which has been installed immediately after the engine core. The highest pressure amplitude value in the loop is 5.3 kPa at the the cold end of the regenerator, and the lowest pressure amplitude value is 2.3 kPa at the mid-point of the loop. Therefore, the resulting pressure standing wave ratio can be estimated by these two pressure amplitude values as 2.3. Pure travelling wave systems have a pressure standing wave ratio equal to 1 (Crocker 1998). Comparing this ideal ratio to the one in the current design reflects that the acoustic reflection within the feedback pipe is relatively high, and the standing wave component contributes to the acoustic losses along the feedback pipe.

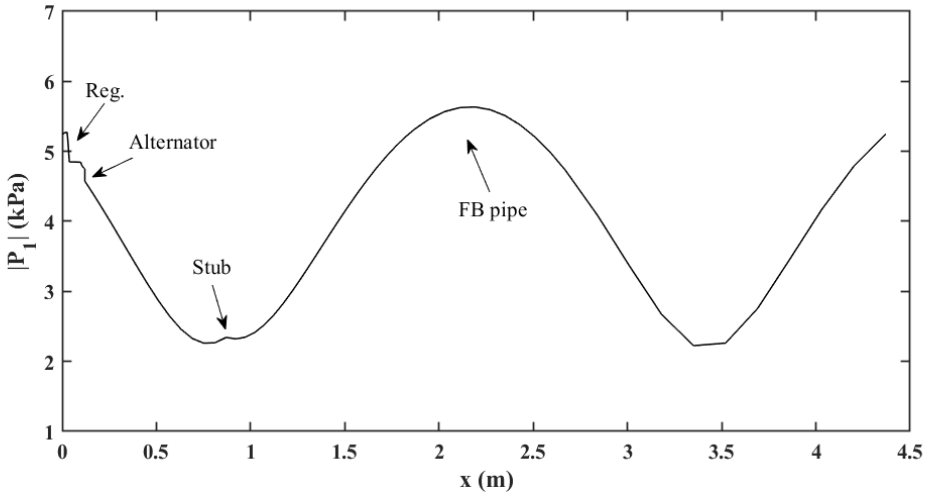


Figure 4.5: Axial distribution of the pressure amplitude of the gas throughout the engine.

As shown in Figure 4.6, the volumetric velocity amplitude increases from 0.027 m^3/sec to 0.034 m^3/sec across the regenerator, because of the temperature difference between the hot and the cold side of the regenerator (Swift 2017). The regenerator locates near the volumetric velocity node, which means the local acoustic impedance within the regenerator is high. For travelling wave thermoacoustic engines, a low value of volumetric velocity is preferred to maintain low viscous dissipations within the regenerator. The low volumetric velocity resulted from the self-configuration mechanism of this engine. Essentially, it is determined by the flow resistance of the regenerator which is relatively high compared to the other system components. For a given pressure amplitude of oscillation, the relatively low velocity is caused by the high flow resistance of the regenerator (Backhaus and Swift 2000). Also, it can be seen that the alternator locates in a region of relatively high volumetric velocity amplitude of about 0.045 m^3/sec, which is good for extracting of electrical power according to the optimum

electrical power output equation:

$$W_e = \frac{1}{8}|U_1|^2 \frac{Bl^2}{R_L * A_{Alt.}^2} \tag{4.11}$$

Here: W_e is the electrical power output, R_L is the load resistance, and $A_{Alt.}$ is the cross-sectional area of the alternator.

The volumetric velocity increases from 0.045 m^3/sec to 0.06 m^3/sec along the pipe that is located between the alternator and the tuning stub. It can also be seen that the volumetric velocity decreases suddenly at the location of the stub branch, which indicates that the stub removes part the volumetric velocity, and this is another design strategy of the current engine. Moreover, in the middle of the feedback loop, the volumetric velocity reaches a minimum value of 0.023 m^3/sec which corresponds to approximately 6 m^3/sec speed of acoustic wave.

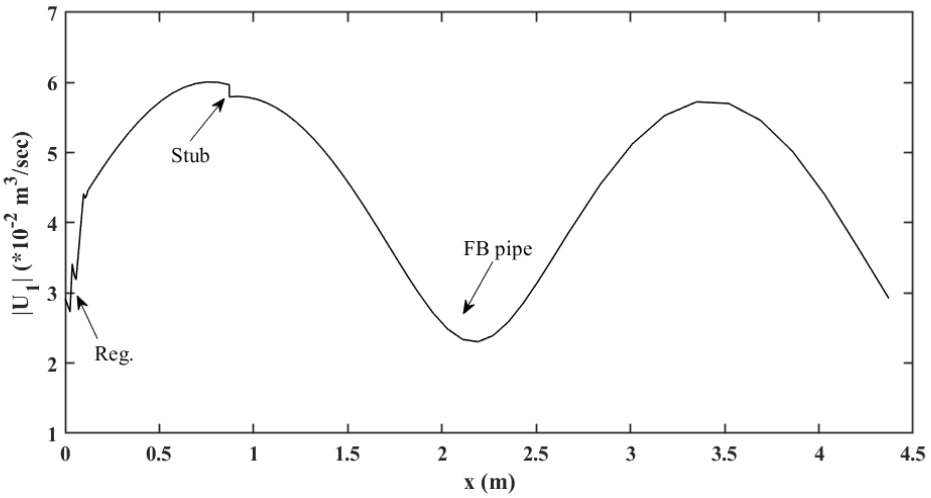


Figure 4.6: Axial distribution of the volumetric velocity amplitude of the gas throughout the engine.

For an acoustic wave, the acoustic impedance is defined as the ratio of the acoustic pressure, P_1, to the acoustic volume flow, U_1:

$$Z = \frac{p_1}{U_1} \tag{4.12}$$

The specific acoustic impedance can be expressed as the ratio of the acoustic pressure to the specific flow, u_1:

$$z = \frac{p_1}{u_1} \tag{4.13}$$

The acoustic pressure, p_1, and the flow velocity, u_1 are given by:

$$p_1 = -\kappa \frac{\partial y}{\partial x} \tag{4.14}$$

$$u_1 = \frac{\partial y}{\partial t} \tag{4.15}$$

a simple displacement solution of the wave equation of sound in compressible lossless gas can be written as a function of position x and time t:

$$y = A\sin(kx - \omega t) \tag{4.16}$$

Where: ω is the angular velocity and k is the wave number, κ is the adiabatic bulk modulus, given by:

$$\kappa = \gamma p = \rho a^2 \tag{4.17}$$

The specific acoustic impedance, z, of a lossless travelling wave should be $\pm\rho a$. However, for a practical regenerator, the $z/(\rho a)$ is greater than one because viscous losses cannot be neglected, and sometimes are the main losses in thermoacoustic engines.

Figure 4.7 shows the distribution of the specific acoustic impedance along the engine. In the cold end of the regenerator, the ratio of the absolute acoustic impedance, |Z|, to the gas characteristic impedance, ρa, is approximately 20 which indicates the acoustic losses are minimized. Within the alternator at a distance x = 0.1 m, there is a slight decrease in the absolute acoustic impedance of about 3.9 kPa.sec/m^3. This decrease in the acoustic impedance has been compensated relatively by the existence of the stub branch tube, where there is a little increase of 1.2 kPa.sec/m^3 in the absolute impedance. The increase in the acoustic impedance at the stub location resulted from the decrease in the volumetric velocity as in Figure 4.6. The highest value of the absolute acoustic impedance in the loop is around 240 kPa.sec/m^3, and it is almost in the middle of the engine.

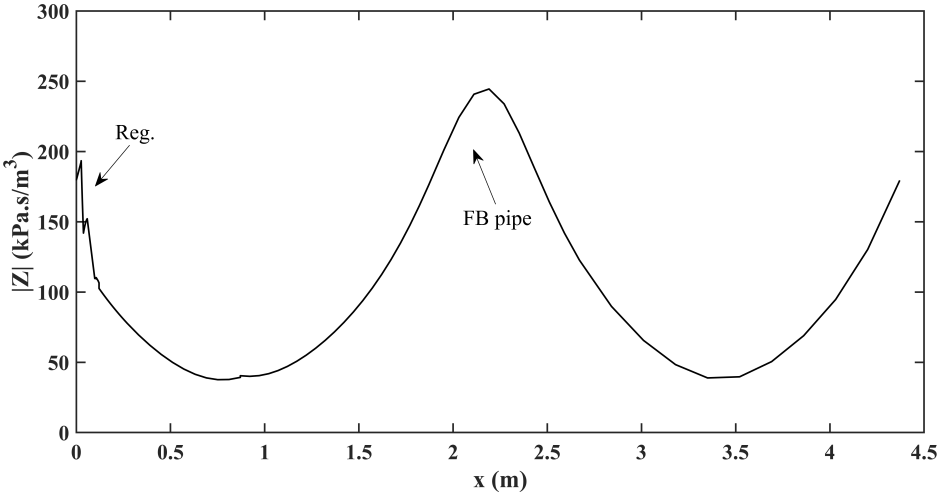


Figure 4.7: Axial distribution of the absolute acoustic impedance along the engine.

The distribution of the phase difference between the pressure and the velocity of oscillation along the engine is shown in Figure 4.8. It can be found that the phase angle, ϕ, in the regenerator section is between -20° and +20°. However, the phase angle in the feedback pipe is closer to 46° or -46°, which confirms that the standing wave is pronounced within the feedback pipe. At a distance x = 0.1 m, where the alternator is located, the phase angle increases to 46° as a result of the power extraction in the alternator which significantly drops the travelling-wave component (Kang, Zhou and Li 2010).

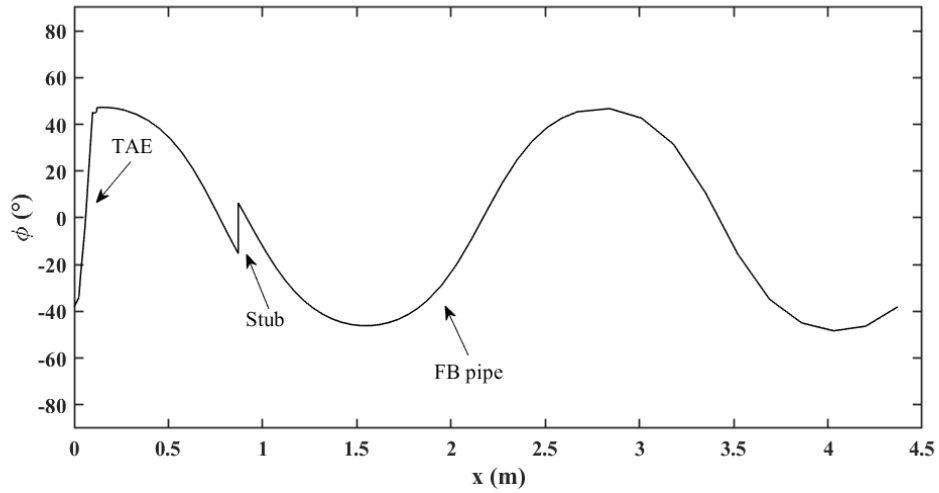


Figure 4.8: Axial distribution of the phase angle difference between the pressure and the volumetric velocity of oscillation along the engine.

Figure 4.9 shows the flow of the acoustic power along the engine. It can be seen that at the starting point where x = 0, there is 60.4 W of acoustic power that flows into the main ambient heat exchanger AHX. Within the AHX, about 0.5 W of acoustic power was dissipated. The remaining acoustic power entered the cold end of the regenerator. After the acoustic power was amplified in the regenerator, about 77.3 W emerged out of the hot end of the regenerator. Part of this acoustic power was dissipated in the HHX, the SAHX, and the TBT before the remaining 73.9 W flowed to the alternator.

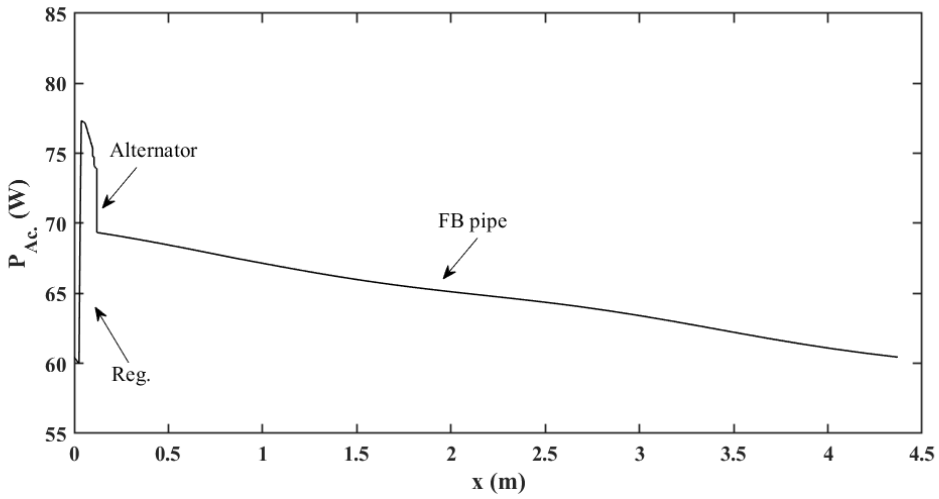


Figure 4.9: Axial distribution of the acoustic power along the engine.

The useful electrical power extracted by the alternator is around 3.5 W. After the alternator, about 69 W of the acoustic power passed along the feedback pipe, where 8.6 W was lost before it passed to the starting point.

4.4 Experimental investigations and validation

4.4.1 Lab device, design and construction

The engine was initially designed to be integrated with a wood burning stove. However, for experimental purposes, an electrical heater was used to supply the heat instead of a fire from burning wood. Using an electrical heater will allow for accurate measuring of the heat input into the engine, and offers optimal acoustic design as the heat supply source is compact, and therefore, it helps with designing structures to transfer heat to the working gas. The electrical heater was placed in an insulated block, and then connected to the case of the thermoacoustic core. The heat supply from the electrical heater can be varied using a rheostat, while the electrical power drawn by the heater was captured using a power meter that connected to the power supply of the heater. The engine was equipped with a single core, connected to a feedback pipe in a loop configuration, as shown in Figure 4.10. Typically, the thermoacoustic engine consists of six main modules: Engine core, Thermal buffer tube (TBT), Secondary ambient heat exchanger (SAHX), Feedback pipe (FB pipe), Linear alternator and Tuning stub. The core of the engine is essentially an acoustic amplifier (Yu and Jaworski 2010). It consists of a regenerator clamped in between a main ambient heat exchanger (AHX) and a hot heat exchanger (HHX).

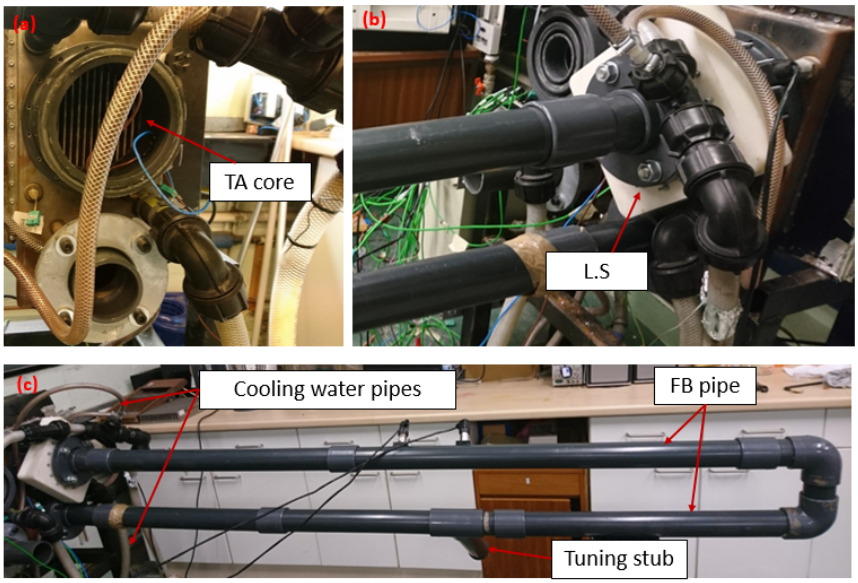


Figure 4.10: A general testing outline of the single core thermoacoustic electricity generator showing the main components: (a) The thermoacoustic (TA) core, (b) The loudspeaker, and (c) the cooling water pipes, feedback pipe and the tuning stub.

The Main Ambient Heat Exchanger

The SCORE Demo 2 engine was designed to dissipate 1.7 kW of heat through the ambient heat exchanger. To meet this design, SCORE project inspected different types of heat exchangers, one of which was the commercially available air cooled heat exchanger. These types of heat exchangers were rejected on the grounds of cost, because it was found that, to dissipate this amount of heat from the system, a large surface area on the gas side is needed. Also, thick metal sections are required to transfer the heat to the large gas surfaces, plus fans to enhance the heat transfer, therefore providing a better performance. It was also realized that it is impossible to hit the target even if the optimal material (aluminium) is used. Then, liquid-cooled heat exchangers were adopted because water can be the liquid transfer medium, and therefore the cost can be reduced. The advantages of the liquid-cooled heat exchangers are their higher heat transfer rate, and their ability to remove more heat due to the higher heat capacity of the liquid. The disadvantages are that extra equipment is needed, and its efficiency is less for small engines. However, the automotive sector has many years' experience in designing efficient low-cost radiators for the cooling system of the automobile engines. Therefore, conventional auto-mobile radiators were selected as the ambient heat exchanger. Riley (2014*b*) suggested that the cost in volume is slightly higher than the targeted cost when using automobile radiators for the design of the AHX, but it is acceptable in the absence of a better alternative.

The ambient heat exchanger, as shown in Figure 4.11, is 250 × 217 mm and made from the core of a typical low-cost automobile radiator, suitably modified to fit the thermoacoustic engine and to enhance the sealing capabilities. The thickness of the AHX is 25 mm, with tube plates at 10 mm pitch, and 10 mm spaced fins. The system uses the water circulation (thermo-siphon) method to dissipate heat whilst maintaining a good path for the hot air along the convoluted plates of the HHX. Therefore, the requirement for a pump in the system was eliminated. The water feed is attached to a 35 mm diameter nozzle at the lower end, to prevent air locks in the radiator channels, which might cause temperature soar, and therefore the possibility of melting the radiator. In the front of the AHX, there are two PVC plastic adaptors that are connected via 120 mm diameter holes, while on the rear of the radiator, two rectangular holes of 200 × 200 mm were drilled for the regenerator. The AHX is sealed to the upper plate using silicon grease.

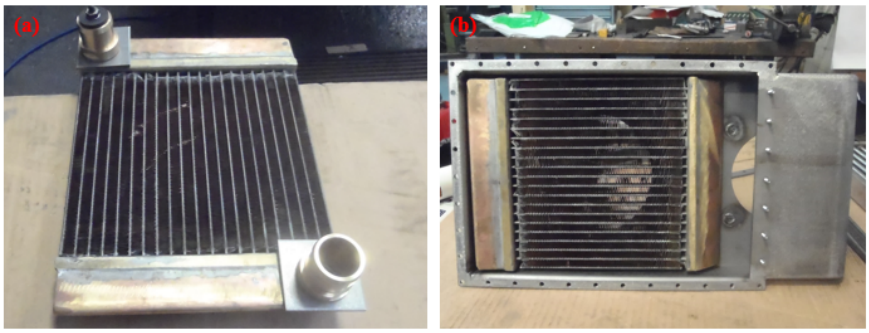


Figure 4.11: Photographs of the ambient heat exchanger. (a) The radiator with two holes drilled for the water inlet and outlet. (b) Assembly of the radiator and the upper housing.

Regenerator

The Regenerator matrix is the most important part of the thermoacoustic engine, as mentioned earlier in the literature review. It acts as a "temporary heat storage" medium for the working gas while it completes a thermodynamic cycle. In this engine, the regenerator is sandwiched between the radiator (AHX) and the hot heat exchanger (HHX), as depicted in Figure 4.12. The volumetric porosity and the hydraulic radius are the two crucial parameters to determine the characteristic of the regenerator. The volumetric porosity, ϕ, is defined as the ratio of gas volume to the total volume of the regenerator, and can be expressed as:

$$\phi = \frac{V_{gas}}{V_{total}} = 1 - \frac{V_{solid}}{V_{total}} \tag{4.18}$$

where V_{gas} and V_{solid} are the volume occupied by the working gas and the solid media, respectively, and V_{total} is the total volume which includes both gas and solid volumes.

For regular geometries, the porosity can be expressed using the cross-sectional area occupied by the gas:

$$\phi = \frac{A_{gas}}{A_{total}} \tag{4.19}$$

For a parallel plate stack with a thickness of $2l$ and a plate spacing of $2y_0$, the volumetric porosity is given as:

$$\phi = \frac{y_0}{y_0 + l} \tag{4.20}$$

The porosity of an array of crossed straight rods, or individual wire segments of a diameter D_w in the plain square-weave screens, that are widely used for regenerators can be expressed as:

$$\phi = 1 - \frac{\pi n D_w}{4}\sqrt{1 + (nD_w)^2} \tag{4.21}$$

Where: n is the mesh number which represents the number of wires per unit length, and D_w is the wire diameter. The hydraulic radius, r_h, is a characteristic linear parameter that is used to quantify the pore size of a porous medium. It is defined as the ratio of the volume occupied by the gas, V_{gas} , to the gas-solid interface area, A_{wetted}:

$$r_h = \frac{V_{gas}}{A_{wetted}} \tag{4.22}$$

For a channel with cross-sectional area A and perimeter Π, the hydraulic radius is conventionally expressed as the ratio of the channel's cross-sectional area to its perimeter.

$$r_h = \frac{A}{\Pi} \tag{4.23}$$

The hydraulic radius of a circular channel equals half of the actual radius of the circle: $r_h = r_0/2$, while for parallel plates with uniform spacings of $2y_0$ between the plates, the hydraulic radius is half of the plate spacing: $r_h = y_0$.
For tortuous porous geometries, the hydraulic radius can be estimated using the porosity, ϕ, and the wire diameter, D_w as follows:

$$r_h = D_w \frac{\phi}{4(1-\phi)} \tag{4.24}$$

The regenerator used in this system is made out of from 50 layers Stainless Steel wire mesh machined to a required size of 200 $\times$ 200 mm. The mesh wire has a diameter of 82 µm and a pitch of 250 µm. The volume porosity of the regenerator is calculated using Equation 4.16 to be around 73.3% for a hydraulic radius of 56 µm. The air thermal penetration depth through the regenerator is much bigger than the hydraulic radius and is about 365 µm. The even sheets are slightly corrugated yielding 12 mm thickness of the regenerator. These mesh layers are positioned in a rectangular hole drilled in the back of the AHX, with approximately 4 mm space left for high temperature insulation.

The stacked mesh layers are then compressed by the HHX. AHX and the HHX are placed on opposing sides of the regenerator to create the thermoacoustic effect that generates a travelling acoustic wave in the feedback tubes.

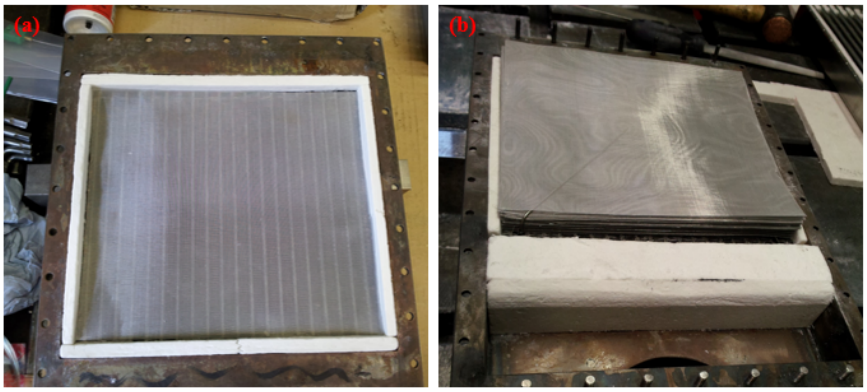


Figure 4.12: Photographs of the regenerator mesh in the thermoacoustic engine unit. (a) The rectangular hole drilled for the mesh layers. (b) The Stainless Steel mesh layers after being stacked together.

The Hot Heat Exchanger

The hot heat exchanger (HHX) is used to transmit heat to the regenerator mesh. To maintain a low cost for the current engine, and to obtain a quick warm-up time, a low-mass convoluted stainless steel plate design is adopted for the HHX, as shown in Figure 4.13. Unlike the conventional thermoacoustic systems, the HHX is built to receive the heat from burning wood. This meant the heat exchange between the combustion gas and the thermoacoustic gas has to take place with the combustion side being particularly vicious due to corrosive compounds produced from wood in the gas stream. The hot heat exchanger is 232.9 $\times$ 307 mm and was made of 3 mm thick 304 low thermal mass Stainless Steel plate with a convoluted profile. The fin height at the inside of the convoluted plate is adjusted by 3 mm thick aluminium plate in order to transfer a large amount of heat to the regenerator in a restricted space from a low power density heat source, such as fire from burning wood. The HHX was placed into the upper frame and its edges were sealed. The plate is welded to a flange that is designed to be directly bolted to the engine housing.

In the current experimental investigations, each convoluted HHX receives heat from a custom-made 2 kW electrical heater that is designed to simulate the combustion of the wood. The electrical heater is made from 12 off, 42 turns of 20 SWG nichrome wire on a 6 mm former, wound to 150 mm length, and stretched to 170 mm to fit screw pitch. A turn at each end is flattened so it can be screwed in, so there are only 40 active turns. Each coil is 1.7 Ω, and twelve are connected in series making 20 Ω total. Resistance changes with temperature, so operating current is 10 Amps at 230 V.

The electrical heater is placed in an insulated enclosure heater box, and then mounted to the engine. The heater is equipped with a PID (proportional-integral-derivative) temperature controller, to control the temperature of the heater. In order to achieve better heat transfer, and to reduce heat dissipations, three layers (25 mm) of heat resistant, low thermal conductivity super wool fibre insulation were applied between the heater box and the engine housing.



Figure 4.13: Convoluted hot heat exchanger of the single thermoacoustic engine. (a) The convolutions. (b) The convolution after being bolted to the lower housing. (c) Back view of the HHX with a completed insulated lower housing unit. (d) Top view of the convoluted HHX and the lower housing.

The Case

After the core parts had been assembled, the AHX pressed the regenerator against the convoluted HHX, to ensure that the regenerator mesh was not moving and was fixed in place. All the other system components were then compressed between two cases (upper and lower). The upper case is made out from 3 mm thick mild steel because it does not experience high working temperatures. Also, the mild steel has a relatively low-cost compared to the stainless steel. The lower frame is directly attached to the convoluted plate HHX, thus it is important to select a metal that has a low thermal conductivity to ensure minimum thermal dissipations. Therefore, the lower case is made from 3 mm thick 304 thermal resistant stainless steel. The lower case is aligned and clamped with the upper housing, and holes are drilled through both housing flanges and fastened together using M8 bolts. For a better fastening, and lower heat conduction, a high heat resistant gasket is applied between the two cases.

The Thermal Buffer Tube

Below the hot heat exchanger, there is a short section of thermal buffer tube (TBT) which is in a direct contact with the secondary ambient heat exchanger (SAHX). The TBT is designed to allow the hot gas to be cooled by the SAHX, immediately after it flows out from the HHX. In this way, the feedback loop will be separated from the hot side of the engine, and hence the heat transfer efficiency will be improved. The TBT is made from a mild steel pipe with the end machined to mate the commercially low-cost drain fittings. The TBT has a wall area of 0.00116 m^2, and it is welded to the front side of the radiator flange.

The Secondary Ambient Heat Exchanger

In the current system, heat is extracted via the AHX augmented by the secondary ambient heat exchanger (SAHX). The SAHX is also used to intercept the heat leaking down the thermal buffer tube, and therefore protect the alternator housing. Similar to the AHX, the SAHX is made from a piece of commercial car radiator to fit tightly inside the thermal buffer tube (TBT). The length of the SAHX is 10, and its volumetric porosity is 71.3%.

The Linear Alternator

To extract the electrical power in this system, a low-cost commercial loudspeaker; model JL 6W3v3-4 was used as a linear alternator and was positioned in the loop in the front of the ambient heat exchanger as depicted in Figure 4.14. The loudspeaker's nominal diameter is 165 mm, and 4 Ω nominal impedance. The specifications and the Thiele & Small parameters are given earlier in Table 4.2.



Figure 4.14: Photograph of the loudspeaker used to extract the electrical power from the acoustic power.

The Tuning Stub

An extra pipe perpendicular to the feedback loop is called the tuning stub and is installed in the system using a T-joint. The stub is used to enhance the impedance matching between the acoustic wave and the linear alternator, and to suppress the acoustic impedance disturbance in the thermoacoustic field caused by the engine's core and the alternator. To adjust the impedance ratio and the phase difference, and therefore to achieve the optimum acoustic power, the length of the stub branch was adjusted manually. However, the length (thus volume) can also be varied by placing a moving piston in the pipe (Jaworski and Mao 2013; Yu, Jaworski and Backhaus 2012). The stub used here in this engine is a section of standard PVC (Polyvinyl Chloride) pipes, which has the same diameter of the main feedback pipe of 70 mm. One end of the stub is connected to the loop, while the other end is closed by a commercially available standard PVC cover. For pressurizing the whole engine, a standard pressurized valve is mounted on the circular PVC cover.

The Feedback pipe

For the connection of the whole system as a closed loop, a high quality solid-wall with 70 mm inner diameter standard underground PVC pipes and fittings are used as shown in Figure 4.15. These pipes are selected instead of metal plate pipes to meet the

desired cost of the system. These plastic pipes also enable investigation into different loop configurations. The acoustic power produced by the thermoacoustic effect in the regenerator mesh is transmitted from the casing via the thermal buffer tube into the feedback pipe. The acoustic wave eventually returns from the feedback pipe via the ambient heat exchanger, where it is continuously amplified by the thermoacoustic effect within the regenerator. The total length of the loop is about 4.4 m, which leads to an operating frequency of 75 Hz. Air leaks can affect acoustic performance, so it is vital to eliminate these. Therefore, silicone grease is applied on each PVC fitting.



Figure 4.15: Photograph of the standards PVC pipes and fittings used to assemble part of the feedback pipe.

4.4.2 Measuring instruments

All the experiments in this piece of work were conducted at atmospheric pressure, and ambient room temperature. Air was used as the working fluid for the thermoacoustic system. The temperatures and oscillating pressures are monitored at certain locations throughout the system. The entire experimental set-up is shown schematically in Figure 4.16. Water flow from a water tap is used to cool the ambient heat exchanger, and the rejected water is flowing into an external water tank. A water flow meter (Type TM-47X, FM-S Rotameter® Series 2000) with an accuracy of $\pm$ 1.2% of indicated flow is adopted for monitoring the water flow rate of the system.

A total of five thermocouples (Type-K RS Components) are utilized for monitoring the temperatures of the working gas and the water. Three of these thermocouples are embedded in the middle of the engine core to capture the temperatures at the cold and the hot sides of the regenerator, as well as the surface temperature of the heater box. The rest of the thermocouples are attached to the water inlet and outlet pipes to monitor the temperature of the cooling water. All the thermocouples used here were certified by the manufacturer to conform to K-Type calibration, which gives an accuracy of

$\pm 1^{\circ}$ C. Two pressure transducers (model IM-A5000-1A4-BXV-00-063) are used to measure the pressure of oscillation in different locations. One of these transducers was placed on the radiator frontal flange to capture the peak pressure amplitude inside the thermoacoustic core, while the other was positioned in the feedback loop to record the strength of the wave there. The pressure sensors were calibrated by the manufacturer, to give an accuracy of $\pm$ 0.1%.

The readings of the thermocouples and the pressure transducers are obtained using a Data Acquisition (NI cDAQ 9172) with one thermocouple module (NI 9211) and one bridge module (NI 9237) to convert the measured signal into a digital signal and thus it could be saved as (*.txt) file. This data acquisition is connected via a USB cable to a data logger system with appropriate software developed by SCORE project. The signal from the pressure sensors is also visualised and saved using an oscilloscope (RS component model PRO IDS 6072A-U) with an accuracy of 0.01%. A wide range variable resistor (model VISHAY®) is adopted as an electrical load for the loudspeaker to extract the electrical power from the system. The electrical power was measured using a power analyser (model KintiQPPA2530) as shown in Figure 4.17, with an accuracy of 0.05%.

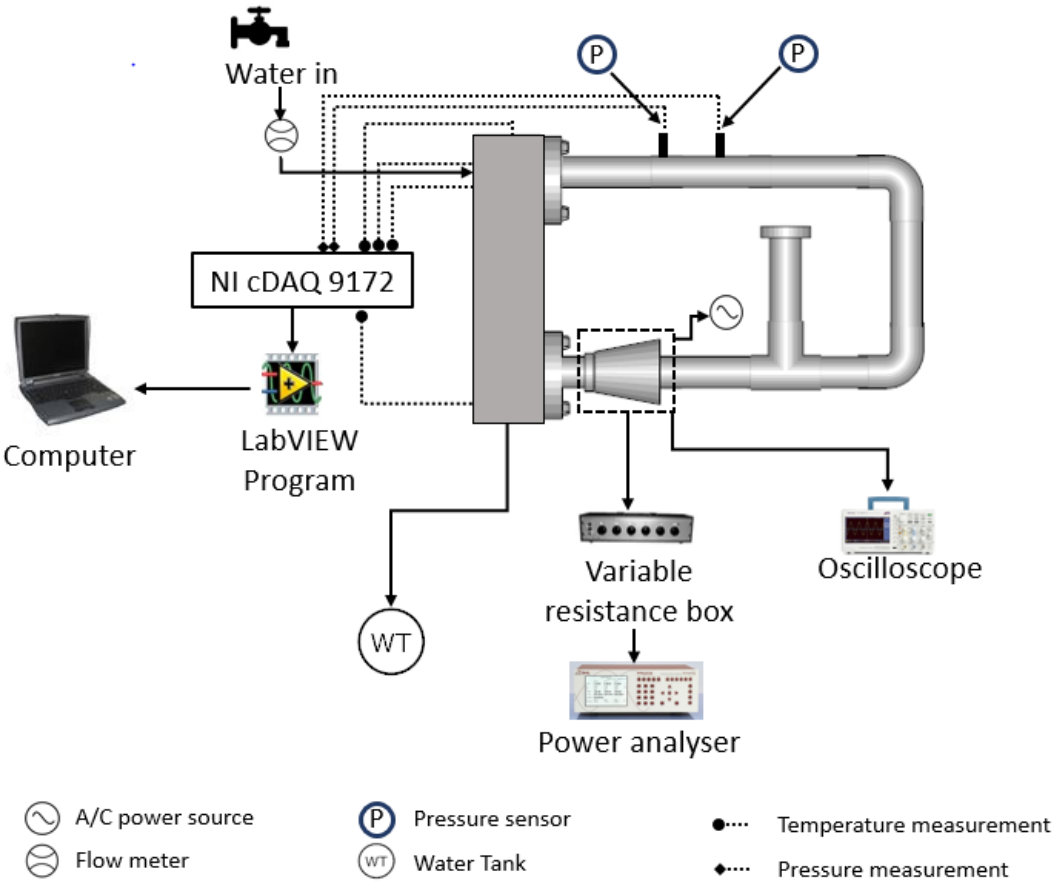


Figure 4.16: Schematic diagram of the experimental apparatus of the single core thermoacoustic electricity generator. The dotted arrows of solid circle ends indicate the temperature measurements, while the ones of solid rhombus ends are to show the pressure measurements. The letter P is to note the location of the pressure sensors.

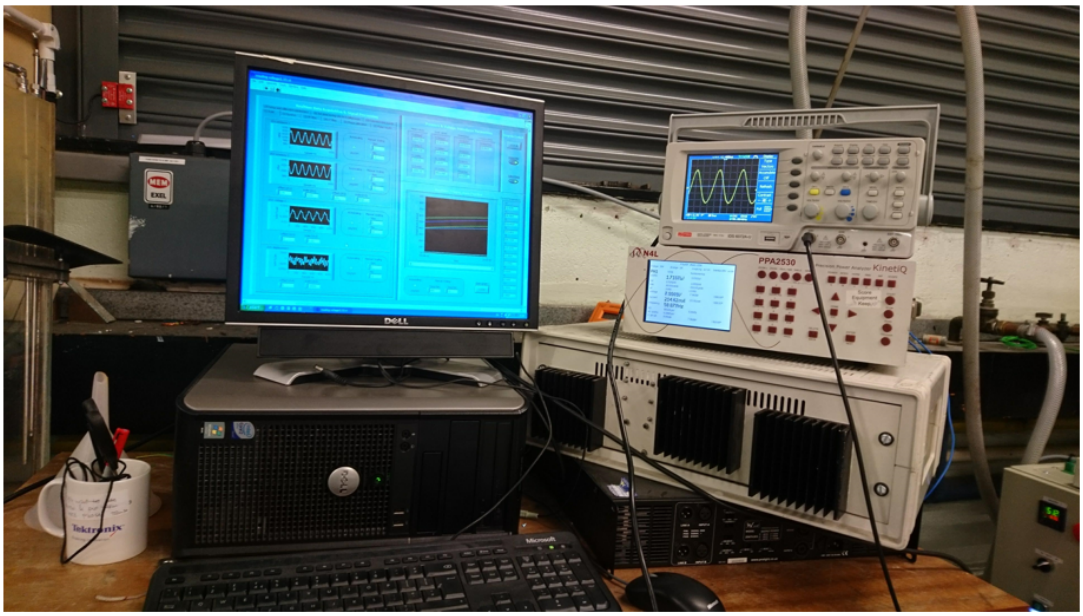


Figure 4.17: SCORE software, the oscilloscope, and the power analyser during the operation of the single core thermoacoustic system.

To estimate the acoustic power flow in the loop, the well known two-sensor power measurement technique is used. The technique used two identical absolute pressure sensors, A and B, that were placed in the feedback pipe with a short distance, Δx, of 8 cm between them to capture the variation in the dynamic pressure, and hence to estimate the acoustic power at the midpoint of the two sensors (Fusco, Ward and Swift 1992). The location of the two sensors in the feedback loop is illustrated in Figure 4.18. The generated acoustic power, $P_{Ac.}$, can be obtained from:

$$P_{Ac.} = \left(\frac{\pi r_0^2}{2\omega\rho_m \Delta x} \right) \mid P_A \mid\mid P_B \mid \sin\phi_{AB} \tag{4.25}$$

Where: r_0 is the radius of the feedback pipe, ω is the angular frequency (rad/sec), ρ_m is the mean density of the working gas (kg/m^3), Δx is the distance separating the two sensors (m). $\mid P_A \mid$ is the absolute pressure at point A (Pa), $\mid P_B \mid$ is the pressure amplitude at point B (Pa), ϕ_{AB} is the phase angle by which the pressure signal at A leads the pressure signal at B (°).

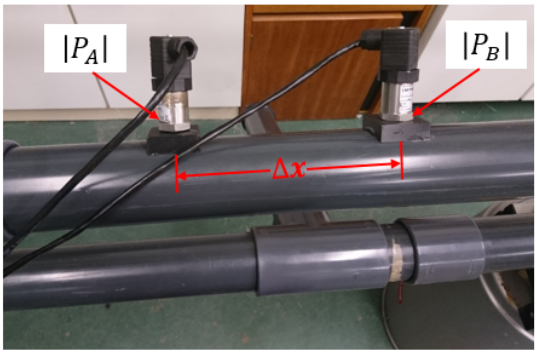


Figure 4.18: The absolute pressure sensors mounted to the feedback pipe to measure the acoustic power throughout the looped-tube single regenerator thermoacoustic engine.

4.4.3 Results and discussion

Studies of the alternator's load resistance

The load resistance of the alternator, R_L, plays a pivotal role in the performance of the system. The variation of the load resistance has a complex effect and should be optimized to achieve a high electrical power output. The effects of changing the load resistance on the electrical power output extracted by the alternator, and the thermal-to-electrical efficiency of the the system were investigated numerically and experimentally. The electrical power was calculated and measured at four different heat input values (1250, 1500, 1750 and 2000 W). As shown in Figure 4.19 and Figure 4.20, the electrical power output and the thermal-to-electrical efficiency both increase when the heat input increases. For a given heating power, there is an optimum load resistance at which a maximum electrical power can be extracted. DeltaEC results

show that, at the maximum heating power of 2 kW, a maximum electrical power of 8.2 W can be achieved at an optimal load resistance of the alternator of 25 Ω. The experimental results agreed that at the same heat input, the optimal load resistance is also 25 Ω at which a maximum electrical power of 7.5 W can be obtained with about 0.4% thermal-to-electrical efficiency. For the heat input power of 1.5kW, a maximum electrical power of 3 W was delivered, at an optimal load resistance of 30 Ω using air at atmospheric pressure with 0.2% thermal to electrical efficiency. For the same heat input power, DeltaEC predicted an electrical power output as high as 17%. Sun et al. (2013) expressed that the electrical power output of the alternator is approximately proportional to the load resistance and the square of the pressure amplitude in front of the alternator when both the mechanical and electrical resonances are achieved. Therefore, when the load resistance decreases, the electrical output increases first as a result of the rapid increase in the square of the pressure amplitude, and after that the output decreases due to the displacement of the loudspeaker diaphragm.

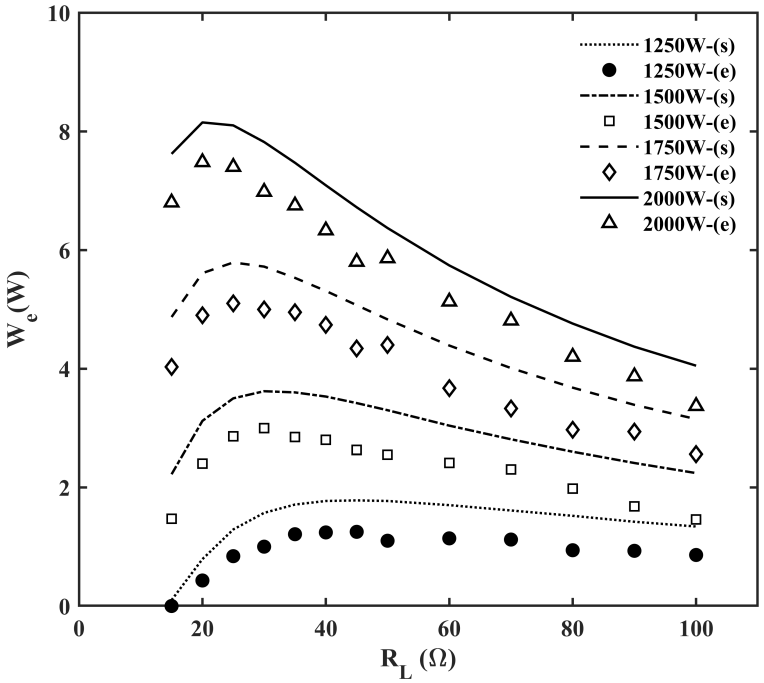


Figure 4.19: Performance characterisation of a single regenerator thermoacoustic engine: Electrical power output at four levels of heating power, when the load resistance is varied. (e) Denotes experimental data, and (s) for simulated ones.

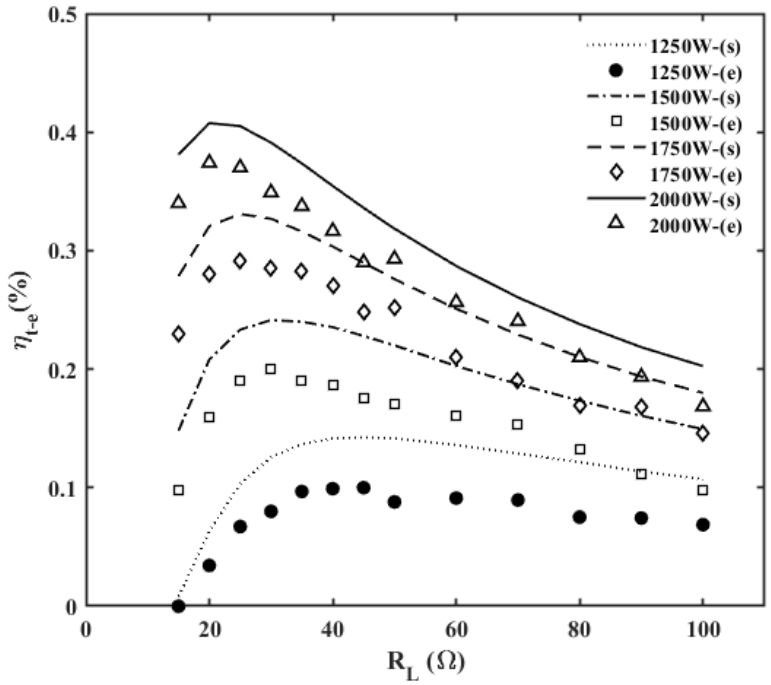


Figure 4.20: Performance characterisation of a single regenerator thermoacoustic engine: Thermal-to-electrical efficiency at four levels of heating power, when the load resistance is varied. (e) Denotes experimental data, and (s) for simulated ones.

The influence of the load resistance on the coil displacement for different heat input power is introduced in Figure 4.21. For the alternator installed in this system, the maximum stroke equals 9.4 mm as illustrated in Table 4.2. The theory predicts that, for heating input power higher than 1750 W, the diaphragm displacement will greatly exceed the allowed limit. Pushing the speaker beyond its limit can damage the speaker as the voice coil either slips out of the magnetic gap or hits the bottom of it. Therefore, to avoid over-excursion, the heating power should be kept below 1750 W. However, the effect of the coil resistance should be also considered because it shows that displacement increases at higher load resistances. For instance, when the heat input power is 1500 W, the displacement of the coil's diaphragm increases from 3.9 mm to 6.5 mm and the load resistance varies from 15 Ω to 50 Ω, which means that the load resistance should be kept less than 50 Ω to meet the displacement condition. Considering the stroke limitation, and the influence of the load resistance on the output power bring that 30 Ω is the optimal load resistance for the currently used alternator. Working beyond the stroke limitation will cut down the thermal-to-electrical efficiency, due to the mechanical losses that occur when the coil displacement approaches its maximum value.

It should be noted that the acoustic dissipations in the thermoacoustic engines are proportional to the square of the pressure amplitudes. Therefore, decreasing the load

resistance would negatively affect the thermal-to-electrical efficiency, because of the much larger acoustic power dissipations.

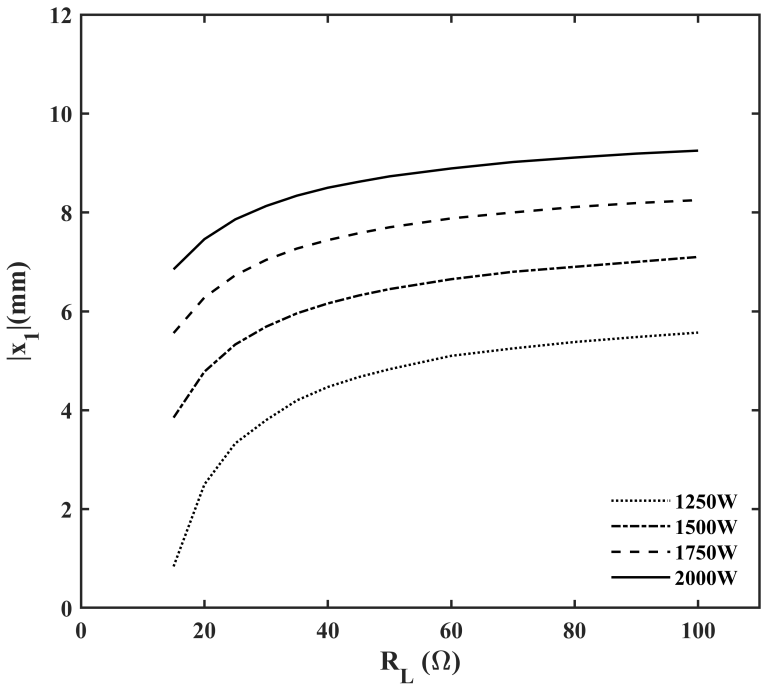


Figure 4.21: The computational peak stroke of the alternator against the load resistance.

As shown in Figure 4.22, the current amplitude of the alternator also depends on the load resistance. For heating power of 1250 W, both numerical and experimental data show that the current of the loudspeaker increases firstly when the load resistance increases from 15 Ω to 30 Ω and then decreases with the increase in the load resistance. For heating power of 1500, 1750 and 2000 W, the theoretical and experimental results reveal that the current decreases when the load resistance increases. Wang et al. (2015) realized that when the load resistance was too small, the operating current of their alternator exceeded its upper limit. Therefore, the operating current should be also considered when varying the load resistance. DeltaEC calculations and experimental data show the same trends in the currents which indicate the ability of DeltaEC simulation to simulate the working characteristics of the current engine.

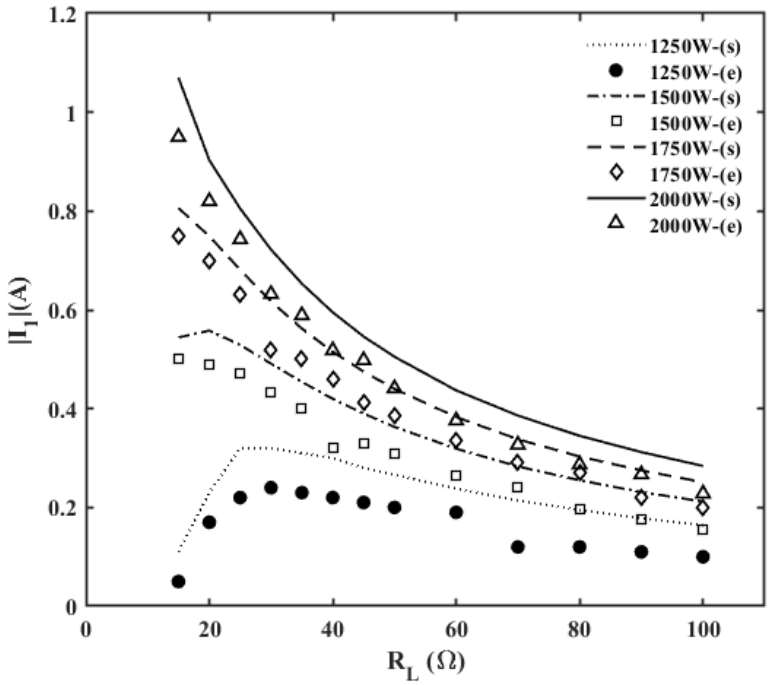


Figure 4.22: Current of the alternator against the load resistance for different heating input power. (e) Denotes experimental data, and (s) for simulated ones.

Figure 4.23 and Figure 4.24 show the computational pressure amplitude and the volumetric velocity amplitude against the load resistance of the loudspeaker, for different values of the heat input power. For all heat input values, both the pressure amplitude and the volumetric velocity amplitude increase gradually with increasing of the load resistance. Meanwhile, as is shown in the electrical power curve Figure 4.19, there is an optimum load resistance that corresponds to a high electrical power output. Therefore, for the most powerful operating condition, one should choose proper values of the pressure amplitude and the volumetric velocity amplitude.

For a given alternator, the extraction of the electrical power depends mainly on coil velocity and load resistance. For a given coil velocity, the load resistance should approach the electrical resistance of the coil in order to extract more electrical power (Yu, Saechan and Jaworski 2011). Therefore, decreasing the load resistance from 100 Ω can greatly enhance the electrical power output. However, further reduction of the load resistance would dramatically increase the equivalent impedance of the alternator, and as a result it would strengthen the disruption to the acoustic field of the system. Consequently, the alternator would cause a higher pressure loss across it's diaphragm as shown in Figure 4.25. However, if the heat input power doesn't change, the achievable pressure amplitude is limited. Therefore, the coil velocity will rapidly decrease by the high acoustic impedance. The reduced velocity will minimize the acoustic power flow

across the alternator, which enters the cold side of the regenerator, and as a result it will reduce the amplified acoustic power within the regenerator.

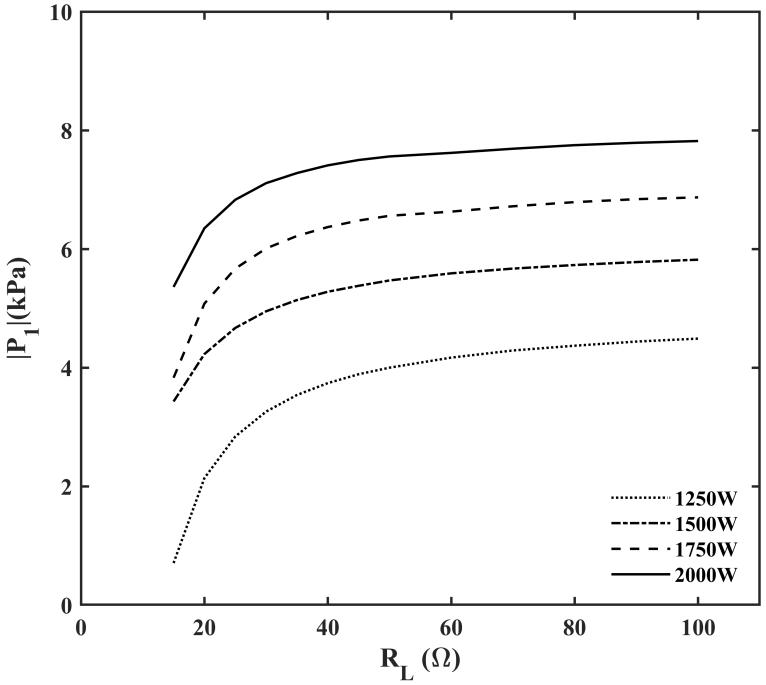


Figure 4.23: The numerical pressure amplitude against the load resistance of the alternator for different heating input power.

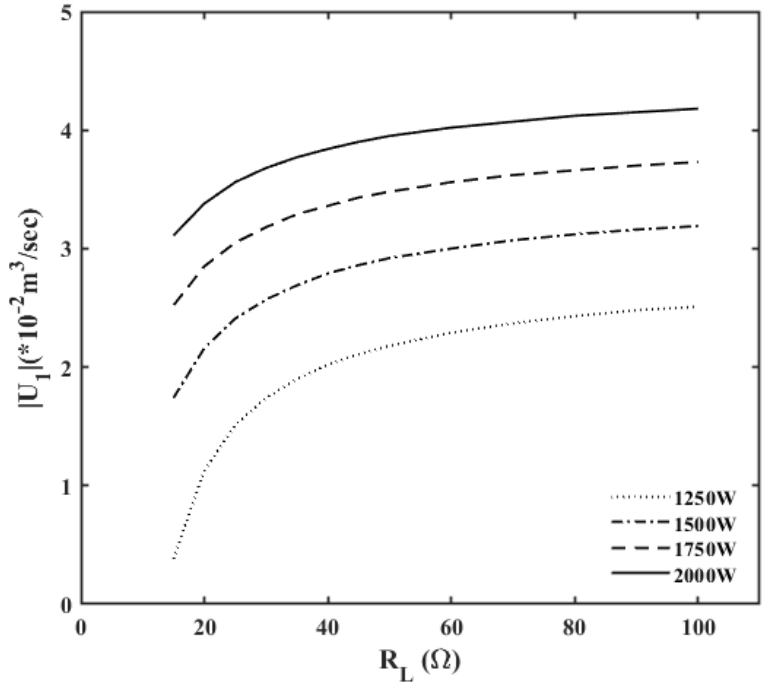


Figure 4.24: The numerical volumetric velocity amplitude against the load resistance of the alternator for different heating input power.

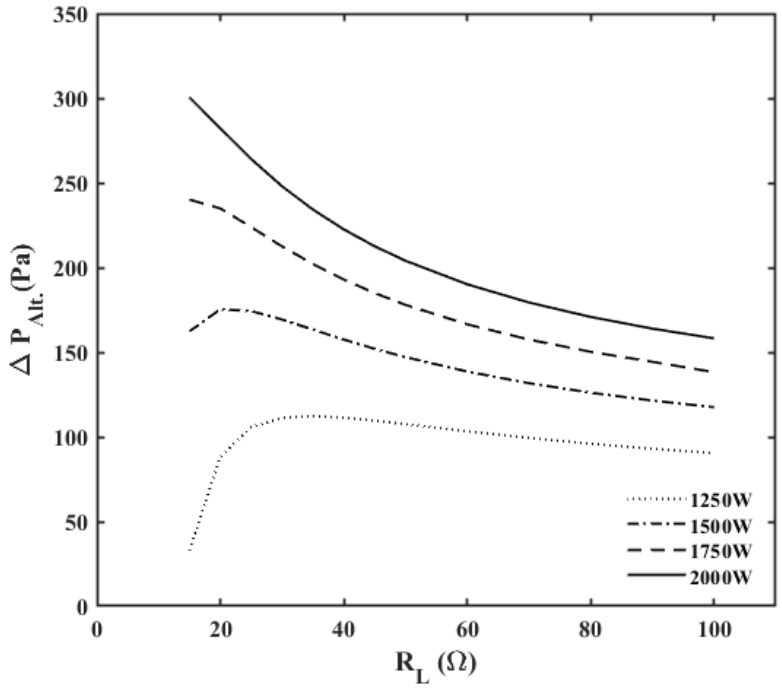


Figure 4.25: The numerical pressure drop across the alternator's diaphragm against the load resistance for different heating input power.

Studies of stub length

In the current system, the alternator is coupled within the loop, which offers the advantages of eliminating Gedeon streaming within the looped engine and also minimizes heat dissipations from the HHX. However, it causes large pressure drop and sharp acoustic impedance drop when the acoustic wave passes through the alternator's diaphragm. Therefore, it is crucial to reduce the changes in the acoustic field caused by the alternator by introducing a phase tuning component. Yu, Jaworski and Backhaus (2012) added a side branch stub to correct the acoustic field altered by a load. They were able to match the acoustic load with the engine's acoustic network, and they minimized the harmful acoustic dissipation within the feedback pipe. They varied and optimized the length of the stub branch using a moving piston to cancel out reflections. Therefore, they proved that the length of the stub branch can be varied to tune acoustic conditions. Kang et al. (2015) used a combination of a tuning stub and a ball valve to adjust the acoustic field. Jin et al. (2016) analysed the mechanism of phase tuning, adding either a compliance tube or a resistance tube to their travelling wave system. They concluded that the compliance tube function is very similar to a stub and it is better to correct the acoustic field than the resistance tube. Al-Kayiem and Yu (2017) tuned the acoustic field utilizing a side-branched volume that functions in a similar way

to a compliance or a stub. Most recently, Kruse et al. (2017) used a stub to adjust the acoustic impedance and phase angle within their system.

Accordingly, a matching stub is installed in the current system, and its location was optimized to be approximately 0.75 m away from the alternator. In this section, investigation of the length of the stub needed to regulate the acoustic impedance and the phase angle will be discussed. Investigations were performed to address the influence of the stub length on the pressure drop through the alternator's diaphragm, the electrical power output, the efficiency, the acoustic conditions within the regenerator, and the phase angle within the feedback pipe. The heat input power and the load resistance of the alternator are fixed at 1.5 kW, and 30 Ω, respectively, for both DeltaEC and the experiments. As illustrated in Figure 4.26, as the length of the tuning stub increases, the pressure drop across the diaphragm significantly increases until it reaches an optimum value of 188 Pa, when the stub length is 61 cm. Also, as seen in Figure 4.27, an optimum electrical power output of 3.5 W can be achieved with about 0.23% thermal-to-electrical efficiency, when the stub length is 61 cm. The experimental data shows similar trend to DeltaEC estimation, which indicates that the DeltaEC model has observed the essence of the experimental apparatus. However, the electrical acoustic power achieved in the lab is less than the simulation, due to the fact that there was a high acoustic dissipation as well as the underestimated parasitic losses.

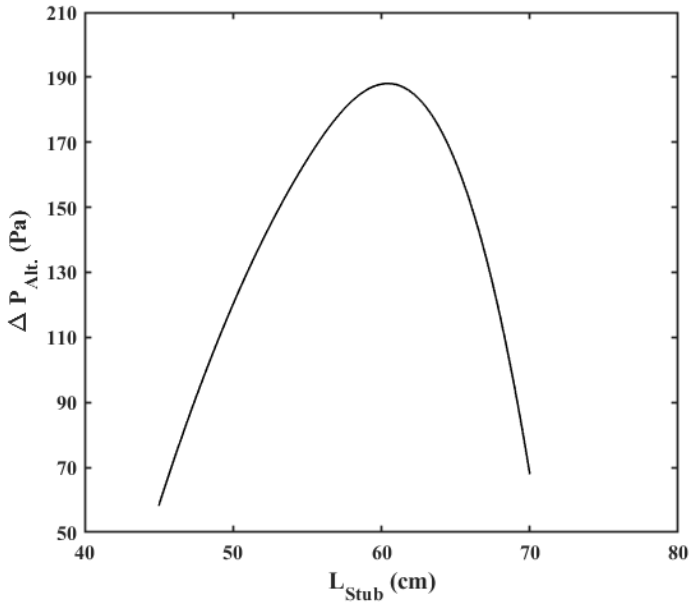


Figure 4.26: DeltaEC results of the pressure drop across the alternator diaphragm when the length of the stub branch varied between 45 and 70 cm.

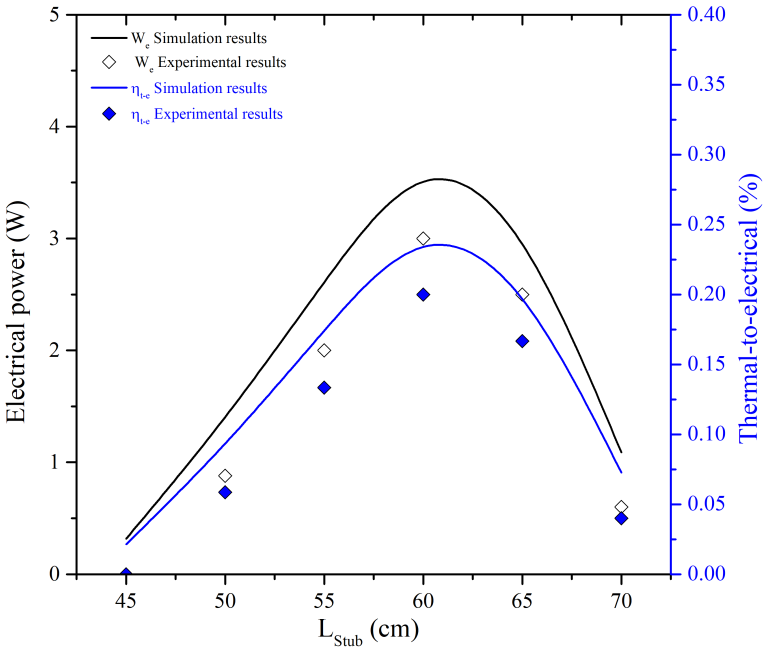


Figure 4.27: Experimental results and DeltaEC results of the electrical power output and the thermal-to-electrical efficiency when the length of the stub branch varied between 45 and 70 cm.

The stub is mainly added to the system to modify the acoustic field changed by the alternator and to reduce the acoustic losses. Therefore, the acoustic conditions within the regenerator and the phase angle within the feedback pipe are plotted as a function of the length of the tuning stub as shown in Figure 4.28. It can be observed that the acoustic impedance in the regenerator, which represents the ratio of the pressure amplitude to the volumetric velocity amplitude, increases as the length of the tuning stub increases from 55 cm to 70 cm. For stub length of the range 45 cm to 55 cm, the local impedance isn't improved significantly. Moreover, the phase angle between the pressure and the volumetric velocity of oscillation in the regenerator and the end of the feedback pipe is affected by increasing the length of the stub. It changes from -53° to 7° in the regenerator when the stub length varies from 45 cm to 70 cm. Meanwhile, the phase angle decreased from 61° to 21° at the end of the feedback pipe. The calculated results showed that, at the optimum electrical power output of 3.5 W, the phase angle in the regenerator is around -21° and about 38° in the feedback pipe. As mentioned earlier, to maximize the generated acoustic power from the system, a near travelling-wave condition should be achieved within the regenerator and the feedback pipe. Therefore, the acoustic power amplification can be enhanced within the regenerator and the reflections can be tuned out along the feedback loop. **??** confirms that the phase angle within the regenerator and the feedback pipe was effectively tuned by the introduction of the stub branch in the system. The functionality of the stub for phase changing justifies the dependence

of the electrical power output on the length of the tuning stub. Therefore, referring to Figure 4.26, Figure 4.27 and Figure 4.28, a 61 cm long stub offers better travelling wave conditions and the highest produced electrical power output. Finally, the simulation and experimental results are provided in Table 4.3.

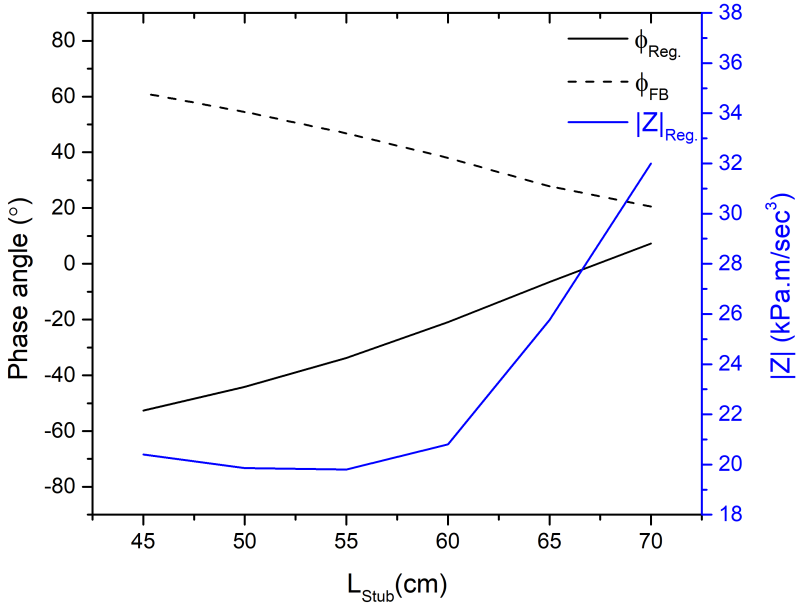


Figure 4.28: DeltaEC results of the local acoustic impedance in the regenerator, the phase angle in the regenerator, and the phase angle in the feedback pipe as a function of the stub length.

Table 4.3: Comparison between the simulation and the lab measurements.

Parameter	**Unit**	**Simulation**	**Experiments**
Heat input power, Q_{in}	(kW)	1.5	1.5
Load resistance, R_L	(Ω)	30	30
Pressure amplitude in front of the AHX, $\mid P_1 \mid$	(kPa)	5.25	3.9
Pressure amplitude in feedback pipe point A (Figure 4.14), $\mid P_A \mid$	(kPa)	4.73	3.51
Pressure amplitude in feedback pipe point B (Figure 4.14), $\mid P_B \mid$	(kPa)	4.21	3.11
Acoustic power of the loop, $P_{Ac.}$	(W)	60.4	45.6
Electrical power output, W_e	(W)	3.5	3
Thermal-to-acoustic efficiency, η_{t-a}	(%)	4.03	3.04
Thermal-to-electrical efficiency, η_{t-e}	(%)	0.23	0.2

Although DeltaEC has captured the trends of performance of the engine, there is still a discrepancy between the theoretical model and experimental data due to several

possible reasons such as the significant heat loss in the experiments which has not been fully considered in the simulation. Moreover, DeltaEC assumes perfect alternators which is not the case in reality. Furthermore, for a looped tube configuration, the acoustic field is very sophisticated and highly sensitive to the design parameters of the physical parts of the system through which the acoustic wave propagates. In addition, DeltaEC is one-dimensional linear thermoacoustic representation and doesn't account for the two-dimensional and three-dimensional thermoacoustic effects such as bends and streaming. Also,it doesn't taken into account the non-linear behaviours which exist in the actual engine. DeltaEC simulation of the single core thermoacoustic system can be found in **Appendix B1**.

4.4.4 Comments on uncertainty in the experimental results

Estimation of a rigorous error in a system of complex physical behaviours such as a thermoacoustic system is relatively difficult. It is well known that every experiment uses some of the known instruments such as thermocouples, pressure transducers, etc. There are some individual/personal errors, in addition to the errors related to the global conditions. The most important aspect of the lab test is whether the observed thermoacoustic effects (i.e. peak pressure, peak volumetric velocity) are 100% reproducible for the same experimental global conditions. Therefore, repeatability can be considered as a more useful measure of the experimental uncertainty, offering a good indication of the compounded value of measurement errors. Here in this research, one potential source of error associated with the experimental conditions such as the atmospheric pressure and the ambient temperature is that the variation in the global conditions was assumed to be too little and to have no significant effect on the measurements. However, these conditions may not be consistent with every measurement, which may affect the temperature of the cooling water, and as a result the amount of heat rejection.
Moreover, the number of thermocouples used to measure the temperature of the gas in different locations throughout the engine is not sufficient to accurately estimate the thermal power flow. One extra source of error is related to the estimation of the flow rate of the cooling water, which also alters the dissipated heat. The water flow rate was estimated by using the average value of the data recorded during the test. Also, a water tap was used to provide the cooling water, and it should be noted that there is a possibility of inconsistency in the water pressure, which may slightly affect the water flow rate. Furthermore, simply measuring the pressure amplitude at one or two positions along the loop does not provide enough data for further analysis, especially when it comes to the distribution of the pressure amplitude along the system components. Additionally, there is the possibility of error in the estimation of the acoustic power using the two-sensor meter. This is due to the possible error in the measurement of the phase difference between the two sensors, which can be eliminated by separating the

two sensors by velocity anti-node distance. Also, the distance separating the sensors should be large (≈ 0.6 m), and the measuring device should have an accuracy greater than 0.01° (De Blok 2013).

4.5 Concluding remarks

A thermoacoustic electricity generator is a type of engine that can convert thermal power into acoustic power, and in turn into electricity. It can potentially be very useful in a wide range of applications, but it can be affected by many design parameters and has a very complex physical behaviour. Therefore, designing and developing such a complex energy conversion system is challenging. In this study, a single core thermoacoustic electricity generator in a looped tube configuration, working at a frequency of 75 Hz, has been examined. The experiments were carried out using air at atmospheric pressure as a working fluid. A numerical model of the thermoacoustic engine has been developed with DeltaEC simulation software.
The system comprises a single engine stage, a feedback pipe, a loudspeaker and a matching stub. The regenerator was heated using an electrical heater and cooled using circulated cooling water. The performance of the engine was predicted and tested under different working conditions. Pressure and temperature measurements are taken at several locations in the system. The important parameters, including heat input power, load resistance, stub length, pressure amplitude, displacement, electrical power, thermal-to-electrical efficiency, etc., are explained in detail and analysed systematically. The distribution of the acoustic parameters along the 4.4 m long loop is firstly illustrated quantitatively. The distributions of acoustic power throughout the system showed that the acoustic power dissipations in the hot heat exchanger, secondary ambient heat exchanger, thermal buffer tube, and the feedback tube are very significant. The predictions showed that acoustic power generation can be effectively enhanced by increasing the heating input power into the system.

The variation in load resistance is employed to change the power output and the efficiency. An optimal power output of 3.5 W is achieved using a load resistance of 30 Ω, when the heating power to the HHX is 1500 W. The thermal-to-electrical efficiency at low load resistance is relatively small because of the large pressure amplitudes inside the thermoacoustic engine, which increases the acoustic dissipations. The changes of the electrical power output and the thermal-to-electric efficiency with the variation of the load resistance are basically due to the changes of the corresponding acoustic impedance of alternator. Also, it is found that by changing the length of the stub, the acoustic conditions in the regenerator in terms of the local acoustic impedance, and the phase difference between pressure and volumetric velocity of oscillation can be accurately adjusted. It is concluded that 61 cm long stub has enhanced the acoustic conditions and

reduced the disturbance in the acoustic field caused by the alternator. The electrical power output is increased from almost zero to about 3.5 W, when the stub length was increased from 45 cm to 61 cm which confirms that the stub branch is a good acoustic tuning mechanism. Moreover, it is realized that the optimum engine performance isn't only influenced by ideal acoustic conditions and geometrical parameters of the regenerator, but also on achieving an optimal acoustic field throughout the system. Therefore, by adjusting both the load resistance and the length of the stub, the load can be matched to the system. It can be inferred that the DeltaEC model has captured the essence of the behaviour of the current single core looped-tube thermoacoustic engine. The theoretical model also shows the existence of a high standing wave in the feedback pipe. This most likely resulted from the acoustic reflection by the thermoacoustic core.

CHAPTER 5

A NOVEL ASYMMETRIC HEATING METHOD FOR A TWO-STAGE TRAVELLING WAVE THERMOACOUSTIC ELECTRICITY GENERATOR

5.1 Introduction

This chapter continues the effort on the development of low-cost thermoacoustic electricity generators for rural households. The results from the previous study of a single core thermoacoustic engine indicated that the maximum acoustic and electricity outputs are 60.4 W and 3.5 W, respectively. As mentioned in the introductory chapter, 20 W electricity output is required to satisfy the basic needs of rural households which is far from the what have been done in the previous chapter. Well-known is that the power density can be improved by placing a thermoacoustic engine of multi regenerator units in a series as previously reported by De Blok (2008). Besides, the system can be utilised to lower the onset temperature without depressing the intensity of the acoustic power. This research outcomes therefore widen the application range of the thermoacoustic technology to include low-temperature source such as 70°C for solar (without concentration), and waste heat of up to 400°C for exhaust gas of a combined heat powered system CHP. Considerable research has proposed the use of multiple thermoacoustic cores in the thermoacoustic travelling wave engine to to enhance the thermoacoustic amplification, and also to enable the onset of oscillation at a much lower temperature (Chen et al. 2012; De Blok and Systemen 2012; Jin et al. 2015; Senga and Hasegawa 2016). Zhang et al. (2016) and Zhang and Chang (2015) concluded that the engine stage

number has to be optimised to take into account a trade-off between the operational temperature difference for onset and the overall cost of the system.

The most advanced and powerful of these multi-stage thermoacoustic systems contain two (Kang et al. 2015), three (Wu et al. 2014*a*) or four (Wang and Qiu 2017) cores, generating 204W, 1.57kW, and 1.2kW of electricity, respectively. This high level of electricity was achieved by pressurizing the helium gas to 18, 50, and 30 bar, respectively. As discussed in Chapter 2, the power density is proportional to the mean pressure of the working gas (Ceperley 1979). Pressurization of the working gas can increase the power output by the order of the square root of the pressure (Piccolo 2018). Using helium and other expensive gases can also enhance the performance, but this is not beneficial for such applications (developing world). Therefore, this work concentrates on the use of air as the working fluid.

Once the engine stages have generated the acoustic power, the electrical power should be harvested using the only moving part included in the thermoacoustic engine. A loudspeaker was used to function as a linear alternator (LA) for this work, although there are other alternatives that are clearly summarized in Chapter 2. For this application, the driving force was the cost and availability of the parts in remote areas such as South Sudan. One of the developments from SCORE is a twin-core design (Chen et al. 2013; Riley 2014*b*). This system is not yet capable of meeting the target but has managed to generate 12.6W from a wood burning stove, using atmospheric air. In this design, the two engine stages were placed side by side so that the hot gases from the fire heated them evenly. The work shown in this study is the continuation of the development of the low cost two-stage travelling wave thermoacoustic electric generator designed by SCORE. The intention is to boost the output power from the air-filled engine. As mentioned earlier in the literature survey (Chapter 3), no study has been focused on distributing the total thermal power between the stages using different heat ratios, and all the available research has used even input power to each engine core. This study explains and proves that the power outputs from this twin-core system can be increased significantly by heating each core by different amounts depending on the location in the feedback tube. This improvement occurs with no change in the geometry or design of the system.

5.2 Design concept of the current system

The current prototype, referred to as SCORE Demo2, is a double core travelling wave thermoacoustic engine that is designed according to the following requirements:

1. A travelling wave condition has to be observed.

- The travelling wave thermoacoustic engine type is chosen instead of standing wave type because of the its high power output, high power density, high overall efficiency and low acoustic dissipations.

2. The system must have a multiple regenerator set-up.
   - This is to overcome the problems related to the single stage thermoacoustic engines, where the excited acoustic oscillation starts at a high temperature and the produced power is low. The multi-stage design offers the advantage of a low onset temperature and a high power output. However, a compromise between the number of the regenerators and the cost of the system should be made. Therefore, SCORE Demo2 was designed using dual regenerators (Riley 2014*b*).
3. A quick appearance of the thermoacoustic effect.
   - Since the current system will also be used to demonstrate the thermoacoustic effect, the start-up time of the system should be short. An adjustable heat source should be implemented in the system to heat-up the two hot heat exchangers.
4. The operating frequency of the thermoacoustic engine, f, considered here should be a trade-off between several factors
   - f should be near the resonance frequency of the alternator to ensure that the alternator can be excited only by a relatively low acoustic pressure or acoustic pressure difference.
   - Increasing the working frequency increases the power density in the loop (Swift 2017), which is beneficial to hit the $100W$ target. However, it requires a very fine regenerator mesh and therefore, the system will be costly and not affordable for low income families.
5. The thermal-to-electrical power converter should be relatively cheap and readily available
   - The ultimate target of a low cost thermoacoustic power generator is likely to consider ordinary audio loudspeakers (resonance frequency range is 40 to 80 Hz), and which can be find in a fraction of cost and they are cheap compared to the commercial linear alternators that of a thousands UK pound cost. However, the acoustic-to-electrical conversion efficiencies tend to be between 30 and 55%
   - Beside the principal function of the alternator as a power converter, one could benefit from coupling the alternator with the loop by stopping acoustic

streaming and as a result improve the performance. However, this arrangement will contribute to unnecessary disturbance in the acoustic field due to the high pressure drop (Yu et al. 2012), which subsequently limits the acoustic power of the loop.

5.3 DeltaEC modelling

Following the design requirements outlined in section 2, and for an in-depth understanding of the behaviour of the thermoacoustic system under consideration, a numerical calculation for the system performance was made. DeltaEC simulation tool is adopted to obtain the acoustic field including the flow of the loop acoustic power. The numerical simulation presented in this study is based on the final built of SCORE Demo2 of a double core configuration. A schematic diagram of the experimental device used to construct the DeltaEC model is presented in Figure 5.1, including the system components. The blue arrows in the diagram are used to illustrate the flow of the acoustic power along the system.

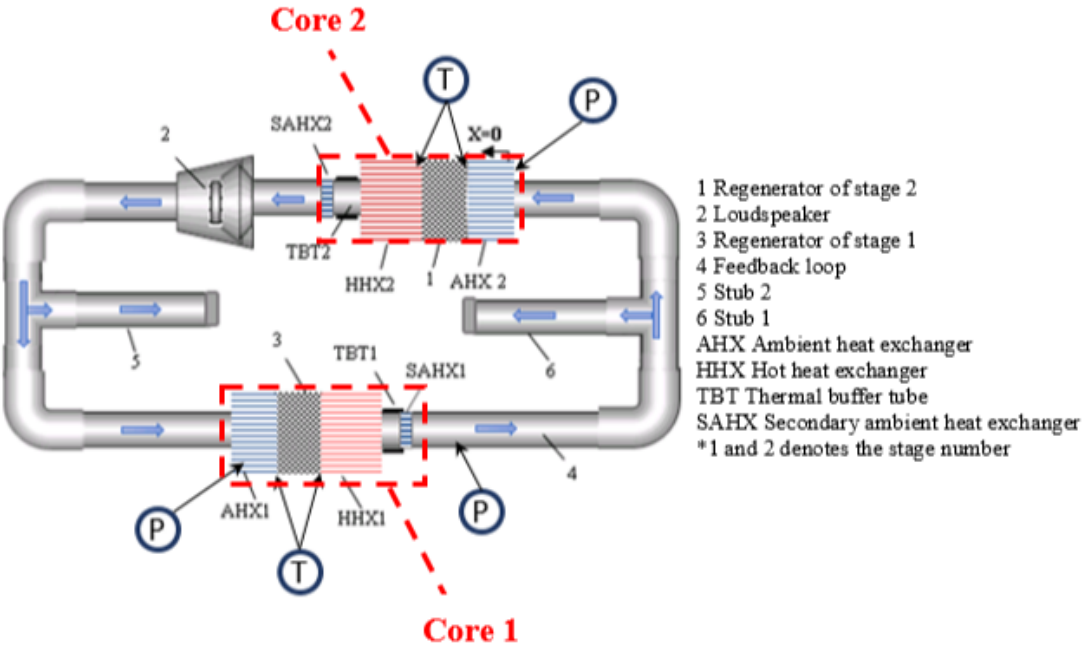


Figure 5.1: Functional diagram of the double core thermoacoustic electricity generator showing the components, the locations of the two cores within the loop, the starting point of the simulation $x = 0$, and the measurements taken to estimate the performance (pressure P and temperature T). A key is provided on the right side of the graph to show the name of the different system components.

Accordingly and based on the experimental rig of a double core design, a schematic diagram of the DeltaEC simulation is developed as presented in Figure 5.2. The model was built using some of DeltaEC physical and logistical segments (Ward and Swift 1994), with the same design parameters of the experimental rig. The model starts at

$x = 0$ which is located at the hot end of the second ambient heat exchanger AHX2, and continues anticlockwise, passes through all system components until it returns back to the initial point. The pressure amplitude, $|p_1|$, the volumetric velocity amplitude, $|U_1|$, and their phases, ϕ_p and ϕ_U, at the final point are targeted to match those in the starting point.

$$|p_1|_{x=0m} = |p_1|_{x=4.1m} \tag{5.1}$$

$$|U_1|_{x=0m} = |U_1|_{x=4.1m} \tag{5.2}$$

$$(\phi_p)_{x=0m} = (\phi_p)_{x=4.1m} \tag{5.3}$$

$$(\phi_U)_{x=0m} = (\phi_U)_{x=4.1m} \tag{5.4}$$

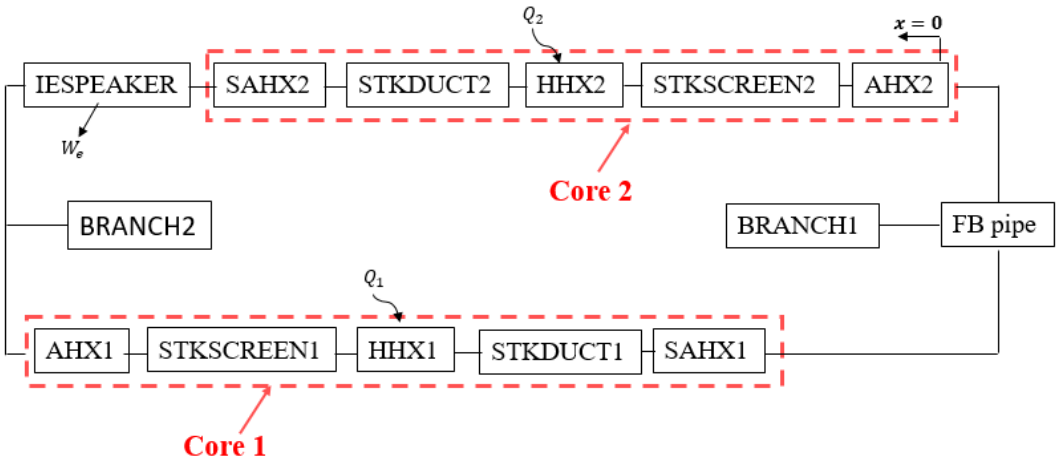


Figure 5.2: Schematic illustration of the segments used to construct DeltaEC model for the double core thermoacoustic electricity generator. The amounts of heat added into the first and the second engines (HHX1 and HHX2) are Q_1 and Q_2, respectively, while the amount of electricity extracted by loudspeaker (IESPEAKER segment) is W_e.

Since the research targets the developing world, atmospheric air is selected as the working gas. The system works at 73 Hz frequency. The total length of the loop is around 4.1m. The maximum temperature for both the hot heat exchangers should be 650 °C to not exceed the tolerances of typical material used for their manufacturing. In order to address the influence of the heating power in the system, the total heating power was varied between 2.1 - 3 kW. The total heat was split into different percentages between the two stages of the thermoacoustic system. To verify the numerical results against the lab data, the load resistance of the loudspeaker was set to 37.5 Ohm, which is the resistance at which the loudspeaker can extract the maximum electrical power.

The main focus of this research is to investigate the ability of improving the system performance applying a novel operational methodology. The idea is that the total heat value, Q_T, is maintained constant in all the cases and only the distribution ratios into

the two heater blocks Q_1/Q_T and Q_2/Q_T are changed. When the heat flows into each thermoacoustic engine (TAE) as shown in the power flow diagram Figure 5.3, part of the heat is dissipated through the AHXs and the TBTs before the rest is amplified within the regenerator. The amplified acoustic power from the two engines TAE1 and TAE2 flows into the feedback pipe where another amount is lost there. The net acoustic power entered the power harvester before it converted into electricity.

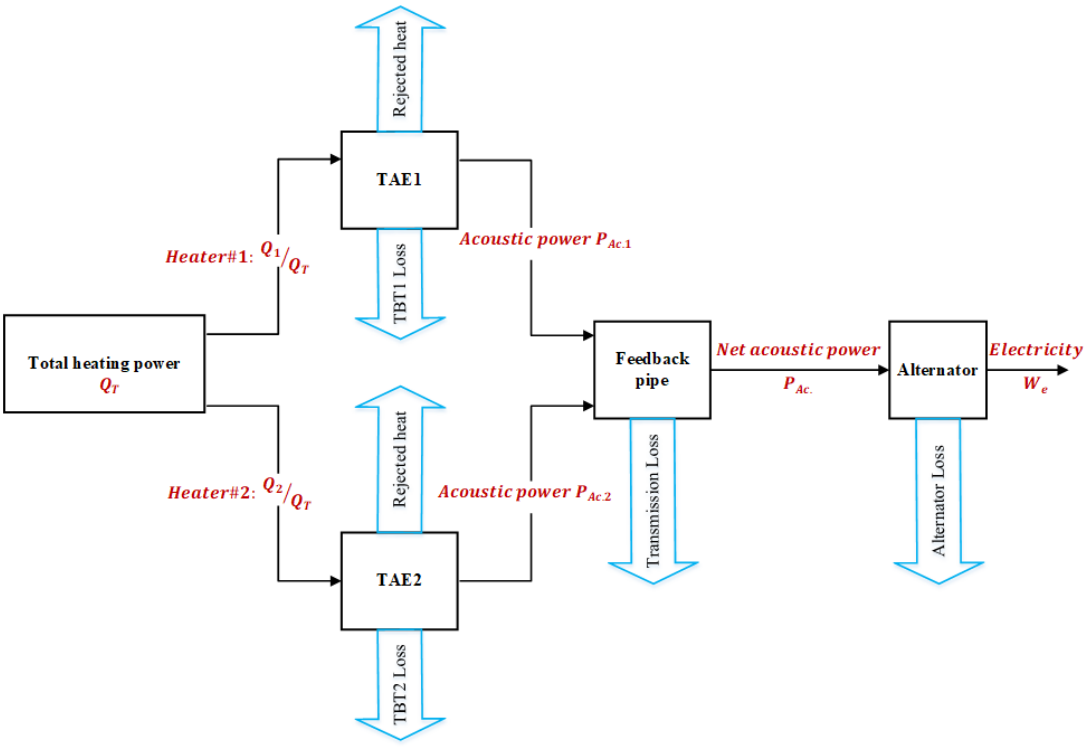


Figure 5.3: Power flow diagram for the double core thermoacoustic electricity generator.

5.3.1 DeltaEC results and discussion

To further demonstrate the influence of the operational methodology on the system performance, the numerical results of the acoustic field in the system are shown in Figure 5.4 to Figure 5.8. The four curves correspond to the various heat input ratio into the two HHXs: 40%, 50 % 55% and 60% of the heat is directed into the HHX1, and the power in core 2 being set so that the total heat supply, Q_T remained constant. No other variables were adjusted. The changes in the pressure amplitude of oscillation is displayed in Figure 5.4. It is obvious that all the curves have the same trend for all the heat supply percentages. The numbers shown in the graphs identify the locations from the schematic representation Figure 5.1. The pressure amplitude drops at each of the two regenerators (location 1 and 3) because of their flow resistance. It also decreases across the linear alternator (location 2) due to its acoustic resistance which is the product of the mechanical resistance R_m, electrical resistance R_e, load resistance R_L, compliance $C_{L.A}$ and inertance $L_{L.A}$. The two stubs don't influence the pressure

amplitude significantly. The pressure standing wave ratio (PSWR) in the system is approximately around 2.97 because of the reflections where the cross sectional area of the resonator changes. For travelling wave systems, PSWR of less than 1.8 are considered good (Riley 2014*b*), and this can be achieved using several techniques such as varying the length of the branch pipe or by using quarter and three quarter length for the feedback tubes. It can be noted there is a higher pressure drop through the alternator when 40% of the heat is directed to the HHX1 which indicates better extraction of the electric power. In other words, a 48% increase of the electrical power output can be achieved when the balance of heat went from 50% to 60% in the second engine. It can be seen that the location of the pressure anti-nodes altered slightly in the four heat supply ratios, particularly near the end of the feedback loop due to the small change in the operating frequency.

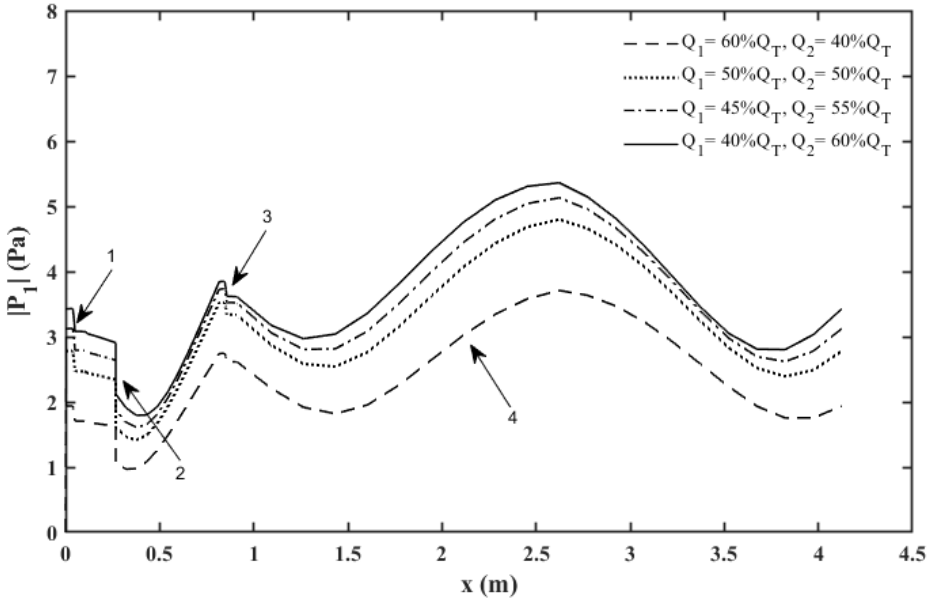


Figure 5.4: The variation of the peak pressure amplitude through the loop using different percentages of the total heat input. Numbers in the graph correspond to that in Figure 5.1: 1 is the regenerator of stage 2, 2 is the loudspeaker, 3 is the regenerator of stage 1 and 4 is the feedback pipe.

The distribution of the acoustic volumetric velocity throughout the loop for different ratios of the heating power is seen in Figure 5.5. No obvious differences are observed in the trend of all curves other than those noted previously. The volumetric velocity is low at the AHX of the regenerator 1 and regenerator 2 (location 1 and 3) which is the expected design to eliminate viscous dissipations and to enhance the amplification of the acoustic power in the system. The volumetric velocity is effectively reduced due to the enlarged cross-sectional area of the thermoacoustic core which is crucial for powerful operation. Also, the curves show that volume flow rate has a third low

value at location 6 which corresponds to the location of the highest pressure amplitude. Moreover, there is a high decrease in the volume velocity at this location which indicates that the stub removes part of the volumetric flow from the loop. In contrast, there is a significant increase in the volume flow rate across the two regenerators (location 1 and 3) as a result of the increasing temperature gradient. After the alternator and before the secondary ambient heat exchanger, there is a region between location 1 and 5 where the pressure amplitude decreases and volumetric velocity increases. From the four heating power ratios, the $Q_1 = 40\%Q_T, Q_2 = 60\%Q_T$ has the highest pressure amplitude and the highest volumetric velocity amplitude compared to the other ratios, whilst the $Q_1 = 60\%Q_T, Q_2 = 40\%Q_T$ produces the minimum oscillations.

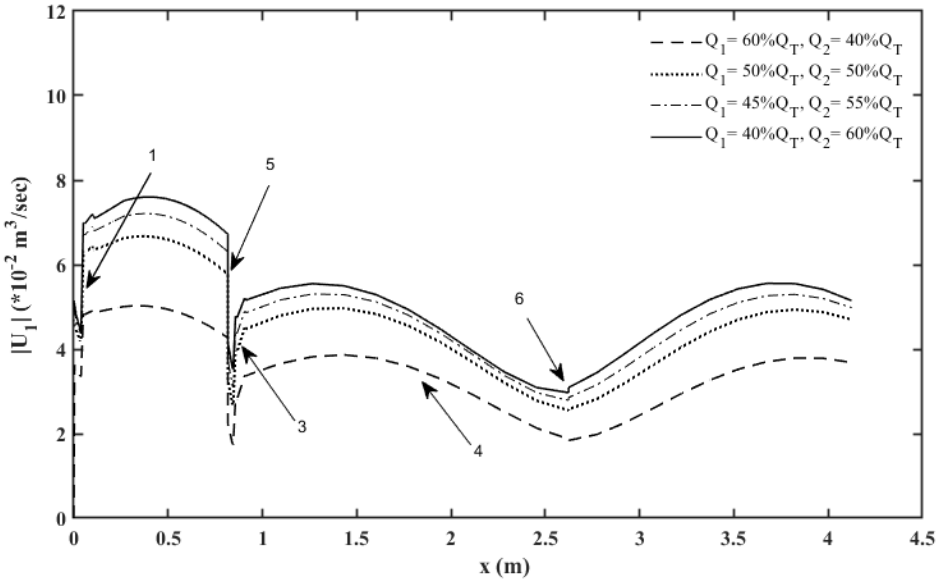


Figure 5.5: The variation of the peak volumetric velocity amplitude through the loop using different percentages of the total heat input. Numbers in the graph correspond to that in Figure 5.1: 1 is the regenerator of stage 2, 3 is the regenerator of stage 1, 4 is the feedback pipe, 5 is stub 2, 6 is stub 1.

The acoustic impedance is plotted in Figure 5.6. For all the heat ratios, there are two higher values of the acoustic impedance that at the location 1 and 3 corresponding to the thermoacoustic regenerators. These values represent 14.4 and 7.2 times the specific acoustic impedance of the gas $\rho_m a/A$ when distributing the heat equally between the two engines. This changes to 11.9 at regenerator 1, and 8.3 at regenerator 2 when applying $40\%/60\%$ percentage which indicates that the impedance in the second core is relatively better when using two third of the heat in the second stage. Table 5.1 summarises the amplification of the acoustic power as well as the ratio of the acoustic impedance to the specific acoustic impedance for the two regenerators. In travelling wave thermoacoustic engine, a standard practise is to set the absolute value of the regenerator impedance within the range of 10-20 times the specific acoustic impedance

to limit the impact of viscous dissipations in the regenerator (Backhaus and Swift 2000; De Blok 2008). The acoustic impedance dropped at the alternator (location 5) where the volumetric velocity is constant at the two sides of the diaphragm. At the locations of the tuning stubs (location 5 and 6), the impedance increased due to the constant pressure amplitude at the junction between the stub and the feedback tube. For optimization of the whole system, the introduction of the stubs within the loop compensate the acoustic impedance drop caused by the alternator.

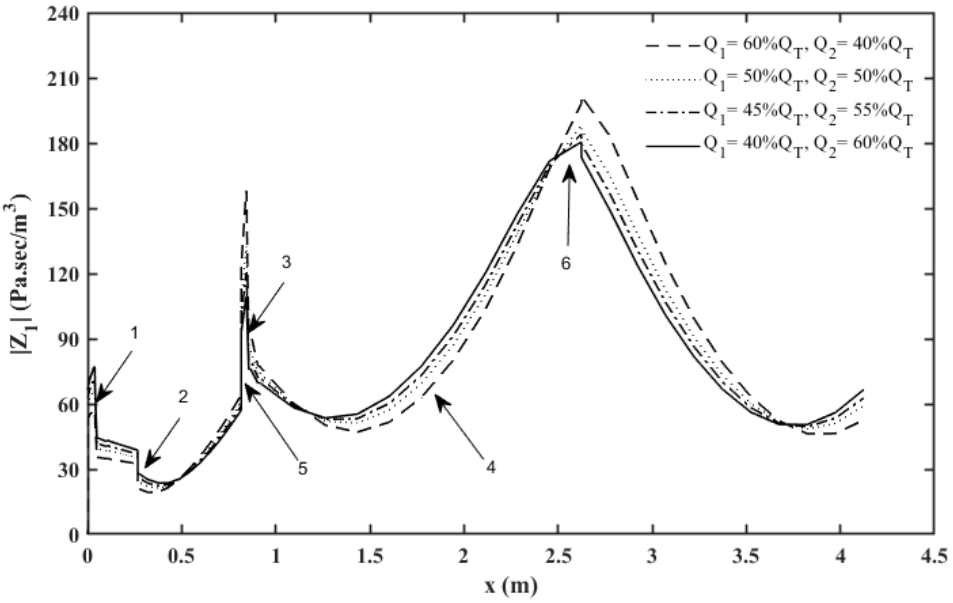


Figure 5.6: The variation of the acoustic impedance through the loop using different percentages of the total heat input. Numbers in the graph correspond to that in Figure 5.1: 1 is the regenerator of stage 2, 2 is the loudspeaker, 3 is the regenerator of stage 1, 4 is the feedback pipe, 5 is stub 2, 6 is stub 1.

Table 5.1: Performance of the two regenerators at several ratios of the thermal power.

Heat ratio, Q_1/Q_T	**Amplified power in reg.1 (W)**	**Impedance ratio at reg.1**	**Amplified power in reg.2 (W)**	**Impedance ratio at reg.2**
0.6	14.1	17.16	9	6.2
0.5	20.94	14.39	20.1	7.16
0.45	21.76	13.13	26.3	7.7
0.4	20.9	11.93	32.6	8.32
0.3	14.98	9.75	44.38	9.85

The phase angle between the pressure and the volumetric velocity of oscillation throughout the loop is illustrated in Figure 5.7. The graph again shares the same trend among

the four different heat ratios being added to the two cores. For all the cases, the two regenerators (location 1 and 3 in the graph) are close to zero which would be expected for a travelling wave. After the alternator (location 2), there is a rapid decrease in the phase angle. In contrast, there are two sharp increases in the phase at the location of the two stubs (location 5 and 6) to counteract the sharp decrease in the phase angle. It can be noted that when adding 2.5 kW heat power, Q_T , using different ratios throughout the two stages, the phase angle within the system is altered. For example, applying $60\%Q_T$ instead of $40\%Q_T$ into the second HHX shifts the phase angle within the first regenerator from -40° to -18° . The phase angle range within the feedback loop changes from $-40^\circ < \phi < 40^\circ$ to $-34^\circ < \phi < 34^\circ$. One of the design strategies to be fulfilled in travelling wave thermoacoustic engine is that the phase angle between the pressure amplitude and the volumetric velocity amplitude should be close to zero or slightly negative within the regenerator. In addition, near travelling wave condition should be maintained in at least one part of the feedback tube. Thereby, the amplification of the acoustic power within the regenerators can be maximized, and the acoustic power dissipation within the feedback pipe can be minimized. The phase angle at 2.7 m distance equals zero when using $60\%Q_T$ in HHX2, thus using one third of the total heat at the first core minimized the phase angle in the loop and in turn the acoustic losses.

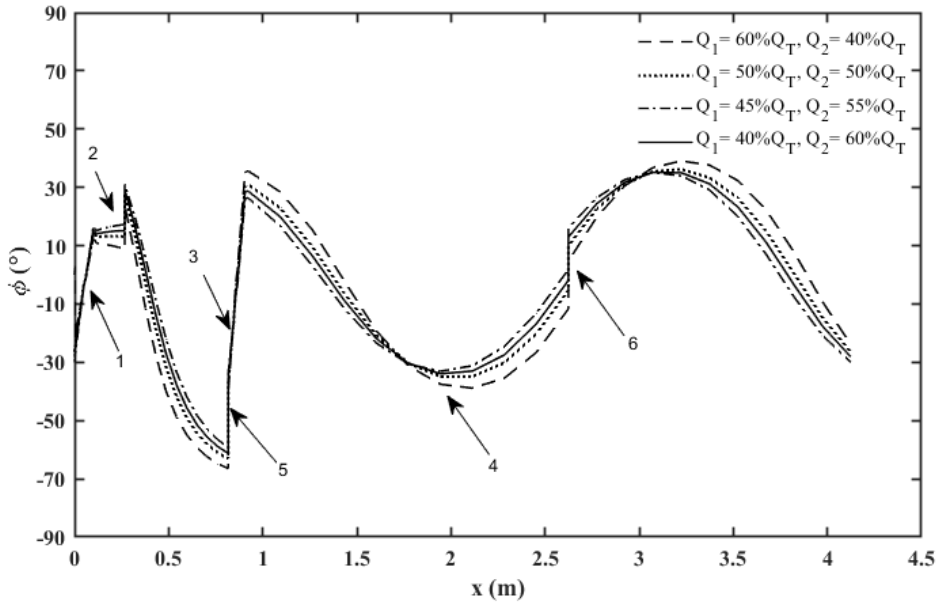


Figure 5.7: The variation of the phase angle through the loop using different percentages of the total heat input. Numbers in the graph correspond to that in Figure 5.1: 1 is the regenerator of stage 2, 2 is the loudspeaker, 3 is the regenerator of stage 1, 4 is the feedback pipe, 5 is stub 2, 6 is stub 1.

The variation in the acoustic power throughout the loop using different heat ratios is given in Figure 5.8. It shows that the acoustic power flow is in the lowest level when

using $2/3$ of the total heat in the first stage, and the acoustic loop power increases gradually when increasing the heat ratio in the second core and reducing the ratio in the first heater. This is due to the fact that the intensity of the acoustic oscillation in the $60\% - 40\%$ is not strong as those in the other three heat ratio sets as presented in Figure 5.4 and Figure 5.5. For all the ratios, the curves again have the same relative characteristics. In the base case where the total heating power splits evenly between the two heaters, DeltaEC predicted that, 58.4 W of the acoustic power from the resonance tube travels towards HHX2. Only 1 W is dissipated within AHX2. The remaining 57.4 W enters the cold side of the regenerator 2 where the acoustic power is amplified to 77.5 W by consuming 1.25 kW total thermal power. Minor losses of 1.8 W occur in HHX2, the thermal buffer tube and SAHX2. 24.4 W electrical power was extracted by the alternator with thermal-to-acoustic conversion efficiency of 2.3%, acoustic-to-electrical efficiency of 41.8%, and thermal-to-electrical efficiency of 0.98%.

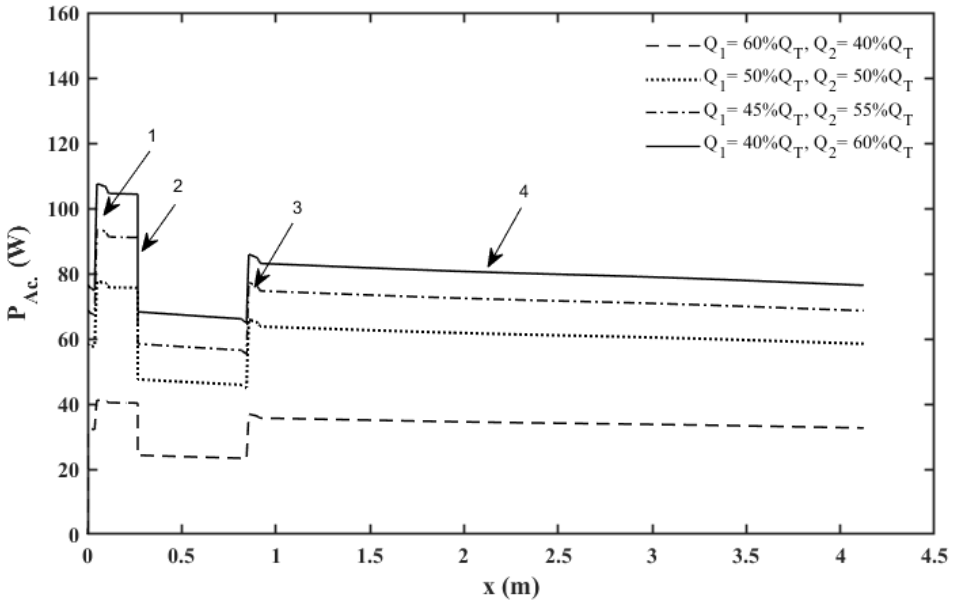


Figure 5.8: The variation of the acoustic power through the loop using different percentages of the total heat input. Numbers in the graph correspond to that in Figure 5.1: 1 is the regenerator of stage 2, 2 is the loudspeaker, 3 is the regenerator of stage 1, 4 is the feedback pipe.

The temperature difference between the hot and cold side of the regenerator is also important to evaluate the performance of the thermoacoustic systems. The efficiency is generally better when the onset temperature (the temperature difference at the starting of spontaneous oscillation) is low. Generally, the onset temperature and the steepness of the acoustic power curve against temperature difference across the regenerator are good indicators of the performance of a thermoacoustic system. A low onset temperature means low dissipation and adequate acoustic matching between the various components of the system. A steep power increase against temperature difference indicates good

heat transfer of the ambient and hot heat exchangers and also reflects low acoustic loss (De Blok 2008).Therefore, to assess the current rig for the tested heat input percentages, the loop acoustic power is plotted against the temperature difference across the two regenerators in Figure 5.9. Clearly, the acoustic power amplification in the second regenerator decreases when the heat ratio into the first core is larger and the temperature difference increases in this case. However, in the first regenerator, the reverse happens. In fact, there is a significant drop in the temperature difference of the second core. This drop is larger in magnitude than the increase in the temperature difference of the first core.

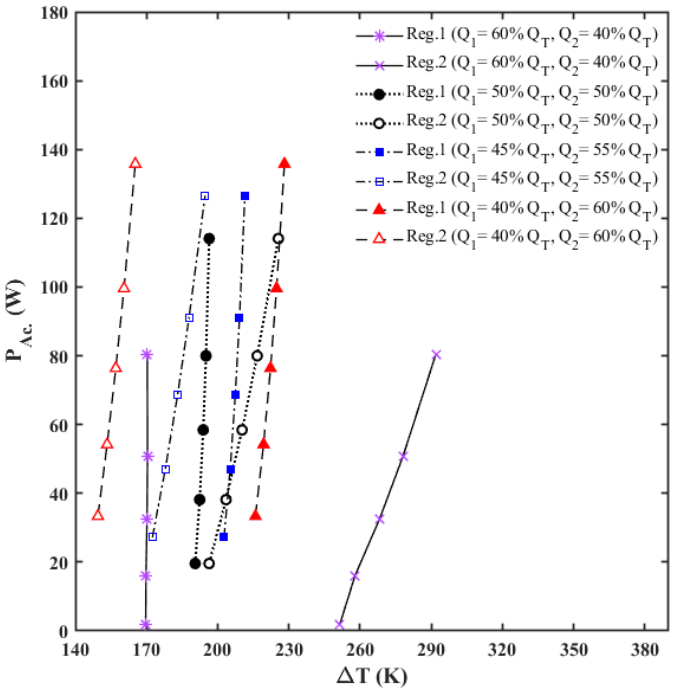


Figure 5.9: Loop acoustic power relation with the temperature difference across the regenerator when different heat percentages are used to add a total heating power range of 2.1 to 3 kW into the system.

Figure 5.10 shows the predicted acoustic power and the electrical power output as functions of the heat input ratio. The horizontal axis displays the ratio of the heat supply into the second core divided by the total heat added into the two heaters Q_2/Q_T. It can be noted that, the predicted acoustic power increases gradually when the heat input power to the first engine is decreased and the heat input power into the second engine is increased until it reaches the highest level of 84 W at $Q_1 = 30\%Q_T$, $Q_2 = 70\%Q_T$. The acoustic power declines when the heat input ratio is greater than 70% in the second stage. This behaviour is mimicked by the electrical power output where the optimal output is 34 W at 70% heat ratio in HHX2. Unfortuantely, it was impossiple to validate the optimal predictions with the present experimental prototype due to material

considerations of the hot heat exchanges, which why the experimental results are restricted to a maximum ratio 40% : 60%.

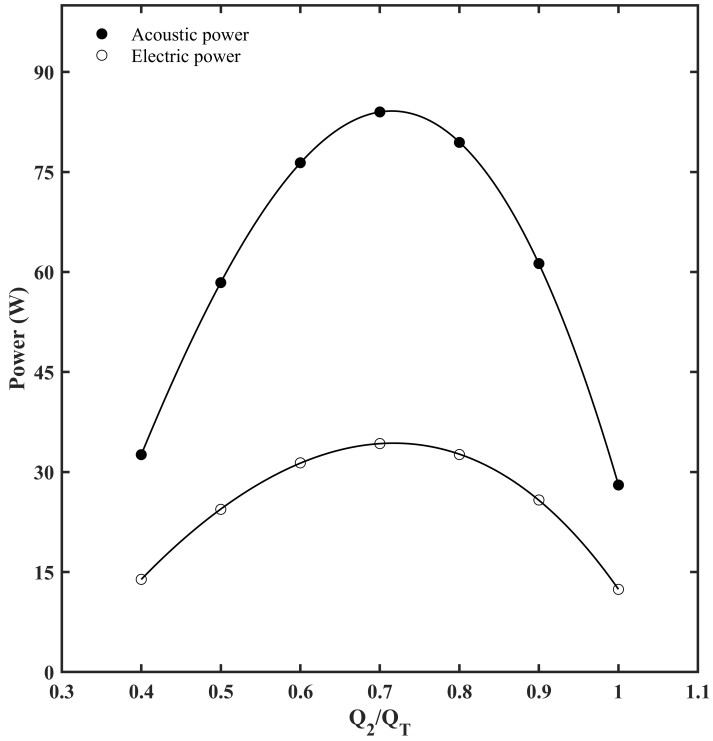


Figure 5.10: Dependences of the acoustic power, and the electric power on the percentage of the heating power into the second engine, when a total heating power of 2.5 kW is added into the system.

At this point, the function of the regenerator and its relation to the power amplification and the heat input ratio can be discussed further. In a travelling wave thermoacoustic engine, the regenerator functions as acoustic amplifier with the amplification factor, τ, given as the ratio of the hot-side temperature, T_H, to cold-side temperature, T_C:

$$\tau = \frac{T_H}{T_C} \tag{5.5}$$

The acoustic power flows out the regenerator can be expressed as:

$$P_{Ac.,out} = \tau P_{Ac.,in} \tag{5.6}$$

Where: $P_{Ac.,in}$ and $P_{Ac.,out}$ are respectively the acoustic power flows into the ambient end and out of the hot end of the regenerator. Therefore, the regenerator produces a net

acoustic power as follows (Backhaus and Swift 1999):

$$P_{Ac.,net} = (\tau - 1)P_{Ac.,in} \tag{5.7}$$

The acoustic power flows into the ambient end of the regenerator can be expressed as a function of the pressure amplitude as:

$$P_{Ac.,in} = \frac{A_g |p_{1,in}|^2}{2n\rho_m a} \tag{5.8}$$

Here: $|p_{1,in}|$ is the pressure amplitude at the ambient end of the regenerator, A_g is the area of the regenerator, ρ_m is the mean density of the working gas, a is the speed of sound, and n is the ratio of the acoustic impedance to the specific acoustic impedance for the regenerator. This ratio (also called the impedance enhancement factor) is set by the system configuration (bypass, or looped tube) (De Blok 2008). Substituting Equation 5.8 with Equation 5.7 gives the net acoustic power produced by the regenerator in the form:

$$P_{Ac.,net} = (\tau - 1)\frac{A_g |p_{1,in}|^2}{2n\rho_m a} \tag{5.9}$$

Equation 5.9 shows that the net acoustic power is a function of the square of the pressure amplitude at the cold side of the regenerator, the amplification factor and the acoustic impedance enhancement factor. Table 5.2 is provided below to illustrate the behavior of the two regenerators with the novel operational methodology applied in this study. The numerical data shows that when the heat input ratio is varied from 0.6 to 0.4 in the second engine, the pressure amplitude, $|p_1|$, at the cold end of regenerator 1 and regenerator 2 increases significantly. Thus, a strong acoustic wave is produced which is clearly seen in Figure 5.11. Also, the volumetric velocity, $|U_1|$, increases in both the regenerators. The thermal dissipation is proportional to $|p_1|^2$, and the viscous dissipation is proportional to $|U_1|^2$, which reflects that the losses become larger with higher heating percentages. The calculated thermal and viscous losses in the two regenerators are less than 1 W in all the tested heat ratios, which means they have no significant effect.

Table 5.2 shows the net produced acoustic power from the two regenerators for the 0.6 heat input ratio in the second engine is significantly increased due to the significant increase in the pressure amplitude in the two regenerators; $|p_1|$ is increased from 2745 to 3949 Pa in regenerator 1, and from 1939 to 3431 in regenerator 2, when the heat ratio is changed from 0.4 to 0.6. As a result, the net acoustic power from regenerator 1 changed from 17.2 to 29 W in regenerator 1, and from 15.1 to 47 W in regenerator 2. Moreover, due to the heat input methodology, the impedance enhancement factor

in both regenerators tends toward 10-20, which is close to the preferred conditions to reduce viscous losses in travelling-wave systems (De Blok 2008).

Table 5.2: Summary of DeltaEC results of the double core thermoacoustic electricity generator when the heat is being distributed into the two heaters with different ratios.

	Heat input percentage, Q_1/Q_T		
Parameter	**0.6**	**0.5**	**0.4**
Total heat input, Q_T (kW)	2.5	2.5	2.5
Pressure at cold end of reg.1, $\lvert p_1 \rvert$ (Pa)	2745	3525	3849
Pressure at at cold end of reg.2, $\lvert p_1 \rvert$ (Pa)	1939	2782	3431
Volumetric velocity at cold end of reg.1, $\lvert U_1 \rvert$ (m^3/sec)	0.017	0.027	0.035
Volumetric velocity at cold end of reg.2, $\lvert U_1 \rvert$ (m^3/sec) (Pa)	0.034	0.042	0.045
Cold temperature of regenerator 1 (K)	369	371	373
Hot temperature of regenerator 1 (K)	637	581	530
Cold temperature of regenerator 2 (K)	363	363	363
Hot temperature of regenerator 2 (K)	533	557	585
Amplification factor at reg. 1, τ	1.73	1.57	1.42
Amplification factor at reg. 2, τ	1.47	1.53	1.61
Impedance enhancement factor at reg. 1, n	17.2	14.4	11.9
Impedance enhancement factor at reg. 2, n	6.2	7.2	8.3
Net acoustic power produced by reg. 1, $P_{Ac.,net}$ (W)	17.2	26.9	29.0
Net acoustic power produced by reg. 2, $P_{Ac.,net}$ (W)	15.1	31.5	47.4
Loop acoustic power (W)	32.6	58.4	76.4
Electrical power output (W)	13.9	24.4	31.4
Thermal-to-acoustic efficiency (%)	1.3	2.3	3.1
Thermal-to-electrical efficiency (%)	0.6	1	1.3
Relative Carnot efficiency for acoustic output(%)	3.5	6.6	9.0

Previous research undertaken by Yu and Al-Kayiem (2014) has identified that the symmetrical geometry conditions led to an asymmetrical acoustic condition in their three-stage travelling wave thermoacoustic engine. Their system used helium at 3.0 MPa as the working gas, and the system was able to produce 1512 W total acoustic power with 10% thermal-to-acoustic efficiency. Although their three engine stages have exactly symmetric configuration, the produced acoustic power and thermodynamic efficiencies are different for each engine stage. This could be a result of the same physical mechanisms, and it might have been that if they had adjusted the input ratio using the current research methodology, their system performance also could have improved. As discussed in the background section, there are many design of systems that have multiple cores. These results suggest that perhaps they should consider asymmetrical input of energy for enhanced system performance. The data produced by the model of the two-stage thermoacoustic system is provided in **Appendix C**.

5.4 Experimental Apparatus

All the experiments were conducted at atmospheric pressure and ambient room temperature. The working gas used for the thermoacoustic system was air. The general experimental set-up is shown schematically in Figure 5.11, which comprises two thermoacoustic engines operating in mainly travelling wave mode, and evenly distributed within a looped resonance tube. To harvest electricity, the system is coupled with a loudspeaker, which functions as a linear alternator, and there are two tuning stubs to correct the disturbance in the acoustic field occurring due to the usage of the loudspeaker. The locations and the lengths of these stub branch pipes were optimized carefully using the same concept applied in the previous single thermoacoustic engine. The current arrangement offers an advantage of using low-temperature heat source with a lower temperature gradient through each engine stage. The two thermaocoustic engines are placed side-by-side, each engine has a regenerator (REG), a main ambient heat exchanger (AHX), a hot heat exchanger (HHX), a thermal buffer tube (TBT) and a secondary ambient exchanger (SAHX). A cooling water pipes and measurement system are also included in the apparatus.

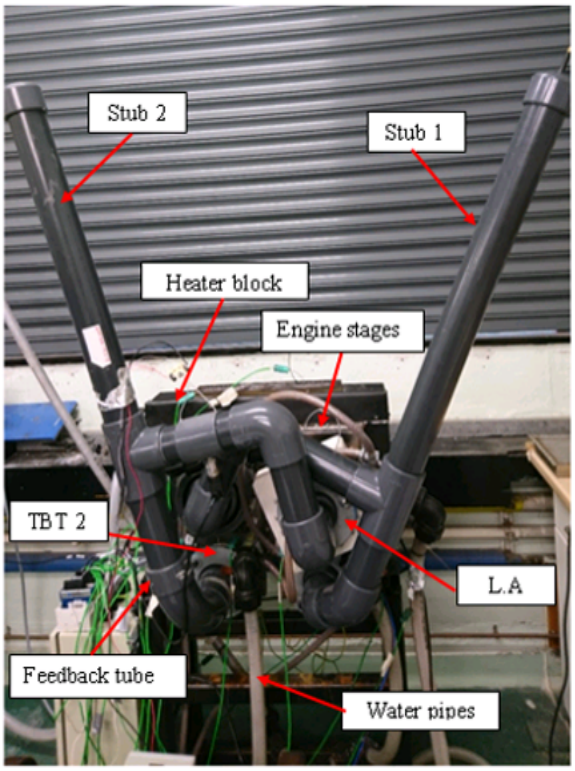


Figure 5.11: Photo of the double core thermoacoustic electricity generator shows the location of the engines, the heater block, the alternator (L.A), the feedback pipe, one of the thermal buffer tubes (TBT2) and the cooling water pipes.

The two hot heat exchangers (HHX1, HHX2) are identical, and they are made out from a convoluted plate of Stainless Steel as seen in Figure 5.12. Both the hot heat exchangers are used to capture and transfer heat to the regenerator mesh of the two engines. It should be mentioned that, the double core thermoacoustic engine was originally developed to be integrated with a wood burning cooking stove which means it will receive heat from a flame. However, for a steady heating power flow, two identical electrical heaters were used to supply the heating power to the hot heat exchangers instead of the wood fire. Both the heaters have a rated power output of 2.5 kW, and they are placed in an insulated heater block that is directly attached to the engine's frame as illustrated in Figure 5.13. The two heaters are separately controlled by PID controller which enables the engine to be operated at various heat inputs. After, heat is introduced to each engine, the convoluted plate heat exchanger then heats up rapidly to a temperature of about 650°C, and transfers heat to one end of each regenerator (hot side).

The total amount of heat, Q_T, flows into a multi-stage system can be found from the following equation:

$$Q_T = \sum_{1}^{n} Q_n \tag{5.10}$$

Where: n is the number of the stages, Q_n is the heat input per stage.

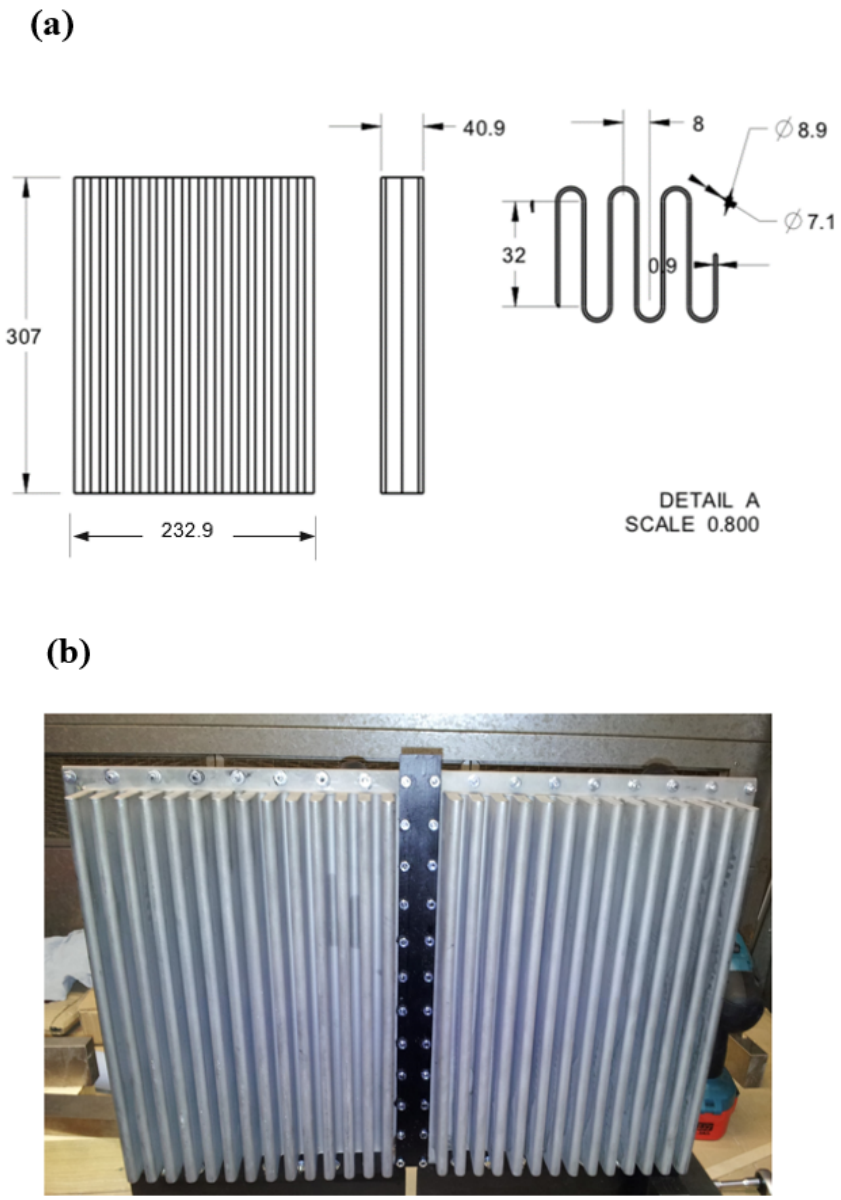


Figure 5.12: The design considered for the hot heat exchangers. (a) The dimensions of the convolutions. (b) The two hot heat exchangers after being bolted to the engine frame.

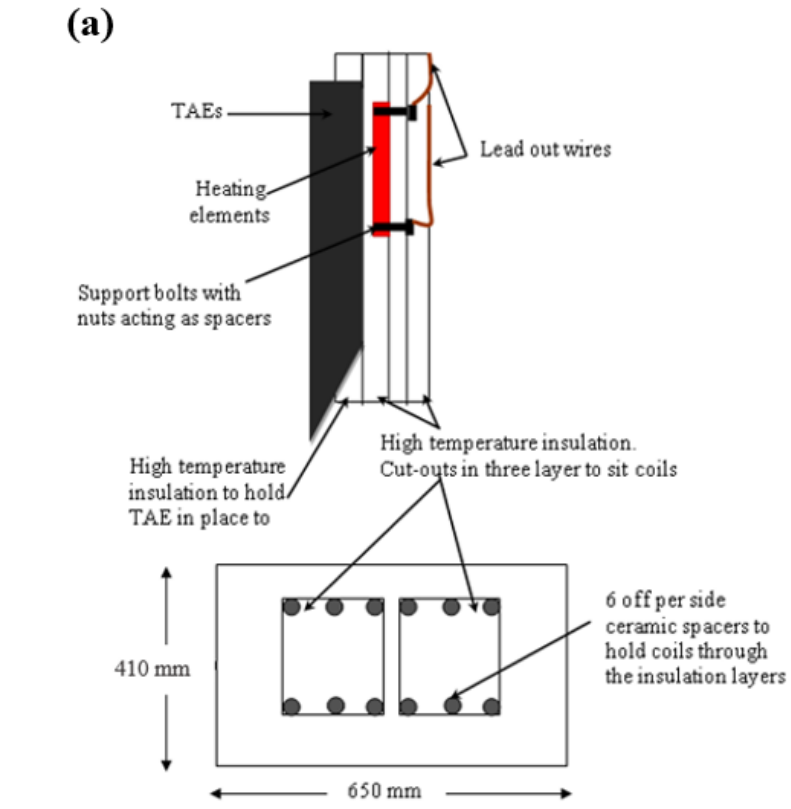


Figure 5.13: The electrical heaters used to supply the heat into the double core thermoacoustic electricity generator. (a) Schematic of the engine shows the location of the heater and the assembly of the heating elements. (b) Photo of the heating elements after being installed.

The ambient and the hot heat exchangers are placed on opposing sides of the regenerator. The regenerator is a stack of stainless steel mesh screen layers, as depicted

in Figure 5.14, that creates a porous cross-sectional area to drive the thermoacoustic effect. The idea is that the acoustic wave passes along the thermoacoustic loop to be regenerated or boosted with more acoustic power when it passes through the regenerator. In the current design, two thermoacoustic cores are utilized to amplify each other, so more acoustic power is created. The specifications of the regenerator mesh are provided in Table 5.3.

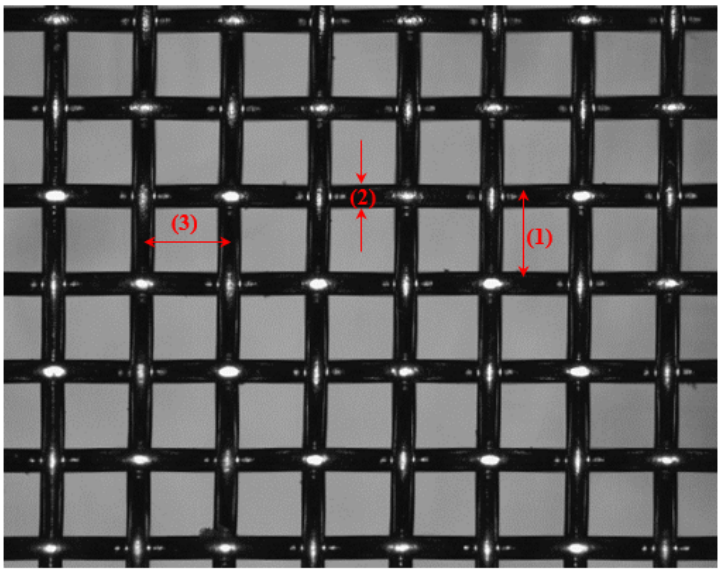


Figure 5.14: Microscopic view for the Stainless Steel mesh used to build the regenerators of the two thermoacoustic cores. (1) is the pitch, (2) is the diameter of the wire, and (3) is the width.

Table 5.3: Specification of the regenerator mesh used in the current design.

Parameter	**Value**	**Unit**
Regenerator width	200	mm
Regenerator length	250	µm
Regenerator length	200	mm
Regenerator thickness	12	mm
Wire diameter	143	µm
Wire spacing	250	µm
Volumetric porosity,ϕ	0.73	-
Solid fraction, $(1-\phi)$	0.27	-
Hydraulic radius	97	µm

The performance of the system is given by the thermal-to-acoustic efficiency, η_{t-a}, and the electrical-to-acoustic efficiency, η_{t-e}, as follows:

$$\eta_{t-a} = \frac{P_{Ac.}}{Q_T} \tag{5.11}$$

$$\eta_{t-e} = \frac{W_e}{Q_T} \tag{5.12}$$

Where: $P_{Ac.}$ is the acoustic power produced by the system (entering the loop), and W_e is the electrical power extracted by the alternator.
The relative Carnot efficiency of the output acoustic power is given as the ratio:

$$\eta_{R,Ac.} = \frac{\eta_{t-a}}{\eta_{Carn.}} \tag{5.13}$$

Where: $\eta_{Carn.}$ is the Carnot efficiency of the system. The ambient heat exchangers are sections of a typical car radiator. The difference between heat captured from the HHX and the ambient heat exchanger AHX will produce the thermoacoustic effect. The cold side of the regenerator is cooled using cooling water that fed via the water pipe. The amount of rejected heat, Q_w can be evaluated from:

$$Q_w = \dot{m}_w c_{p,w}(T_{w,out} - T_{w,in}) \tag{5.14}$$

Where: $\dot{m}_w$ is the mass flow rate of the cooling water, $c_{p,w}$ is the specific heat capacity of the water, $T_{w,in}$ the temperature of the water inside the inlet pipe. $T_{w,out}$ is the temperature of the water flows inside the outlet pipe.

The two thermal buffer tubes are sections of Stainless Steel pipe, each TBT is positioned immediately below the HHX to separate the secondary ambient heat exchanger from the hot gases and also to minimize thermal losses. The secondary heat exchangers are used to cool down the air before it flows into the loudspeaker's housing. As shown in Figure 5.4, the two engine stages are connected to each other using two different lengths of 70 mm inner diameter standard PVC pipes. These lengths of the PVC pipes are named feedback loop.

The two stub branch pipes are also 70 mm diameter PVC pipes, installed perpendicular to the feedback loop to enhance the impedance matching between the acoustic wave and the loudspeaker, and to maintain the required phase condition between the velocity and the pressure of oscillation through the regenerators. All the pipe works and the fittings are PVC to cut down the manufacturing cost of the system. A detailed specifications of the different parts of the current system including the material and the dimensions is presented in Table 5.4, while detail drawings contain all the information required for manufacturing the two-stage thermoacoustic system are included in **Appendix C**.

Table 5.4: Design parameters of the components of the double core thermoacoustic electricity generator.

Part	**Parameter**	**Value**
Main ambient heat exchangers	Length (mm)	25
	Porosity, ϕ	0.7
	Plate spacing, $2y_0$ (mm)	2.934
	Material	Copper
Hot heat exchangers	Length (mm)	40
	Porosity, ϕ	0.75
	Plate spacing, $2y_0$ (mm)	9
	Material	Stainless Steel
Thermal buffer tubes	Wall area (m^2)	1.16E-03
	Length (mm)	80
	Material	Stainless Steel
Secondary ambient heat exchangers	Length (mm)	10
	Porosity, ϕ	0.713
	Plate spacing, $2y_0$ (mm)	2.934
	Material	Copper
Tuning stub1	Area (m^2)	3.85E-03
	Length (cm)	90
	Material	PVC
Tuning stub2	Area (m^2)	3.85E-03
	Length (cm)	70
	Material	PVC
Feedback pipe	Area (m^2)	3.85E-03
	Material	PVC

The acoustic power of the loop that is produced from the thermoacoustic engines is captured by a low-cost commercial audio loudspeaker. The loudspeaker is connected in series to the thermoacoustic loop, and it is positioned at the cold side of the second engine stage. The series configuration aids suppression of the acoustic streaming that might cause non-linear heat dissipations from the hot heat exchanger. The specifications of the electrical and mechanical parameters of the loudspeaker are summarized in Table 5.5 (Riley 2014*b*).

Table 5.5: Specification of electromechanical parameters of the loudspeaker.

Parameter	**Value**	**Unit**
Area, $A_{L.S}$	0.0196	m^2
Force factor, Bl	14	T.m
Coil electrical resistance, R_e	4	Ω
Coil electrical inductance, L_e	10	mH
Moving mass, M	20	g
Stiffness, K	4778	N/m
Mechanical resistance, R_m	0.18	N.sec/m

5.4.1 Principle of operation

The experimental tests start with supplying power to the thermoacoustic system via a transformer, and a voltage divider to control the supplied power. Electrical power is provided into the two identical electrical heaters at a $50V$ maximum voltage, and a $10A$ maximum current from an AC power supply. In all the experimental tests, the thermoacoustic rig was started from room temperature. The maximum temperatures of HHXs were maintained at around 650°C in order to have comparable conditions for the experiments, and because of the limited material strength.

Each HHX received the heat from the electrical heater, and then the heat was transferred into the regenerator. The temperature of the regenerator side that adjacent to the HHX is increased. It should be mentioned that the heat input power from each heater block was ramped up to the maximum value instantaneously at the start of the experiments rather than being increased gradually. As a result, non-linear temperature profiles will occur across the regenerators. However, it is more practical to directly adjust the required heat input power to ensure quick warm-up which is preferable for practical thermoacoustic engines. As the heat is added into the first engine, the temperature of HHX1 and the hot

sides of regenerator1 increase rapidly until the difference between these temperatures reaches a critical value, and the gas in the system starts to oscillate spontaneously from stationary state.

After this stage, the heat transfer from HHX1 to the hot side of regenerator 1 becomes faster, and as a result, the temperature of HHX1 drops sharply, while the temperature of the hot side of regenerator 1 increases rapidly. This continues until the temperature of HHX1 and the regenerator's hot side reach a steady state, with the spontaneous oscillation continuing and regenerator 1 generates acoustic power. The acoustic power produced from regenerator 1 flows into the AHX1, the TBT1, the SAHX1 before it enters the second thermoacoustic engine. In the regenerator of the second thermoacoustic unit, the acoustic power will be amplified again and the transfer process repeated.
In order to measure the changes in the gas and the solid temperatures along the system, three thermocouples are used for each engine and they are embedded in the hot and cold sides of the regenerators and the center of the convoluted HHXs. The pressure of the acoustic wave is measured and monitored using pressure sensors. The thermocouples and the pressure sensors all are connected to the data acquisition (DAQ) card. After the temperatures and the pressure measurements obtained, the thermoacoustic engine can be analysed.

5.4.2 Data acquisition (DAQ) system

In the current dual core thermoacoustic electricity generator, several measurements are required to evaluate the performance such as the hot and cold temperatures of the working gas, temperatures of the cooling water, gas pressure, and time delay between the pressure signals. For temperature measurements, eight thermocouples (type K, $\pm 1^{\circ}$C accuracy) are impeded in different locations along the system. For the pressure measurements, three absolute pressure transducers (model IM-A5000-1A4-BXV-00-063, $\pm 0.1\%$ accuracy) and one differential pressure sensor (RS component, model ABPMJJT, $\pm 0.25\%$ accuracy) are distributed in the system. The distribution of the measuring instruments along the current system is shown in and Figure 5.15, while a summary of each measurement is Table 5.6.

Table 5.6: Summary of the measurements used to evaluate the performance of the current thermoacoustic system.

Parameter	Location	Parameter	Location
T_0	Temperature of hot end of Reg.2	P_1	Peak pressure in front of AHX1
T_1	Temperature of hot end of Reg.1	P_2	Peak pressure in front of AHX2
T_2	Temperature of cold end of Reg.2	p_1	Peak pressure in FB pipe
T_3	Temperature of cold end of Reg.1	Δp_1	Differential pressure in FB pipe
T_4	outside convolutions of HHX2		
T_5	outside convolutions of HHX1		
T_6	Inlet water total		
T_7	Outlet water total		

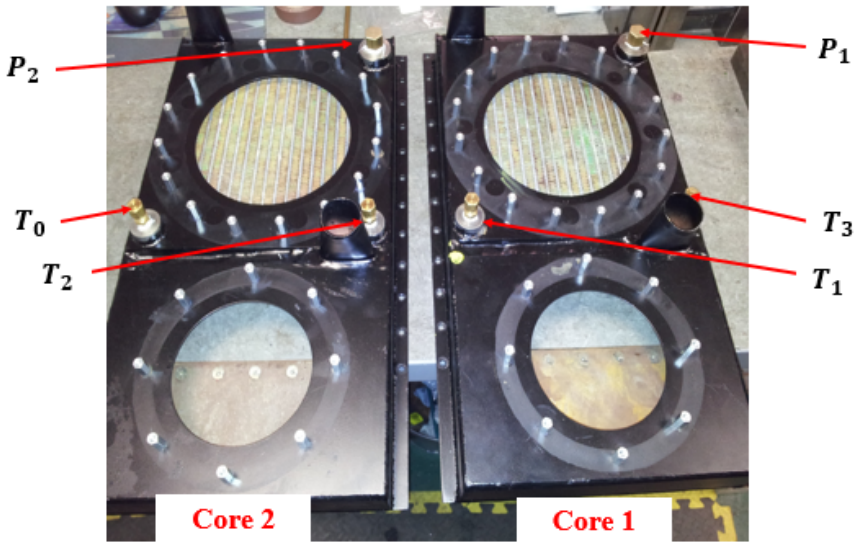


Figure 5.15: Photo of the locations of the pressure and the temperature sensors in the two cores of the current thermoacoustic system.

The signals from the thermocouples and the pressure sensors is passed via a data acquisition (DAQ) card, and the data displayed on the SCORE measurement software (Figure 5.16) before it is being saved on the computer.

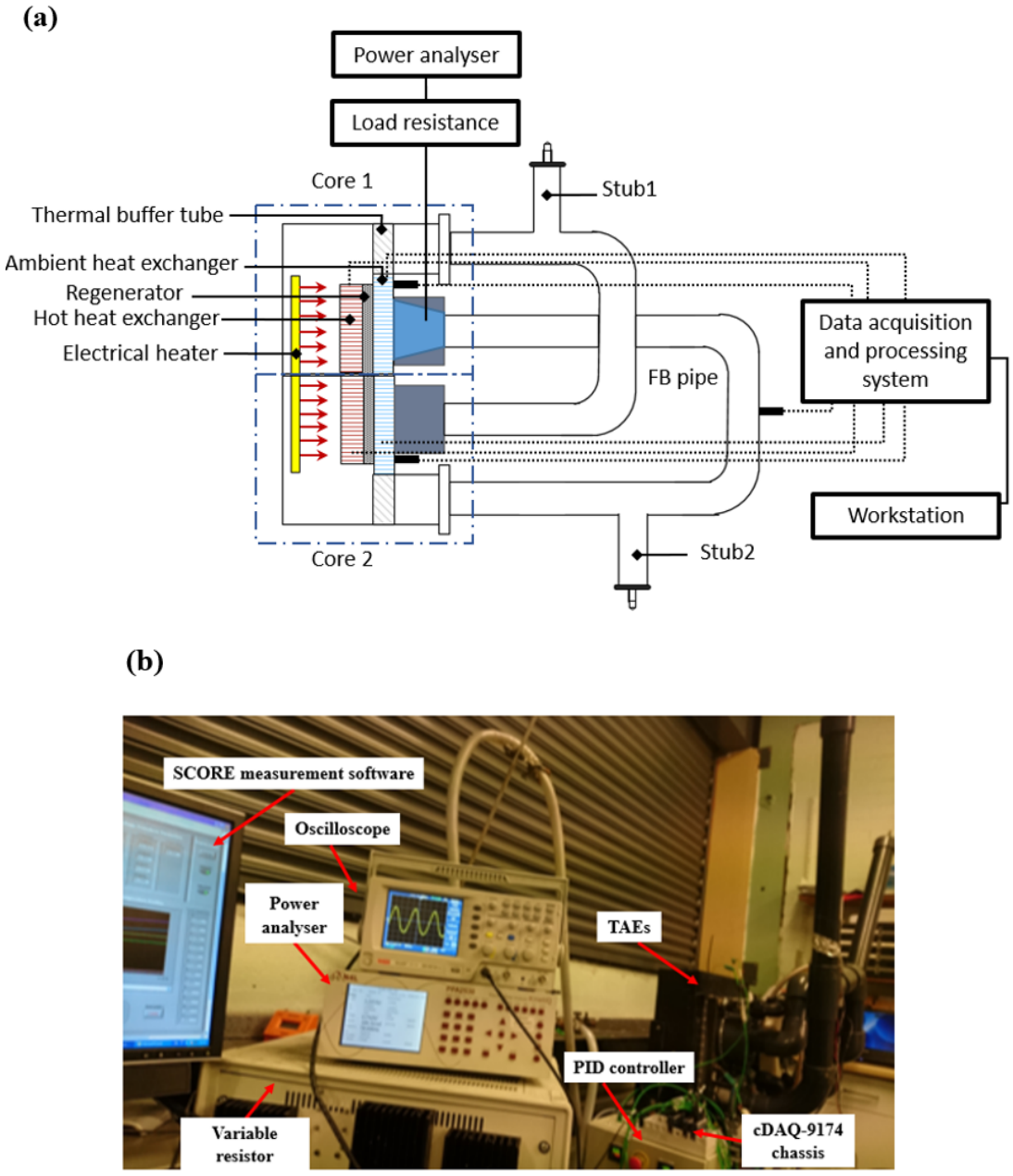


Figure 5.16: The double core thermoacoustic engine and the measuring instrumentations. (a) Schematic illustration for for the connection of the pressure and temperature sensors with the cDAQ. (b) Photo of the system while measurements are recorded.

The measurements devices (Figure 5.16) are the same ones reported in Chapter 4.

The SCORE measurement software allows plotting of temperature curves in real time, and pressure distribution curves over time, which enables the user monitoring the changes in the temperatures and also visualising the variation in the pressure.
It should be noted that, beside the above mentioned measurements, the dimensions of the system components are also required for both the experimental analysis and

DeltaEC modelling. Therefore, a measuring tape is used to measure the length of the feedback pipe, the tuning stubs and the heat exchangers, while small dimensions (< 1cm) are measured using a Vernier.

5.4.3 Measurement of the acoustic power

In order to quantify the performance of the system, it is important to determine the heating power, the acoustic power and the electric power output. The most complicated parameter to measure is the acoustic power which is defined as a time-average energy flux accompanied by pressure oscillations and velocity of the working gas. Accordingly, measurements of the pressure amplitude and the volumetric velocity amplitude and their phases are mandatory for estimating the loop acoustic power.
To obtain an accurate measure of the acoustic power in the current system, a more durable way alternative method referred as "gradient method" is employed (De Blok 2013). The gradient method employs one differential pressure sensor plus one absolute pressure transducer based on the acoustic pressure gradient in the working gas (as seen in Figure 5.17), to directly calculate the mass of the air between the two sensors, the acoustic velocity, and the acceleration. The distance between the two sensors is small compared to the two-microphone method. Thereby, no empirical correction for acoustic loss is required. Acoustic power propagation in the feedback loop can be expressed as:

$$P_{Ac.} = \frac{1}{2} Re(p_1 u_1^*) \tag{5.15}$$

Here: A is the cross-sectional area of the feedback loop (m^2), p_1 is the pressure amplitude of oscillation (Pa), which is the signal obtained from the absolute sensor, u_1 is the acoustic velocity (m/sec) and can be given as:

$$u_1 = \frac{\Delta p_1}{\omega \rho_m \Delta x}(-i\cos\phi + \sin\phi) \tag{5.16}$$

Where: Δp_1 is the output signal from the differential pressure sensor (Pa), Δx is the distance separates the two probes of the differential sensor (= 8 cm), ϕ is the measured phase between p_1 and Δp_1, ω is the angular velocity (rad/sec), ρ_m is the mean density (kg/m^3). Subsequently, the acoustic power can be found by substitute the real part of the acoustic velocity in Equation 5.15

$$P_{Ac.} = A.\hat{p_1} \frac{\Delta p_1}{2\omega \rho_m \Delta x} \sin\phi \tag{5.17}$$

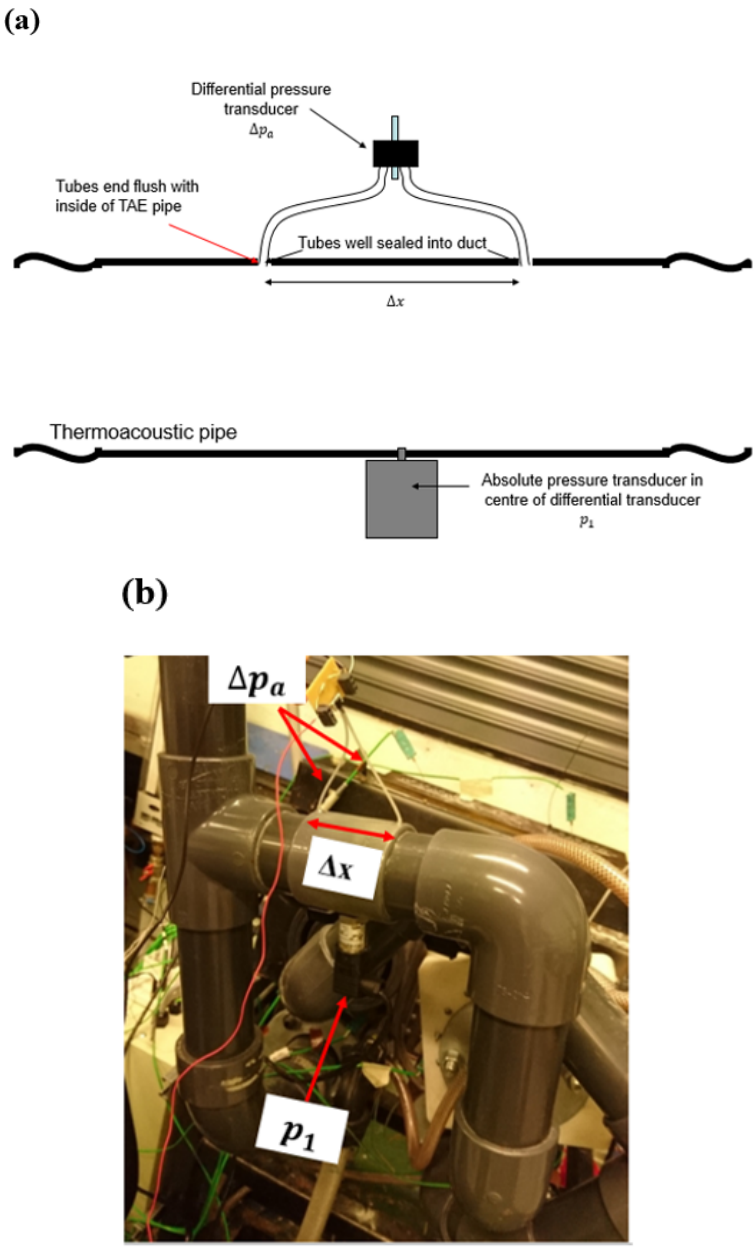


Figure 5.17: Measurement of the acoustic power flows in the thermoacoustic feedback pipe. (a) The arrangement of the differential and the absolute pressure transducer in the thermoacoustic pipe. (b) Photo for the transducers after being mounted on the thermoacoustic pipe.

5.4.4 Experimental results and validation

The results of the numerical modelling were surprising, and it showed that the heat input ratio has a great impact on the system performance. Therefore, to verify the software data, a series of experimental investigations was carried using the same operational concept (changing the distribution ratio, while maintaining the total input power). For all the tests, atmospheric air was the working gas. The data obtained from the double core thermoacoustic system is illustrated in Figure 5.18 and Figure 5.19. In Figure 5.18,

($T_H - T_C$) curve represents the time history of the temperature difference across the regenerator of the first engine, when 2.5 kW total heat is introduced into the system. The experiments were carried out by supplying total amount of heat of 2.5 kW through the electric heaters of the two engine cores. As indicated with the blue arrow in the temperature difference curve ($T_H - T_C$), the heat addition into the system was done 6 minutes (t = 300 s) after it reached the steady state. Due to this, the temperature difference across the regenerator increases rapidly with time until it reaches a maximum of 368°C. It took approximately 4 minutes after the system was heated up to start the oscillation (at t = 540 s) as seen in the pressure curve Figure 5.19. As the temperature difference keep rising up, a strong acoustic oscillation was occurred.

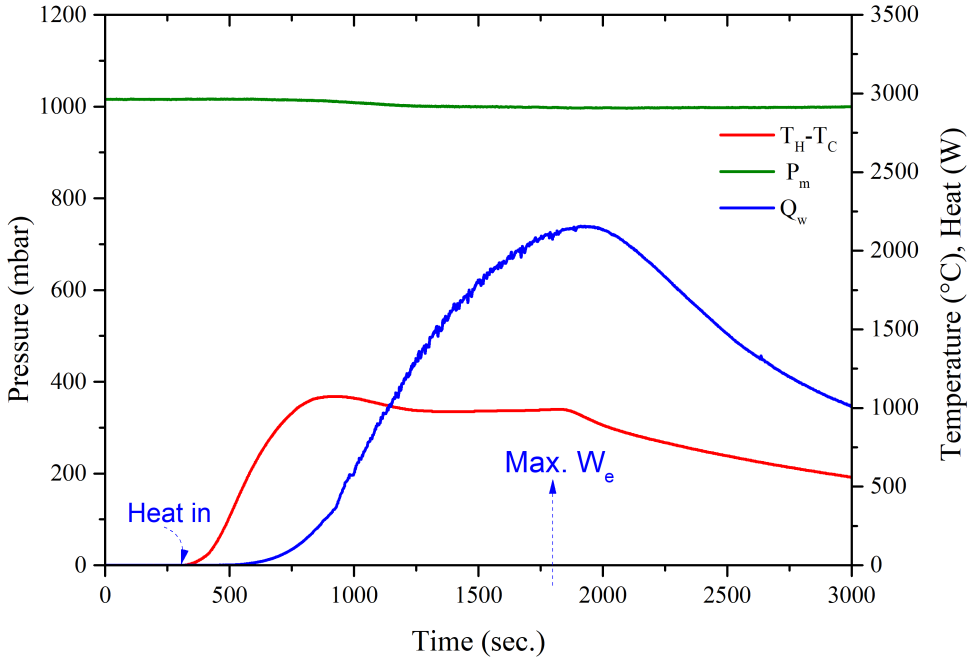


Figure 5.18: Measurement results of the performance of the double core thermoacoutsic electricity generator shows the mean pressure P_m, the amount of heat rejection Q_w, and the temperature difference across the regenerator $T_H - T_C$ as a function of time, with air at atmospheric pressure condition.

The observed frequency was 70 Hz. After that, the temperature difference $T_H - T_C$ decreased gradually from its maximum value until it reached a steady state of 336°C at t = 1250 s of operation. The steady state is indicated by the constant temperature difference ($T_H - T_C$), which can be understood that the amount of these heat energy (temperatures drop) is converted into acoustic power (acoustic oscillation).

Figure 5.19 shows the measured pressure amplitude and the acoustic power flow inside the feedback loop. The maximum electrical power extracted by the alternator was

about 16.5 W (recorded from the power analyser) with 35.5Ω load resistance, and was achieved when the acoustic power of the loop was 48 W at 1800 s of operation. The acoustic power dropped at 1800 s as a result of electricity harvesting. At the maximum output power, the pressure amplitude within the feedback loop was about 3130 Pa, and the heat removed by the cooling water was approximately 2 kW.

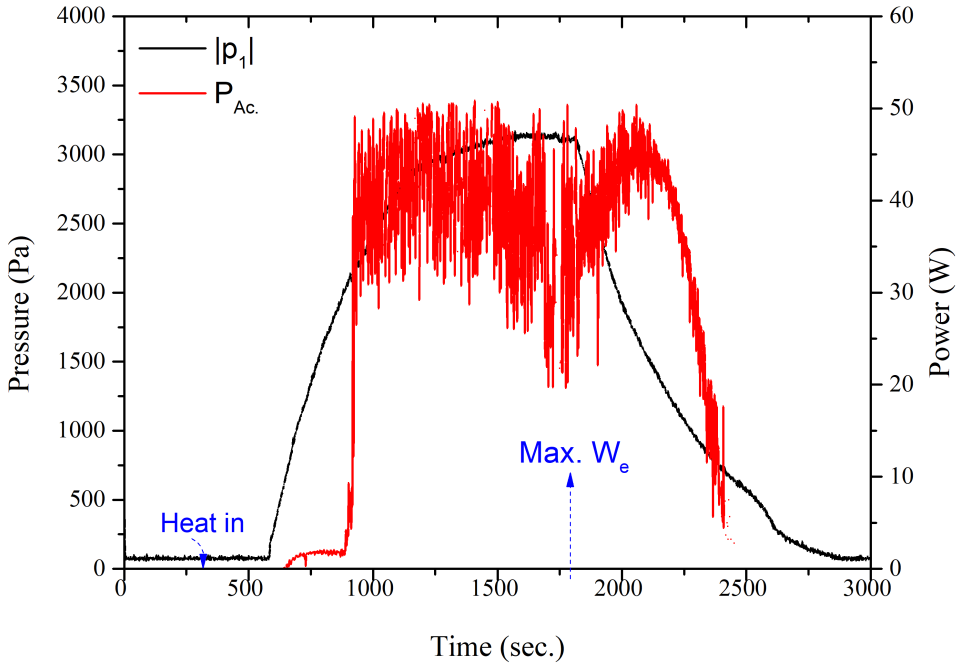


Figure 5.19: Experimental data for the peak pressure amplitude and the acoustic power as a function of time, when air at atmospheric pressure is used and a total heat input of 2.5 kW is evenly distributed between the two electrical heaters.

Comparing the obtained results from the current system with that achieved by SCORE for the same experimental conditions reveal that, the electrical power output achieved here is 4 W higher than that reported by Riley (2014*b*), where the system performance was highly degraded due to the high parasitic heat losses.

It is worth mentioning that, at the beginning of the experimental tests, it was realized that the insulation layers inside the heater block was partially damaged and some of the heating elements were not tightly fixed in their place. Therefore, both the heaters were replaced with completely new coils, and all the insulation layers were replaced with extra layers added near the upper case which might contribute to their improved performance. Figure 5.20 and Figure 5.21 compare DeltaEC results with the lab results, for the acoustic power and the electrical power, when several heat supply percentages are used to heat up the two cores. All the data are obtained when air at atmospheric pressure is employed as the working gas, and the total heat input into the system is

varied as a consequence of heat input range 2.1 to 3 kW. The load resistance of the loudspeaker is adjusted to be same as that used in DeltaEC simulation (37.5Ω). From Figure 5.20 to Figure 5.23 it can be observed how the investigated parameters increase with the total heat input. Both the acoustic power Figure 5.20, and the electrical power output Figure 5.21, increase linearly with the total heat input.

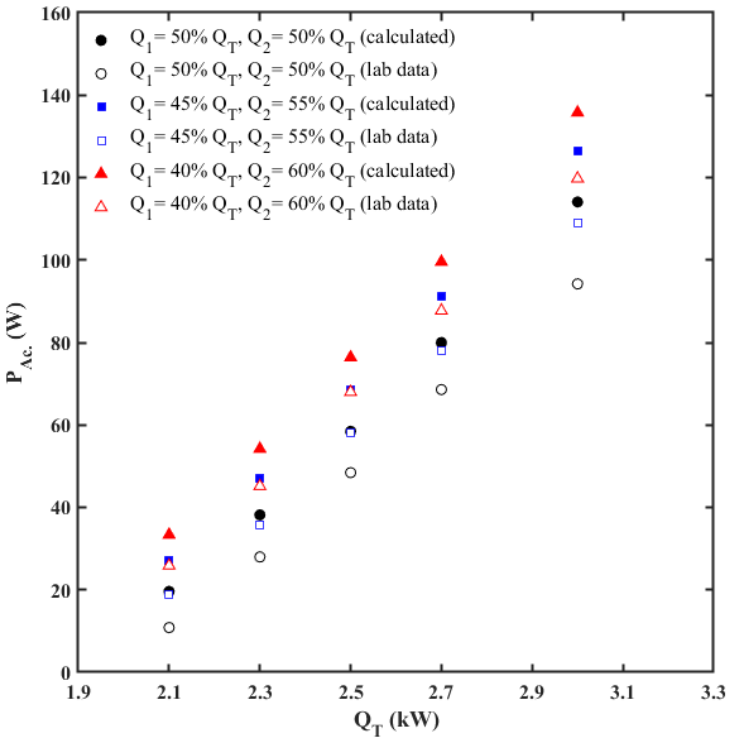


Figure 5.20: The loop acoustic power as a function of the heat input percentage, when a total heat input power range of 2.1 - 3 kW is added into the thermoacoustic system.

Extra power could be gained from the system by simply supplying a higher heat ratio into the second core and lower values in the first one. Using 2.5 kW power with equal distribution among the two engines generated an acoustic power of 48.4 W. This power is raised by approximately 40.5% to be 68 W when applying 40% Q_1,60% Q_2. It implies that if a higher output power is required from the current design, one should apply lower heat power into core 1 and higher into core 2. It is obvious that, at low power level, DeltaEC predictions are closer to the measured values for all the heat input ratios than the higher heat in calculation. There is a significant overestimation in the numerical power outputs at high input level. This could be mainly due to the fact that the heat dissipations to the ambient are considerably higher at a higher heat input.

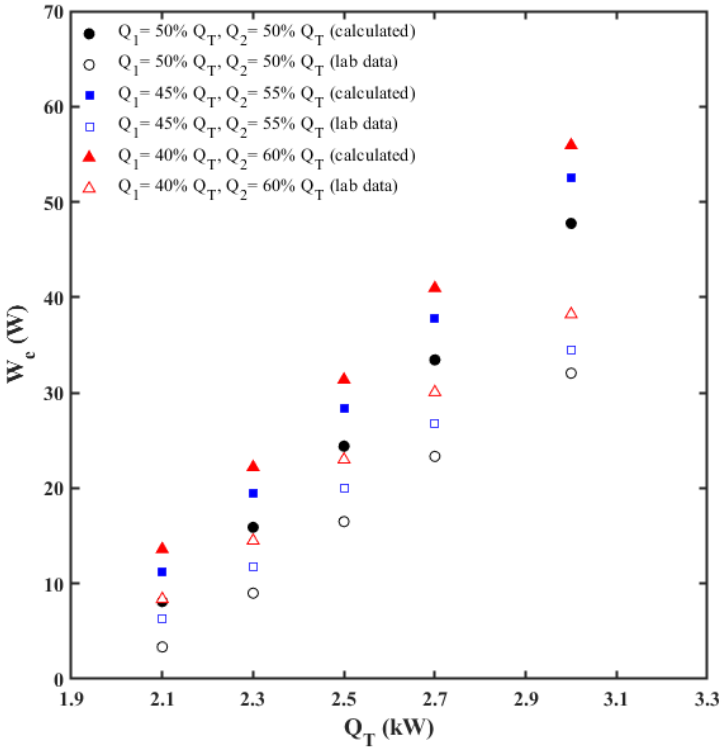


Figure 5.21: The harvested electrical power as a function of the heat input percentage, when the total heat input range of 2.1 - 3 kW is supplied into the thermoacoustic system.

The working principle of the current system is that, heat is added into the first core where the regenerator amplifies the acoustic power. The produced power is then passed into the second core where it get amplified for a second time before it enters the loudspeaker. It is important to note that the system is equipped only with one loudspeaker, which is connected immediately after the second engine. Therefore, if the heat is supplied with a higher rate into the first core, the resulting acoustic parameters (pressure amplitude $|p_1|$, and volumetric velocity amplitude $|U_1|$) will become higher. As a result, both the thermal and viscous dissipations parts will increase (thermal dissipation is proportional to $|p_1|^2$, and the viscous loss is proportional to $|U_1|^2$). Due to this, a strong acoustic wave will enter the second core where another high acoustic dissipation will be happen. Therefore, less acoustic power for electricity production. On the contrary, less losses can be obtained if the heat is added in small rate into the first core, and after the acoustic wave passes away from the first core to the second one it will be amplified again using higher heat ratio, leading to a stronger wave that enters the loudspeaker, where the harvesting of electricity will be enhanced. Moreover, for the range of the total heating power of 2.1 - 3 kW, using three different heat ratios at HHX1 (0.4, 0.45, and 0.6), it can be seen clearly that DeltaEC simulation predicted loop acoustic power values that are of the order of as $0.1 - 0.8\%$ higher than the experimental ones, and electrical

power values of the order of $0.4 - 1.4\%$ higher than the lab data. This suggests that the model does not account for all losses in converting thermal power into acoustic power, and that the heat dissipation is potentially an issue. For example, a considerable amount of the heat was being lost to the feedback pipe walls, and at the top of the engine housing instead of being directed down into the working gas factors which aren't considered by DeltaEC. Furthermore, there is only one power extractor in this system compared to other practical multi-stage "self-matching engines", where every stage has an independent electrical power harvesting point which prevents high power spots and reduces losses (Bi et al. 2017) (De Blok 2010) (De Blok and Systemen 2012) (Wu et al. 2014*a*). Another important point is that the alternator used in this system is placed next to the cold side of the second engine. At this location, the acoustic impedance has a minimum value. In fact, the maximum alternator stroke is reached at 3 kW thermal power, which puts some limitations on the maximum produced electricity. Therefore, if more electrical power is to be extracted and to avoid the stroke limitation, the driver should be installed in a high impedance zone.

Riley (2014*b*) showed that from the same configuration and using atmospheric air the system delivered 12.6 W electric power. In this work after the heaters were maintained and the insulation was improved, the obtained electric power increased up to 16.5 W at $50\% - 50\%$ heat input ratio among the two cores. While, the electrical output enhanced further to around 23.4 W electrical power when the heat input was distributed by 40% of the total heat in the first engine stage, and the rest directed into the second stage. This is around 86% increase in electrical power (12.6 W to 23.4 W) with no additional changes to the system other than using a novel methodology to distribute the heat flow (asymmetrical input).

Figure 5.22 and Figure 5.23 compare the DeltaEC model against the experimental values for the conversion efficiencies of the current system, using different percentages of the heat input into the two cores. The experimental results yielded a maximum value of the thermal-to-acoustic efficiency of 4% achieved when using one-third and two-third of the total heat through the first and the second heaters, respectively. At the same ratio, the thermal-to-electric efficiency reached a maximum value of 1.27%, which is indeed much lower than that noted in Backhaus et al. (2004), where the linear alternator acted as a transduction mechanism as well as a mechanical resonator with 75% transduction efficiency compared to only 34% of the loudspeaker used in the current design.

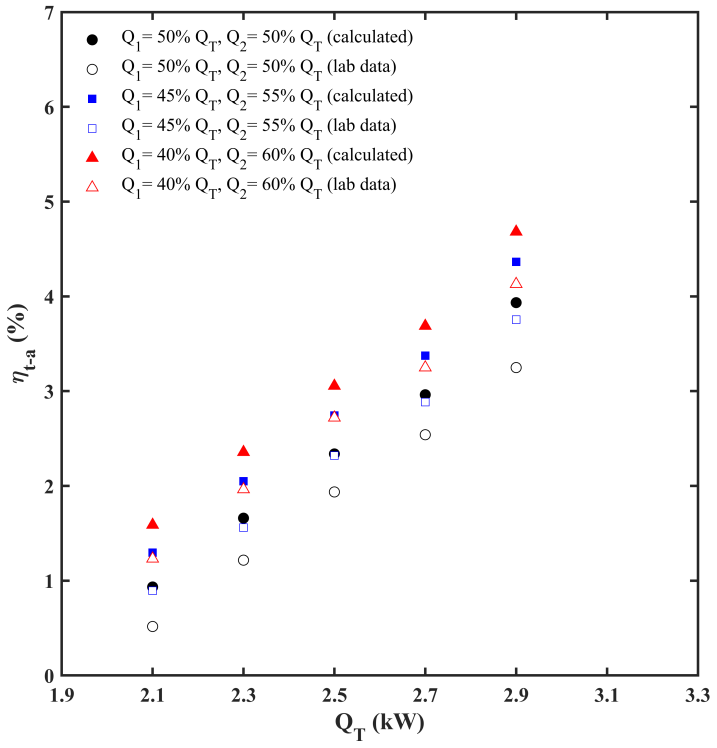


Figure 5.22: The effect of the heat input percentage on the thermal-to-acoustic efficiency, considering a total heat input power range of 2.1 - 3 kW.

In our current design, two main reasons contribute to the poorer efficiencies for the experimental data. The first reason is higher real-world parasitic losses through the casing. The second reason is that the transduction efficiency of the loudspeaker is lower than the theoretical value (around 34%) which lowers the extracted electric power. It is possible that the measured electric output could be doubled by using the alternator reported in (Saha et al. 2012) which was approximately 60% efficient. However, this linear alternator is too expensive compared to our loudspeaker and this counteracts the affordability of the system for rural communities.

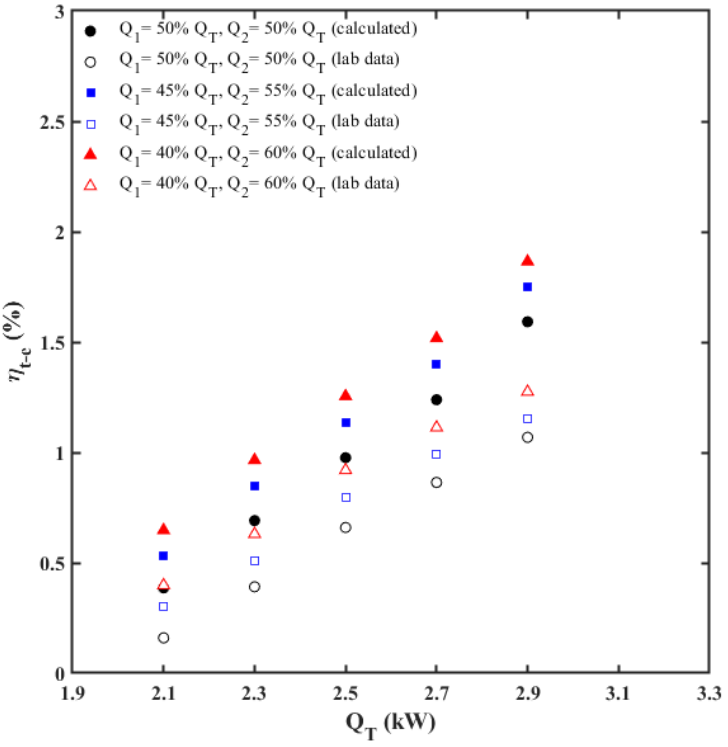


Figure 5.23: The effect of the heat input percentage on the thermal-to-electrical efficiency, using a total heat input power range of 2.1 - 3 kW.

5.5 Concluding remarks

In this work, a TAE is used to convert thermal energy into acoustic power and then into electricity with air at atmospheric pressure as the working gas. The system comprises two engine cores/stages, a loudspeaker, a feedback pipe and two matching stub pipes. Each engine core consists of a regenerator installed in between a cold and a hot heat exchanger, a secondary ambient heat exchanger and a thermal buffer tube. A numerical model of the looped-tube double-core TAE has been developed with the simulation software DeltaEC, which is validated later through experimental tests. Previous research on multistage systems has based operational criteria on equal heat inputs in the engine cores/stages. The current study proposes a new operational methodology for the heating power. The total heating power into the two-core system is varied to be asymmetrical by changing the distribution ratio into the two heater blocks ($Q_1/Q_T - Q_2/Q_T$) from $50\% - 50\%$ to $30\% - 70\%$. The pressure amplitude, volumetric velocity amplitude, their phases, and the acoustic impedance are significantly influenced by the way of splitting the total heat input. The overall onset temperature of the system is decreased and, therefore, the amplification factor, the impedance enhancement ratio and the produced acoustic power are changed. As a result, a significant increase in both acoustic and electrical power is achieved. The simulated power output was shown to

be greatest at heat ratio $30\% - 70\%$. However, using this ratio in the experimental tests was not possible due to the strength limitation of the material of the HHX. The simulated loop acoustic power increased from 58.4 W for $50\% - 50\%$ to 68.6 W for $40\% - 60\%$ heat input with no other changes to configuration. For the same ratio, the electrical power increased from 24.4 W to 31.4 W. A similar 39% increase of electrical output was observed in the experimental results (from 16.5 W to 23.5 W), showing that this is not an artefact of the DeltaEC program. SCORE project tests of the same experimental apparatus showed that, using air as the working gas and even distribution of the heating power of 2500 W produces 12.6 W electrical power. The current work improved the electrical output by 149% (from 12.6 W to 31.4 W).

The numerical and the experimental results suggested that the applied operational methodology is beneficial for multi-stage thermoacoustic systems that have a single power extraction point (one alternator), and it could be integrated into a new, more compact design that still meets the cost requirements. Besides, this new heat input strategy makes it possible to meet the 100 W limit identified as a requirement if this technology is to be implemented in the field.

CHAPTER 6

OPTIMISATION OF THE REGENERATORS OF A DOUBLE CORE THERMOACOUSTIC ENGINE WITH ASYMMETRIC HEAT INPUTS

6.1 Introduction

In a travelling-wave thermoacoustic engine, the regenerator is the heart of the engine. It realizes the thermal interaction between the working fluid and the solid material, and therefore, the energy conversion is yielded. The working principle of the regenerator in a travelling-wave thermoacoustic engine is to ensure that the gas parcels displaced during acoustic oscillations follow the temperature of the adjacent solid surface by having excellent thermal contact. The shape of the regenerator is more of a solid, porous material which offers an advantage of better thermal contact, and indicates an enhanced performance over the stack that is used in a standing wave engine.

To obtain excellent thermal contact at the frequency of interest, the design of the regenerator should be very narrow channels. However, the narrower the channels are, the higher is the acoustic pressure drop and, therefore, the production of the acoustic power will be influenced by these losses. The rate of acoustic amplification within the regenerator is determined by the temperature gradient along its end, as well as the phase difference between the pressure and volumetric velocity. The required time phase condition between the pressure and volumetric velocity in the regenerator can be achieved by having excellent heat transfer between the gas parcels and the solid plate. On the other hand, the temperature gradient is maintained by placing a high temperature source in one end of the regenerator, and a heat sink in the other, the three

parts forming the so-called thermoacoustic core. The thermoacoustic effect that is essential for generating travelling waves in the thermoacoustic core is created by the combination of these three components: a cold heat exchanger, a regenerator, and a hot heat exchanger.

Several attempts have been made to better understand the mechanisms of acoustic power amplification within the regenerator. Backhaus and Swift (2001) assessed the performance of their Thermoacoustic-Stirling Heat Engine TASHE with a parallel-plate regenerator. The system was tested with two different shapes of the regenerator; a stacked-screen type, and a parallel-plate type. Their measurements demonstrated that the fabrication of the regenerator is crucial for the performance. The study showed that the parallel-plate regenerator design offered excellent performance over the screen-based one. The power output from the TASHE was approximately doubled (increased from 890 to 1750 W), and the efficiency was also improved significantly (from 22% to 30%) when a parallel-plate regenerator was employed (Backhaus and Swift 1999; 2001). The study provided quantitative analysis for the viscous losses which contributed to the difference in performance between the two regenerator designs. However, the thermal dissipations and their influence on the performance were only qualitatively analysed. To further enhance the thermoacoustic performance of the TASHE, Napolitano, Dragonetti and Romano (2017) proposed an optimization procedure based on a Matlab code validated by a DeltaEC simulation. The optimisation procedure revealed that the length and hydraulic radius of the regenerator should be chosen carefully to achieve the maximum acoustic power conversion.

A strong relationship between the hydraulic radius of the regenerator pore and the performance has been reported in literature. Yu et al. (2005) inspected the influence of the ratio of the thermal penetration depth to the hydraulic radius, of a stacked-screen mesh regenerator in a travelling-wave thermoacoustic engine. The experimental data showed that the relative radius is crucial for the excitation of the system, and there is an optimal value for this ratio that provides the lowest temperature difference across the regenerator. Additionally, decreasing the hydraulic radius will lead to a high viscous resistance in the regenerator which in turn will reduce the produced acoustic power. Similarly, Kruse et al. (2017) examined the impact of the geometrical parameters of a regenerator of a single stage thermoacoustic engine on the overall performance. The optimum operating conditions in the system were found to be highly affected by the length, porosity and hydraulic radius of the regenerator.

In another research, Yu and Jaworski (2010) investigated a travelling-wave thermoacoustic engine with two different regenerator designs; a parallel-plate regenerator, and a stacked-screen regenerator. A discrepancy in the acoustic power production was observed and attributed to the different flow passages, and the different flow resis-

tance between the two designs. It is found that for a given pressure amplitude, a high flow resistance reduced the volumetric velocity along the regenerator and, as a result, the impedance of the regenerator increased. The authors concluded that, the flow resistance of the regenerator can be decreased by decreasing its length, increasing its cross-sectional area, or by having a regular configuration design for the regenerator such as parallel-plate design.

Previous research work has shown that the pore and length of the regenerator plays a key role in the performance of a travelling-wave thermoacoustic engine. However, the process of optimisation of the regenerator for a particular application is a complex process, particularly when the cost of the regenerator is an important consideration. Also, the complexity increases when the thermoacoustic system has more than one regenerator. This piece of work focuses on the regenerators of the double core travelling-wave thermoacoustic engine tested in the previous work. The effect of the regenerator design parameters on the power conversion is studied and explained in detail. The motivation behind this work is driven by a desire to improve the performance of the double core engine by increasing the power output to move forward the SCORE design aim (100 W electrical power output).

6.2 Principle of the regenerator

The regenerator, the thermal-acoustic energy conversion field, pumps acoustic power into the working gas when the temperature gradient through its ends is high enough. The variation in the acoustic power, $dP_{Ac.}$, through a length dx of the regenerator channel, in x-direction can be depicted as follows:

$$\frac{dP_{Ac.}}{dx} = \overline{P_{Ac.,g}} + \overline{P_{vis.}} + \overline{P_{T,diss.}} \tag{6.1}$$

Where: $\overline{P_{Ac.,g}}$ describes the acoustic power generated from the regenerator as result of the temperature gradient, $\overline{P_{vis.}}$ is the viscous dissipation due to the motion of the working gas, and $\overline{P_{T,diss.}}$ is the thermal dissipation within the regenerator.

The generated acoustic power is approximately proportional to the temperature gradient through the regenerator, and it should ideally be much larger than the losses at the channel walls. In addition, part of the acoustic power is always consumed by these losses, whatever the temperature gradient is. The viscous dissipation, $\overline{P_{vis.}}$, is proportional to the square of the volumetric velocity amplitude $|U_1|^2$ and is independent of the thermal conductivity of the working gas. The thermal-relaxation dissipation, $\overline{P_{T,diss.}}$, is proportional to the square of the pressure amplitude, $|p_1|^2$, and is independent of viscosity. The produced acoustic power, the viscous loss, and the thermal dissipation

can be expressed as:

$$\overline{P_{Ac.,g}} = \frac{1}{2} Re[g\tilde{p_1} U_1] \tag{6.2}$$

$$\overline{P_{vis.}} = -\frac{r_\nu}{2} |U_1|^2 \tag{6.3}$$

$$\overline{P_{T,diss.}} = -\frac{1}{2r_\kappa} |p_1|^2 \tag{6.4}$$

Here: r_ν and $1/r_\kappa$ are the viscous resistance and thermal relaxation per unit length of the channel, respectively, g is the complex gain constant for the volumetric flow, p_1 and U_1 are the pressure and volumetric velocity amplitude, respectively. r_ν, $1/r_\kappa$, and g are given as

$$r_\nu = \frac{\omega \rho_m}{A_g} \frac{Im[-f_\nu]}{|1-f_\nu|^2} \tag{6.5}$$

$$\frac{1}{r_\kappa} = \frac{\gamma - 1}{\gamma} \frac{\omega A_g}{P_m} Im[-f_\kappa] \tag{6.6}$$

and

$$g = \frac{(f_\kappa - f_\nu)}{(1-f_\nu)(1-\sigma)} \frac{1}{T_m} \frac{dT_m}{dx} \tag{6.7}$$

Where: P_m, ρ_m, and T_m are the mean pressure, mean density and mean temperature of the working gas, respectively, ω is the angular velocity, A_g is the cross-sectional area of the gas channel in the regenerator which can be expressed as: $A_g = \phi A$; where ϕ is the porosity of the regenerator and A is the total cross-sectional area of the regenerator, σ is Prandtl number, f_ν and f_κ are spatially averaged viscous and thermal functions, respectively, and their expressions depend on the shape of the regenerator pores (see **Appendix A**).

6.3 The double core thermoacoustic engine

As mentioned in the previous chapter, the double core thermoacoustic engine consists of a looped PVC tube containing two thermoacoustic stages, a loudspeaker for electrical power extraction, and two tuning stubs for impedance matching. The space between the two engine cores is approximately a quarter wave-length, $\lambda/4$. The enlarged cross-sectional area of the thermoacoustic cores is designed to insure appropriate acoustic conditions (De Blok 2010). The engine is filled with air at atmospheric pressure and works at an operating frequency of 73 Hz. The total heat addition into the two identical heater blocks is 2500 W, distributed as 1000 W into the first stage, and 1500 W into the second. The heat input ratio was selected according to the validated results stated previously in Chapter 5, where the 40-60% ratio showed the optimum power output. The aim is to further improve the performance of the thermoacoustic system by

optimising the parameters of the regenerator part. No changes are made in the other geometrical parameters. As the main focus of this study is the regenerator, it would be useful to re-mention the specification of the regenerators used in the existed prototype. Each regenerator is a pile of fine mesh stainless-steel screens. The diameter of the screen wire is 143 μm, the volumetric porosity $\phi = 73\%$ and the hydraulic radius r_h = 97 μm. The length of each regenerator L = 12 mm.
In the double core thermoacoustic system, the cross-sectional area of the thermoacoustic core has been enlarged to obtain high acoustic impedance, thus the acoustic dissipation can be minimized and the output power will be higher.

6.4 Optimisation of the two regenerators

The numerical optimisation of the two regenerators was performed based on the thermoacoustic simulation software DeltaEC (Ward, Clark and Swift 2008). Referring to the thermoacoustic linear theory (Swift 2017), the pressure, velocity, and the time-averaged acoustic power, generated from a staked-screen regenerator of a length dx, can be approximately expressed as:

$$\frac{dp_1}{dx} = -i\omega\rho_m\left[1+\frac{(1-\phi^2)}{2(2\phi-1)}\langle u_1\rangle\right] - \frac{\mu_m}{r_h^2}\left(\frac{c_1(\phi)}{8}+\frac{c_2(\phi)NR_1}{3\pi}\right)\langle u_1\rangle \tag{6.8}$$

$$\frac{d\langle u_1\rangle}{dx} = \frac{-i\omega\gamma}{\rho_m a^2}p_1 + \frac{\beta dT_m}{dx}\langle u_1\rangle + i\omega\beta\left[\frac{T_m\beta}{\rho_m c_p}\frac{\varepsilon_s+(g_c+2e^{2i\theta_p}g_v)\varepsilon_h}{1+\varepsilon_s+\varepsilon_h(g_c+e^{2i\theta_T}g_v)}p_1 - \frac{1}{i\omega}\frac{dT_m}{dx}\frac{\varepsilon_s+(g_c-g_v)\varepsilon_h}{1+\varepsilon_s+(g_c+e^{2i\theta_T}g_v)\varepsilon_h}\langle u_1\rangle\right] \tag{6.9}$$

$$\frac{dP_{Ac.}}{dx} = \frac{1}{2}A_g Re\left[i\omega\left(\beta\frac{T_m\beta}{\rho_m c_p}\frac{\varepsilon_s+(g_c+e^{2i\theta_p}g_v)\varepsilon_h}{1+\varepsilon_s+(g_c+e^{2i\theta_T}g_v)\varepsilon_h}-\frac{\gamma}{\rho_m a^2}\right)|p_1|^2 - i\omega|\langle u_1\rangle|^2 - \frac{\mu}{r_h^2}\left(\frac{c_1(\phi)}{8}+\frac{c_2(\phi)NR_1}{3\pi}\right)|\langle u_1\rangle|^2 + \beta\frac{dT_m}{dx}\left(1-\frac{\varepsilon_s+(g_c-g_v)\varepsilon_h}{1+\varepsilon_s+(g_c+e^{2i\theta_T}g_v)\varepsilon_h}\right)\tilde{p_1}\langle u_1\rangle\right] \tag{6.10}$$

Where: A_g is the cross-sectional area available for the working gas, $Re[\,]$ denotes the real part of a complex number, β is the thermal expansion coefficient, γ and μ are the ratio of the specific heats and the dynamic viscosity of the working gas, respectively. $\langle u_1\rangle$ is the spatial average oscillatory velocity $\langle U_1\rangle/\phi A$, where ϕ is volumetric porosity and A is regenerator cross-sectional area; $b(\phi)$, $c_1(\phi)$, $c_2(\phi)$, $g_c(NR_1)$ and $g_v(NR_1)$ are factors resulting from the fitting of data of Kays and London (1984), NR_1 is a positive

real number called Reynolds. More details of these variables and definitions can be found in (Swift and Ward 1996). Using:

$$\theta_p = phase(\langle u_1 \rangle) - phase(p_1),\ \theta_T = phase(\langle u_1 \rangle) - phase(\langle T_{u,1} \rangle) \tag{6.11}$$

$$\varepsilon_s = \frac{\phi \rho_m c_p}{(1-\phi)\rho_s c_s},\ \varepsilon_h = \frac{8ir_h^2}{b(\phi)\sigma^{1/3}\delta_\kappa^2} \tag{6.12}$$

$$NR_1 = \frac{4|\langle u_1 \rangle| r_h \rho_m}{\mu} \tag{6.13}$$

The first term in the right hand side of Equation 6.10 represents the loss in acoustic power due to thermal relaxation effects, the second and third terms together represent the loss in acoustic power due to the flow resistance in the regenerator, the fourth term represents the amount of acoustic power produced from thermal energy as a result of the thermoacoustic effect.

Of substantial interest is the relationship between the pressure losses in oscillatory flows and those under steady-flow conditions. The steady-flow loss data reported by Kays and London (1984) have been coded by Swift and Ward (1996) with the pressure drop, Δp_1 given as a function of the gas velocity u_1 as follows:

$$\Delta p_1 = \frac{L\rho u_1^2}{2r_h}\left(\frac{c_1(\phi)}{NR_1} + c_2(\phi)\right) \tag{6.14}$$

$$= \frac{L}{D_w}\frac{\mu u_1}{2r_h}c_1(\phi) + \frac{4L}{D_w}\frac{\rho u_1^2}{2}c_2(\phi) \tag{6.15}$$

Swift and Ward (1996) proposes $c_1(\phi) = 1268 - 3545\phi + 2544\phi^2$, and $c_2(\phi) = -2.82 + 10.7\phi - 8.6\phi^2$.

The first term in Equation 6.15 expresses the the pressure loss through the regenerator due to viscous losses, and the second expresses the separated flow part.

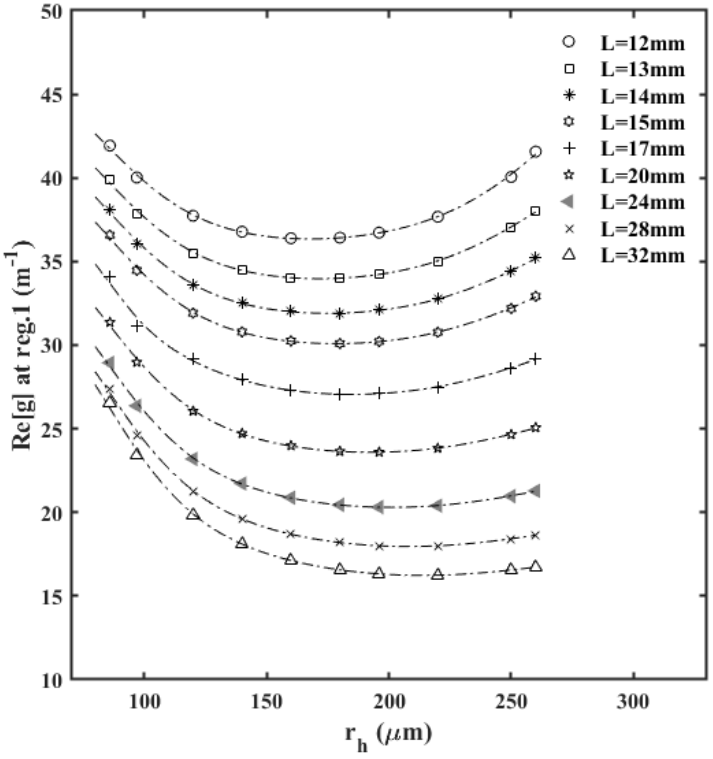
A schematic representation of the double core thermoacoustic system used in DeltaEC simulation is shown earlier in Chapter 5; Figure 5.1. The outcomes of the optimisation will be discussed in details in the next sections.

6.4.1 Acoustic amplification within the regenerators

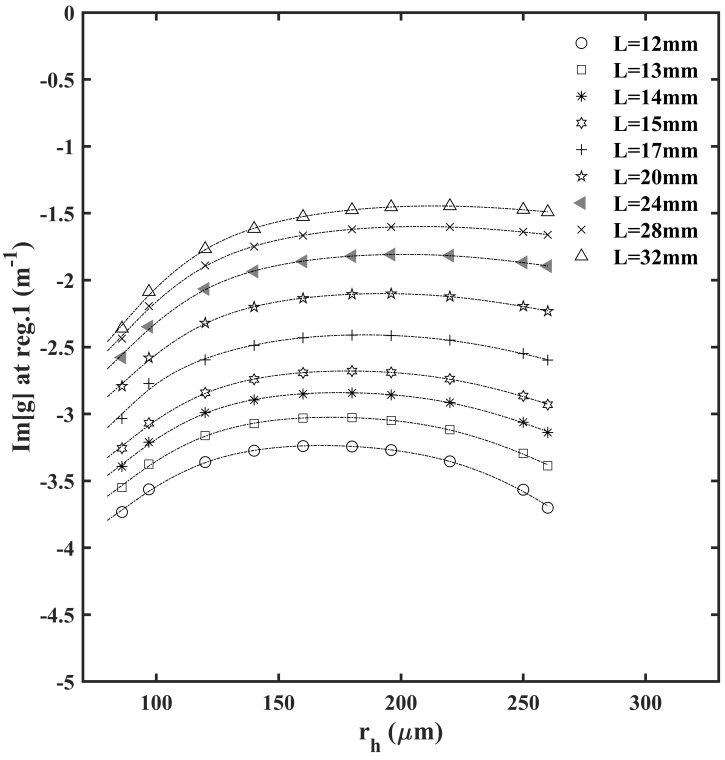
The gain factor, g, influences the thermal-to-acoustic conversion inside the regenerator. This factor relates to the temperature gradient across the regenerator, the mean temperature of the working gas, the length of the regenerator, and the spatially averaged thermal and viscous functions, ΔT, T_m, L, f_κ, and f_ν, respectively. Both f_κ and f_ν are functions of r_h. Therefore, variations in the regenerator length and hydraulic radius will change the gain factor which in turn will affect the acoustic power generated within

the regenerator. Both f_κ and f_ν are predicted by the model. Figure 6.1 and Figure 6.2 report the trend of the gain factor when the length of the regenerator is varied between 12 and 32 mm, and the hydraulic radius is varied between 86 - 280 μm. It is possible to note that the real part of the gain factor, $Re[g]$, for regenerator 1 and regenerator 2 is always positive and this guarantees a useful conversion of thermal energy into acoustic power.

For all tested ranges of L and r_h, it shows that the real part of g in regenerator 1 is smaller than the one for regenerator 2 (Figure 6.2), and this is can be justified by the fact that the amount of heat added into the first stage is less than that in the second. For a given length of the regenerator, $Re[g]$ decreases slightly in both regenerators with the increase of the hydraulic radius until it reaches a lowest point, after which it increases again. Moreover, $Re[g]$ decreases with the increase in the length of the regenerator and this is confirmed by Equation 6.7. Considering the design specifications of the regenerators of the dual core system, where the hydraulic radius selected by SCORE is 97 μm, the numerical results show that increasing the length of the regenerator from 12 mm to 32 mm will decrease $Re[g]$ by approximately 41.4% in regenerator 1 and by 39.4% in regenerator 2.

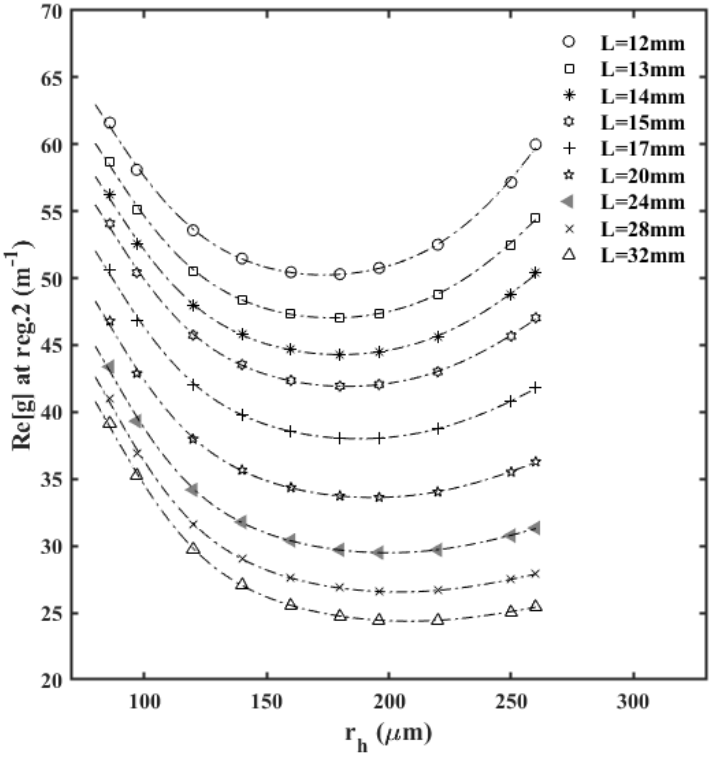


(a)

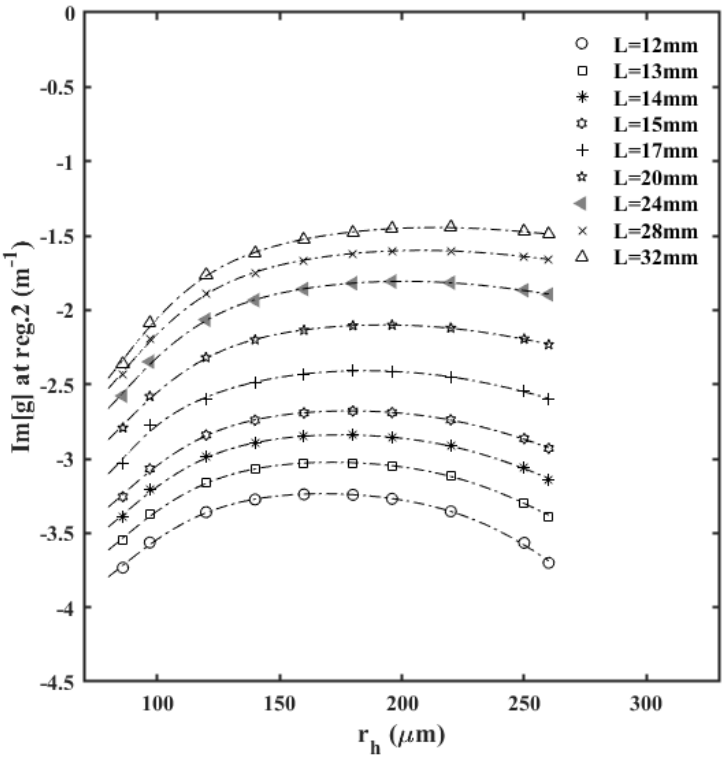


(b)

Figure 6.1: Numerical calculations of the change in the gain factor, g, in regenerator 1 of the dual core thermoacoustic electricity generator, when the length of the regenerator is varied in the range of 12-32 mm, and the hydraulic radius is also changed in the range of 86 - 260 µm. (a) The real part of the gain $Re[g]$. (b) The imaginary part of the gain $Im[g]$.



(a)



(b)

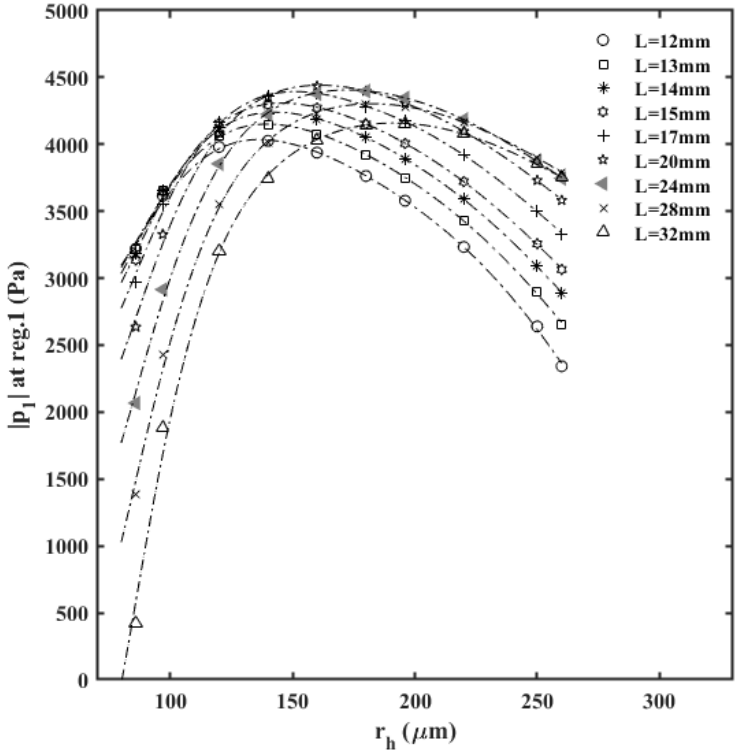
Figure 6.2: Numerical calculations of the change in the gain factor, g, in regenerator 2 of the dual core thermoacoustic electricity generator, when the length of the regenerator is varied in the range of 12-32 mm, and the hydraulic radius is also changed in the range of 86 - 260 μm. (a) The real part of the gain $Re[g]$. (b) The imaginary part of the gain $Im[g]$.

6.4.2 Acoustic dissipation

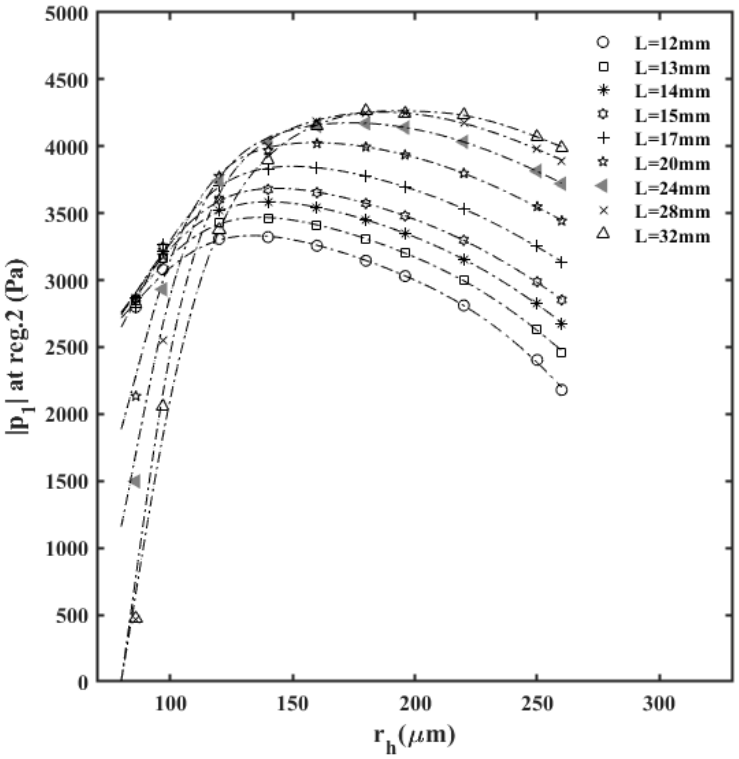
The aim of this study is to maximise the acoustic power produced from the double core engine whilst reducing the acoustic losses and, therefore, improving overall performance. The acoustic losses from the regenerator are one of the major issues that contribute to the low efficiency of the system. The thermoacoustic field would be greatly enhanced if these losses were minimized. Therefore, the optimization of the two regenerators also requires careful consideration of the thermal and viscous losses. By considering Equation 6.3 and Equation 6.4 it is possible to note that the viscous and thermal dissipation components are related to the volumetric velocity amplitude and the pressure amplitude. Both the thermal and viscous losses consume part of the generated acoustic power, and as a result the acoustic conversion is degraded. On the contrary, the acoustic amplification is proportional to $|U_1|$ and $|p_1|$ as given in Equation 6.2. In this respect, it is possible to use the pressure amplitude, and the volumetric velocity amplitude as performance indicators due to the fact that they influence both the amplification and dissipation acoustic parts.

Thermal-relaxation dissipation

The influence of the regenerator design parameters on the pressure amplitude, and the thermal-relaxation dissipation are presented in Figure 6.3 and Figure 6.4, respectively. The length of each regenerator was varied in the range of 12-32 mm, while the range for its hydraulic radius was varied from 86 - 260 μm, without altering the symmetrical design aspect of the two regenerators. Here, the pressure amplitude, $|p_1|$ represents half of the peak-to-peak pressure oscillation. What is obvious from Figure 6.3(a) and Figure 6.3(b) is that the pressure amplitude curves for regenerator 1 and regenerator 2 are very similar in character. The increase in pressure amplitude in the regenerators of the two engine stages due to the change in the length and hydraulic radius shows several expected trends. For a given length of the regenerator, the pressure amplitude increases almost gradually with the hydraulic radius until they reach a maximum point, after which their performance drops abruptly.

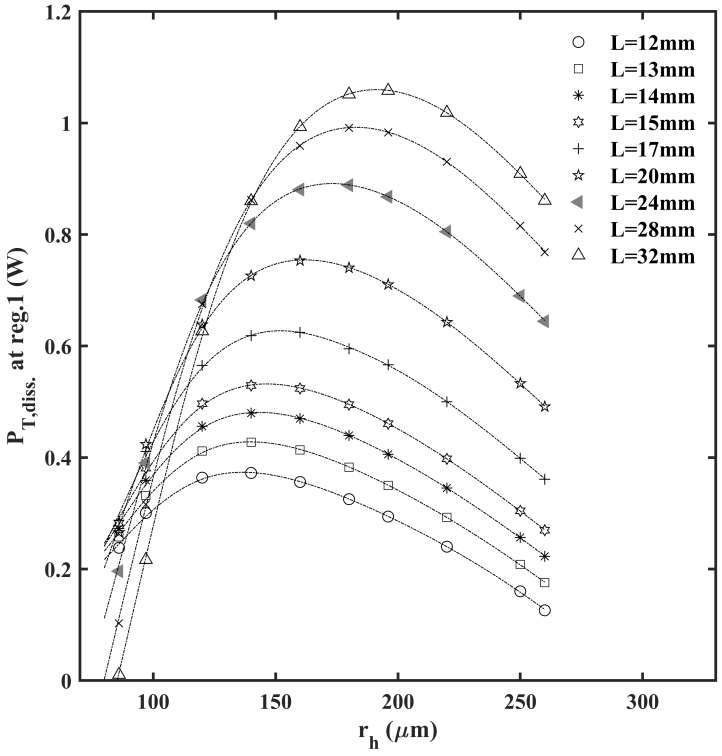


(a)

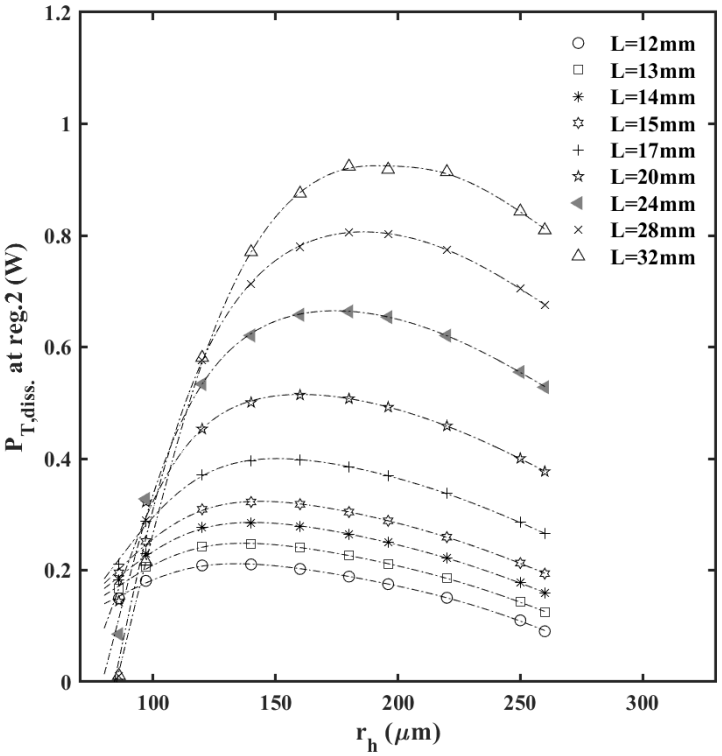


(b)

Figure 6.3: The simulated pressure amplitude, $|p_1|$, in the regenerators of the double core thermoacoustic electricity generator when the length of the mesh is varied in the range of 12-32 mm, and the hydraulic radius is changed in the range of 86 - 260 µm. (a) At regenerator 1. (b) At regenerator 2.



(a)



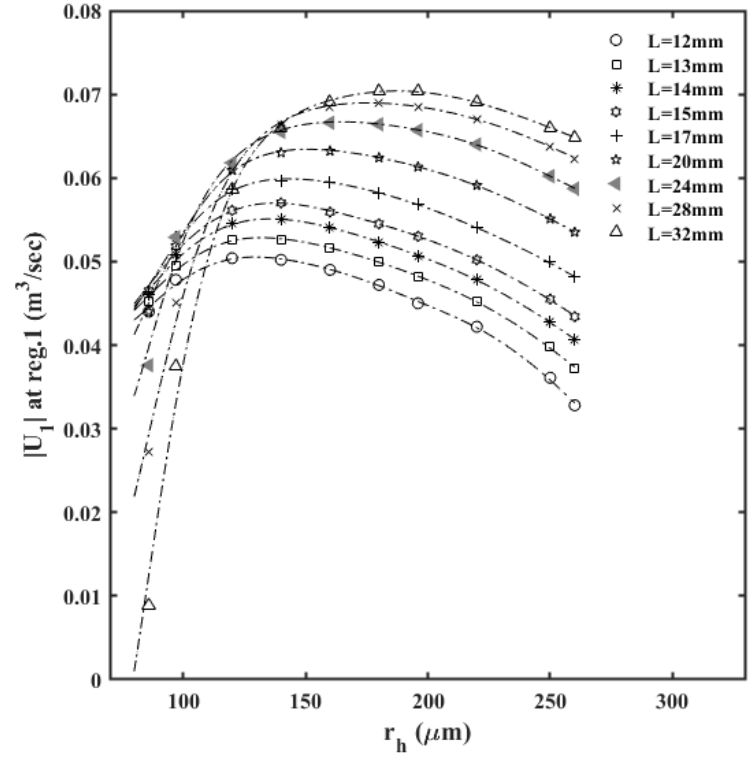
(b)

Figure 6.4: Numerical calculations of the thermal-relaxation dissipation components resulting from variation of the lengths and the hydraulic radii of the regenerators of the double core system. The length of each regenerator is varied in the range of 12-32 mm, while the hydraulic radius is varied in the range of 86-260 μm. (a) At regenerator 1. (b) At regenerator 2.

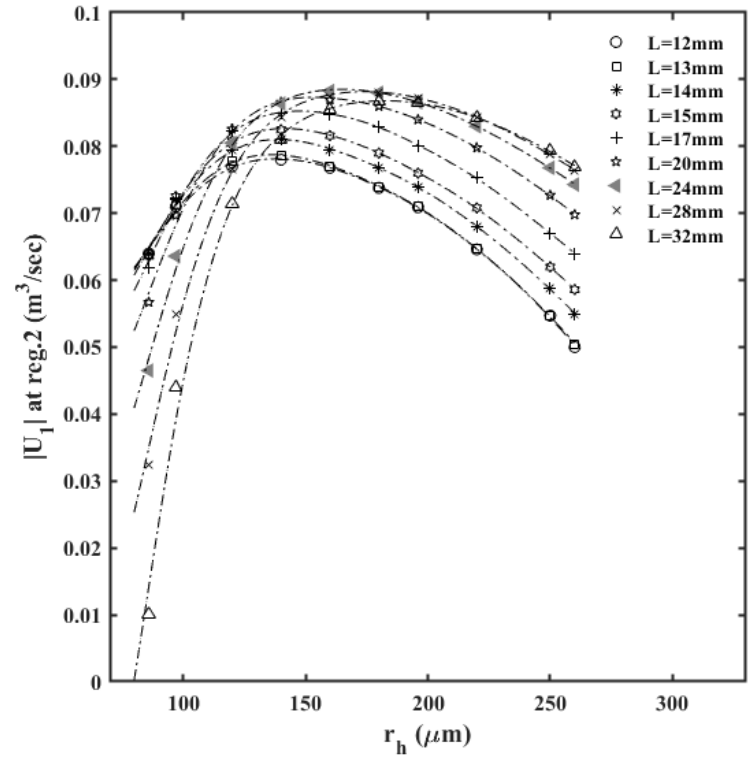
The data showed an optimal acoustic power of 131 W when the parameters of the regenerator are: L= 28 mm and r_h = 180 µm. Due to the increase in the length from 12 mm to 28 mm and hydraulic radius from 97 µm to 180 µm, the pressure amplitude in regenerator 1 increased significantly by almost 19% (from 3617.2 to 4300.1 Pa), while it increased by approximately 38% in regenerator 2 (from 3080.9 to 4253.3 Pa).
The largest observed pressure amplitude of 4436 Pa is observed in regenerator 1 at L = 20 mm and r_h = 160 µm, while the highest value of 4262 Pa is obtained with L = 32 mm and r_h = 180 µm in regenerator 2. Due to the increase of $|p_1|$ in the regenerators, the useful work from each engine stage could be maximized, but the consequences of this increase on the thermal-relaxation losses should be considered.
Consequently, the acoustic loss in the regenerators of the double core system because of thermal leaks are depicted in Figure 6.4(a) and Figure 6.4(b). For all the hydraulic radii considered in this optimisation, a longer regenerator results in a higher thermal dissipation. The highest thermal loss that can be obtained is almost 1 W in the first regenerator, and is even smaller in the second regenerator, but these are not significant figures. This indicates that the dissipations due to conduction heat leaks become less important as the intensity of the acoustic power grows. These thermal-relaxation dissipations are increased, but not as fast as the generated acoustic power, $P_{Ac.,g}$.

Viscous dissipation

In the regenerator of a travelling-wave engine, the amplitude of the acoustic volumetric velocity plays a vital role since it directly influences the loss in acoustic energy. The volumetric velocity represents the volume of working gas passing through the regenerator per unit time. Equation 6.3 indicates that the viscous dissipated part is proportional to the square of the volumetric velocity $|U_1|^2$, and is independent of thermal conductivity. One important note is that the viscous dissipation within the regenerator is always greater than the thermal-relaxation dissipation. Low volumetric velocity leads to high acoustic impedance which is advantageous for reducing the viscous losses in the regenerator, contrary to high volumetric velocity which leads to low acoustic impedance, and therefore, low power conversion.
Figure 6.5 and Figure 6.6 present that the volumetric velocity, and the viscous loss increases significantly with increasing length of the regenerator. For a given regenerator length, there is a value of r_h where $|U_1|$ becomes the maximum. For the first regenerator, the volumetric flow is smaller than that in the second one, due to the lower heating power in the first core. The highest observed $|U_1|$ in regenerator 1 is 0.07 m^3/sec at 32 mm length and 180 µm radius, and is 0.09 m^3/sec in regenerator 2 at 24 mm and 160 µm.

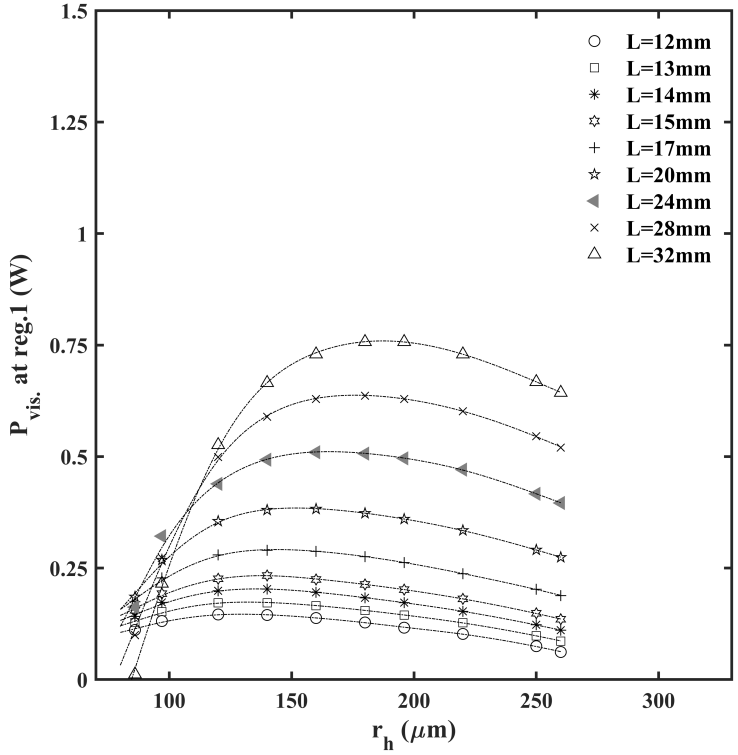


(a)

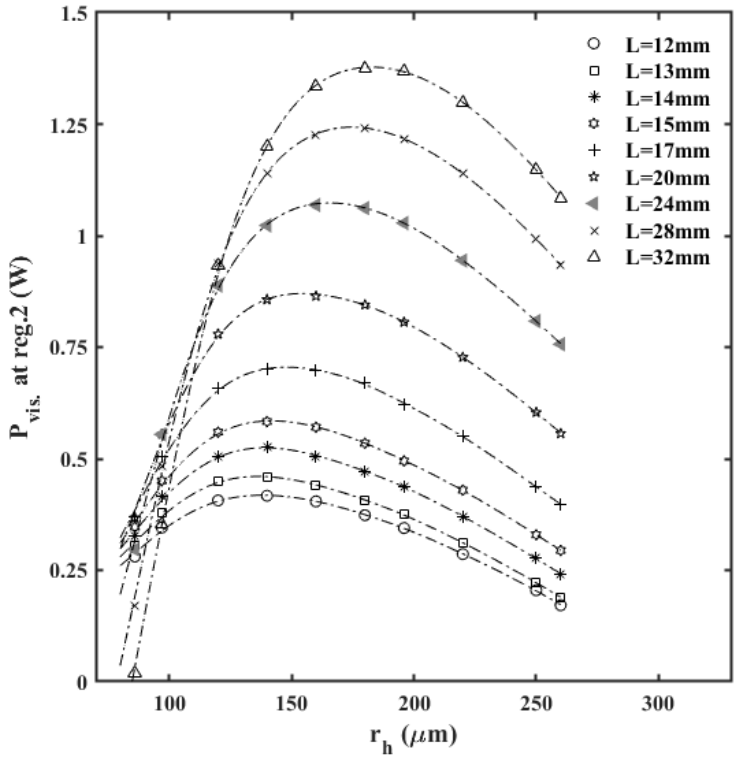


(b)

Figure 6.5: The simulated volumetric velocity $|U_1|$ in the regenerators of the double core thermoacoustic electricity generator when the length of the mesh is varied in the range of 12 - 32 mm, and the hydraulic radius is changed in the range of 86 - 260 µm. (a) At regenerator 1. (b) At regenerator 2.



(a)



(b)

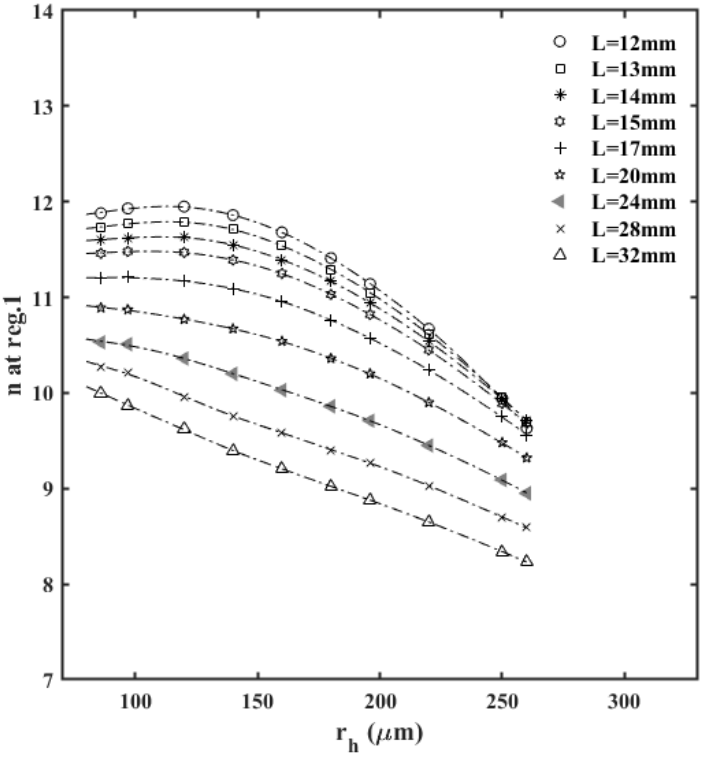
Figure 6.6: Numerical calculations of the viscous dissipation components, $P_{vis.}$, resulted from variation of the lengths and the hydraulic radii of the regenerators of the double core thermoacoustic electricity generator. The length of each regenerator is varied in the range of 12-32 mm, while the hydraulic radius is varied in the range of 86-260 μm. (a) At regenerator 1. (b) At regenerator 2.

On the other hand, the maximum viscous energy loss obtained in regenerator 1 is 0.8 W, and 1.4 W within regenerator 2, both at a length of 32 mm and r_h of 180 µm. The reduction of the volumetric velocity amplitude within regenerator 1 contributed to the suppression of the viscous losses. In practice, travelling-wave thermoacoustic engines should have a local impedance (p_1/U_1) greater than the characteristic impedance of the gas (ρa) to limit the impact of the large viscous dissipations which occur as a result of the high acoustic velocities (Ceperley 1985; Yazaki et al. 1998). Additionally, the produced acoustic power is proportional to the pressure amplitude, and inversely proportional to the local acoustic impedance at the cold side of the regenerator. Higher impedance will result in a low acoustic power being fed into the cold side of the regenerator. A regenerator with a high flow resistance leads to a low acoustic velocity within the regenerator, and hence, a high acoustic impedance at the cold side of the regenerator. By contrast, a regenerator with a low flow resistance and a high pressure amplitude is preferable for higher acoustic power production. Therefore, it's crucial to study the impact of the regenerator optimisation on the volumetric velocity amplitude inside the regenerator, and thus, the loss in the acoustic power that occurs because of this.

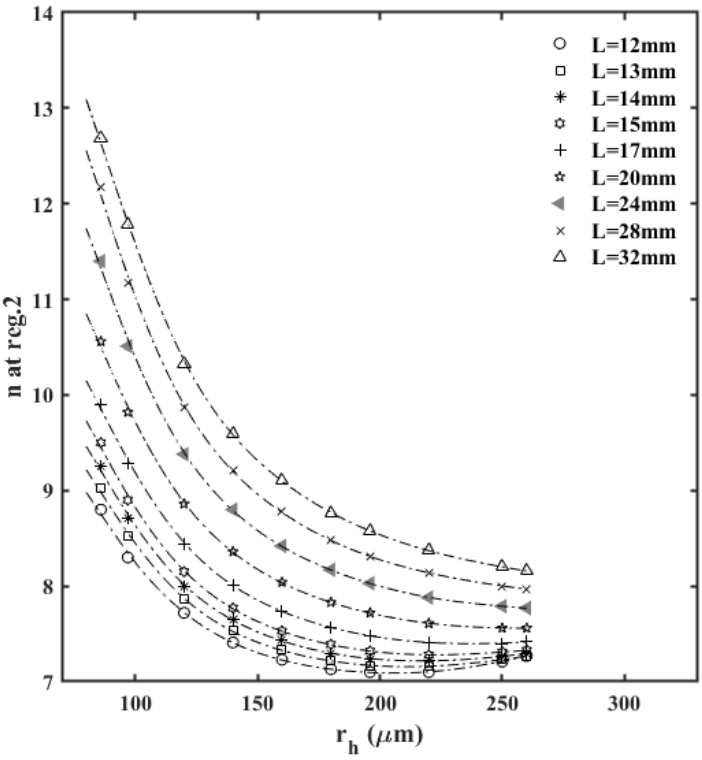
From Figure 6.1, Figure 6.2, Figure 6.4, and Figure 6.6 it is obvious that the real gain factor which corresponds to the useful acoustic work is always greater than the thermal and viscous dissipation components. This implies that for the entire length range of the regenerator (12 - 32 mm), it is possible to produce useful acoustic power. Figure 6.7 shows the estimated values of the impedance enhancement, n, for the two regenerators with the different tested ranges of the lengths and the hydraulic radii of the regenerator. n is the ratio between the acoustic impedance and the characteristics impedance of the gas. It can be found that at the optimum power output, n values are 9.4 and 8.5 at the cold end of regenerator 1 and regenerator 2, respectively.

The pressure drop due to viscous loss across the two regenerators is presented in Figure 6.8. According to Equation 6.14 and Equation 6.15, the pressure drop across the regenerator is proportional to its length and directly proportional to its hydraulic radius. For the length of the regenerator in the range 12 - 20 mm, there is a reduction in the pressure drop with the increase of the r_h, while for the length's range of 24 - 32 mm, the pressure drop increases until it reaches a maximum value, after which it decreases. This increase in the pressure drop is due to the increase of the volumetric velocity, which increases the second term on the left-hand side of Figure 6.5. The values of c_1 and c_2 in Figure 6.5 are calculated using 73% porosity as -2675.5 and 0.4, respectively. The behaviour of regenerator 1 shows that a maximum pressure drop value of about 524 Pa is obtained with L = 32 mm and r_h = 120 µm. Regenerator 2 has the highest pressure drop at the same L and r_h but the pressure drop is 23% greater than

that realized at regenerator 1 (around 644 Pa). For existing regenerators (12 mm and 97 μm) the pressure dropped by 231 and 350 Pa along regenerator 1, and regenerator 2, respectively.

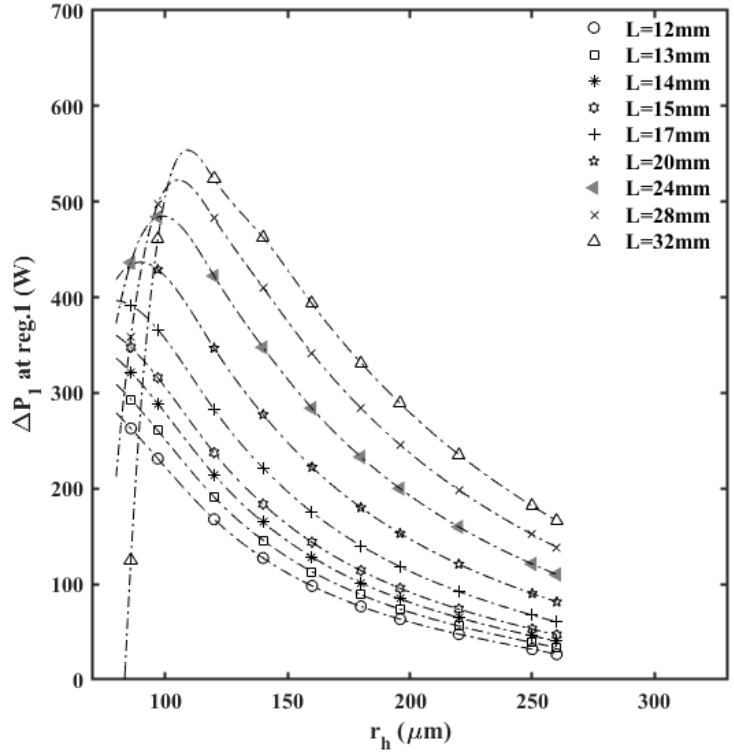


(a)

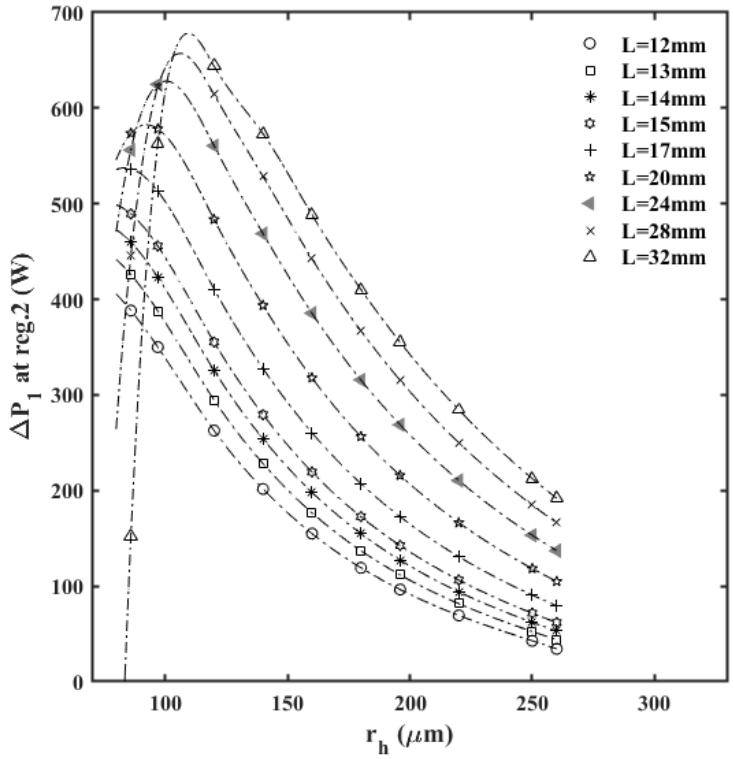


(b)

Figure 6.7: DeltaEC calculations of the impedance enhancement factor, *n*, at the cold end of the regenerators of the dual core thermoacoustic electricity generator, when the length of the regenerator is varied in the range of 12-32 mm, and the hydraulic radius is also changed in the range of 86 - 260 µm. (a) Conditions through regenerator 1. (b) Conditions through regenerator 2.



(a)



(b)

Figure 6.8: DeltaEC results of pressure drop, ΔP_1, across the regenerators of the double core thermoacoustic electricity generator when the length of the regenerator is varied in the range of 12-32 mm, and the hydraulic radius is changed in the range of 86 - 260 μm. (a) Values of Δp_1 at regenerator 1. (b) Values of Δp_1 at regenerator 2.

Certainly, higher pressure drop could degrade the overall system performance. However, it is possible that the system will operate relatively well and deliver considerable amounts of acoustic power which is enough to overcome the effect of the high pressure drop, viscous, and thermal dissipations. Therefore, there should be compromise between the amount of acoustic power generated and dissipation components, according to the requirements of the different applications.

6.4.3 Temperature profile across the regenerator

The effect of the regenerator length on the temperature difference between its hot and cold ends, and therefore, the acoustic gain, can be further demonstrated by integrating the acoustic power generated from the regenerator in Equation 6.10, over the length of the regenerator, and neglecting the thermal and viscous losses. This produces:

$$\Delta P_{Ac.} = \frac{1}{2} A_g \beta_m \int_0^L Re \left[\left(1 - \frac{\varepsilon_s + (g_c - g_v)\varepsilon_h}{1 + \varepsilon_s + (g_c + e^{2i\theta_T} g_v)} \varepsilon_h \right) \tilde{p}_1 u_1 \frac{dT_m}{dx} \right] dx \tag{6.16}$$

Therefore, and according to Equation 6.16, it is clear that the acoustic power produced within the regenerator is proportional to the length, the temperature gradient, and the acoustic power flows into the cold end of the regenerator, L, $\frac{dT_m}{dx}$, and $\tilde{p}_1 u_1$, respectively. Accordingly, increasing these three parameters will increase the power production from the regenerator. However, the temperature gradient across the regenerator is inversely proportional to it's length.

$$\frac{dT_m}{dx} = \frac{T_H - T_C}{L} \tag{6.17}$$

For a given temperature gradient, the difference between the hot side and cold side of the regenerator, T_H, and T_C increases as the length of the regenerator increases. Therefore, a balance should be made to obtain the optimal length of the regenerator when the design seeks a particular temperature difference. DeltaEC results of the relationship between the temperature difference across the regenerator and the regenerator length for a given hydraulic radius of the pore are presented in Figure 6.9. For a 12 mm long regenerator, with r_h = 180 μm, simulation showed temperature differences across regenerator 1 and regenerator 2 of 143 K, and 192 K, respectively. To demonstrate the impact of the length on the temperature difference along the regenerator, Figure 6.10 is plotted for the optimal r_h of 180 μm. Doubling the actual length of the regenerator results in an extra 24 K in the temperature difference along regenerator 1, and an additional 35 K in ΔT across regenerator 2. This is reflected by approximately a 96% increase in the delivered loop acoustic power, which reflects that it is beneficial to consider a longer regenerator.

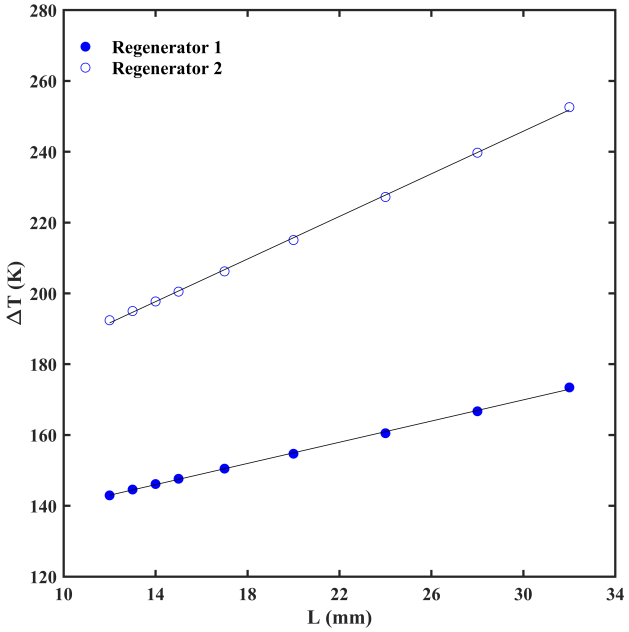
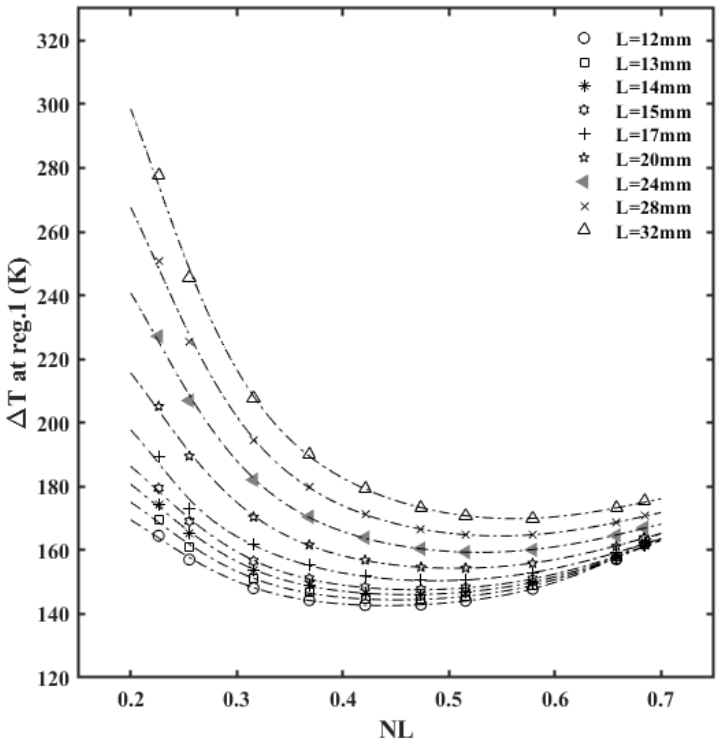
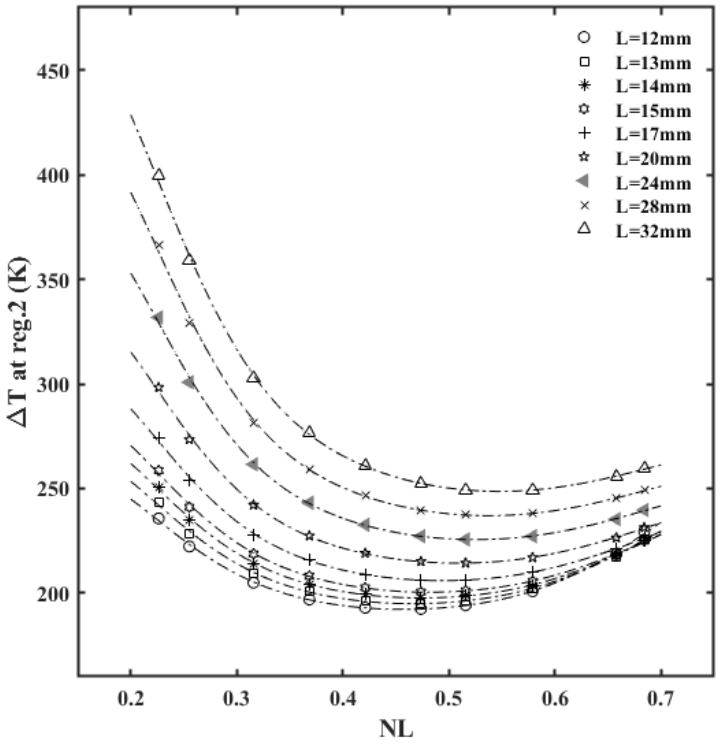


Figure 6.9: DeltaEC simulation results showing the temperature difference between the hot and cold ends of the regenerators of the double core thermoacoustic electricity generator when the length of each regenerator is changed between 12 to 32 mm, and the hydraulic radius is adjusted as 180 µm. (a) Data of regenerator 1. (b) Data of regenerator 2.

In the thermoacoustic effect, the heat transfer between the working gas and the solid media depends strongly on a dimensionless ratio known as the Lautrec number, *NL*. Lautrec number can be defined as the ratio of the hydraulic radius to the thermal penetration depth, $NL = r_h/\delta_\kappa$. The Lautrec number has been used by Garrett (2004) as an indicator of the difference between a stack in standing-wave systems and the regenerator in travelling-wave systems. If the value of Lautrec number, $NL \gg 1$, the porous medium used to transfer heat to the working gas is a stack, while it is a regenerator if $NL \ll 1$. Broadly, *NL* is used to explain the effect of the hydraulic radius on the performance of the engine. However, the optimisation of the system should involve achieving the lowest attainable difference across the regenerator. Hence, the relationship between the temperature difference along regenerator 1 and regenerator 2 and *NL* is illustrated in Figure 6.10(a), and Figure 6.10(b), respectively, when the length of each regenerator is varied between 12 - 32 mm. For both the regenerators, the curves have similar trends. What can be clearly seen is the decrease in the temperature difference across both regenerators with the increase in the Lautrec number, until it fell to a low point. Equation 6.18 gives that the temperature difference across the regenerator is directly proportional to its length and the temperature gradient. The temperature gradient is proportional to $f_n u$ which itself is inversely proportional of *NL* as shown in Equation 6.7.



(a)



(b)

Figure 6.10: The relationship between the temperature difference along the regenerators of the dual core thermoacoustic electricity generator and Lautrec number *NL* as a result of varying the hydraulic radius of the pore in the range 86 - 260 μm, for length's range of 12-32 mm. (a) conditions at regenerator 1. (b) Conditions at regenerator 2.

When the regenerator is short, the temperature difference along the regenerator becomes less. For a 12 mm long regenerator, the numerical results showed about 157 K temperature difference across the first regenerator, and around 222 K across the second one at a Lautrec $NL \simeq 0.26$. With optimal acoustic power production of 131 W (Figure 6.11), the temperature difference across regenerator 1 and regenerator 2 are increased by 10 and 18 K, respectively, at $NL = 0.47$. Therefore, a balance between the amplified acoustic power and the temperature difference along the regenerator is important for selecting the length of the regenerator.

It is encouraging to compare these findings with the so-called "thermoacoustic Stirling heat engine" (TASHE) developed by Backhaus and Swift (2000) where an optimum range of NL of 0.1 - 0.3 was identified for the system. Likewise, in a four-stage travelling-wave thermoacoustic engine, Zhang and Chang (2015) concluded that the best characteristics are achievable with NL range of 0.2 - 0.33. On the other hand, Yu et al. (2005) found that the Lautrec number affects the temperature difference across the regenerator, and the engine excitation in their thermoacoustic system. Data from their study suggested an optimum range of NL of 0.2 - 0.33 at which the lowest temperature difference was observed. Also, other numerical research highlighted the effect of the Lautrec on the regenerator length (Kruse et al. 2017); $NL = 0.3$ when $L = 5$ mm, and $NL = 0.55$ when $L = 25$ mm. It is possible that Lautrec number depends also on the impedance enhancement ratio, n Yu and Jaworski (2010) obtained an optimal NL of 0.25 with n =35, and NL of 0.5 with $n = 6$.
It is important to bear in mind that the previously stated values of NL are mostly recognized for the lowest temperature difference. However, in a practical thermoacoustic system, the optimum NL will most likely be different, depending on the design aim, e.g. if the system is designed for maximum power production at a given temperature.

Further analysis of the performance of the double core thermoacoustic electricity generator is based on investigating the amount of acoustic power running through the feedback loop. This acoustic power flow is called loop acoustic power (De Blok 2008). The magnitude of the loop acoustic power and the temperature gradient across the regenerator reflect the performance of the regenerator. The loop acoustic power, $P_{Ac.}$ of the double core thermoacoustic system with various lengths and hydraulic radii of the regenerators is shown in Figure 6.11. $P_{Ac.}$ and starts at a relatively low level of loop acoustic power, but it grows rapidly with the hydraulic radius and subsequently levels off. The sudden drop in loop acoustic power corresponds to the amplitude drop. Of course the level of the loop acoustic power is different for the nine lengths of the

regenerator considered here. For each length of the regenerator, there is an optimal hydraulic radius that corresponds to the optimal acoustic power production.

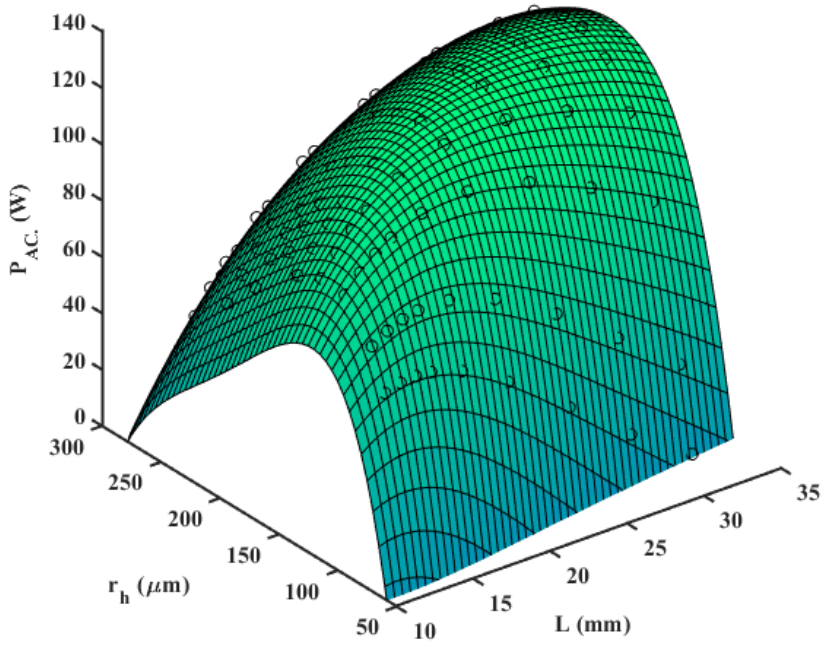
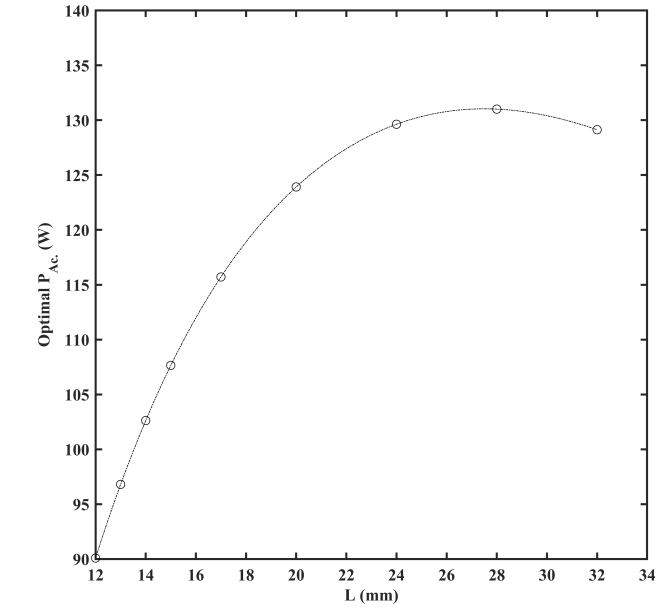
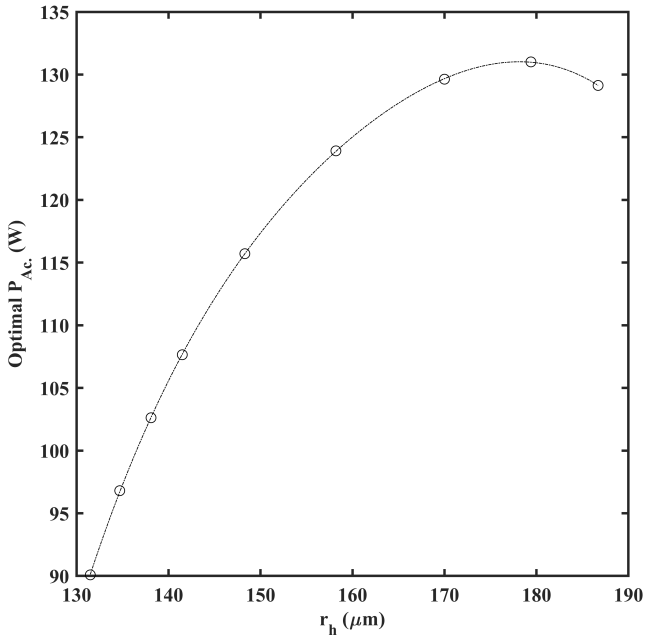


Figure 6.11: The numerical results of the acoustic power flowing within the thermoacoustic loop of the double core engine when the lengths and hydraulic radii of the two regenerators are varied in the ranges 12 - 32 mm, and 86 - 260 μm, respectively.

The optimal loop acoustic power was found to be 131 W when each regenerator is 28 mm long, and both have a hydraulic radius r_h = 180 μm. These findings reflect an increase of about 71.5% in the acoustic power output when the lengths is varied from 12 to 28 mm and the mesh size is changed from 97 to 180 μm. The optimal characteristics of the double core thermoacoustic engine for the range of L and r_h considered in this optimisation are presented in Figure 6.12. The acoustic amplification could be increased by having extra mesh layers but this would enhance the attenuation effect. Therefore, the length of the regenerator must be selected wisely by compromising between the amount of useful work and attenuation.



(a)



(b)

Figure 6.12: The numerical results of the optimal loop acoustic power $P_{Ac.}$ produced from the double core thermoacoustic electricity generator. (a) As a function of the regenerator's length L. (b) As a function of the regenerator's hydraulic radius r_h.

The results obtained from the analysis of Lautrec and the power output are presented in Figure 6.13. For a given length of the regenerator, there is an optimal NL that corresponds to the maximum acoustic output. The simulation results provided the same optimal NL of 0.37 for the length range 12 - 17 mm. For 20 mm length of the

regenerator, *NL* is increased slightly to 0.42, while it is increased further to 0.47 for the 24, 28, and 32 mm lengths.

Table 6.1: Optimal loop acoustic power and the coressponding Lautrec number *NL* for the different lengths of the regenerator.

Length, *L* **(mm)**	**Maximum acoustic power,** $P_{Ac.}$ **(W)**	**Lautrec number** *NL*	**Impedance factor,** *n* **at regenerator 1**	**Impedance factor,** *n* **at regenerator 2**
12	89.4	0.37	11.9	7.4
13	96.5	0.37	11.7	7.5
14	102.5	0.37	11.6	7.7
15	107.5	0.37	11.4	7.8
17	115	0.37	11.1	8
20	123.9	0.42	10.5	8
24	129	0.47	9.9	8.2
28	131	0.47	9.4	8.5
32	128.6	0.47	9	8.8

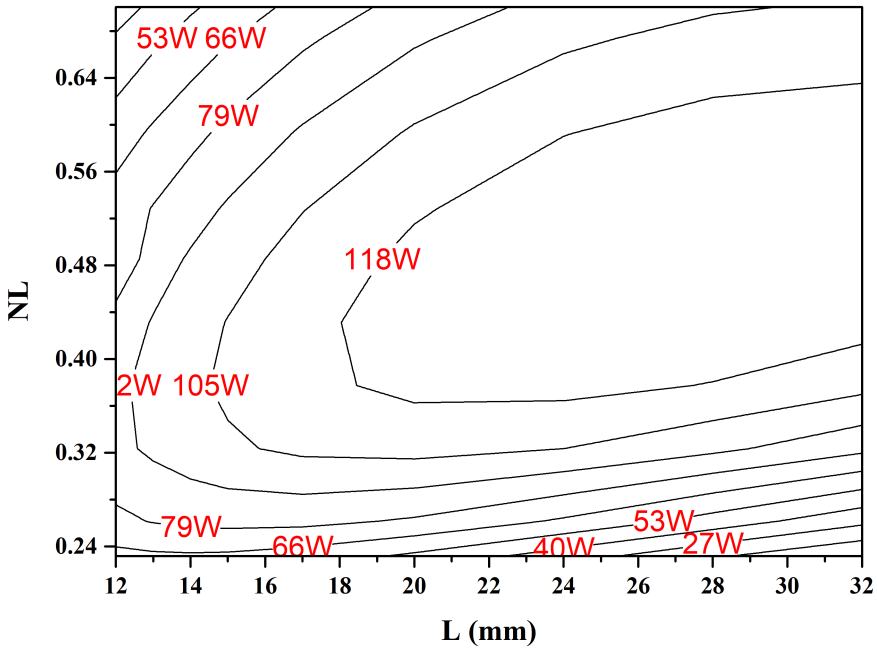


Figure 6.13: Contour plot of the effect of Lautrec number, *NL*, and the regenerator length, *L*, on the acoustic power produced from the double core thermoacoustic electricity generator system.

The thermoacoustic energy conversion within the regenerator can be controlled by a dimensionless parameter. This parameter is the product of the angular frequency of gas oscillation, ω, and the thermal relaxation time, τ. The thermal relaxation time τ is defined as the time required for thermal equilibrium in the cross-section at the flow channel, and it can be expressed as:

$$\tau = \frac{C_g}{G_{g-s}} = \frac{\rho_m c_p AL}{hA_s} \tag{6.18}$$

Here: C_g is the thermal capacity of the gas in the open space of the regenerator (J/K), G_{g-s} is the total amount of heat transfer between the gas and the solid material of the regenerator (W/K), A_s is the area of the surface of the material m^2), AL is the gas volume (m^3), and h is the heat transfer coefficient per unit area (W/m^2.K). For woven screen regenerators with channel space r_h, the thermal relaxation time can be expressed as Lawn 2012; 2014:

$$\tau = \frac{r_h^2}{3\alpha} \tag{6.19}$$

Where: α is the thermal diffusivity of the working gas (m^2/sec).
$\omega\tau$ has a significant impact on the amplification of the acoustic power within the regenerator and influences the induced heat flow along the regenerator. The ideal regenerator of a travelling-wave engine has $\omega\tau = 0$ which indicates that the working gas experiences isothermally reversible thermodynamic processes in the flow channels. As a result, the loop acoustic power would be equivalent to the amount of heat flow into the system, and the thermal to acoustic conversion efficiency equivalent to the Carnot factor. At increased value of $\omega\tau$, the heat flow also increases until it reaches a maximum for $\omega\tau = 1$ (case of stack). On the other hand, when $\omega\tau = \infty$, heat flows go to zero which means the working gas oscillates adiabatically (Biwa et al. 2011).

Numerical data for the impact of $\omega\tau$ on the amplified acoustic power, and the thermal to acoustic conversion for different lengths of the regenerator are shown in Figure 6.14 and Figure 6.15, respectively. $\omega\tau$ increases from 0.04 to 0.32 as a result of varying the hydraulic radius from 86 to 260 μm. An optimal acoustic power of 131 W with 5.2 % thermal-to-acoustic conversion efficiency is obtained from the thermoacoustic loop at $\omega\tau$ =0.15. The value of $\omega\tau = 0.04$ for the regenerators before this optimisation due to the small value of r_h, where τ is a function of r_h^2.

(Lawn 2012; 2013) observed the influence of the design parameters of a woven-steel mesh regenerator on the acoustic power output and the thermoacoustic conversion. In their research, coarse and fine mesh types were tested to identify the optimal characteristics of the system. The coarser type has shown a slightly better generating performance when its length is selected to be be three times the finer one, hence providing compara-

ble pressure drop. The optimum thermoacoustic conversion was obtained at a range of $\omega\tau$ of 0.05 - 0.2.

Yu and Jaworski (2010) evaluated numerically the acoustic losses in a regenerator of the travelling-wave engine with different configurations and dimensions. The detected theoretical optimum of their randomly stacked screen regenerators was achieved when Lautrec number was within the range of NL = 0.25 - 0.5, and $\omega\tau$ = 0.04-0.07, which are correlated to the system investigated in this study.

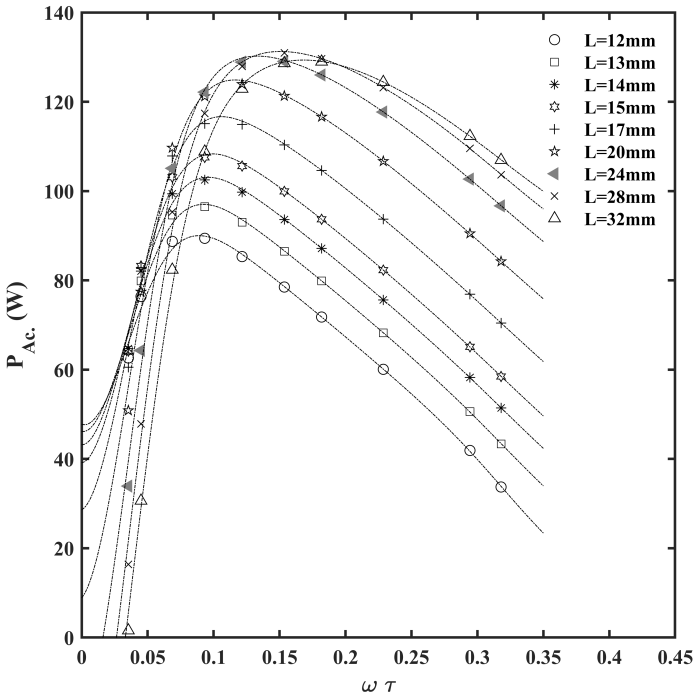


Figure 6.14: The numerical results of the loop acoustic power of the double core thermoacoustic electricity generator for selected range of length: 12 - 32 mm, and hydraulic radii: 86 - 260 µm.

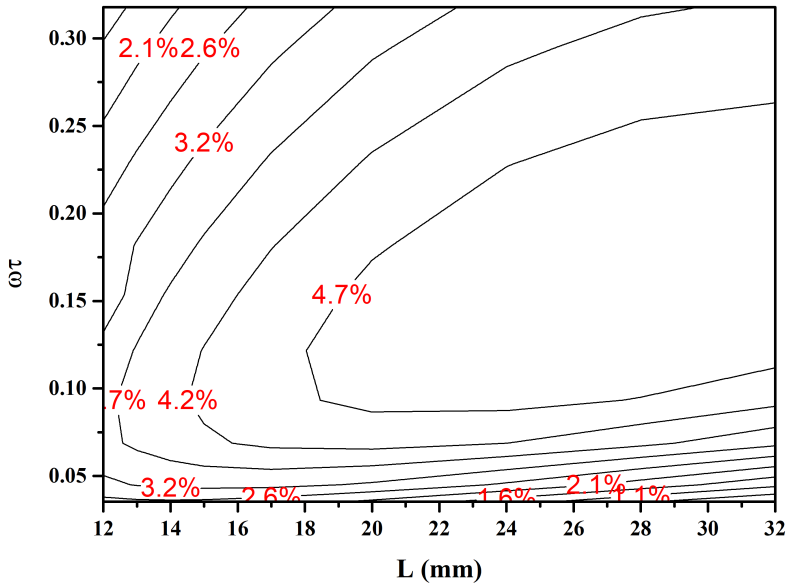


Figure 6.15: Contour plot of the effect of $\omega\tau$, and the regenerator length, L, on the acousto-electric energy conversion of the double core thermoacoustic electricity generator.

6.4.4 Extracting of electrical power

As mentioned earlier in Chapter 3 coupling the thermoacoustic engines with electrodynamic transducers enables direct conversion of acoustic power into electricity. The work discussed here is a next step from the previous "proof-of-concept": designing a low-cost electricity-generating cooking stove for high-volume implementation (Riley 2014*b*). The technology prototype was capable of producing approximately 12.6 W electrical power using two custom made electrical heaters to simulate biomass combustion, and an ordinary loudspeaker connected in series to the thermoacoustic loop. Later, and as a part of the current project, it was found that the output could be enhanced to 31.4 W considering the heat input ratio concept. By optimizing both regenerators, DeltaEC data revealed a remarkable increase in the loop acoustic power. According to the arrangement of the system, a low-cost ordinary loudspeaker is used to extract electricity from the thermoacoutsic loop. The results of the amount of electricity, W_e, that can be harvested from the optimised thermoacoustic engine are set out in Figure 6.16.

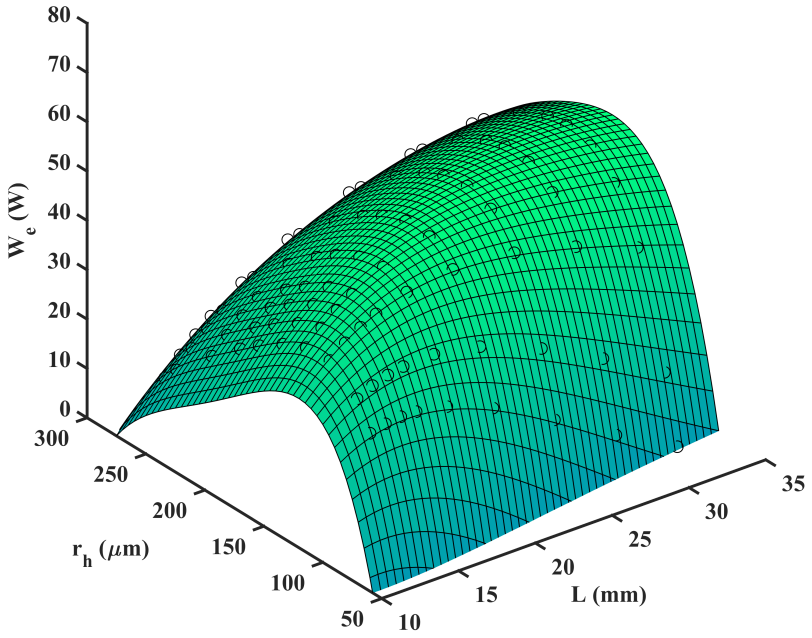


Figure 6.16: The numerical results of the electricity extracted from the double core thermoacoustic engine when the lengths and hydraulic radii of the two regenerators are varied in the ranges 12 - 32 mm, and 86 - 260 μm, respectively.

Again, greatest performance is reached for the electrical power output. For L = 28 mm, and r_h = 180 μm, W_e is approximately 52.4 W with 67% increase (was 31.4 W). This is a rather remarkable outcome, which proves that the regenerators can be optimised for the maximum acoustic amplification. The performance predicted by the DeltaEC model for the multi-stage travelling-wave thermoacoustic electricity generator is summarized in Table 6.2. The DeltaEC model of the double core thermoacoustic engine with the optimum regenerator parameters is attached in **Appendix D**.

Table 6.2: Summary of DeltaEC simulation of the double core thermoacoustic electricity generator after optimisation of the two regenerators.

Symbol	Definition	Value and unit
$Q_{in,1}$	Heat input into HHX1	1000 W
$Q_{in,2}$	Heat input into HHX2	1500 W
$\|p_1\|_{reg.1}$	Pressure amplitude in reg.1	4301 Pa
$\|U_1\|_{reg.1}$	Volumetric velocity amplitude in reg.1	0.069 m^3/sec
$\|p_1\|_{reg.2}$	Pressure amplitude in reg.2	4253 Pa
$\|U_1\|_{reg.2}$	Volumetric velocity amplitude in reg.2	0.088 m^3/sec
$P_{Ac.,in1}$	Acoustic power inlet into reg.1	115 W
$P_{Ac.,out1}$	Acoustic power inlet into reg.1	148 W
$P_{Ac.,in2}$	Acoustic power inlet into reg.2	128 W
$P_{Ac.,out2}$	Acoustic power inlet into reg.2	187 W
$P_{Ac.,net1}$	Net acoustic power produced in reg.1	33 W
$P_{Ac.,net2}$	Net acoustic power produced in reg.2	59 W
$P_{Ac.}$	Acoustic power of the loop	131 W
$T_{H,1}$	Gas temperature at the hot side of reg.1	542 K
$T_{C,1}$	Gas temperature at the cold side of reg.1	375 K
$T_{H,2}$	Gas temperature at the hot side of reg.2	603 K
$T_{C,2}$	Gas temperature at the cold side of reg.2	363 K
W_e	Electrical power output	52.4 W
η_{t-a}	Thermal-to-acoustic conversion efficiency	5.2 %
η_{t-e}	Thermal-to-electrical conversion efficiency	2.1 %
$\eta_{R,Ac.}$	Relative Carnot efficiency for acoustic output	14.8 %

6.5 Concluding remarks

In this piece of research, many facets of the design of the core of a two-stage thermoacoustic engine have been explored numerically, based on the dimensions and operational parameters reported in Chapter 5. Bearing in mind the ultimate requirement for low

cost and the type of application, attention has been drawn to the unpressurised air-filled duct, with a simple design for the thermoacoustic core and loop. One of the most important design features in travelling-wave thermoacoustic engines is the choice of the regenerator, as it functions as an amplifier for the acoustic power. The SCORE project focused on the development of thermoacoustic engines that can be integrated into cooking stoves to generate electricity for families in the developing world. The SCORE aim was to produce 100 W of electricity with 2.5 kW heating power supplied to the double core thermoacoustic engine, using air at the same atmospheric pressure as the working gas. However, for the thermoacoustic stove to be commercially viable its acoustic power output must be increased by 88 W to generate 100 W of electrical power using 1 bar air in its thermoacoustic loop.

The aim of this work is to increase the power output closer to the 20 - 100 W goal. Accordingly, an optimization procedure is proposed for the regenerator's geometry, which is shown to enhance the thermoacoustic performance of the two-stage thermoacoustic engine. A *STKSCREEN* DeltaEC segment is used to reflect the design parameters of the regenerator. Afterwards, for the two stacked-screen regenerators, better hydraulic radius of 180 μm and length of 28 mm are obtained by employing the optimisation scheme outlined in this study. A fundamental analysis of the performance of the two regenerators in terms of resistance to the flow, relation to heat transfer, and the heat capacity of the working gas provided quantitative and qualitative measures for arbitrary geometries. Furthermore, the sensitivity of acoustic power production to the thermal relaxation time, and the temperature difference across the regenerator is demonstrated. The ratio of the hydraulic radius to the thermal penetration depth, the impedance enhancement factor, are also explained.

By varying the length and the pore shape of the regenerator, we realized the possibility of achieving maximum acoustic and electrical power outputs of 131, and 52.4 W, respectively. Compared to SCORE results, the acoustic power increased by 63.8% (from 80 W to 131 W), while the electricity output improved by 316% (from 12.6 W to 52.4 W). The Relative Carnot efficiency for acoustic output is increased from 5.3% to 14.8%. The data revealed that as the regenerator length is increased, the loss in acoustic power due to viscous and thermal-relaxation will also be increased, reducing the overall efficiency of the system. Nevertheless, a longer regenerator enabled the higher conversion of the heating power into the acoustic one. As a result, higher temperature differences across the regenerator and larger acoustic output can be achieved. The optimal regenerator length should be obtained by balancing these effects. It is also shown that for each length of the regenerator, the optimal hydraulic radius is not the same, and therefore, must be carefully selected. The advantage of greater length and hydraulic radius is sufficient to overcome the acoustic losses.

CHAPTER 7

CONCLUSIONS AND RECOMMENDATIONS FOR FUTURE WORK

7.1 Conclusion

In closing this thesis, this chapter provides the main concluding remarks that can be drawn from the research work, followed by a relevant discussion. Suggestions for future developments based on the research gap that was identified during the analysis of the results are provided in section 7.2.

7.1.1 Statement of the project's aim and objectives

The overarching theme of this research work was to investigate the viability of providing a reliable, sustainable, and affordable energy supply for the rural dwellers utilising thermoacoustic technology. The aim is to boost the electricity output from a dual-core thermoacoustic engine developed by the SCORE team to meet the 20 - 100 W target using waste heat from traditional biomass cooking stoves. Such a system would be particularly suitable for cooking, lighting, and heating solutions in areas where people live mostly in the dark such as South Sudan. The system would be more attractive if it were constructed using minimum moving parts and at a low cost. Therefore, all the research work presented in this thesis focused only on low-cost design philosophy, particularly air-filled systems and standard PVC pipes and fittings. However, cost analysis is out of the scope of the current research. The purpose of the work done during the project is summarised in the following statements of objectives:

1. Gain understanding of the thermoacoustic effect, the acoustoelectric conversion, and the process of modelling thermoacoustic systems using DeltaEC tool.

2. Develop an optimisation procedure and build predictive models for a single core looped-tube thermoacoustic electricity generator to mimic the wave performance throughout the different components.
3. Examine the effect of the loudspeaker's load resistance on the harvested electricity.
4. Prove that the stub pipe functions as an impedance modifier to compensate for the disturbance in the acoustic field resulting from using a loudspeaker.
5. Perform experimental tests of the single-core thermoacoustic engine.
6. Validate the DeltaEC results against the lab data and assess the feasibility of a single-core air-filled system for electricity production.
7. Further develop the DeltaEC model of the double-core looped tube thermoacoustic electricity generator developed by SCORE.
8. Investigate a novel operational technique for the double-core engine numerically.
9. Demonstrate the potential of the proposed technique to boost the power output with no additional cost.
10. Conduct experimental investigations of the double-core generator to obtain the optimum conditions.
11. Confirm the DeltaEC results with the experiments and prove the validity of the suggested operating method.
12. Optimise both regenerators of the double-core system using DeltaEC software.
13. Evaluate the overall performance of the optimised double-core thermoacoustic system compared to that achieved previously by the SCORE team.

7.1.2 Level of attainment of the objectives

From a purely practical point of view, the investigations required to meet the aim and the objectives were carried out in two stages. Both stages used a looped tube configuration for the feedback loop, which is the most attractive option for this application due to its simplest implementation, as concluded from Chapter 3. In the broadest sense, the initial stage of study concerned a single-core travelling wave engine using air at atmospheric pressure (Chapter 4), while the second stage (Chapters 5 and 6) addressed the challenges posed by having atmospheric air working gas in a multi-stage travelling wave engine, and bearing in mind the differences between the two engines in terms of size, parts, heating power.

The single regenerator travelling wave thermoacoustic system

Objectives (2) – (6) have been achieved through the research activities outlined in Chapter 4 devoted to the optimisation and experimental investigation of a single regenerator engine working with air at 1 bar. However, in a detailed description, these are reported as follows:

- Detailed optimisation procedure of a single core looped-tube travelling wave thermoacoustic engine coupled with a loudspeaker has been set out based on DeltaEC simulation code. A predictive model representing the actual geometry has been developed. DeltaEC modelling enabled physical understanding of the behaviour of the thermoacoustic system in terms of the axial distribution of the pressure and volumetric velocity amplitudes, the impedance, the phase angle, the amplification and dissipation of the acoustic power throughout the system, and extraction of the electrical power by the loudspeaker.
- The laboratory device was tested under different working conditions. Spontaneous oscillations of the working gas were observed within the feedback loop. The system was examined at 75 Hz corresponding to a loop length of 4.4 m. The engine functioned as an energy conversion system producing acoustic power. The loudspeaker extracted electrical power from the generated acoustic power. The effect of the load resistance and the current of the loudspeaker on the electricity output was determined, and the optimum resistance was 30Ω. The impact of the length of the tuning stub pipe on the thermoacoustic field was also realized and compared with the analytical estimations of DeltaEC. The disturbance in the acoustic field caused by the installation of the loudspeaker The installation of the was partially compensated by the stub. The optimum length was found to be 61 cm. From DeltaEC results, the system achieved 3.5 W of electricity with 4.03% thermal-to-acoustic conversion and 0.23% thermal-to-electrical. A fair degree of agreement between the lab data and the numerical results was obtained. One of the important findings was that the acoustic dissipation through the feedback pipe was high, which is consequently degraded the overall performance. This does not accurately meet the SCORE original aim but could be regarded as a "proof of concept" outlining the principles of thermoacoustic power and thermoacoustic modelling.

The multi-stage travelling wave thermoacoustic electricity generator

Objectives (7) – (11) have been met through the study outlined in this chapter (Chapter 5):

- The multi-stage looped-tube travelling wave thermoacoustic engine developed by SCORE. The engine delivered 12.6 W electricity with 0.5% thermal-to-electrical efficiency using an atmospheric air-filled resonator. In this piece of research, a DeltaEC model was constructed to capture the essence of the system. The heat supply into the two engine stages was varied to be asymmetric without affecting the total heat supply. A series of DeltaEC simulations were developed accordingly, where a variation in the overall performance for the same heating power was discovered. Those used lower heat percentages in the first thermoacoustic stage, and a higher rate in the second one performed better compared to those using the opposite. The resulting acoustic wave propagated throughout the thermoacoustic system was much stronger in terms of pressure amplitude, volumetric velocity amplitude, and the phase difference between them. Also, a lower temperature difference, acoustic power production, thermoacoustic and thermoelectric conversion efficiencies were obtained as a result of applying unevenly distributed heat inputs.

- Similarly, the experimental apparatus was tested to verify DeltaEC estimations. The results confirmed the potential of the heat input ratio in enhancing the thermoacoustic performance with no additional cost. From a fundamental acoustic research point of view, unevenly heated thermoacoustic cores cause asymmetric acoustic impedance distribution along the system, which in turn affects the amplified acoustic power from each regenerator.

- The simulated power output was shown to be highest at a heat ratio of 30% : 70%. However, it was impossible to use this ratio in the experimental device because of the strength limitation of the material of the HHX. The simulated loop acoustic power increased from 58.4 W for 50% : 50% to 68.6 W for 40% : 60% heat input with no other changes to the configuration. For the same ratio, the electrical power increased from 24.4 W to 31.4 W. The data from the experimental rig agreed well with the numerical predictions in terms of optimal applicable heat ratio, generated acoustic power, and electricity output.

- Comparing this with the SCORE achievable power output, the innovative heat input technique enhanced the electricity output by nearly 149% (from 12.6 W to 31.4 W) using the same total heat supply of 2500 W and with a 1 bar air-filled resonator. The most crucial point to be highlighted is that power output was achieved with no additional cost of verification which meets the aim of increasing the power output without affecting the total cost (section 1 in the introduction chapter).

According to author knowledge, the work presented in this chapter has not been investigated before, and the open literature only identified that the conventional method is to supply equal heat amounts. Such a concept for thermal power distribution has considerable consequences for acoustic research in multi-stage travelling wave thermoacoustic electricity generators, and this breakthrough may be of assistance to other researchers who consider multi-stage thermoacoustic electricity generators. Besides, this part of the research includes a technique that directly monitors the acoustic volumetric velocity, "the gradient method", by placing one absolute pressure transducer and one differential pressure sensor within the feedback pipe, and accordingly, the acoustic power was obtained. The literature survey shows that the two-sensor power technique is commonly used to estimate the loop acoustic power in thermoacoustic engines, and the gradient method has not been applied before.

Optimisation of the regenerators of a double core thermoacoustic engine with asymmetric heat inputs

Attention has been drawn to the regenerator part because it is the place where the thermodynamic interaction between the acoustic wave and solid material, and therefore, the power amplification, takes place. However, far too little attention has been paid to simultaneously optimising multiple regenerators due to the complexity of such a system. The work described in this chapter (Chapter 6) has led to objectives (12) – (13) being met as follows:

- Based on the DeltaEC model of the multi-stage system developed in the previous chapter, a further numerical study was carried out on the regenerator units. The influence of design parameters of the regenerator on the performance characteristics was studied. The geometry of the two regenerators was optimised with the help of DeltaEC. The optimisation was carried out using the optimum heat input ratio determined previously in Chapter 5. The optimisation procedure suggested by this work can be implemented to capture the complexities of the thermoacoustic amplification in such a multi-stage system.
- By changing the geometry of the two regenerators, it is shown that, only for optimised ranges of the length and the hydraulic radius, it is possible to obtain the maximum acoustic production. Additionally, the results of the numerical calculations indicated the necessity of balancing the acoustic gain and the acoustic dissipations.
- For the optimised dual regenerator thermoacoustic engine with atmospheric air as the working gas and total heating power of 2500 W distributed asymmetrically into 1000 W in the first engine and the rest in the second one, the optimal

acoustic power achieved 131 W. At this loop acoustic power, the loudspeaker delivered 52.4 W, which is 39.4 W higher than that reported by SCORE. This 316% increase in the electricity output has shown the potential of the dual-core thermoacoustic engine to meet the needs of rural households. The investigation carried out in this study has improved the Relative Carnot efficiency for acoustic output from 5.3% to 14.8%.

7.1.3 Contribution of the thesis

The most important novel aspects of the work contributed by this thesis are the validated modelling of all aspects of the thermoacoustic engines developed by the SCORE consortium with correct geometry. The asymmetric heat input distribution method was applied to the multi-stage travelling wave thermoacoustic electricity generator coupled with one loudspeaker. This new method was implemented successfully in the experimental apparatus, and it was recognised to enhance power amplification. The novelty of such an operational methodology is that a stronger travelling wave is generated in the loop, and therefore, the power harvester delivered a higher electrical output. Such uneven distribution of the heat input power in multi-stage thermoacoustic electricity generators was not found in the literature.

The technique applied for monitoring the velocity of the working gas in a thermoacoustic feedback loop presented in the thesis has not applied before, according to the literature. Both the numerical modelling and the experimental results have demonstrated that the proposed technique can accurately estimate the acoustic power of the loop.

Successful optimisation of the regenerators of the multi-stages travelling wave thermoacoustic engine was carried out with an acoustoelectric converter. This contributed to improving the system's performance and demonstrated the potentiality of the system for developing an inexpensive electricity generator. Some literature was found regarding optimisation of the geometrical parameters of thermoacoustic engines of a single regenerator unit. The optimisation of multiple regenerators (multi-stage engines) has not been attempted prior to this work according to the literature survey.

In spite of its limitations regarding the type of the working gas and the cost, the study certainly adds to our understanding of the problems encountered with the SCORE thermoacoustic systems. There is still uncertainty, however, whether a thermoacoustic engine is filled with air at atmospheric pressure has the potential to deliver acceptable levels of electricity. The research reported in this thesis proved the viability of using an atmospheric air-filled resonator to generate up to 52 W of electricity. The outcome of this research could be beneficial to meet a combined smoke-free stove design with electricity generation for low-income households of South Sudan or any other rural areas in the developing world, to meet the basic needs, particularly for charging mobile phones and both indoor and torch lighting.

7.2 Recommendation for future research

Unfortunately, generally in research there is no completed research, and there are always opportunities for further enhancements. This is especially so when the topic is still in its growth stage, such as thermoacoustic power, where many areas remained unexplored. There have been many proposals for new research directions or suggestions on how to improve the already obtained results. The most important ideas are discussed in this section. Part of these recommendations have already been treated separately within the related chapters of this thesis, but some will be repeated here for the sake of completeness.

1. The design of the hot heat exchanger can be improved to enhance the heat transfer rate, and therefore, ensure a considerable amount of the heat is transferred to the hot heat exchangers and heat dissipation is minimised. For example, adding staggered fins will increase the heat transfer area of the hot heat exchanger.

2. Metal pipes can be used for the feedback loop to allow using high-pressure air and also to reduce the loss in energy due to the expansion and contraction of PVC pipes which may occur as a result of the vibration. MATLAB software or Tina^{TM} can be used to predict the size and length of the feedback tube required to tune the system.

3. Other technologies for phase matching can be considered to tune the phase difference between the pressure and velocity oscillations, and hence to adequately meet the travelling wave conditions.

4. Another possible area of improvement is to increase the acoustoelectric conversion by installing a bi-directional turbine or a loudspeaker that has more favourable electromechanical characteristics.

5. The measurement techniques could be improved further; for example, the possibility of obtaining pressure signals at the two ends of the regenerator and within the thermal buffer tube. The benefit of this approach is to capture the complexities of the acoustic field and possible future developments.

6. Experimental work is needed to better understand the relative performance of different pore shapes, physical properties, and length of the regenerator. The regenerator should be precisely assembled to obtain the required porosity and hydraulic radius by selecting the correct size and numbers of the wire.

7. Further studies are required to extend the optimization procedure suggested for the regenerator part to cover operating parameters such as the working frequency, the type of the working gas, and the wave condition at the inlet of the regenerator.

8. Investigations into using elevated mean pressure of the working gas in the acoustic pipes should be considered, after resolving the sealing issues. The effects of pressurising the system on the power density should be investigated.

9. Using the models generated in this work, robust design of the multi-stage engine can be implemented for a manufactured product by vertically arranging the thermoacoustic cores. The vertical design enables placing the thermoacoustic core inside the chimney in case integrating the engine with a cooking stove, and therefore, the occupied area can be reduced.

If these recommendations were studied, the electrical power output could exceed 100 W at a low cost. Likewise, the thermoacoustic technology can be the solution for the electricity shortage in rural areas such as South Sudan and would have a significant impact on both residential, and industrial sectors. Additionally, this thermoacoustic stove would decrease the total household air pollution, which will profoundly affect regional health. Using electric lighting would also benefit health by reducing smoke from kerosene lamps used for lighting.

APPENDIX A

DELTAEC CALCULATIONS

A.1 Physical segments

This section provides a list of the DeltaEC segments used to construct the models and the equations needed to estimate the wave performance throughout the model based on the user-guide (Ward et al. 2008):

A.1.1 DUCT

$$\frac{dp_1}{dx} = \frac{-i\omega\rho_m}{(1-f_v)A}U_1 \tag{A.1}$$

$$\frac{dU_1}{dx} = \frac{-i\omega A}{\rho_m a^2}\left(1+\frac{\gamma-1}{1+\varepsilon_s}f_\kappa\right)p_1 \tag{A.2}$$

which are equivalent to

$$\left(1+\frac{\gamma-1}{1+\varepsilon_s}f_\kappa\right)p_1 + \frac{\omega^2}{a^2}(1-f_v)\frac{d^2p_1}{dx^2} = 0 \tag{A.3}$$

In laminar DUCTs of length Δx, these are equivalent to:

$$p_{1,out} = p_{1,in}cos\kappa\Delta x - \frac{i\omega\rho_m}{(1-f_v)\kappa A}U_{1,in}sin\kappa\Delta x \tag{A.4}$$

$$U_{1,out} = U_{1,in}cos\kappa\Delta x - \frac{i(1-f_v)\kappa A}{\omega\rho_m}p_{1,in}sin\kappa\Delta x \tag{A.5}$$

Here the complex wave number κ is given by

$$\kappa = \frac{\omega}{a}\sqrt{\frac{1+(\gamma-1)f_\kappa/(1+\varepsilon_s)}{1-f_\nu}} \tag{A.6}$$

In DUCTs, the effective radius r_0 defined as $r_0 = A/\Pi$ which represents the radius of the circle in circular cross sections and equals twice the hydraulic radius in the other cross sections.
In narrow DUCTs, for $r_0/\delta_j < 25$, f_κ and $f\nu$ are calculated using complex Bessel functions as follows:

$$f_j = \frac{2J_1[(i-1)r_0/\delta_j]}{(i-1)(r_0/\delta_j)J_0[(i-1)r_0/\delta_j]} \quad for\ j = \kappa\ or\ \nu \tag{A.7}$$

In wide DUCTs, where $r_0/\delta_j > 25$

$$f_j = (1-i)\Pi\delta_j/2A \quad for\ j = \kappa\ or\ \nu \tag{A.8}$$

For intermediate values, linear interpolation is applied to make a smooth match between the two regimes To anticipate for turbulence, the software increases the resistive component of the pressure gradient, and therefore the viscous power loss, by

$$m_\nu = \frac{\delta_\nu^2 N_R}{24\pi r_h^2}\frac{[f_M(1-9\pi/32)NR_1 df_M/dNR_1]}{Re[i/(1-f_\nu)]} \tag{A.9}$$

The moody friction factor can be evaluated as a Reynolds number, NR_1 and the roughness ε as follows:

$$\frac{1}{\sqrt{f_M}} = 1.7385 - 2log_{10}\left(2\varepsilon + \frac{18.574}{NR_1\sqrt{f_M}}\right) \tag{A.10}$$

A.1.2 HX

In *HX*, wave propagation is calculated using the following equations:

$$\frac{dp_1}{dx} = \frac{-i\omega\rho_m}{(1-f_\nu)A_{gas}}U_1 \tag{A.11}$$

$$\frac{dU_1}{dx} = \frac{-i\omega A_{gas}}{\rho_m a^2}\left(1+\frac{\gamma-1}{1+\varepsilon_s}f_\kappa\right)p_1 \tag{A.12}$$

HX uses parallel plate geometry to compute the spatially averaged thermal and viscous functionas as follows:

$$f_j = \frac{\tanh[(1+i)y_0/\delta_j]}{(1+i)y_0/\delta_j} \tag{A.13}$$

for $j = \kappa$ or ν For $\dot{N} = 0$, temperature and power are given as

$$\frac{dT_m}{dx} = 0 \tag{A.14}$$

$$\frac{d\dot{H}_{tot}}{dx} = \frac{\dot{Q}}{\Delta x} \tag{A.15}$$

$$T_{solid} = T_m + \frac{\dot{Q}}{hA_{gas}x_{eff}/r_h} \tag{A.16}$$

Here: Δx is the length of the heat exchanger, $\dot{Q}$ is the heat added into the heat exchanger, h is the heat transfer coefficient which can be estimated with

$$h = \frac{\kappa}{y_{eff}} \tag{A.17}$$

$$x_{eff} = min[2 \mid \xi_1 \mid, \Delta x] \tag{A.18}$$

$$y_{eff} = min[\delta_\kappa, r_h] \tag{A.19}$$

For $\dot{N} \neq 0$, temperature and power are given as

$$\frac{dT_m}{dx} = F_{\dot{Q}\dot{N}}\frac{\dot{Q}/\Delta x}{\dot{N}mc_p} \tag{A.20}$$

$$\frac{d\dot{H}_{tot}}{dx} = \frac{\dot{Q}}{\Delta x} \tag{A.21}$$

If $\dot{Q} > 0$

$$T_{solid} = max[T_m(0) + T_m(\Delta x)] + \frac{\dot{Q}}{hA_{gas}x_{eff}/r_h} \tag{A.22}$$

If $\dot{Q} < 0$

$$T_{solid} = min[T_m(0) + T_m(\Delta x)] + \frac{\dot{Q}}{hA_{gas}x_{eff}/r_h} \tag{A.23}$$

A.1.3 STKSCREEN

In *STKSCREEN* regenerators, the acoustic parameters evolve according to

$$\frac{dp_1}{dx} = -i\omega\rho_m\left[1 + \frac{(1-\phi^2)}{2(2\phi-1)}\langle u_1\rangle\right] - \frac{\mu_m}{r_h^2}\left(\frac{c_1(\phi)}{8} + \frac{c_2(\phi)NR_1}{3\pi}\right)\langle u_1\rangle \tag{A.24}$$

$$\frac{d\langle u_1\rangle}{dx} = \frac{-i\omega\gamma}{\rho_m a^2}p_1 + \frac{\beta dT_m}{dx}\langle u_1\rangle + i\omega\beta\left[\frac{T_m\beta}{\rho_m c_p}\frac{\varepsilon_s + (g_c + 2e^{2i\theta_p}g_v)\varepsilon_h}{1 + \varepsilon_s + \varepsilon_h(g_c + e^{2i\theta_T}g_v)}p_1 -\right.$$

$$\frac{1}{i\omega}\frac{dT_m}{dx}\frac{\varepsilon_s+(g_c-g_v)\varepsilon_h}{1+\varepsilon_s+(g_c+e^{2i\theta_T}g_v)\varepsilon_h}\langle u_1\rangle\Bigg] \quad \text{(A.25)}$$

$$\frac{dT_m}{dx}=\left(Re\left[\left(T_m\beta\frac{\varepsilon_s+\varepsilon_h(g_c+e^{2i\theta_p}g_v)}{1+\varepsilon_s+\varepsilon_h(g_c+e^{2i\theta_T}g_v)}+1-T_m\beta\right)p_1\langle\tilde{u_1}\rangle\right]-\frac{2\dot{H}_{2,\kappa}}{\phi A}\right)$$
$$/\left(\frac{\rho_m c_p}{\omega}Im\left[\frac{\varepsilon_s+\varepsilon_h(g_c+e^{2i\theta_p}g_v)}{1+\varepsilon_s+\varepsilon_h(g_c+e^{2i\theta_T}g_v)}\right]\langle u_1\rangle\langle\tilde{u_1}\rangle+2\left[\kappa_{s,eff}\frac{1-\phi}{\phi}+\kappa\right]\right) \quad \text{(A.26)}$$

using

$$c_1(\phi)=1268-3545\phi+2544\phi^2,\ c_2(\phi)=-2.82+10.7\phi-8.6\phi^2 \quad \text{(A.27)}$$

$$b(\phi)=3.81-11.29\phi+9.47\phi^2 \quad \text{(A.28)}$$

$$\theta_p=phase(\langle u_1\rangle)-phase(p_1),\ \theta_T=phase(\langle u_1\rangle)-phase(\langle T_{u,1}\rangle) \quad \text{(A.29)}$$

$$\varepsilon_s=\frac{\phi\rho_m c_p}{(1-\phi)\rho_s c_s},\ \varepsilon_h=\frac{8ir_h^2}{b(\phi)\sigma^{1/3}\delta_\kappa^2} \quad \text{(A.30)}$$

$$NR_1=\frac{4|\langle u_1\rangle|r_h\rho_m}{\mu} \quad \text{(A.31)}$$

A.1.4 STKDUCT

In the *STKDUCT* segment, the pressure propagates according to Rott's wave approximation equation, given in the form:

$$\frac{dp_1}{dx}=\frac{-i\omega\rho_m}{(1-f_\nu)A_{gas}}U_1 \quad \text{(A.32)}$$

$$\frac{dU_1}{dx}=\frac{-i\omega A_{gas}}{\rho_m a^2}\left(1+\frac{\gamma-1}{1+\varepsilon_s}f_\kappa\right)p_1+\frac{\beta(f_\kappa-f_\nu)}{(1-f_\nu)(1-\sigma)(1+\varepsilon_s)}\frac{dT_m}{dx}U_1 \quad \text{(A.33)}$$

$$\frac{dT_m}{dx}=\frac{2\dot{H}_{2,\kappa}-\frac{1}{2}Re\left[p_1\tilde{U}_1\left(1-\frac{T_m\beta(f_\kappa-\tilde{f}_\nu)}{(1-\varepsilon_s)(1+\sigma)(1-f_\nu)}\right)\right]}{\frac{\rho_m c_p|U_1|^2}{2\omega A_{gas}(1-\sigma)|1-f_\nu|^2}Im\left[\tilde{f}_\nu+\frac{(f_\kappa-\tilde{f}_\nu)(1+\varepsilon_s f_\nu/f_\kappa)}{(1+\varepsilon_s)(1+\sigma)}\right]}-A_{gas}k-A_{solid}k_s \quad \text{(A.34)}$$

$$f_j=(1-i)\Pi\delta_j/2A,\ for j=\kappa\ or\ \nu \quad \text{(A.35)}$$

$$\varepsilon_s=\left(\frac{k\rho_m c_p}{k_s\rho_s c_s}\right)^2\frac{1}{\tanh\left[(1+i)l/\delta_s\right]} \quad \text{(A.36)}$$

Where:

$$l = \frac{Wall\ cross-sectional\ area}{perimeter} \tag{A.37}$$

A.1.5 IESPEAKER

An Enclosed transducer *IESPEAKER* is an object connected in series with other segments. The volume flow rate U_1 is nearly unchanged (except for surface thermal-hysteresis losses). However, pressure is changed by the force exerted by the transducer, obeying the complex equations

$$V_1 = Z_e I_1 - \tau U_1 \tag{A.38}$$

$$P_{out} - P_{in} = \tau' I_1 - Z_m U_1 \tag{A.39}$$

The complex electrical impedance Z_e, the transduction coefficient τ, and the complex mechanical impedance Z_m are given as:

$$Z_e - R_e + i\omega L \tag{A.40}$$

$$\tau = -\tau' = \frac{Bl}{A} \tag{A.41}$$

$$Z_m = \frac{R_m}{A^2} + \frac{i(\omega M - k/\omega)}{A^2} \tag{A.42}$$

Enclosed speakers have area A exposed to $p_{1,in}$ and area A exposed to $p_{1,out}$, because both sides of the speaker experience oscillatory pressure. This thermal hysteresis on those two surfaces manifests itself as a small change in volume flow rate, according to:

$$U_{1,out} = U_{1,in} - \frac{\omega}{\rho_m a^2}\frac{\gamma-1}{1+\varepsilon_s}\frac{\delta_k}{2}A(p_{1,in} + p_{1,out}) \tag{A.43}$$

U_1 in Equation A.38 and Equation A.39 is actually the value after the first thermal-hysteresis loss:

$$U_1 = U_{1,in} - \frac{\omega}{\rho_m a^2}\frac{\gamma-1}{1+\varepsilon_s}\frac{\delta_k}{2}Ap_{1,in} \tag{A.44}$$

This segment doesn't affect the mean temperature T_m.

A.1.6 BRANCH

A *BRANCH* is a side branch with complex impedance $Z_{br.}$ where the pressure is unchanged in the trunk, but volume flow rate in the trunk changes according to

$$U_{1,out} = U_{1,in} - p_1/Z_{br.} \tag{A.45}$$

For a BRANCH of a radius r where the wave number is $k = \omega/a$, the complex impedance is given by:

$$Z_{br.} = \frac{\rho_m a}{A}\left[1 - \frac{2J_1(2kr)}{2kr} + i\left(\frac{4/\pi}{2kr} + \frac{\sqrt{8/\pi}\sin(2kr - 3\pi/4)}{(2kr)^{3/2}}\right)\right] \; if \; 2kr > 2.68 \tag{A.46}$$

$$Z_{br.} = \frac{\rho_m a}{A}\left[1 - \frac{2J_1(2kr)}{2kr} + i\left(\frac{(4/\pi)2kr}{3}\left(1 - \frac{(2kr)^2}{15}\right)\right)\right] \; otherwise \tag{A.47}$$

This segment doesn't affect the mean temperature T_m.
The trunk exiting energy flow is computed as

$$\dot{H}_{2,k,out} = \dot{H}_{2,k,in} - \dot{H}_{br.} \tag{A.48}$$

A.1.7 JOIN

The *JOIN* segment is used to account for small discontinuities in the thermoacoustic parameters at the interface between a heat exchanger or other isothermal segment and an unmixed, thermally stratified, adiabatic region such as a pulse tube. When a model encounters a *JOIN* segment, DeltaEC looks both upstream and downstream to figure out whether the "heat exchanger" is upstream and the "pulse tube" is downstream, or vice versa. The discontinuity in the mean temperature at a *JOIN* segment can be calculated as follows:

$$T_{m,out} - T_{m,in} = \left(-\frac{T_m\beta}{\rho_m c_p}|p_1|\sin\theta - \frac{|U_1|_{in}}{\omega A_{gas}}\frac{dT_m}{dx}\right)F \tag{A.49}$$

Here: θ is the phase difference between p_1 and U_1; $dT_m = dx$ is evaluated on the thermally stratified, adiabatic side of the *JOIN*, and F is a factor to account for the two-dimensional nature of the *JOIN* problem and it can be given by

$$F = \sqrt{\frac{2(A_{gas}kdT_m/dx)^2}{(A_{gas}kdT_m/dx)^2 + (\dot{H}_{2,k} - \dot{E})^2}} \tag{A.50}$$

The discontinuity in volume flow rate U_1 at *JOIN* is given by

$$|U_1|_{out} = |U_1|_{in} - \frac{\delta}{3\pi}\frac{(\gamma-1)}{\rho_m a^2}|p_1||U_1|_{in}\cos\theta = |U_1|_{in} - \frac{16}{3\pi}\frac{(\gamma-1)}{\rho_m a^2}\dot{E} \tag{A.51}$$

There is no discontinuity in the pressure p_1, in the phase of U_1, or in $\dot{H}_{2,k}$.

A.2 The thermoviscous function and its spatial average

This section provides the thermoviscous function and its spatial average for different stack geometries. For wide-open channels with $y = 0$ at the wall, the thermoviscous function, h and its spatial average, f can be given as:

$$h = e^{-(1+i)y/\delta} \tag{A.52}$$

$$f = \frac{(1-i)\delta}{2r_h} \tag{A.53}$$

For parallel plates with separation $2y_0 = 2r_h$ where y_0 is the center between the plates. h and f are:

$$h = \frac{\cosh[(1+i)y/\delta]}{\cosh[(1+i)y_0/\delta]} \tag{A.54}$$

$$f = \frac{\tanh[(1+i)y/\delta]}{(1+i)y_0/\delta} \tag{A.55}$$

For rectangular channels of dimensions $2y_0 \times 2z_0$:

$$h = 1 - \frac{16}{\pi^2}\sum_{m,n\ odd}\frac{\sin(m\pi y/2y_0)\sin(n\pi z/2z_0)}{mnC_{mn}} \tag{A.56}$$

$$f = 1 - \frac{64}{\pi^4}\sum_{m,n\ odd}\frac{1}{m^2n^2C_{mn}} \tag{A.57}$$

Where:

$$C_{mn} = 1 - i\frac{\pi^2\delta^2}{8y_0^2z_0^2}(m^2z_0^2 + n^2y_0^2) \tag{A.58}$$

Theses functions are also known for circular pores with radius $R = 2r_h$:

$$h = \frac{J_0[(i-1)r/\delta]}{J_0[(i-1)R/\delta]} \tag{A.59}$$

$$f = \frac{2J_1[(i-1)R/\delta]}{J_0[(i-1)R/\delta](i-1)R/\delta} \tag{A.60}$$

For pins arranged in a triangular array with the spaces between pins oriented along the direction of acoustic oscillations. Each pin of radius r_i and the center-to-center distance

between the pins is $2\pi r_0/\sqrt[4]{3} \simeq 1.905 r_0$ (Swift and Keolian 1993):

$$h \simeq \frac{Y_1(\alpha_0)J_0(\alpha) - J_1(\alpha_0)Y_0(\alpha)}{Y_1(\alpha_0)J_0(\alpha_i) - J_1(\alpha_0)Y_0(\alpha_i)} \tag{A.61}$$

Here: Y is Neumann function, J is Bessel function

$$f \simeq \frac{2\alpha_i}{\alpha_0^2 - \alpha_i^2} \frac{Y_1(\alpha_0)J_1(\alpha_i) - J_1(\alpha_0)Y_1(\alpha_i)}{Y_1(\alpha_0)J_0(\alpha_i) - J_1(\alpha_0)Y_0(\alpha_i)} \tag{A.62}$$

Where $\alpha = (i-1)r/\delta$

A.3 The correlations for the thermal properties factor

For parallel plates

$$\varepsilon_s = \left[\frac{k\rho_m c_p}{k_s \rho_s c_s}\right]^{1/2} \left[\frac{\tanh[(i+1)y_0/\delta_k}{\tanh[(i+1)l/\delta_s}\right] \tag{A.63}$$

For rectangular channels

$$\varepsilon_s = \left[\frac{k\rho_m c_p}{k_s \rho_s c_s}\right]^{1/2} \left[\frac{f_k(i+1)ab/\delta_k(a+b)}{\tanh[(i+1)l/\delta_s]}\right] \tag{A.64}$$

For circular pores

$$\varepsilon_s = \left[\frac{k\rho_m c_p}{k_s \rho_s c_s}\right]^{1/2} \left[\frac{f_k(i+1)r_0/2\delta_k}{\tanh[(i+1)l/\delta_s]}\right] \tag{A.65}$$

For pin arrays

$$\varepsilon_s = \left[\frac{k\rho_m c_p}{k_s \rho_s c_s}\right]^{1/2} \left[\frac{J_0\sqrt{-i\omega/\kappa_s} r_i}{J_1\sqrt{-i\omega/\kappa_s} r_i} f_k \sqrt{-i\omega/k} \frac{r_0^2 - r_i^2}{2r_i}\right] \tag{A.66}$$

$$\kappa = \frac{k}{\delta_k c_p}, \kappa_s = \frac{k_s}{\delta_s c_s} \tag{A.67}$$

$$r_0^2 = \frac{\sqrt{3}}{2\pi}(2y_0)^2 \tag{A.68}$$

Here: the superscript, s, is used for all the properties of the solid material. For parallel plate geometry: y_0 represents half of the plate spacing, and l is half of the plate thickness. For rectangular pore structure: a is half of the rectangular pore's width, and b is half of the pore's breadth. For circular pores, r_0 and l are the radius of the pores and half of the thickness of the solid sheet between the pores, respectively. For pin array structure, r_i and y_0 are pin radius and the center-to-center distance between adjacent pins in the hexagonal array arrangements of pins, respectively.

APPENDIX B

SUPPLEMENTARY DATA FOR CHAPTER 4

B.1 DeltaEC model of the single core thermoacoustic system

```
TITLE
!->C:\Users\eaxwk\Desktop\DeltaEC output files\1500_09102018_60cm.out
!Created@19:41:07  25-Sep-2019 with DeltaEC version 6.4b2.7!under win32,
using Win 6.2.9200 () under Python 2.7.9.
!---------------------------------  0 ---------------------------------
BEGIN      the setup
 1.0132E+5  a Mean P Pa
   75.905   b Freq   Hz       G
  363.00    c TBeg   K
 5248.0     d |p|    Pa       G
     0.0000 e Ph(p)  deg
 2.9247E-2  f |U|    m^3/s    G
   38.025   g Ph(U)  deg      G
air           Gas type
!---------------------------------  1 ---------------------------------
RPN        Edot passing this point
     0.0000 a G or T                    60.455                    A Watt
                                        60.455                    B Watt
Htot ; Edot
!---------------------------------  2 ---------------------------------
HX         AHX
 5.4250E-2  a Area   m^2                 5276.7     A |p|    Pa
    0.1150  b GasA/A                    -0.55243    B Ph(p)  deg
 2.5000E-2  c Length m                   2.7431E-2  C |U|    m^3/s
```

```
 1.4670E-3  d y0     m                    33.449   D Ph(U)  deg
 -794.95    e HeatIn W        G         -734.5     E Htot   W
  300.00    f SolidT K                   59.999   F Edot   W
                                        363.00    G GasT   K
ideal           Solid type              247.50    H SolidT K
!--------------------------------  3 --------------------------------
RPN        Dissipation of PAc. in AHX
     0.0000 a G or T                  0.45548                  A ChngeMe
1A 2F -
!--------------------------------  4 --------------------------------
DUCT       Regen cold end dead space
 1.4250E-2  a Area   m^2               5277.2     A |p|    Pa
    0.7400  b Perim  m                -0.56057    B Ph(p)  deg
 1.0000E-3  c Length m                 2.7289E-2  C |U|    m^3/s
                                         33.008   D Ph(U)  deg
                                       -734.5     E Htot   W
stainless          Solid type           59.996   F Edot   W
!--------------------------------  5 --------------------------------
RPN        Complex Z
     0.0000 a G or T                  20.828                   A ChngeMe
                                      -33.569                  B ChngeMe
                                      3.6471E-4                C ChngeMe
dk ; p1 U1 / arg ; p1 U1 / 6a * mag rho / a /
!--------------------------------  6 --------------------------------
STKSCREEN  Regenerator
 4.0000E-2  a Area   m^2               4848.6     A |p|    Pa
    0.7330  b VolPor                    -3.0319  B Ph(p)  deg
 1.2000E-2  c Length m                 3.4159E-2  C |U|    m^3/s
 5.6000E-5  d rh     m                   17.912   D Ph(U)  deg
    0.3000  e ksFrac                   -734.5     E Htot   W
                                         77.339   F Edot   W
                                        363.00    G TBeg   K
stainless          Solid type           519.65    H TEnd   K
!--------------------------------  7 --------------------------------
RPN        Onset temperature difference
     0.0000 a G or T                  156.65                   A ChngeMe
6H 6G -
!--------------------------------  8 --------------------------------
RPN        Phi in reg.
     0.0000 a G or T                  -20.944                  A ChngeMe
6B 6D -
!--------------------------------  9 --------------------------------
DUCT       All regen hot end dead space
 3.1500E-2  a Area   m^2               4850.0     A |p|    Pa
    2.0000  b Perim  m                   -3.1106  B Ph(p)  deg
 2.0000E-2  c Length m                 3.1884E-2  C |U|    m^3/s
                                          0.33447 D Ph(U)  deg
```

```
                                        -734.5     E Htot   W
stainless           Solid type            77.178   F Edot   W
!---------------------------------- 10 ----------------------------------
HX          HHX heat transfer area used/not acoustic area
 7.1500E-2  a Area   m^2                4845.6     A |p|    Pa
    0.7000  b GasA/A                     -3.209   B Ph(p)  deg
 4.0000E-2  c Length m                  4.4207E-2  C |U|    m^3/s
 4.5000E-3  d y0     m                   -48.467   D Ph(U)  deg
 1500.0     e HeatIn W                   765.50    E Htot   W
  578.00    f SolidT K                    75.391   F Edot   W
                                         519.65    G GasT   K
stainless           Solid type         1033.6     H SolidT K
!---------------------------------- 11 ----------------------------------
JOIN        Change Me
                                        4845.6     A |p|    Pa
                                          -3.209   B Ph(p)  deg
                                        4.3846E-2  C |U|    m^3/s
                                         -48.467   D Ph(U)  deg
                                         765.50    E Htot   W
                                          74.776   F Edot   W
                                         519.65    G TBeg   K
                                         522.82    H TEnd   K
!---------------------------------- 12 ----------------------------------
STKDUCT     Thermal Buffer Tube
 1.8000E-3  a Area   m^2      Mstr      4793.2     A |p|    Pa
 0.15025    b Perim  m        12a         -3.8136  B Ph(p)  deg
 8.0000E-2  c Length m                  4.3846E-2  C |U|    m^3/s
 1.1600E-3  d WallA  m^2                 -48.464   D Ph(U)  deg
                                         765.50    E Htot   W
                                          74.756   F Edot   W
                                         522.82    G TBeg   K
stainless           Solid type          363.00    H TEnd   K
!---------------------------------- 13 ----------------------------------
RPN         Force TBT ambient temperature
sameas   0c a =A?                     363.00                    A ChngeMe
Tm
!---------------------------------- 14 ----------------------------------
RPN         how much heat must be rejected here? Resonator is insulated
  100.00    a G or T                  -644.59                   A ChngeMe
10e 2e + 1A - ~
!---------------------------------- 15 ----------------------------------
JOIN        Change Me
                                        4793.2     A |p|    Pa
                                          -3.8136  B Ph(p)  deg
                                        4.3488E-2  C |U|    m^3/s
                                         -48.464   D Ph(U)  deg
                                         765.50    E Htot   W
```

```
                                          74.146   F Edot   W
                                         363.00    G TBeg   K
                                         365.72    H TEnd   K
!--------------------------------- 16 ---------------------------------
HX         Change Me
 7.1818E-3  a Area   m^2                4759.1     A |p|    Pa
    0.7130  b GasA/A                     -4.1392  B Ph(p)  deg
 1.0000E-2  c Length m                  4.4069E-2  C |U|    m^3/s
 1.4670E-3  d y0     m                   -49.303   D Ph(U)  deg
sameas  14A e HeatIn W                   120.91    E Htot   W
     0.0000 f SolidT K                    73.937   F Edot   W
                                         365.72    G GasT   K
ideal           Solid type               148.25    H SolidT K
!--------------------------------- 17 ---------------------------------
DUCT
 1.0000E-2  a Area   m^2      Mstr       4751.7     A |p|    Pa
    0.4526  b Perim  m        17a          -4.2254  B Ph(p)  deg
 5.0000E-3  c Length m                  4.4639E-2  C |U|    m^3/s
                                         -50.032   D Ph(U)  deg
                                         120.91    E Htot   W
stainless           Solid type            73.929   F Edot   W
!--------------------------------- 18 ---------------------------------
IESPEAKER  Linear Alternator
 1.9000E-2  a Area   m^2                4573.8     A |p|    Pa
    4.0000  b R      ohms                 -2.9047  B Ph(p)  deg
 1.0000E-3  c L      H                  4.4609E-2  C |U|    m^3/s
    7.0000  d BLProd T-m                 -50.072   D Ph(U)  deg
 2.0000E-2  e M      kg                  117.40    E Htot   W
 4337.0     f K      N/m                  69.356   F Edot   W
    0.1800  g Rm     N-s/m                -3.5071  G WorkIn W
    0.48353 h |I|    A        G           14.508   H Volts  V
  -50.052   i Ph(I)  deg      G            0.48353 I Amps   A
                                         179.09    J Ph(V/I) deg
                                         207.80    K |Px|   Pa
stainless           Solid type           145.29    L Ph(Px) deg
!--------------------------------- 19 ---------------------------------
RPN        DP across the alternator
     0.0000 a G or T                   177.86                    A ChngeMe
17A 18A -
!--------------------------------- 20 ---------------------------------
DUCT
 3.8000E-3  a Area   m^2      Mstr       3927.5     A |p|    Pa
    0.2790  b Perim  m        20a          -10.894  B Ph(p)  deg
    0.1500  c Length m                  5.0569E-2  C |U|    m^3/s
                                         -56.86    D Ph(U)  deg
                                         117.40    E Htot   W
stainless           Solid type            69.026   F Edot   W
```

```
!---------------------------------- 21 ----------------------------------
DUCT
 3.8000E-3  a Area   m^2      Mstr       2343.3     A |p|    Pa
    0.2790  b Perim  m        21a         -90.633   B Ph(p)  deg
    0.6000  c Length m                   5.9699E-2  C |U|    m^3/s
                                          -75.384   D Ph(U)  deg
                                          117.40    E Htot   W
stainless           Solid type            67.483   F Edot   W
!---------------------------------- 22 ----------------------------------
BRANCH     Stub
     0.0000 a Re(Zb) Pa-s/m^3            2343.3     A |p|    Pa
-1.0549E+5  b Im(Zb) Pa-s/m^3             -90.633   B Ph(p)  deg
     0.0000 c HtotBr W                   5.7965E-2  C |U|    m^3/s
                                          -97.083   D Ph(U)  deg
                                          117.40    E Htot   W
                                           67.483   F Edot   W
                                             0.0000 G EdotBr W
!---------------------------------- 23 ----------------------------------
DUCT
 3.8000E-3  a Area   m^2      Mstr       3611.6     A |p|    Pa
    0.2790  b Perim  m        23a        -156.26    B Ph(p)  deg
    0.5000  c Length m                   5.0390E-2  C |U|    m^3/s
                                         -113.0     D Ph(U)  deg
                                          117.40    E Htot   W
ideal           Solid type              66.273     F Edot   W
!---------------------------------- 24 ----------------------------------
RPN        Phi
     0.0000 a G or T                  -43.254                   A ChngeMe
23B 23D -
!---------------------------------- 25 ----------------------------------
DUCT
 3.8000E-3  a Area   m^2      Mstr       5318.9     A |p|    Pa
    0.2790  b Perim  m        25a        -179.66    B Ph(p)  deg
    0.5000  c Length m                   3.0197E-2  C |U|    m^3/s
                                         -144.09    D Ph(U)  deg
                                          117.40    E Htot   W
ideal           Solid type              65.325     F Edot   W
!---------------------------------- 26 ----------------------------------
DUCT
!P_A is measured here
 3.8000E-3  a Area   m^2      Mstr       4730.4     A |p|    Pa
    0.2790  b Perim  m        26a         155.37    B Ph(p)  deg
    0.8000  c Length m                   3.8571E-2  C |U|    m^3/s
                                          109.99    D Ph(U)  deg
                                          117.40    E Htot   W
ideal           Solid type              64.081     F Edot   W
!---------------------------------- 27 ----------------------------------
```

```
DUCT
!P_B is measured here
 3.8000E-3  a Area   m^2      Mstr       4208.9     A |p|    Pa
    0.2790  b Perim  m        27a         149.15    B Ph(p)  deg
    0.1400  c Length m                   4.4373E-2  C |U|    m^3/s
                                          102.26    D Ph(U)  deg
                                          117.40    E Htot   W
ideal           Solid type                 63.816   F Edot   W
!---------------------------------- 28 ----------------------------------
DUCT
 3.8000E-3  a Area   m^2      Mstr       5248.0     A |p|    Pa
    0.2790  b Perim  m        28a        2.6065E-14 B Ph(p)  deg
    1.5600  c Length m                   2.9247E-2  C |U|    m^3/s
                                            38.025  D Ph(U)  deg
                                          117.40    E Htot   W
ideal           Solid type                 60.455   F Edot   W
!---------------------------------- 29 ----------------------------------
RPN        stroke (mm peak-to-peak), max 18mm
   17.000   a G or T                    6.4552                    A mm p-p
U1 mag 18a / w / 2 * 1000 *
!---------------------------------- 30 ----------------------------------
RPN        What capacitance would "cancel" the alternator's inductance?
     0.0000 a G or T                    4.3964E-3                 A Farad
w sqrd 18c * inv
!---------------------------------- 31 ----------------------------------
RPN        a = Load Resistor (Ohm). A = complex load impedance
   30.000   a G or T                    (30.000, -0.47692)        A Ohm
inp i w * 30A * inv +
!---------------------------------- 32 ----------------------------------
RPN        Target V\I = magnitude of electrical impedance
     0.0000 a =A?                       -3.5527E-15               A Ohm
18H 18I / 31A mag -
!---------------------------------- 33 ----------------------------------
RPN        Target phase(V/I) = phase(electrical impedance)
     0.0000 a =A?                       3.9857E-14                A ChngeMe
18J 180 - 31A arg -
!---------------------------------- 34 ----------------------------------
RPN        Electrical output
sameas  18G a G or T                    3.5071                    A ChngeMe
18G -1 *
!---------------------------------- 35 ----------------------------------
RPN        Force electrical load to be resistive
 -180.0     a G or T                    179.09                    A ChngeMe
18J
!---------------------------------- 36 ----------------------------------
RPN        Thermal-to-electrical efficiency
     0.0000 a G or T                    0.2338                    A ChngeMe
```

```
18G 10e / 100 * -1 *
!---------------------------------- 37 ----------------------------------
RPN        Thermal-to-acoustic conversion efficiency
     0.0000 a G or T                    4.0303                     A ChngeMe
Edot 10e / 100 *
!---------------------------------- 38 ----------------------------------
RPN        Set p1 mag
    1.0000  a =A?                       1.0000                     A ChngeMe
p1 mag 0d /
!---------------------------------- 39 ----------------------------------
RPN        Set p1 phase
    1.0000  a =A?                       1.0000                     A ChngeMe
p1 arg 0e - 1 +
!---------------------------------- 40 ----------------------------------
RPN        Set mag U1
    1.0000  a =A?                       1.0000                     A ChngeMe
U1 mag 0f /
!---------------------------------- 41 ----------------------------------
RPN        Set U1 phase
    1.0000  a =A?                       1.0000                     A ChngeMe
U1 arg 0g - 1 +
!---------------------------------- 42 ----------------------------------
RPN        Generator efficiency
     0.0000 a G or T                    0.43838                    A ChngeMe
18G 800.0 / 100 * -1 *
! The restart information below was generated by a previous run
! and will be used by DeltaEC the next time it opens this file.
guessz   0b   0d   0f   0g   2e  18h  18i
xprecn -1.4619E-4  -4.3217E-2   1.5903E-7  -1.2058E-4  -6.5458E-4   3.7277E-6  -2.6504E-4
targs   13a  32a  33a  38a  39a  40a  41a
hilite 2F 6F 9F 10F 12F 18G 21C 22C 22F 28F
mstr-slave 9 12 -2 17 -2 20 -2 21 -2 23 -2 25 -2 26 -2 27 -2 28 -2
! Plot start, end, and step values.  May be edited if you wish.
! Outer Loop:                       | Inner Loop .
```

B.2 Calibration certificate for the pressure transducers

IMPRESS
SENSORS & SYSTEMS

Unit 6 Mercury House, Calleva Park
Aldermaston, Berkshire, RG7 8PN
Tel: +44 (0)118 981 7980
Fax:+44 (0)118 981 7990
e-mail: sales@impress-sensors.co.uk
Website: www.impress-sensors.co.uk

Pressure - Temperature - Level - Distance - Control - Indication - Data logging

Calibration Certificate

Customer Order Number Quote IMPQ11777-2		Impress Sales Order IMPS-9482 Line 1	
Type IMP-A5000-1A4-BXV-00-063		Operator Robin Stacey	Date 07/03/12
Supply 2 - 30V dc	Range 0 - 5 Bar Abs	Output mV/V / 4-wire	Test Voltage 10Vdc

Serial Number		Zero	FSO	Span	Non-Linearity		
168425		-1.210	32.530	33.740	-0.075		
168426		-1.389	32.830	34.219	-0.118	2922	196
168427		-0.450	32.300	32.750	-0.084		
168428		-1.454	32.150	33.604	-0.116		
168429		-2.095	23.790	25.885	-0.110	5863	420
168430		-1.288	29.900	31.188	-0.139	3206	205
168431		-1.133	30.700	31.833	-0.068	3141	153
168432		2.103	32.280	30.177	-0.102		

Score
Equipment
Camera centre

Note: Non-Linearity = % of Span BFSL

Wiring Designation		Small Plug & Socket (Code A)	Large Plug & Socket (Code B)	IP66 Cable (Code C)	AMP 6-pin Bayonnet (Code D)	IP68 Vented Cable (Code E)	Binder 6-pin connector (Code F)	M12x1, 4-pin connector (Code G)
2-wire	+ve Supply	Pin 1	Pin 1	Red	Pin 1	Red	Pin 1	Pin 1
	-ve Supply	Pin 2	Pin 2	Blue	Pin 2	Blue	Pin 2	Pin 2
	Ground	Earth Pin	Earth Pin	Green	Earth Pin	White	Pin 3	Pin 3
3-wire	+ve Supply	Pin 1	Pin 1	Red	Pin 1	Red	Pin 1	Pin 1
	-ve Supply	Pin 2	Pin 2	Blue	Pin 2	Blue	Pin 2	Pin 2
	+ve Output	Pin 3	Pin 3	Green	Pin 3	White	Pin 3	Pin 3
	Ground	Earth Pin	Earth Pin	Yellow	Earth Pin	Yellow	Pin 4	Pin 4
4-wire	+ve Supply	Pin 1	Pin 1	Red	Pin 1	Red	Pin 1	Pin 1
	-ve Supply	Pin 2	Pin 2	Blue	Pin 2	Blue	Pin 2	Pin 2
	+ve Output	Pin 3	Pin 3	Green	Pin 3	White	Pin 3	Pin 3
	-ve Output	Earth Pin	Earth Pin	Yellow	Pin 4	Yellow	Pin 4	Pin 4

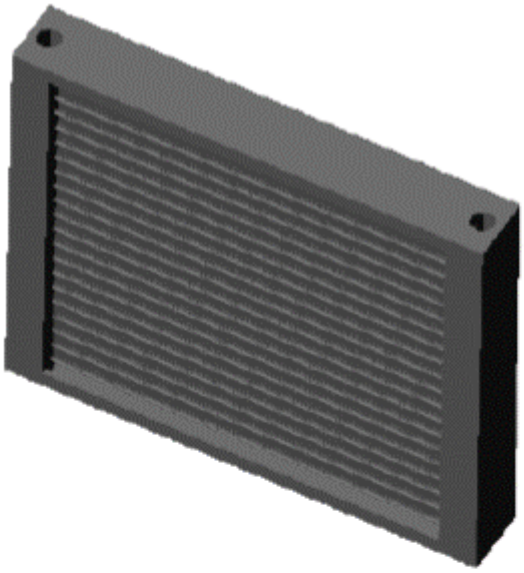
APPENDIX C

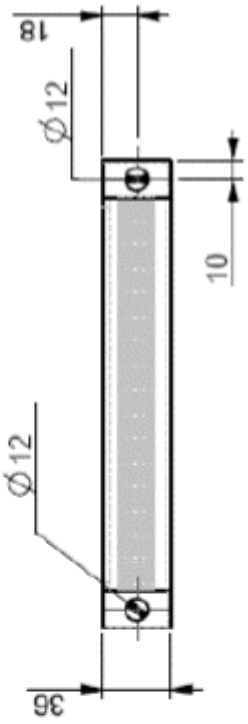
SUPPLEMENTARY DATA FOR CHAPTER 5

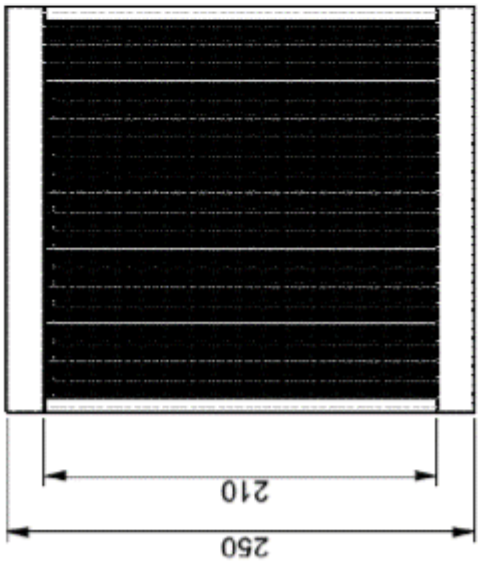
C.1 Detailed drawings of the double core thermoacoustic system

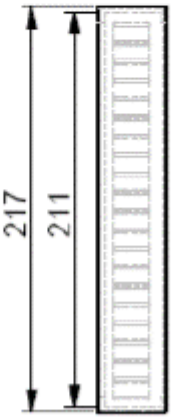
* All units are in mm

(C.1.1) The ambient heat exchanger AHX

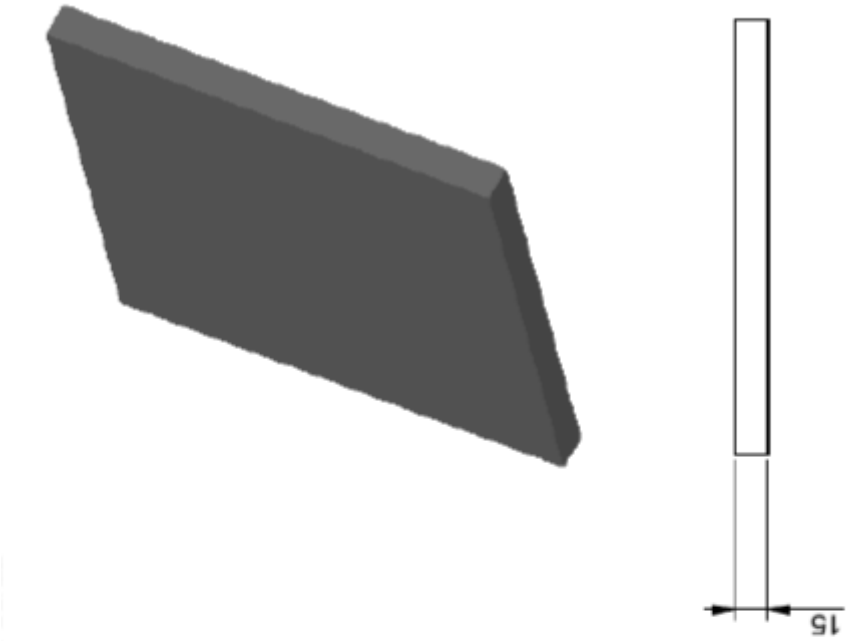




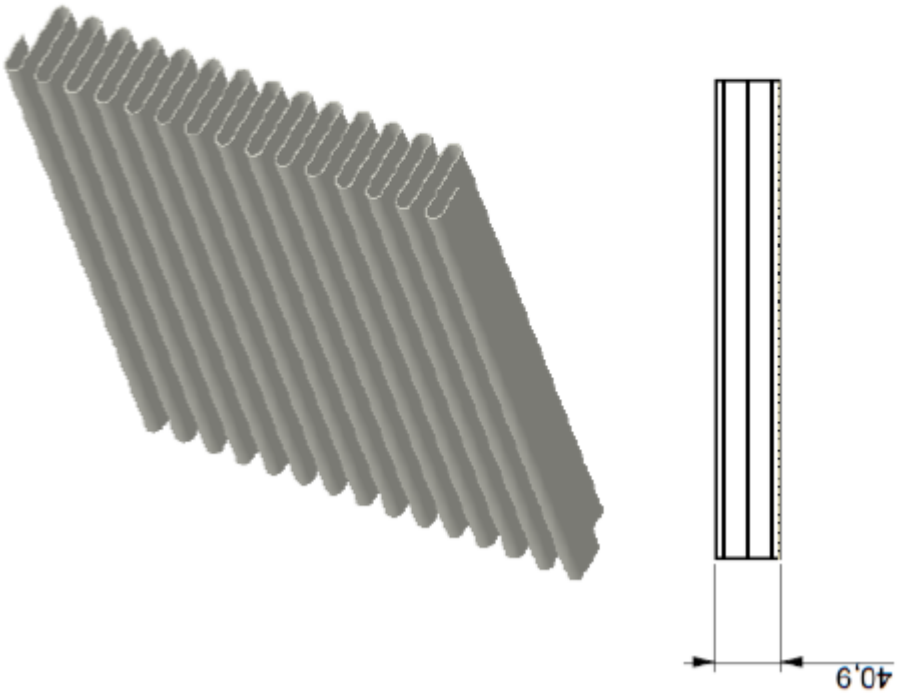


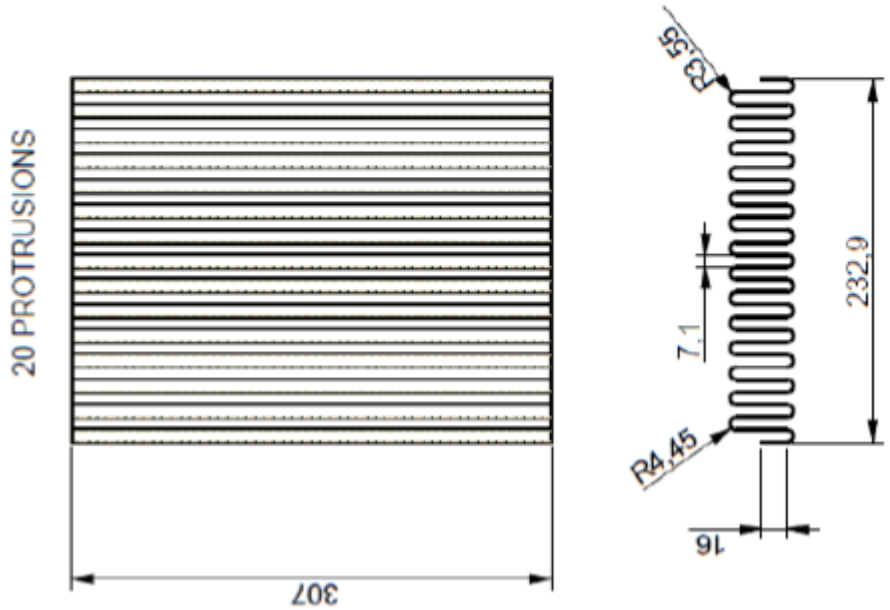


(C.1.2) The regenerator

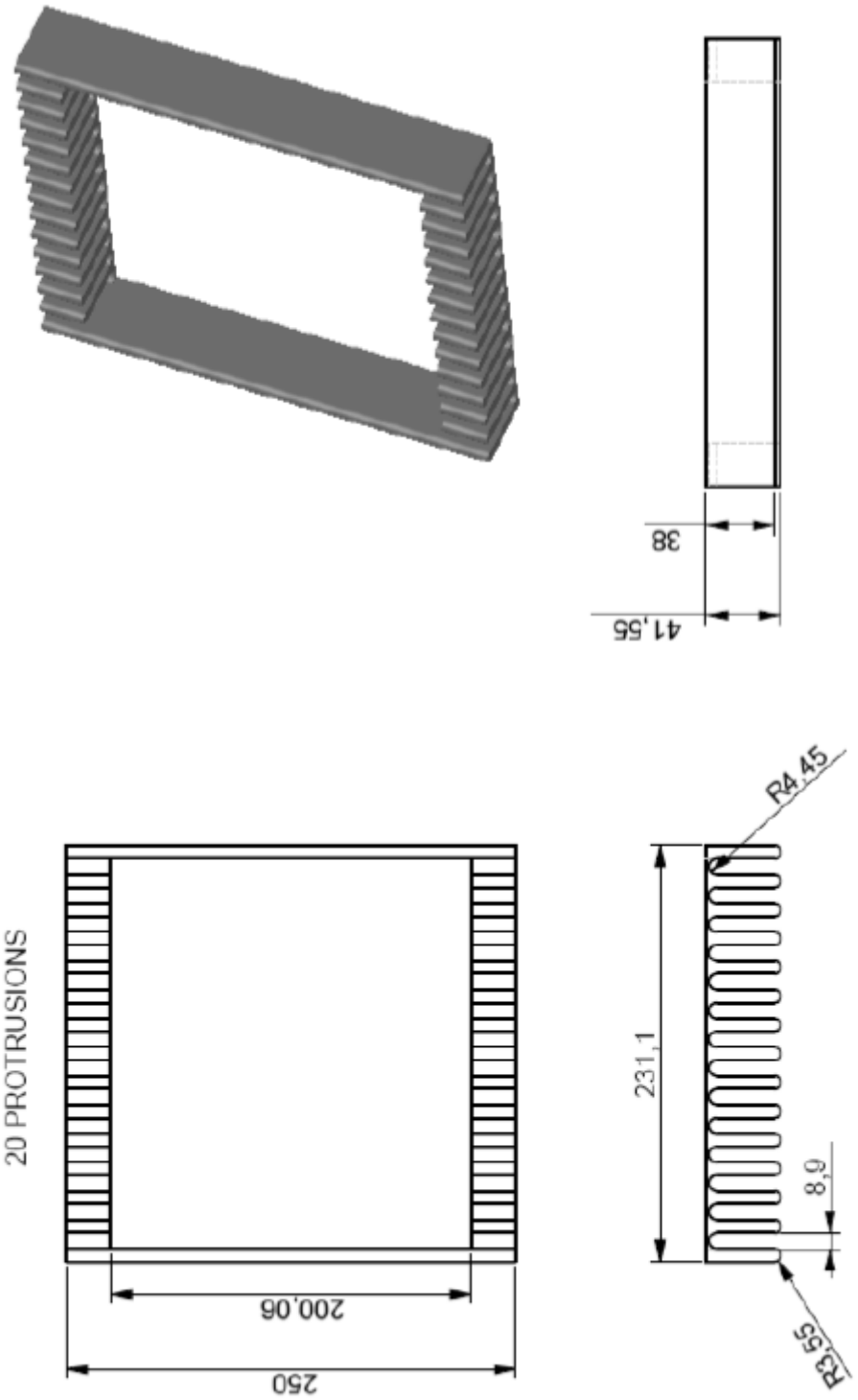


(C.1.3) The hot heat exchanger HHX

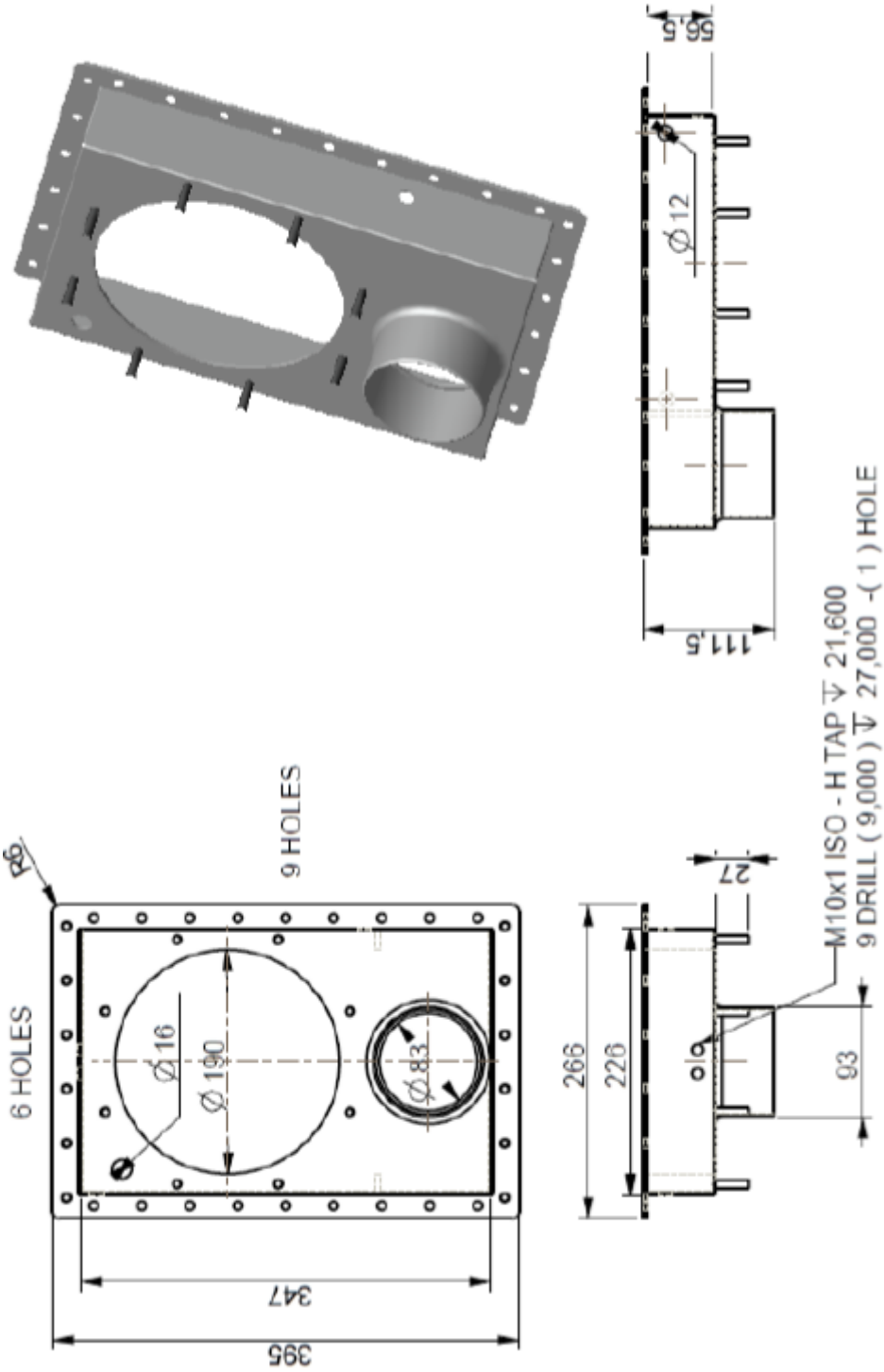




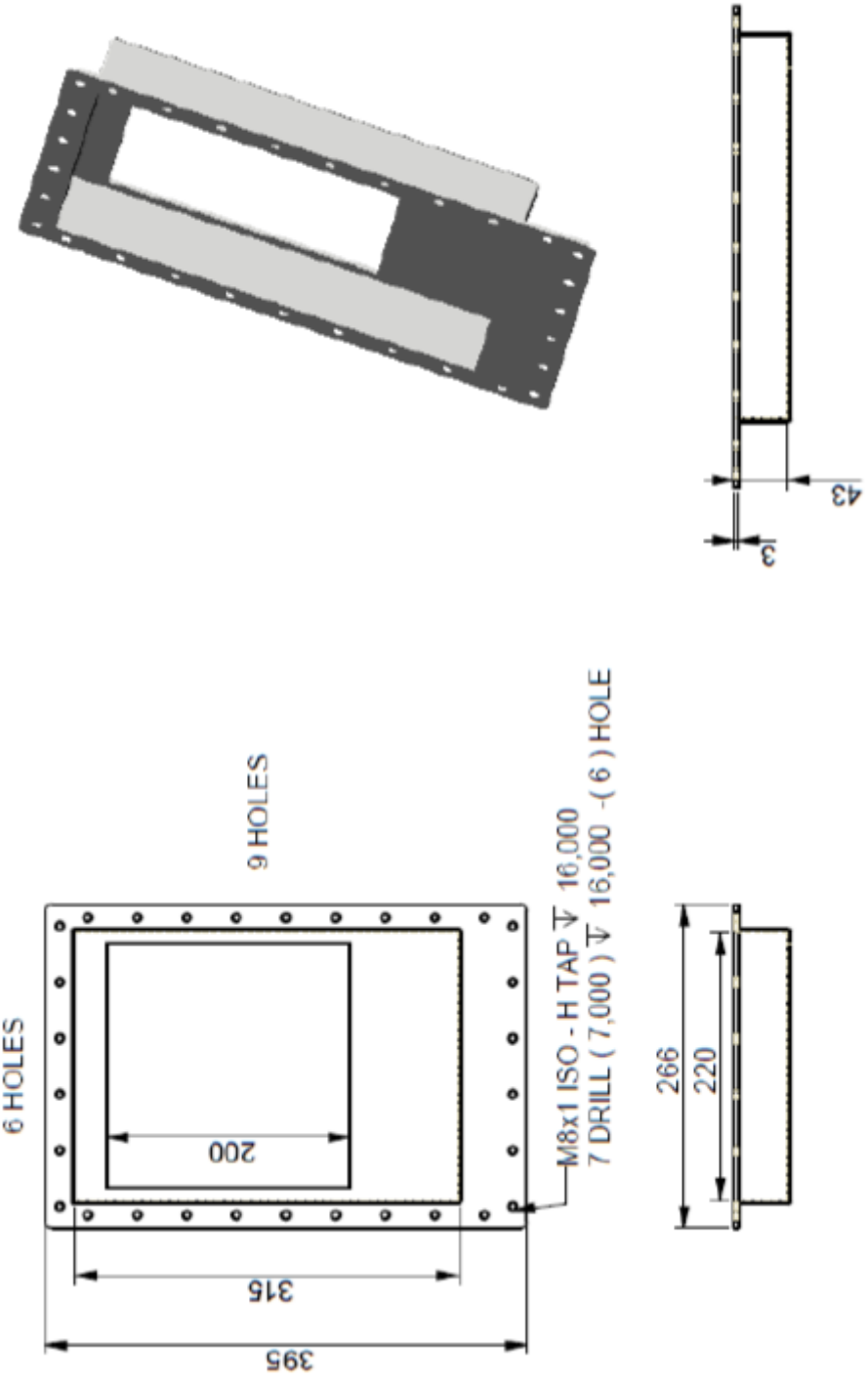
(C.1.4) HHX Insulator



(C.1.5) The upper housing

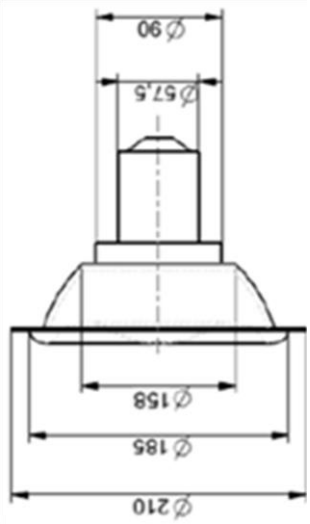


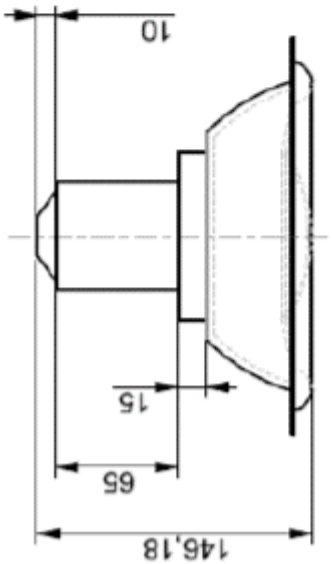
(C.1.6) The lower housing

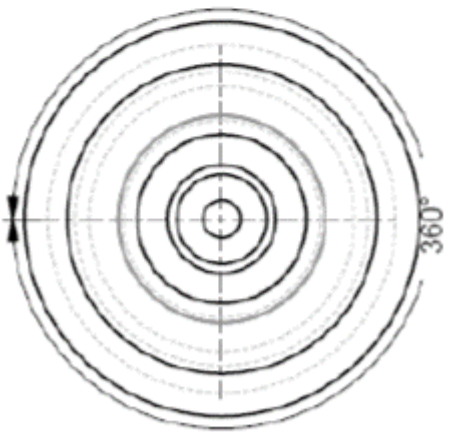


(C.1.7) The loudspeaker









C.2 DeltaEC output file for evenly heated twin-core system

```
TITLE
!->C:\Users\eaxwk\Desktop\DeltaEC output files\last_run\50%_50%.out
!Created@19:17:22  25-Sep-2019 with DeltaEC version 6.4b2.7!under win32,
using Win 6.2.9200 () under Python 2.7.9.
!--------------------------------  0 --------------------------------
BEGIN      the setup
 1.0132E+5  a Mean P Pa
 73.047     b Freq   Hz       G
 363.00     c TBeg   K
 2777.7     d |p|    Pa       G
 0.0000     e Ph(p)  deg
 4.7001E-2  f |U|    m^3/s    G
 26.452     g Ph(U)  deg      G
air           Gas type
!--------------------------------  1 --------------------------------
RPN        Edot passing this point
     0.0000 a G or T                   58.444                    A Watt
                                       58.444                    B Watt
Htot ; Edot
!--------------------------------  2 --------------------------------
DUCT       Change Me
sameas   4a a Area   m^2      Mstr       2779.2     A |p|    Pa
    0.82567 b Perim  m        2a        -7.1600E-2  B Ph(p)  deg
 1.0000E-2  c Length m                   4.5031E-2  C |U|    m^3/s
 5.0000E-4  d Srough                       20.886   D Ph(U)  deg
                                           58.444   E Htot   W
ideal           Solid type                58.436   F Edot   W
!--------------------------------  3 --------------------------------
JOIN       Change Me
                                        2779.2     A |p|    Pa
                                       -7.1600E-2  B Ph(p)  deg
                                        4.4751E-2  C |U|    m^3/s
                                          20.886   D Ph(U)  deg
                                          58.444   E Htot   W
                                          58.073   F Edot   W
                                         363.00    G TBeg   K
                                         363.00    H TEnd   K
!--------------------------------  4 --------------------------------
HX         Ambient heat exchanger AHX2
 5.4250E-2  a Area   m^2               2781.4     A |p|    Pa
    0.7000  b GasA/A                  -0.35799    B Ph(p)  deg
 2.5000E-2  c Length m                 4.1930E-2  C |U|    m^3/s
 1.4670E-3  d y0     m                    9.5843  D Ph(U)  deg
 -645.07    e HeatIn W        G        -586.63    E Htot   W
```

```
  300.00    f SolidT K                    57.436   F Edot   W
                                         363.00    G GasT   K
ideal           Solid type               302.88    H SolidT K
!---------------------------------  5 ---------------------------------
DUCT       Regen cold end dead space
 1.4250E-2  a Area   m^2                2782.1     A |p|    Pa
    0.7400  b Perim  m                 -0.44335    B Ph(p)  deg
 3.1750E-3  c Length m                  4.1859E-2  C |U|    m^3/s
                                           9.0336  D Ph(U)  deg
                                        -586.63    E Htot   W
stainless          Solid type            57.433   F Edot   W
!---------------------------------  6 ---------------------------------
RPN        Complex Z
     0.0000 a G or T                  7.1584                    A ChngeMe
                                      -9.4769                   B ChngeMe
                                      3.7177E-4                 C ChngeMe
dk ; p1 U1 / arg ; p1 U1 / 7a * mag rho / a /
!---------------------------------  7 ---------------------------------
STKSCREEN  Regenerator2
 4.0000E-2  a Area   m^2                2470.0     A |p|    Pa
    0.7300  b VolPor                     -1.2866  B Ph(p)  deg
 1.2000E-2  c Length m                  6.2888E-2  C |U|    m^3/s
 9.7000E-5  d rh     m                     1.9495  D Ph(U)  deg
    0.1500  e ksFrac                    -586.63    E Htot   W
                                          77.544   F Edot   W
                                         363.00    G TBeg   K
stainless          Solid type            556.90    H TEnd   K
!---------------------------------  8 ---------------------------------
RPN        Temperature difference across reg.2
     0.0000 a G or T                  193.90                    A ChngeMe
7H 7G -
!---------------------------------  9 ---------------------------------
RPN        TAE2 amplified power
     0.0000 a G or T                  20.108                    A ChngeMe
7F 4F -
!--------------------------------- 10 ---------------------------------
DUCT       All regen hot end dead space
 3.1500E-2  a Area   m^2                2470.1     A |p|    Pa
    2.0000  b Perim  m                   -1.4053  B Ph(p)  deg
 8.7000E-3  c Length m                  6.2785E-2  C |U|    m^3/s
 6.0000E-4  d Srough                   -5.9545E-2  D Ph(U)  deg
                                        -586.63    E Htot   W
stainless          Solid type            77.523   F Edot   W
!--------------------------------- 11 ---------------------------------
HX         HHX2 heat transfer area used/not acoustic area
 7.1500E-2  a Area   m^2                2467.8     A |p|    Pa
    0.7500  b GasA/A                     -1.7338  B Ph(p)  deg
```

```
 4.0000E-2  c Length m                    6.4341E-2  C |U|    m^3/s
 4.5000E-3  d y0     m                     -15.878   D Ph(U)  deg
 1250.0     e HeatIn W                     663.37    E Htot   W
  578.00    f SolidT K                      76.983   F Edot   W
                                           556.90    G GasT   K
stainless           Solid type            810.22    H SolidT K
!---------------------------------- 12 ----------------------------------
JOIN
                                          2467.8     A |p|    Pa
                                            -1.7338  B Ph(p)  deg
                                          6.3973E-2  C |U|    m^3/s
                                           -15.878   D Ph(U)  deg
                                           663.37    E Htot   W
                                            76.542   F Edot   W
                                           556.90    G TBeg   K
                                           565.23    H TEnd   K
!---------------------------------- 13 ----------------------------------
STKDUCT    Thermal Buffer Tube TBT2
 8.3300E-3  a Area   m^2      Mstr        2462.3     A |p|    Pa
 0.32323    b Perim  m        13a           -2.2251  B Ph(p)  deg
 8.0000E-2  c Length m                    6.3962E-2  C |U|    m^3/s
 1.1600E-3  d WallA  m^2                   -16.216   D Ph(U)  deg
                                           663.37    E Htot   W
                                            76.412   F Edot   W
                                           565.23    G TBeg   K
stainless           Solid type            363.00    H TEnd   K
!---------------------------------- 14 ----------------------------------
RPN        Force TBT ambient temperature
sameas   0c a =A?                        363.00                   A ChngeMe
Tm
!---------------------------------- 15 ----------------------------------
RPN        ChangeMe
     0.0000 a G or T                     29.222                   A ChngeMe
0.5 1A *
!---------------------------------- 16 ----------------------------------
RPN        how much heat must be rejected here? Resonator is insulated
     0.0000 a G or T                    -575.71                   A ChngeMe
11e 4e + 15A - ~
!---------------------------------- 17 ----------------------------------
JOIN       Change Me
                                          2462.3     A |p|    Pa
                                            -2.2251  B Ph(p)  deg
                                          6.3597E-2  C |U|    m^3/s
                                           -16.216   D Ph(U)  deg
                                           663.37    E Htot   W
                                            75.975   F Edot   W
                                           363.00    G TBeg   K
```

```
                                        370.84    H TEnd   K
!--------------------------------- 18 ---------------------------------
HX         Secondary ambient heat exchanger SAHX2
 7.1818E-3  a Area   m^2                2441.3     A |p|    Pa
    0.7130  b GasA/A                     -3.5478  B Ph(p)  deg
 1.0000E-2  c Length m                 6.3676E-2  C |U|    m^3/s
 1.4670E-3  d y0     m                  -16.594   D Ph(U)  deg
sameas  16A e HeatIn W                   87.666   E Htot   W
     0.0000 f SolidT K                   75.720   F Edot   W
                                        370.84    G GasT   K
ideal           Solid type              172.64    H SolidT K
!--------------------------------- 19 ---------------------------------
DUCT
 1.0000E-2  a Area   m^2      Mstr       2340.4     A |p|    Pa
    0.4526  b Perim  m        19a         -13.54    B Ph(p)  deg
    0.1500  c Length m                 6.6295E-2  C |U|    m^3/s
                                        -26.60    D Ph(U)  deg
                                         87.666   E Htot   W
stainless           Solid type           75.572   F Edot   W
!--------------------------------- 20 ---------------------------------
IESPEAKER  Linear Alternator
 1.9600E-2  a Area   m^2                1614.2     A |p|    Pa
 4.0000     b R      ohms                  0.73702 B Ph(p)  deg
 1.0000E-3  c L      H                  6.6277E-2  C |U|    m^3/s
 14.000     d BLProd T-m                -26.605   D Ph(U)  deg
 2.0000E-2  e M      kg                   63.262   E Htot   W
 4778.0     f K      N/m                  47.516   F Edot   W
 0.1800     g Rm     N-s/m               -24.404   G WorkIn W
 1.1409     h |I|    A        G           42.785   H Volts  V
-26.602     i Ph(I)  deg      G            1.1409  I Amps   A
                                        179.30    J Ph(V/I) deg
                                        872.21    K |Px|   Pa
stainless           Solid type          139.30    L Ph(Px) deg
!--------------------------------- 21 ---------------------------------
RPN        DP
     0.0000 a G or T                  726.21                    A ChngeMe
19A 20A -
!--------------------------------- 22 ---------------------------------
DUCT
 3.8000E-3  a Area   m^2      Mstr       3520.3     A |p|    Pa
    0.2790  b Perim  m        22a         -98.574   B Ph(p)  deg
    0.5500  c Length m                 5.7708E-2  C |U|    m^3/s
                                        -35.425   D Ph(U)  deg
                                         63.262   E Htot   W
stainless           Solid type           45.879   F Edot   W
!--------------------------------- 23 ---------------------------------
BRANCH     Stub No.2
```

```
     0.0000 a Re(Zb) Pa-s/m^3            3520.3     A |p|    Pa
-1.1078E+5  b Im(Zb) Pa-s/m^3             -98.574   B Ph(p)  deg
     0.0000 c HtotBr W                   3.2678E-2  C |U|    m^3/s
                                          -61.48    D Ph(U)  deg
                                           63.262   E Htot   W
                                           45.879   F Edot   W
                                          7.1054E-15 G EdotBr W
!---------------------------------- 24 ----------------------------------
HX          Ambient heat exchanger AHX1
 5.4250E-2  a Area   m^2                 3523.8     A |p|    Pa
    0.7000  b GasA/A                     -98.716   B Ph(p)  deg
 2.5000E-2  c Length m                   2.6818E-2  C |U|    m^3/s
 1.4670E-3  d y0     m                    -80.479   D Ph(U)  deg
 -634.6     e HeatIn W        G          -571.34    E Htot   W
  300.00    f SolidT K                     44.878   F Edot   W
                                           370.84    G GasT   K
ideal            Solid type              284.54    H SolidT K
!---------------------------------- 25 ----------------------------------
DUCT        Regen cold end dead space
 1.4250E-2  a Area   m^2                 3524.6     A |p|    Pa
    0.7400  b Perim  m                    -98.757   B Ph(p)  deg
 3.1750E-3  c Length m                   2.6659E-2  C |U|    m^3/s
                                          -81.535   D Ph(U)  deg
                                          -571.34    E Htot   W
stainless           Solid type            44.874   F Edot   W
!---------------------------------- 26 ----------------------------------
RPN         Complex Z
     0.0000 a G or T                   14.393                    A ChngeMe
                                       -17.221                   B ChngeMe
                                       3.7921E-4                 C ChngeMe
dk ; p1 U1 / arg ; p1 U1 / 27a * mag rho / a /
!---------------------------------- 27 ----------------------------------
STKSCREEN   Regenerator1
 4.0000E-2  a Area   m^2                 3338.7     A |p|    Pa
    0.7300  b VolPor                     -99.391   B Ph(p)  deg
 1.2000E-2  c Length m                   3.9602E-2  C |U|    m^3/s
 9.7000E-5  d rh     m                    -93.966   D Ph(U)  deg
    0.1500  e ksFrac                    -571.34    E Htot   W
                                           65.812   F Edot   W
                                           370.84    G TBeg   K
stainless           Solid type            581.10    H TEnd   K
!---------------------------------- 28 ----------------------------------
RPN         Temperature difference across reg.1
     0.0000 a G or T                   210.26                    A ChngeMe
27H 27G -
!---------------------------------- 29 ----------------------------------
RPN         TAE1 Amplification
```

```
     0.0000 a G or T                    20.935                    A ChngeMe
27F 24F -
!---------------------------------- 30 ----------------------------------
DUCT       All regen hot end dead space
 3.1500E-2  a Area   m^2                3338.8     A |p|    Pa
    2.0000  b Perim  m                   -99.444   B Ph(p)  deg
 8.7000E-3  c Length m                  3.9409E-2  C |U|    m^3/s
 6.0000E-4  d Srough                    -98.283   D Ph(U)  deg
                                        -571.34    E Htot   W
stainless           Solid type           65.776   F Edot   W
!---------------------------------- 31 ----------------------------------
HX         HHX1 heat transfer area used/not acoustic area
 7.1500E-2  a Area   m^2                3335.9     A |p|    Pa
    0.7500  b GasA/A                     -99.589   B Ph(p)  deg
 4.0000E-2  c Length m                  4.5067E-2  C |U|    m^3/s
 4.5000E-3  d y0     m                  -130.06    D Ph(U)  deg
 1250.0     e HeatIn W                   678.66    E Htot   W
  578.00    f SolidT K                    64.787   F Edot   W
                                         581.10    G GasT   K
stainless           Solid type           964.12    H SolidT K
!---------------------------------- 32 ----------------------------------
JOIN       Change Me
                                        3335.9     A |p|    Pa
                                         -99.589   B Ph(p)  deg
                                        4.4757E-2  C |U|    m^3/s
                                        -130.06    D Ph(U)  deg
                                         678.66    E Htot   W
                                          64.342   F Edot   W
                                         581.10    G TBeg   K
                                         588.01    H TEnd   K
!---------------------------------- 33 ----------------------------------
STKDUCT    Thermal Buffer Tube TBT1
 8.3300E-3  a Area   m^2      Mstr      3328.2     A |p|    Pa
 0.32323    b Perim  m        33a        -99.809   B Ph(p)  deg
 8.0000E-2  c Length m                  4.5015E-2  C |U|    m^3/s
 1.1600E-3  d WallA  m^2                -130.71    D Ph(U)  deg
                                         678.66    E Htot   W
                                          64.273   F Edot   W
                                         588.01    G TBeg   K
stainless           Solid type           363.00    H TEnd   K
!---------------------------------- 34 ----------------------------------
RPN        ChangeMe
     0.0000 a G or T                    29.222                    A ChngeMe
0.5 1A *
!---------------------------------- 35 ----------------------------------
RPN        Force TBT ambient temperature
  363.00    a =A?                      363.00                    A ChngeMe
```

```
Tm
!---------------------------------- 36 ----------------------------------
RPN        how much heat must be rejected here? Resonator is insulated
     0.0000 a G or T                    -591.0                     A ChngeMe
31e 24e + 20G + ~
!---------------------------------- 37 ----------------------------------
JOIN       Change Me
                                       3328.2     A |p|    Pa
                                        -99.809   B Ph(p)  deg
                                       4.4707E-2  C |U|    m^3/s
                                       -130.71    D Ph(U)  deg
                                        678.66    E Htot   W
                                         63.834   F Edot   W
                                        363.00    G TBeg   K
                                        369.70    H TEnd   K
!---------------------------------- 38 ----------------------------------
HX         Secondary ambient heat exchanger SAHX1
 7.1818E-3  a Area   m^2               3302.1     A |p|    Pa
    0.7130  b GasA/A                   -100.39    B Ph(p)  deg
 1.0000E-2  c Length m                 4.4980E-2  C |U|    m^3/s
 1.4670E-3  d y0     m                 -131.37    D Ph(U)  deg
sameas  36A e HeatIn W                   87.666   E Htot   W
     0.0000 f SolidT K                   63.673   F Edot   W
                                        369.70    G GasT   K
ideal           Solid type             166.29    H SolidT K
!---------------------------------- 39 ----------------------------------
DUCT
 3.8000E-3  a Area   m^2      Mstr     4797.2     A |p|    Pa
    0.2790  b Perim  m        39a       123.06    B Ph(p)  deg
    1.7000  c Length m                 2.5491E-2  C |U|    m^3/s
                                        128.48    D Ph(U)  deg
                                         87.666   E Htot   W
ideal           Solid type              60.869   F Edot   W
!---------------------------------- 40 ----------------------------------
BRANCH     Stub No. 1
     0.0000 a Re(Zb) Pa-s/m^3          4797.2     A |p|    Pa
-7.0000E+5  b Im(Zb) Pa-s/m^3           123.06    B Ph(p)  deg
     0.0000 c HtotBr W                  2.5763E-2  C |U|    m^3/s
                                        113.12    D Ph(U)  deg
                                         87.666   E Htot   W
                                         60.869   F Edot   W
                                       -7.1054E-15 G EdotBr W
!---------------------------------- 41 ----------------------------------
DUCT
 3.8000E-3  a Area   m^2      Mstr     2777.7     A |p|    Pa
    0.2790  b Perim  m        41a      2.7437E-13 B Ph(p)  deg
    1.5000  c Length m                 4.7001E-2  C |U|    m^3/s
```

```
                                        26.452   D Ph(U)  deg
                                        87.666   E Htot   W
ideal           Solid type              58.444   F Edot   W
!---------------------------------- 42 ----------------------------------
RPN        Alternator's stroke (mm peak-to-peak)
     0.0000 a G or T                   10.450                    A mm p-p
U1 mag 20a / w / 2 * 1000 *
!---------------------------------- 43 ----------------------------------
RPN        What capacitance would "cancel" the alternator's inductance?
     0.0000 a G or T                   4.7472E-3                 A Farad
w sqrd 20c * inv
!---------------------------------- 44 ----------------------------------
RPN        a = Load Resistor (Ohm). A = complex load impedance
   37.500   a G or T                   (37.500, -0.45897)        A Ohm
inp i w * 43A * inv +
!---------------------------------- 45 ----------------------------------
RPN        Target V\I = magnitude of electrical impedance
     0.0000 a =A?                      -4.9738E-14               A Ohm
20H 20I / 44A mag -
!---------------------------------- 46 ----------------------------------
RPN        Target phase(V/I) = phase(electrical impedance)
     0.0000 a =A?                      3.7859E-14                A ChngeMe
20J 180 - 44A arg -
!---------------------------------- 47 ----------------------------------
RPN        Electrical output
sameas  20G a G or T                   24.404                    A ChngeMe
20G -1 *
!---------------------------------- 48 ----------------------------------
RPN        Force electrical load to be resistive
 -180.0     a G or T                   179.30                    A ChngeMe
20J
!---------------------------------- 49 ----------------------------------
RPN        Total heat in
     0.0000 a G or T                   2500.0                    A ChngeMe
11e 31e +
!---------------------------------- 50 ----------------------------------
RPN        Thermal-to-acoustic efficiency
     0.0000 a G or T                   2.3378                    A ChngeMe
Edot 49A / 100 *
!---------------------------------- 51 ----------------------------------
RPN        Thermal-to-Electrical efficiency
     0.0000 a G or T                   0.97617                   A ChngeMe
20G 49A / 100 * -1 *
!---------------------------------- 52 ----------------------------------
RPN        Acoustic-to-Electrical efficiency
     0.0000 a G or T                   51.360                    A ChngeMe
20G 20F / 100 * -1 *
```

```
!---------------------------------- 53 ----------------------------------
RPN        Set p1 mag
    1.0000  a =A?                       1.0000                     A ChngeMe
p1 mag 0d /
!---------------------------------- 54 ----------------------------------
RPN        Set p1 phase
    1.0000  a =A?                       1.0000                     A ChngeMe
p1 arg 0e - 1 +
!---------------------------------- 55 ----------------------------------
RPN        Set mag U1
    1.0000  a =A?                       1.0000                     A ChngeMe
U1 mag 0f /
!---------------------------------- 56 ----------------------------------
RPN        Set U1 phase
    1.0000  a =A?                       1.0000                     A ChngeMe
U1 arg 0g - 1 +
! The restart information below was generated by a previous run
! and will be used by DeltaEC the next time it opens this file.
guessz   0b   0d   0f   0g   4e  20h  20i  24e
xprecn  1.0972E-4   8.7028E-3   3.4325E-7  -5.3629E-5   6.5512E-5  -4.3481E-5  -2.8799E-4
targs   14a  35a  45a  46a  53a  54a  55a  56a
hilite 4F 7F 10F 11F 13F 20G 23F 33H 39F
mstr-slave 7 2 -2 13 -2 19 -2 22 -2 33 -2 39 -2 41 -2
! Plot start, end, and step values.  May be edited if you wish.
! Outer Loop:                       | Inner Loop .
```

APPENDIX D

SUPPLEMENTARY DATA FOR CHAPTER 6

D.1 DeltaEC output file for the double core system with optimised regenerators

```
TITLE
!->C:\Users\eaxwk\Desktop\DeltaEC output files\Final_run\180 & 28 mm.out
!Created@09:51:38  27-Sep-2019 with DeltaEC version 6.4b2.7!under win32,
using Win 6.2.9200 () under Python 2.7.9.
!---------------------------------  0 ---------------------------------
BEGIN      the setup
 1.0132E+5  a Mean P Pa
 72.003     b Freq   Hz       G
 363.00     c TBeg   K
 4608.8     d |p|    Pa       G
 0.0000     e Ph(p)  deg
 7.1023E-2  f |U|    m^3/s    G
 36.855     g Ph(U)  deg      G
air           Gas type
!---------------------------------  1 ---------------------------------
RPN        Edot passing this point
     0.0000 a G or T                    130.96                    A Watt
                                        130.96                    B Watt
Htot ; Edot
!---------------------------------  2 ---------------------------------
DUCT       Change Me
sameas   4a a Area   m^2      Mstr       4611.9     A |p|    Pa
    0.82567 b Perim  m        2a        -5.7471E-2  B Ph(p)  deg
 1.0000E-2  c Length m                   6.6529E-2  C |U|    m^3/s
```

```
 5.0000E-4  d Srough                        31.350   D Ph(U)  deg
                                           130.96    E Htot   W
ideal           Solid type                 130.93    F Edot   W
!--------------------------------  3 --------------------------------
JOIN       Change Me
                                          4611.9     A |p|    Pa
                                         -5.7471E-2  B Ph(p)  deg
                                          6.5902E-2  C |U|    m^3/s
                                            31.350   D Ph(U)  deg
                                           130.96    E Htot   W
                                           129.70    F Edot   W
                                           363.00    G TBeg   K
                                           363.00    H TEnd   K
!--------------------------------  4 --------------------------------
HX         Ambient heat exchanger AHX2
 5.4250E-2  a Area   m^2                    4618.5     A |p|    Pa
    0.7000  b GasA/A                       -0.29163   B Ph(p)  deg
 2.5000E-2  c Length m                      5.8880E-2  C |U|    m^3/s
 1.4670E-3  d y0     m                        19.443   D Ph(U)  deg
 -594.09    e HeatIn W        G             -463.13    E Htot   W
  300.00    f SolidT K                       127.98    F Edot   W
                                             363.00    G GasT   K
ideal           Solid type                   324.81    H SolidT K
!--------------------------------  5 --------------------------------
DUCT       Regen cold end dead space
 1.4250E-2  a Area   m^2                    4620.3     A |p|    Pa
    0.7400  b Perim  m                      -0.35973   B Ph(p)  deg
 3.1750E-3  c Length m                      5.8655E-2  C |U|    m^3/s
                                              18.829   D Ph(U)  deg
                                            -463.13    E Htot   W
stainless           Solid type              127.98    F Edot   W
!--------------------------------  6 --------------------------------
RPN        Complex Z
     0.0000 a G or T                     8.4842                    A ChngeMe
                                         -19.188                   B ChngeMe
                                         3.7446E-4                 C ChngeMe
dk ; p1 U1 / arg ; p1 U1 / 7a * mag rho / a /
!--------------------------------  7 --------------------------------
STKSCREEN  Regenerator 2
 4.0000E-2  a Area   m^2                    4253.2     A |p|    Pa
    0.7300  b VolPor                          -1.4447  B Ph(p)  deg
 2.8000E-2  c Length m                      8.8071E-2  C |U|    m^3/s
 1.8000E-4  d rh     m                        1.0775   D Ph(U)  deg
    0.1500  e ksFrac                        -463.13    E Htot   W
                                             187.11    F Edot   W
                                             363.00    G TBeg   K
stainless           Solid type              602.73    H TEnd   K
```

```
!---------------------------------  8 ---------------------------------
RPN        f_k
 1.8000E-4  a G or T                    (0.99549, -6.1144E-2)     A ChngeMe
(1,1) inp * dk / tanh lstx /
!---------------------------------  9 ---------------------------------
RPN        f_n
 1.8000E-4  a G or T                    (0.98941, -9.3360E-2)     A ChngeMe
(1,1) inp * dn / tanh lstx /
!--------------------------------- 10 ---------------------------------
RPN        Complex p1
     0.0000 a G or T                    4251.9                    A ChngeMe
                                        -107.23                   B ChngeMe
                                        4253.2                    C ChngeMe
p1 mag ; p1 imag ; p1 real
!--------------------------------- 11 ---------------------------------
RPN        Temperature difference across reg.2
     0.0000 a G or T                    239.73                    A ChngeMe
7H 7G -
!--------------------------------- 12 ---------------------------------
RPN        TAE2 Amplification
     0.0000 a G or T                    59.129                    A ChngeMe
7F 4F -
!--------------------------------- 13 ---------------------------------
RPN        ChangeMe
     0.0000 a G or T                    367.11                    A ChngeMe
5A 7A -
!--------------------------------- 14 ---------------------------------
DUCT       All regen hot end dead space
 3.1500E-2  a Area   m^2                4253.3     A |p|    Pa
    2.0000  b Perim  m                    -1.5327  B Ph(p)  deg
 8.7000E-3  c Length m                  8.7955E-2  C |U|    m^3/s
 6.0000E-4  d Srough                      -1.3599  D Ph(U)  deg
                                        -463.13    E Htot   W
stainless           Solid type          187.05    F Edot   W
!--------------------------------- 15 ---------------------------------
HX         HHX heat transfer area used/not acoustic area
 7.1500E-2  a Area   m^2                4249.3     A |p|    Pa
    0.7500  b GasA/A                      -1.776   B Ph(p)  deg
 4.0000E-2  c Length m                  9.2011E-2  C |U|    m^3/s
 4.5000E-3  d y0     m                   -20.29    D Ph(U)  deg
 1500.0     e HeatIn W                  1036.9     E Htot   W
  578.00    f SolidT K                   185.37    F Edot   W
                                         602.73    G GasT   K
stainless           Solid type          817.83    H SolidT K
!--------------------------------- 16 ---------------------------------
JOIN       Change Me
                                        4249.3     A |p|    Pa
```

```
                                        -1.776   B Ph(p)  deg
                                      9.1124E-2  C |U|    m^3/s
                                       -20.29    D Ph(U)  deg
                                      1036.9     E Htot   W
                                       183.59    F Edot   W
                                       602.73    G TBeg   K
                                       616.72    H TEnd   K
!---------------------------------- 17 ----------------------------------
STKDUCT    Thermal Buffer Tube TBT2
 8.3300E-3  a Area   m^2      Mstr       4239.8     A |p|    Pa
 0.32323    b Perim  m        17a          -2.149   B Ph(p)  deg
 8.0000E-2  c Length m                   9.1160E-2  C |U|    m^3/s
 1.1600E-3  d WallA  m^2                  -20.672   D Ph(U)  deg
                                      1036.9     E Htot   W
                                       183.24    F Edot   W
                                       616.72    G TBeg   K
stainless           Solid type         363.00    H TEnd   K
!---------------------------------- 18 ----------------------------------
RPN        Force TBT ambient temperature
sameas   0c a =A?                     363.00                   A ChngeMe
Tm
!---------------------------------- 19 ----------------------------------
RPN        how much heat must be rejected here? Resonator is insulated
  100.00    a G or T                  -827.34                   A ChngeMe
15e 4e + 78.57 - ~
!---------------------------------- 20 ----------------------------------
JOIN       Change Me
                                       4239.8     A |p|    Pa
                                         -2.149   B Ph(p)  deg
                                      9.0283E-2  C |U|    m^3/s
                                       -20.672   D Ph(U)  deg
                                      1036.9     E Htot   W
                                       181.48    F Edot   W
                                       363.00    G TBeg   K
                                       375.33    H TEnd   K
!---------------------------------- 21 ----------------------------------
HX         SAHX2
 7.1818E-3  a Area   m^2              4204.1     A |p|    Pa
    0.7130  b GasA/A                    -3.1763  B Ph(p)  deg
 1.0000E-2  c Length m                 9.0476E-2  C |U|    m^3/s
 1.4670E-3  d y0     m                  -21.116   D Ph(U)  deg
sameas  19A e HeatIn W                  209.53    E Htot   W
     0.0000 f SolidT K                  180.94    F Edot   W
                                       375.33    G GasT   K
ideal           Solid type              88.186   H SolidT K
!---------------------------------- 22 ----------------------------------
DUCT
```

```
 1.0000E-2  a Area   m^2      Mstr       3995.0     A |p|    Pa
    0.4526  b Perim  m        22a         -11.067   B Ph(p)  deg
    0.1500  c Length m                  9.7102E-2  C |U|    m^3/s
                                         -32.466   D Ph(U)  deg
                                         209.53    E Htot   W
stainless           Solid type           180.59    F Edot   W
!--------------------------------- 23 ---------------------------------
IESPEAKER  Linear Alternator
 1.9600E-2  a Area   m^2                3088.6     A |p|    Pa
    4.0000  b R      ohms                  4.1010  B Ph(p)  deg
 1.0000E-3  c L      H                  9.7072E-2  C |U|    m^3/s
   14.000   d BLProd T-m                 -32.475   D Ph(U)  deg
 2.0000E-2  e M      kg                  157.17    E Htot   W
 4778.0     f K      N/m                 120.38    F Edot   W
    0.1800  g Rm     N-s/m               -52.353   G WorkIn W
    1.6710  h |I|    A        G           62.666   H Volts  V
  -32.47    i Ph(I)  deg      G            1.6710  I Amps   A
                                         179.31    J Ph(V/I) deg
                                        1296.7     K |Px|   Pa
stainless           Solid type           130.38    L Ph(Px) deg
!--------------------------------- 24 ---------------------------------
RPN        DP across L.A
     0.0000 a G or T                   906.47                    A ChngeMe
22A 23A -
!--------------------------------- 25 ---------------------------------
DUCT       FB
 3.8000E-3  a Area   m^2      Mstr       4577.2     A |p|    Pa
    0.2790  b Perim  m        25a         -97.757   B Ph(p)  deg
    0.5500  c Length m                  9.0218E-2  C |U|    m^3/s
                                         -42.183   D Ph(U)  deg
                                         157.17    E Htot   W
stainless           Solid type           116.73    F Edot   W
!--------------------------------- 26 ---------------------------------
BRANCH     Stub No.2
     0.0000 a Re(Zb) Pa-s/m^3           4577.2     A |p|    Pa
-1.1078E+5  b Im(Zb) Pa-s/m^3            -97.757   B Ph(p)  deg
     0.0000 c HtotBr W                  6.0803E-2  C |U|    m^3/s
                                         -64.775   D Ph(U)  deg
                                         157.17    E Htot   W
                                         116.73    F Edot   W
                                           0.0000  G EdotBr W
!--------------------------------- 27 ---------------------------------
HX         Ambient heat exchanger AHX1
 5.4250E-2  a Area   m^2                4583.3     A |p|    Pa
    0.7000  b GasA/A                     -97.966   B Ph(p)  deg
 2.5000E-2  c Length m                  5.3545E-2  C |U|    m^3/s
 1.4670E-3  d y0     m                   -77.544   D Ph(U)  deg
```

```
 -442.74    e HeatIn W        G          -285.57    E Htot   W
  300.00    f SolidT K                    114.99    F Edot   W
                                          375.33    G GasT   K
ideal           Solid type                344.20    H SolidT K
!--------------------------------- 28 ---------------------------------
DUCT       Regen cold end dead space
 1.4250E-2  a Area   m^2                 4585.0     A |p|    Pa
    0.7400  b Perim  m                    -98.026   B Ph(p)  deg
 3.1750E-3  c Length m                   5.3314E-2  C |U|    m^3/s
                                          -78.212   D Ph(U)  deg
                                         -285.57    E Htot   W
stainless           Solid type            114.99    F Edot   W
!--------------------------------- 29 ---------------------------------
RPN        Complex Z
     0.0000 a G or T                    9.4186                    A ChngeMe
                                        -19.814                   B ChngeMe
                                        3.8623E-4                 C ChngeMe
dk ; p1 U1 / arg ; p1 U1 / 30a * mag rho / a /
!--------------------------------- 30 ---------------------------------
STKSCREEN  Regenerator 1
 4.0000E-2  a Area   m^2                 4300.9     A |p|    Pa
    0.7300  b VolPor                     -98.934   B Ph(p)  deg
 2.8000E-2  c Length m                   6.8935E-2  C |U|    m^3/s
 1.8000E-4  d rh     m                    -97.114   D Ph(U)  deg
    0.1500  e ksFrac                    -285.57    E Htot   W
                                          148.17    F Edot   W
                                          375.33    G TBeg   K
stainless           Solid type            542.03    H TEnd   K
!--------------------------------- 31 ---------------------------------
RPN        f_k
 1.8000E-4  a G or T                   (0.99344, -7.3647E-2)     A ChngeMe
(1,1) inp * dk / tanh lstx /
!--------------------------------- 32 ---------------------------------
RPN        f_n
 1.8000E-4  a G or T                   (0.98501, -0.11077)       A ChngeMe
(1,1) inp * dn / tanh lstx /
!--------------------------------- 33 ---------------------------------
RPN        Complex p1
     0.0000 a G or T                    -667.94                   A ChngeMe
                                        -4248.7                   B ChngeMe
                                        4300.9                    C ChngeMe
p1 mag ; p1 imag ; p1 real
!--------------------------------- 34 ---------------------------------
RPN        Temperature difference across reg.1
     0.0000 a G or T                    166.70                    A ChngeMe
30H 30G -
!--------------------------------- 35 ---------------------------------
```

```
RPN        TAE1 Amplification
     0.0000 a G or T                    33.173                     A ChngeMe
30F 27F -
!--------------------------------- 36 ---------------------------------
RPN        ChangeMe
     0.0000 a G or T                    284.09                     A ChngeMe
28A 30A -
!--------------------------------- 37 ---------------------------------
DUCT       All regen hot end dead space
 3.1500E-2  a Area   m^2                4300.8     A |p|    Pa
    2.0000  b Perim  m                   -99.01    B Ph(p)  deg
 8.7000E-3  c Length m                  6.8890E-2  C |U|    m^3/s
 6.0000E-4  d Srough                    -100.26    D Ph(U)  deg
                                        -285.57    E Htot   W
stainless           Solid type          148.11    F Edot   W
!--------------------------------- 38 ---------------------------------
HX         HHX1 ( heat transfer area used/not acoustic area)
 7.1500E-2  a Area   m^2                4296.3     A |p|    Pa
    0.7500  b GasA/A                     -99.218   B Ph(p)  deg
 4.0000E-2  c Length m                  7.5096E-2  C |U|    m^3/s
 4.5000E-3  d y0     m                  -123.91    D Ph(U)  deg
 1000.0     e HeatIn W                   714.43    E Htot   W
  578.00    f SolidT K                   146.56    F Edot   W
                                         542.03    G GasT   K
stainless           Solid type          719.15    H SolidT K
!--------------------------------- 39 ---------------------------------
JOIN       Change Me
                                        4296.3     A |p|    Pa
                                         -99.218   B Ph(p)  deg
                                        7.4394E-2  C |U|    m^3/s
                                        -123.91    D Ph(U)  deg
                                         714.43    E Htot   W
                                         145.19    F Edot   W
                                         542.03    G TBeg   K
                                         550.75    H TEnd   K
!--------------------------------- 40 ---------------------------------
STKDUCT    Thermal Buffer Tube TBT1
 8.3300E-3  a Area   m^2      Mstr      4285.4     A |p|    Pa
 0.32323    b Perim  m        40a        -99.525   B Ph(p)  deg
 8.0000E-2  c Length m                  7.4624E-2  C |U|    m^3/s
 1.1600E-3  d WallA  m^2                -124.43    D Ph(U)  deg
                                         714.43    E Htot   W
                                         145.02    F Edot   W
                                         550.75    G TBeg   K
stainless           Solid type          363.00    H TEnd   K
!--------------------------------- 41 ---------------------------------
RPN        Force TBT ambient temperature
```

```
  363.00    a =A?                      363.00                    A ChngeMe
Tm
!---------------------------------- 42 ----------------------------------
RPN         how much heat must be rejected here? Resonator is insulated
  100.00    a G or T                  -504.88                    A ChngeMe
38e 27e + 52.38 - ~
!---------------------------------- 43 ----------------------------------
JOIN        Change Me
                                       4285.4     A |p|    Pa
                                        -99.525   B Ph(p)  deg
                                      7.3930E-2   C |U|    m^3/s
                                      -124.43     D Ph(U)  deg
                                        714.43    E Htot   W
                                        143.68    F Edot   W
                                        363.00    G TBeg   K
                                        371.05    H TEnd   K
!---------------------------------- 44 ----------------------------------
HX          SAHX1
 7.1818E-3  a Area   m^2             4249.0     A |p|    Pa
    0.7130  b GasA/A                 -100.32    B Ph(p)  deg
 1.0000E-2  c Length m               7.4204E-2  C |U|    m^3/s
 1.4670E-3  d y0     m               -124.96    D Ph(U)  deg
sameas  42A e HeatIn W                209.55    E Htot   W
     0.0000 f SolidT K                143.29    F Edot   W
                                      371.05    G GasT   K
ideal           Solid type           195.97    H SolidT K
!---------------------------------- 45 ----------------------------------
DUCT        FB
 3.8000E-3  a Area   m^2      Mstr    7389.9     A |p|    Pa
    0.2790  b Perim  m        45a      132.27    B Ph(p)  deg
    1.7000  c Length m                3.7632E-2  C |U|    m^3/s
                                      122.34    D Ph(U)  deg
                                      209.55    E Htot   W
ideal           Solid type            136.97    F Edot   W
!---------------------------------- 46 ----------------------------------
BRANCH      Stub No. 1
     0.0000 a Re(Zb) Pa-s/m^3         7389.9     A |p|    Pa
-7.0000E+5  b Im(Zb) Pa-s/m^3          132.27    B Ph(p)  deg
     0.0000 c HtotBr W                4.0801E-2  C |U|    m^3/s
                                      107.57    D Ph(U)  deg
                                      209.55    E Htot   W
                                      136.97    F Edot   W
                                         0.0000 G EdotBr W
!---------------------------------- 47 ----------------------------------
DUCT        FB
 3.8000E-3  a Area   m^2      Mstr    4608.8     A |p|    Pa
    0.2790  b Perim  m        47a    -2.3461E-13 B Ph(p)  deg
```

```
    1.5000  c Length m                  7.1023E-2  C |U|    m^3/s
                                          36.855   D Ph(U)  deg
                                         209.55    E Htot   W
ideal           Solid type               130.96    F Edot   W
!---------------------------------- 48 ----------------------------------
RPN        stroke (mm peak-to-peak)
     0.0000 a G or T                    16.019                    A mm p-p
U1 mag 23a / w / 2 * 1000 *
!---------------------------------- 49 ----------------------------------
RPN        What capacitance would "cancel" the alternator's inductance?
     0.0000 a G or T                    4.8858E-3                 A Farad
w sqrd 23c * inv
!---------------------------------- 50 ----------------------------------
RPN        a = Load Resistor (Ohm). A = complex load impedance
   37.500   a G or T                    (37.500, -0.45241)        A Ohm
inp i w * 49A * inv +
!---------------------------------- 51 ----------------------------------
RPN        Target V\I = magnitude of electrical impedance
     0.0000 a =A?                       7.1054E-15                A Ohm
23H 23I / 50A mag -
!---------------------------------- 52 ----------------------------------
RPN        Target phase(V/I) = phase(electrical impedance)
     0.0000 a =A?                       -1.4211E-14               A ChngeMe
23J 180 - 50A arg -
!---------------------------------- 53 ----------------------------------
RPN        Electrical output
sameas  23G a G or T                    52.353                    A ChngeMe
23G -1 *
!---------------------------------- 54 ----------------------------------
RPN        Force electrical load to be resistive
 -180.0     a G or T                    179.31                    A ChngeMe
23J
!---------------------------------- 55 ----------------------------------
RPN        Total heat in
     0.0000 a G or T                    2500.0                    A ChngeMe
15e 38e +
!---------------------------------- 56 ----------------------------------
RPN        Heat input ratios (Q1/QT, Q2/QT)
     0.0000 a G or T                    0.6000                    A ChngeMe
                                        0.4000                    B ChngeMe
38e 55A / ; 15e 55A /
!---------------------------------- 57 ----------------------------------
RPN        Thermal-to-acoustic efficiency
     0.0000 a G or T                    5.2382                    A ChngeMe
Edot 55A / 100 *
!---------------------------------- 58 ----------------------------------
RPN        Thermal-to-Electrical efficiency
```

```
     0.0000 a G or T                    2.0941                     A ChngeMe
23G 55A / 100 * -1 *
!---------------------------------- 59 ----------------------------------
RPN        Acoustic-to-Electrical efficiency
     0.0000 a G or T                    43.488                     A ChngeMe
23G 23F / 100 * -1 *
!---------------------------------- 60 ----------------------------------
RPN        Carnot efficiency for TAE 1
     0.0000 a G or T                    30.755                     A ChngeMe
1 30G 30H / - 100 *
!---------------------------------- 61 ----------------------------------
RPN        Carnot efficiency for TAE 2
     0.0000 a G or T                    39.774                     A ChngeMe
1 7G 7H / - 100 *
!---------------------------------- 62 ----------------------------------
RPN        Average Carnot
     0.0000 a G or T                    35.265                     A ChngeMe
60A 61A + 2 /
!---------------------------------- 63 ----------------------------------
RPN        Carnot efficiency for acoustic output
     0.0000 a G or T                    14.854                     A ChngeMe
57A 62A / 100 *
!---------------------------------- 64 ----------------------------------
RPN        Set p1 mag
    1.0000  a =A?                       1.0000                     A ChngeMe
p1 mag 0d /
!---------------------------------- 65 ----------------------------------
RPN        Set p1 phase
    1.0000  a =A?                       1.0000                     A ChngeMe
p1 arg 0e - 1 +
!---------------------------------- 66 ----------------------------------
RPN        Set mag U1
    1.0000  a =A?                       1.0000                     A ChngeMe
U1 mag 0f /
!---------------------------------- 67 ----------------------------------
RPN        Set U1 phase
    1.0000  a =A?                       1.0000                     A ChngeMe
U1 arg 0g - 1 +
! The restart information below was generated by a previous run
! and will be used by DeltaEC the next time it opens this file.
guessz   0b   0d   0f   0g   4e  23h  23i  27e
xprecn  3.1474E-4  -1.5826E-2  -4.8485E-7   3.0813E-4   4.6793E-3  -2.3818E-5   3.0611E-4
targs   18a  41a  51a  52a  65a  66a  67a  68a
hilite 4F 7F 14F 15F 17F 23G 26F 40H 45F
mstr-slave 7 2 -2 17 -2 22 -2 25 -2 40 -2 45 -2 47 -2
! Plot start, end, and step values.  May be edited if you wish.
! Outer Loop:                       | Inner Loop .
```

BIBLIOGRAPHY

Abdoulla-Latiwish, K. O., Mao, X. and Jaworski, A. J., 2017. 'Thermoacoustic micro-electricity generator for rural dwellings in developing countries driven by waste heat from cooking activities', *Energy* **134**, 1107–1120.

Akhavan, R., Kamm, R. D. and Shapiro, A. H., 1991. 'An investigation of transition to turbulence in bounded oscillatory Stokes flows Part 1. Experiments', *Journal of Fluid Mechanics* **225**, 395–422.

Al-Kayiem, A. and Yu, Z., 2017. 'Using a side-branched volume to tune the acoustic field in a looped-tube travelling-wave thermoacoustic engine with a RC load', *Energy Conversion and Management* **150**, 814–821.

Aldraihem, O. and Baz, A., 2012. 'Onset of self-excited oscillations of traveling wave thermo-acoustic-piezoelectric energy harvester using root-locus analysis', *Journal of Vibration and Acoustics* **134**(1), 011003.

Alemany, A., Francois, M., de Blok, K., Pierre, R. J., Gerard, P., Zeminiani, E., Gaia, E., Roy, P. J. E., Chillet, C., Freiberg, J., Nikoluškins, R., Gerbeth, G. and Eckert, S., 2015. Space thermoacoustic radio—isotopic power system: SpaceTRIPS, *in* '3 rd INTERNATIONAL WORKSHOP ON THERMOACOUSTICS', p. 70.

Anton, S. R. and Sodano, H. A., 2007. 'A review of power harvesting using piezoelectric materials (2003–2006)', *Smart Materials and Structures* **16**(3), R1.

Arnott, W. P., Bass, H. E. and Raspet, R., 1991. 'General formulation of thermoacoustics for stacks having arbitrarily shaped pore cross sections', *The Journal of the Acoustical Society of America* **90**(6), 3228–3237.

Avent, A. W. and Bowen, C. R., 2015. 'Principles of thermoacoustic energy harvesting', *The European Physical Journal Special Topics* **224**(14-15), 2967–2992.

Backhaus, S. and Swift, G. W., 1999. 'A thermoacoustic Stirling heat engine', *Nature* **399**(6734), 335.

Backhaus, S. and Swift, G. W., 2000. 'A thermoacoustic Stirling heat engine: Detailed study', *The Journal of the Acoustical Society of America* **107**(6), 3148–3166.

Backhaus, S. and Swift, G. W., 2001. Fabrication and use of parallel plate regenerators in thermoacoustic engines, *in* 'Proc. 36th Intersociety Energy Conversion Engineering Conf.(IECEC), 2001', Vol. 1, ASME, pp. 453–458.

Backhaus, S., Tward, E. and Petach, M., 2004. 'Traveling-wave thermoacoustic electric generator', *Applied Physics Letters* **85**(6), 1085–1087.

Bejan, A., 2016. *Advanced engineering thermodynamics*, Hoboken, New Jersey: John Wiley & Sons.

Bi, T., Wu, Z., Zhang, L., Yu, G., Luo, E. and Dai, W., 2017. 'Development of a 5 kw traveling-wave thermoacoustic electric generator', *Applied Energy* **185**, 1355–1361.

Biwa, T., Komatsu, R. and Yazaki, T., 2011. 'Acoustical power amplification and damping by temperature gradients', *The Journal of the Acoustical Society of America* **129**(1), 132–137.

Boluriaan, S. and Morris, P. J., 2003. 'Acoustic streaming: from Rayleigh to today', *International Journal of Aeroacoustics* **2**(3), 255–292.

Burks, A. W., Warren, D. W. and Wright, J. B., 1954. 'An analysis of a logical machine using parenthesis-free notation', *Mathematical Tables and Other Aids to Computation* **8**(46), 53–57.

Callen, H. B., 1985. *Thermodynamics and an Introduction to Thermostatistics, 2nd Edition*, New York: John Wiley & Sons.

Ceperley, P. H., 1979. 'A pistonless Stirling engine—the traveling wave heat engine', *The Journal of the Acoustical Society of America* **66**(5), 1508–1513.

Ceperley, P. H., 1985. 'Gain and efficiency of a short traveling wave heat engine', *The Journal of the Acoustical Society of America* **77**(3), 1239–1244.

Chen, B. M., Abakr, Y. A., Riley, P. H. and Hann, D. B., 2012. Development of thermoacoustic engine operating by waste heat from cooking stove, *in* 'AIP Conference Proceedings', Vol. 1440, AIP, pp. 532–540.

Chen, B. M., Riley, P. H., Abakr, Y. A., Pullen, K., Hann, D. B. and Johnson, C. M., 2013. 'Design and development of a low-cost, electricity-generating cooking Score-Stove™', *Proceedings of the Institution of Mechanical Engineers, Part A: Journal of Power and Energy* **227**(7), 803–813.

Chinn, D. G., 2010. Piezoelectrically Driven Thermoacoustic Refrigerator, PhD thesis.

Crocker, M. J., 1998. *Handbook of acoustics*, New York: John Wiley & Sons.

Dagne, T., 2012. *The Republic of South Sudan: Opportunities and Challenges for Africa's Newest Country*, DIANE Publishing.

De Blok, C. M. and Van Rijt, N. A. H. J., 2001. '*Thermo-acoustic system*'. US Patent 6,314,740.

De Blok, K., 2008. 'Low operating temperature integral thermo acoustic devices for solar cooling and waste heat recovery', *Journal of the Acoustical Society of America* **123**(5), 3545–3550.

De Blok, K., 2010. Novel 4-stage traveling wave thermoacoustic power generator, *in* 'ASME 2010 3rd joint US-European fluids engineering summer meeting collocated with 8th international conference on nanochannels, microchannels, and minichannels', American Society of Mechanical Engineers, pp. 73–79.

De Blok, K., 2013. 'Acoustic power measurements in thermoacoustic systems', *Aster Thermoacoustics* . http://www.aster-thermoacoustics.com/wp-content/uploads/2013/07/Measuring-acoustic-power.pdf.

De Blok, K., Owczarek, P. and François, M. X., 2014. Bi-directional turbines for converting acoustic wave power into electricity, *in* 'Proceedings of 9th PAMIR International Conference on Fundamental and Applied MHD'.

De Blok, K. and Systemen, A. T., 2012. Multi-stage traveling wave thermoacoustics in practice, *in* '19th Int. Congress Sound Vibration, Vilnius', Citeseer. http://www.aster-thermoacoustics.com/wp-content/uploads/2013/02/Multi-stage-traveling-wave-feedback-thermoacoustics-in-practice-Kees-de-Blok.pdf.

Dunn, F., Hartmann, W. M., Campbell, D. M. and Fletcher, N. H., 2015. *Springer handbook of acoustics*, New York: Springer-Verlag.

Ehsan, M. D., Sarker, M., Mahmud, R. and Riley, P. H., 2015. 'Performance of an electricity-generating cooking stove with pressurized kerosene burner', *Procedia Engineering* **105**, 619–627.

Feldman Jr, K. T., 1968*a*. 'Review of the literature on Rijke thermoacoustic phenomena', *Journal of Sound and Vibration* **7**(1), 83–89.

Feldman Jr, K. T., 1968*b*. 'Review of the literature on Sondhauss thermoacoustic phenomena', *Journal of Sound and Vibration* **7**(1), 71–82.

Fusco, A. M., Ward, W. C. and Swift, G. W., 1992. 'Two-sensor power measurements in lossy ducts', *The Journal of the Acoustical Society of America* **91**(4), 2229–2235.

Gardner, D. L. and Swift, G. W., 2003. 'A cascade thermoacoustic engine', *The Journal of the Acoustical Society of America* **114**(4), 1905–1919.

Garrett, S. L., 2004. 'Resource letter: TA-1: Thermoacoustic engines and refrigerators', *American Journal of Physics* **72**(1), 11–17.

Garrett, S. L., 2017. 'Understanding acoustics', *Cham, CH: Springer* .

Gedeon, D., 1997. DC gas flows in Stirling and pulse tube cryocoolers, *in* 'Cryocoolers 9', Boston, MA: Springer, pp. 385–392.

Ghorbanian, K. and Karimi, M., 2014. 'Design and optimization of a heat driven thermoacoustic refrigerator', *Applied Thermal Engineering* **62**(2), 653–661.

Gifford, W. E. and Longsworth, R. C., 1966. Surface heat pumping, *in* 'Advances in cryogenic engineering', Boston, MA: Springer, pp. 171–179.

Goh, J. H., 2019. Performance mapping of a two-stage travelling wave thermoacoustic engine for heat recovery, PhD thesis, University of Nottingham.

Hariharan, N. M., Sivashanmugam, P. and Kasthurirengan, S., 2013. 'Influence of operational and geometrical parameters on the performance of twin thermoacoustic prime mover', *International Journal of Heat and Mass Transfer* **64**, 1183–1188.

Hartley, R. V. L., 1951. '*Electric power source*'. US Patent 2,549,464.

Higgins, B., 1802. 'On the sound produced by a current of hydrogen gas passing through a tube', *Journal of Natural Philosophy, Chemistry and the Arts* **1**(129-131), 2.

Hino, M., Kashiwayanagi, M., Nakayama, A. and Hara, T., 1983. 'Experiments on the turbulence statistics and the structure of a reciprocating oscillatory flow', *Journal of Fluid Mechanics* **131**, 363–400.

Jaworski, A. J. and Mao, X., 2013. 'Development of thermoacoustic devices for power generation and refrigeration', *Proceedings of the Institution of Mechanical Engineers, Part A: Journal of Power and Energy* **227**(7), 762–782.

Jensen, C. and Raspet, R., 2010. 'Thermoacoustic power conversion using a piezoelectric transducer', *The Journal of the Acoustical Society of America* **128**(1), 98–103.

Jin, T., Huang, J., Feng, Y., Yang, R., Tang, K. and Radebaugh, R., 2015. 'Thermoacoustic prime movers and refrigerators: Thermally powered engines without moving components', *Energy* **93**, 828–853.

Jin, T., Yang, R., Wang, Y., Liu, Y. and Feng, Y., 2016. 'Phase adjustment analysis and performance of a looped thermoacoustic prime mover with compliance/resistance tube', *Applied Energy* **183**, 290–298.

Kang, H., Cheng, P., Yu, Z. and Zheng, H., 2015. 'A two-stage traveling-wave thermoacoustic electric generator with loudspeakers as alternators', *Applied Energy* **137**, 9–17.

Kang, H., Zhou, G. and Li, Q., 2010. 'Thermoacoustic effect of traveling–standing wave', *Cryogenics* **50**(8), 450–458.

Kays, W. M. and London, A. L., 1984. *Compact heat exchangers*, McGraw-Hill, New York, NY.

Kirkconnell, C. S., 2002. Experimental investigation of a unique pulse tube expander design, *in* 'Cryocoolers 10', Boston, MA: Springer, pp. 239–247.

Kruse, A., Ruziewicz, A., Tajmar, M. and Gnutek, Z., 2017. 'A numerical study of a looped-tube thermoacoustic engine with a single-stage for utilization of low-grade heat', *Energy Conversion and Management* **149**, 206–218.

Lawn, C. J., 2012. Assessment of the performance of regenerators in travelling-wave thermoacoustic engines, *in* 'International Congress on Sound and Vibration, Vilnius, in July', Vol. 2, pp. 1589–1596.

Lawn, C. J., 2013. 'Development of a thermoacoustic travelling-wave engine', *Proceedings of the Institution of Mechanical Engineers, Part A: Journal of Power and Energy* **227**(7), 783–802.

Lawn, C. J., 2014. 'Acoustic pressure losses in woven screen regenerators', *Applied Acoustics* **77**, 42–48.

Lihoreau, B., Lotton, P., Bruneau, M. and Gusev, V., 2002. 'Piezoelectric source exciting thermoacoustic resonator: Analytical modelling and experiment', *Acta Acustica united with Acustica* **88**(6), 986–997.

Lord, R., 1945. *The theory of sound*, Vol. II, Dover, New York.

Luo, E. C., Dai, W., Zhang, Y. and Ling, H., 2006. 'Experimental investigation of a thermoacoustic-Stirling refrigerator driven by a thermoacoustic-Stirling heat engine', *Ultrasonics* **44**, e1531–e1533.

Luo, E., Huang, Y., Dai, W., Zhang, Y. and Wu, Z., 2005. 'A high-performance thermoacoustic refrigerator operating in room-temperature range', *Chinese Science Bulletin* **50**(22), 2662–2664.

Marrison, W. A., 1958. '*Heat-controlled acoustic wave system*'. US Patent 2,836,033.

Matveev, K. I., Wekin, A., Richards, C. D. and Shafrei-Tehrany, N., 2007. On the coupling between standing-wave thermoacoustic engine and piezoelectric transducer, *in* 'ASME 2007 International Mechanical Engineering Congress and Exposition', American Society of Mechanical Engineers, pp. 765–769.

Merkli, P. and Thomann, H., 1975*a*. 'Thermoacoustic effects in a resonance tube', *Journal of Fluid Mechanics* **70**(1), 161–177.

Merkli, P. and Thomann, H., 1975*b*. 'Transition to turbulence in oscillating pipe flow', *Journal of Fluid Mechanics* **68**(3), 567–576.

Migliori, A. and Swift, G. W., 1988. 'Liquid-sodium thermoacoustic engine', *Applied Physics Letters* **53**(5), 355–357.

Napolitano, M., Dragonetti, R. and Romano, R., 2017. 'A method to optimize the regenerator parameters of a thermoacoustic engine', *Energy Procedia* **126**, 525–532.

Nouh, M., Aldraihem, O. and Baz, A., 2013. Analysis and optimization of thermoacoustic-piezoelectric energy harvesters: an electrical circuit analogy approach, *in* 'Active and Passive Smart Structures and Integrated Systems 2013', Vol. 8688, International Society for Optics and Photonics, p. 86880L.

Nouh, M., Aldraihem, O. and Baz, A., 2014. 'Transient characteristics and stability analysis of standing wave thermoacoustic-piezoelectric harvesters', *The Journal of the Acoustical Society of America* **135**(2), 669–678.

Olson, J. R. and Swift, G. W., 1997. 'Acoustic streaming in pulse tube refrigerators: tapered pulse tubes', *Cryogenics* **37**(12), 769–776.

Pereiras, B., Castro, F., El Marjani, A. and Rodríguez, M. A., 2011. 'An improved radial impulse turbine for OWC', *Renewable Energy* **36**(5), 1477–1484.

Piccolo, A., 2018. 'Design issues and performance analysis of a two-stage standing wave thermoacoustic electricity generator', *Sustainable Energy Technologies and Assessments* **26**, 17–27.

Poese, M. E. and Garrett, S. L., 2000. 'Performance measurements on a thermoacoustic refrigerator driven at high amplitudes', *The Journal of the Acoustical Society of America* **107**(5), 2480–2486.

Poese, M. E., Smith, R. W., Garrett, S. L., Van Gerwen, R. and Gosselin, P., 2004. Thermoacoustic refrigeration for ice cream sales, *in* 'Proceedings of 6th IIR Gustav Lorentzen Conference', Citeseer.

Putnam, A. A. and Dennis, W. R., 1956. 'Survey of organ-pipe oscillations in combustion systems', *The Journal of the Acoustical Society of America* **28**(2), 246–259.

Qiu, L. M., Sun, D. M., Tan, Y. X., Deng, X. and Chen, G. B., 2006. Investigation on Gedeon streaming in a traveling wave thermoacoustic engine, *in* 'AIP Conference Proceedings', Vol. 823, AIP, pp. 1115–1122.

Rayleigh, J. W. S. B., 1896. *The theory of sound*, Vol. 2, London: Macmillan.

Rijke, P. L., 1859. 'Notiz über eine neue Art, die in einer an beiden Enden offenen Röhre enthaltene Luft in Schwingungen zu versetzen', *Annalen der Physik* **183**(6), 339–343.

Riley, P. H., 2014*a*. 'Affordability for sustainable energy development products', *Applied energy* **132**, 308–316.

Riley, P. H., 2014*b*. *Designing a low-cost electricity-generating cooking stove for high-volume implementation*, PhD thesis, University of Nottingham.

Rott, N., 1969. 'Damped and thermally driven acoustic oscillations in wide and narrow tubes', *Zeitschrift für angewandte Mathematik und Physik ZAMP* **20**(2), 230–243.

Rott, N., 1973. 'Thermally driven acoustic oscillations. part II: Stability limit for helium', *Zeitschrift für angewandte Mathematik und Physik ZAMP* **24**(1), 54–72.

Rott, N., 1975. 'Thermally driven acoustic oscillations, part III: Second-order heat flux', *Zeitschrift für angewandte Mathematik und Physik ZAMP* **26**(1), 43–49.

Rott, N., 1980. 'Thermoacoustics', *Advances in Applied Mechanics* **20**, 135–175.

Rott, N. and Zouzoulas, G., 1976. 'Thermally driven acoustic oscillations, part IV: tubes with variable cross-section', *Zeitschrift für angewandte Mathematik und Physik (ZAMP)* **27**(2), 197–224.

Saechan, P. and Jaworski, A. J., 2018. 'Thermoacoustic cooler to meet medical storage needs of rural communities in developing countries', *Thermal Science and Engineering Progress* **7**, 164–175.

Saha, C. R., Riley, P. H., Paul, J., Yu, Z., Jaworski, A. J. and Johnson, C. M., 2012. 'Halbach array linear alternator for thermo-acoustic engine', *Sensors and Actuators A: Physical* **178**, 179–187.

Sanchez, T., Dennis, R. and Pullen, K. R., 2013. 'Cooking and lighting habits in rural Nepal and Uganda', *Proceedings of the Institution of Mechanical Engineers, Part A: Journal of Power and Energy* **227**(7), 727–739.

Sanchez, T., Owala, H. and Okello, V., 2012. Research into the behaviour of rural families to technology changes, *in* 'Proceedings of international conference on low-cost, electricity generating heat engines for rural areas'.

Senga, M. and Hasegawa, S., 2016. 'Four-stage loop-type cascade traveling-wave thermoacoustic engine', *Applied Thermal Engineering* **104**, 258–262.

Setoguchi, T. and Takao, M., 2006. 'Current status of self rectifying air turbines for wave energy conversion', *Energy Conversion and Management* **47**(15-16), 2382–2396.

Shahsavari, A. and Akbari, M., 2018*a*. 'Potential of solar energy in developing countries for reducing energy-related emissions', *Renewable and Sustainable Energy Reviews* **90**, 275–291.

Shahsavari, A. and Akbari, M., 2018*b*. 'Potential of solar energy in developing countries for reducing energy-related emissions', *Renewable and Sustainable Energy Reviews* **90**, 275–291.

Shen, C., He, Y., Li, Y., Ke, H., Zhang, D. and Liu, Y., 2009. 'Performance of solar powered thermoacoustic engine at different tilted angles', *Applied Thermal Engineering* **29**(13), 2745–2756.

Smoker, J., Nouh, M., Aldraihem, O. and Baz, A., 2012. 'Energy harvesting from a standing wave thermoacoustic-piezoelectric resonator', *Journal of Applied Physics* **111**(10), 104901.

Sondhauss, C., 1850. 'Über die Schallschwingungen der Luft in erhitzten Glasröhren und in gedeckten Pfeifen von ungleicher Weite', *Annalen der Physik* **155**(1), 1–34.

Sugita, H., Matsubara, Y., Kushino, A., Ohnishi, T., Kobayashi, H. and Dai, W., 2004. 'Experimental study on thermally actuated pressure wave generator for space cryocooler', *Cryogenics* **44**(6-8), 431–437.

Sun, D. M., Wang, K., Zhang, X. J., Guo, Y. N., Xu, Y. and Qiu, L. M., 2013. 'A traveling-wave thermoacoustic electric generator with a variable electric RC load', *Applied Energy* **106**, 377–382.

Sun, D., Qiu, L., Wang, B. and Xiao, Y., 2009. 'Novel Helmholtz resonator used to focus acoustic energy of thermoacoustic engine', *Applied Thermal Engineering* **29**(5-6), 945–949.

Swift, G., 1988*a*. 'A liquid-metal magnetohydrodynamic acoustic transducer', *The Journal of the Acoustical Society of America* **83**(1), 350–361.

Swift, G. and Keolian, R., 1993. 'Thermoacoustics in pin-array stacks', *The Journal of the Acoustical Society of America* **94**(2), 941–943.

Swift, G. W., 1988*b*. 'Thermoacoustic engines', *The Journal of the Acoustical Society of America* **84**(4), 1145–1180.

Swift, G. W., 1992. 'Analysis and performance of a large thermoacoustic engine', *The Journal of the Acoustical Society of America* **92**(3), 1551–1563.

Swift, G. W., 2000. Streaming in thermoacoustic engines and refrigerators, *in* 'AIP Conference Proceedings', Vol. 524, AIP, pp. 105–114.

Swift, G. W., 2003. *Thermoacoustics: A unifying perspective for some engines and refrigerators*, ASA.

Swift, G. W., 2017. *Thermoacoustics: a unifying perspective for some engines and refrigerators*, USA: Springer.

Swift, G. W., Gardner, D. L. and Backhaus, S., 1999. 'Acoustic recovery of lost power in pulse tube refrigerators', *The Journal of the Acoustical Society of America* **105**(2), 711–724.

Swift, G. W. and Ward, W. C., 1996. 'Simple harmonic analysis of regenerators', *Journal of Thermophysics and Heat Transfer* **10**(4), 652–662.

Taconis, K. W., Beenakker, J. J. M., Nier, A. O. C. and Aldrich, L. T., 1949. 'Measurements concerning the vapour-liquid equilibrum of solutions of He^3 in He^4 below 2.19 K', *Physica* **15**(8-9), 733–739.

Tang, K., Lei, T., Lin, X. G., Jin, T. and Zhang, Y., 2011. 'Lumped parameter model for resonant frequency estimation of a thermoacoustic engine with gas-liquid coupling oscillation', *Journal of Zhejiang University-SCIENCE A* **12**(3), 232–237.

Telesz, M. P., 2006. Design and testing of a thermoacoustic power converter, PhD thesis, Georgia Institute of Technology.

Thakker, A., Jarvis, J. and Sahed, A., 2008. 'Quasi-steady analytical model benchmark of an impulse turbine for wave energy extraction', *International Journal of Rotating Machinery* **2008**.

The University of Nottingham, 2007. 'The Score Project', http://www.score.uk.com/. Accessed: 2019-07-04.

Thompson, M. W. and Atchley, A. A., 2005. 'Simultaneous measurement of acoustic and streaming velocities in a standing wave using laser doppler anemometry', *The Journal of the Acoustical Society of America* **117**(4), 1828–1838.

Tijani, M. E. H., Zeegers, J. C. H. and De Waele, A. T. A. M., 2002. 'Design of thermoacoustic refrigerators', *Cryogenics* **42**(1), 49–57.

Timmer, M. A., de Blok, K. and van der Meer, T. H., 2018. 'Review on the conversion of thermoacoustic power into electricity', *The Journal of the Acoustical Society of America* **143**(2), 841–857.

Vogin, C. and Alemany, A., 2007. 'Analysis of the flow in a thermo-acoustic mhd generator with conducting walls', *European Journal of Mechanics-B/Fluids* **26**(4), 479–493.

Wang, K. and Qiu, L., 2017. 'Numerical analysis on a four-stage looped thermoacoustic Stirling power generator for low temperature waste heat', *Energy Conversion and Management* **150**, 830–837.

Wang, K., Sun, D., Zhang, J., Xu, Y., Luo, K., Zhang, N., Zou, J. and Qiu, L., 2016. 'An acoustically matched traveling-wave thermoacoustic generator achieving 750 W electric power', *Energy* **103**, 313–321.

Wang, K., Sun, D., Zhang, J., Xu, Y., Zou, J., Wu, K., Qiu, L. and Huang, Z., 2015. 'Operating characteristics and performance improvements of a 500 W traveling-wave thermoacoustic electric generator', *Applied Energy* **160**, 853–862.

Ward, B., Clark, J. and Swift, G. W., 2008. 'Design environment for low-amplitude thermoacoustic energy conversion', *Software Users Guide, Los Alamos National Laboratory, LA-CC-01-13. (www. lanl. gov/thermoacoustics)* .

Ward, W. C. and Swift, G. W., 1994. 'Design environment for low-amplitude thermoacoustic engines', *The Journal of the Acoustical Society of America* **95**(6), 3671–3672.

Wheatley, J. C., Swift, G. W. and Migliori, A., 1986*a*. 'The natural heat engine', *Los Alamos Science* **14**(2), 2–33.

Wheatley, J. C., Swift, G. W. and Migliori, A., 1986*b*. 'Thermoacoustic magnetohydrodynamic electrical generator'. US Patent 4,599,551.

Wu, Z., Dai, W., Man, M. and Luo, E., 2012. 'A solar-powered traveling-wave thermoacoustic electricity generator', *Solar Energy* **86**(9), 2376–2382.

Wu, Z., Man, M., Luo, E., Dai, W. and Zhou, Y., 2011. 'Experimental investigation of a 500 W traveling-wave thermoacoustic electricity generator', *Chinese Science Bulletin* **56**(19), 1975.

Wu, Z., Yu, G., Zhang, L., Dai, W. and Luo, E., 2014*a*. 'Development of a 3 kW double-acting thermoacoustic stirling electric generator', *Applied energy* **136**, 866–872.

Wu, Z., Yu, G., Zhang, L., Dai, W. and Luo, E., 2014*b*. 'Investigation on a 1 kW traveling-wave thermoacoustic electrical generator', *Applied Energy* **124**, 140–147.

Yang, R., Wang, Y., Feng, Y., Jin, T. and Tang, K., 2019. 'Performance of a looped thermoacoustic engine with multiple loads capable of utilizing heat source below 200° C', *Applied Thermal Engineering* **148**, 516–523.

Yazaki, T., Iwata, A., Maekawa, T. and Tominaga, A., 1998. 'Traveling wave thermoacoustic engine in a looped tube', *Physical Review Letters* **81**(15), 3128.

Yazaki, T. and Tominaga, A., 1998. Measurement of sound generation in thermoacoustic oscillations, *in* 'Proceedings of the Royal Society of London A: Mathematical, Physical and Engineering Sciences', Vol. 454, The Royal Society, pp. 2113–2122.

Yu, G. Y., Luo, E. C., Dai, W. and Wu, Z. H., 2007. 'An energy-focused thermoacoustic-Stirling heat engine reaching a high pressure ratio above 1.40', *Cryogenics* **47**(2), 132–134.

Yu, Z. and Al-Kayiem, A., 2014. 'Numerical analysis of a thermally driven thermoacoustic heat pump for low-grade heat recovery', *Computational Thermal Sciences: An International Journal* **6**(4).

Yu, Z. B., Li, Q., Chen, X., Guo, F. Z. and Xie, X. J., 2005. 'Experimental investigation on a thermoacoustic engine having a looped tube and resonator', *Cryogenics* **45**(8), 566–571.

Yu, Z., Backhaus, S. and Jaworski, A., 2009. Design and testing of a travelling-wave looped-tube engine for low-cost electricity generators in remote and rural areas, *in* '7th International Energy Conversion Engineering Conference', p. 4540.

Yu, Z. and Jaworski, A. J., 2010. 'Impact of acoustic impedance and flow resistance on the power output capacity of the regenerators in travelling-wave thermoacoustic engines', *Energy Conversion and Management* **51**(2), 350–359.

Yu, Z., Jaworski, A. J. and Backhaus, S., 2010*a*. Design of a low-cost thermoacoustic electricity generator and its experimental verification, *in* 'ASME 2010 10th Biennial Conference on Engineering Systems Design and Analysis', American Society of Mechanical Engineers, pp. 191–199.

Yu, Z., Jaworski, A. J. and Backhaus, S., 2010*b*. 'A low-cost electricity generator for rural areas using a travelling-wave looped-tube thermoacoustic engine', *Proceedings of the Institution of Mechanical Engineers, Part A: Journal of Power and Energy* **224**(6), 787–795.

Yu, Z., Jaworski, A. J. and Backhaus, S., 2012. 'Travelling-wave thermoacoustic electricity generator using an ultra-compliant alternator for utilization of low-grade thermal energy', *Applied Energy* **99**, 135–145.

Yu, Z., Saechan, P. and Jaworski, A. J., 2011. 'A method of characterising performance of audio loudspeakers for linear alternator applications in low-cost thermoacoustic electricity generators', *Applied Acoustics* **72**(5), 260–267.

Zhang, X. and Chang, J., 2015. 'Onset and steady-operation features of low temperature differential multi-stage travelling wave thermoacoustic engines for low grade energy utilization', *Energy Conversion and Management* **105**, 810–816.

Zhang, X., Chang, J., Cai, S. and Hu, J., 2016. 'A multi-stage travelling wave thermoacoustic engine driven refrigerator and operation features for utilizing low grade energy', *Energy Conversion and Management* **114**, 224–233.

Zhao, D., 2013. 'Waste thermal energy harvesting from a convection-driven rijke–zhao thermo-acoustic-piezo system', *Energy conversion and management* **66**, 87–97.

Zhou, G., Li, Q., Li, Z. Y. and Li, Q., 2008. 'A miniature thermoacoustic Stirling engine', *Energy Conversion and Management* **49**(6), 1785–1792.